https://doi.org/10.15388/vu.thesis.528
https://orcid.org/0000-0002-4992-9158

VILNIUS UNIVERSITY
CENTER FOR PHYSICAL SCIENCES AND TECHNOLOGY

Karolina Maleckaitė

# Photophysical Properties of Boron Dipyrromethene (BODIPY)-Based Fluorescent Molecular Sensors

**DOCTORAL DISSERTATION**

Natural Sciences,
Physics (N 002)

VILNIUS 2023

This dissertation was written between 2019 and 2023 at Center for Physical Sciences and Technology.
The research was supported by the Research Council of Lithuania: funding for the one-month research visit to Imperial College London (UK) in 2022, support for participation in the Faraday Joint Interest Group Conference in Sheffield (UK) in 2023, and a scholarship for academic achievements awarded in 2023.

**Academic supervisor:**
**Dr. Aurimas Vyšniauskas** (Center for Physical Sciences and Technology, Natural Sciences, Physics – N 002).

**Dissertation Defense Panel:**

**Chairman – Prof. Dr. Artūras Katelnikovas** (Vilnius University, Natural Sciences, Chemistry – N 003).

**Members:**
**Dr. Guido Bolognesi** (University College London, Natural Sciences, Physics – N 002),
**Dr. Danielis Rutkauskas** (Center for Physical Sciences and Technology, Natural Sciences, Physics – N 002),
**Prof. Dr. Simas Šakirzanovas** (Vilnius University, Natural Sciences, Chemistry – N 003),
**Dr. Marijonas Tutkus** (Center for Physical Sciences and Technology, Natural Sciences, Physics – N 002).

The dissertation shall be defended at a public meeting of the Dissertation Defense Panel at 10:00 on 22 September 2023 in Room A101 of the Center for Physical Sciences and Technology.
Address: Saulėtekio av. 3, NFTMC, Room A101, Vilnius, Lithuania.
Tel. +370 5 264 8884; email: office@ftmc.lt.

The text of this dissertation can be accessed at the Vilnius University Library, as well as on the website of Vilnius University: www.vu.lt/naujienos/ivykiu-kalendorius.

https://doi.org/10.15388/vu.thesis.528
https://orcid.org/0000-0002-4992-9158

VILNIAUS UNIVERSITETAS
FIZINIŲ IR TECHNOLOGIJOS MOKSLŲ CENTRAS

Karolina Maleckaitė

# Fluorescuojančių molekulinių jutiklių paremtų boro dipyrometeno (BODIPY) grupe fotofizikinės savybės

**DAKTARO DISERTACIJA**

Gamtos mokslai,
Fizika (N 002)

VILNIUS 2023

Disertacija rengta 2019–2023 metais Fizinių ir technologijos mokslų centre. Mokslinius tyrimus rėmė Lietuvos mokslo taryba: 2022 m. finansuota vieno mėnesio trukmės stažuotė Londono imperatoriškajame koledže (Jungtinėje Karalystėje), 2023 m. skirtas finansavimas dalyvavimui „Faraday Joint Interest Group“ konferencijoje Šefilde (Jungtinėje Karalystėje), bei 2023 m. skirta stipendija už akademinius pasiekimus.

**Mokslinis vadovas:**
**Dr. Aurimas Vyšniauskas** (Fizinių ir technologijos mokslų centras, gamtos mokslai, fizika – N 002).

**Gynimo taryba:**

**Pirmininkas – Prof. Dr. Artūras Katelnikovas** (Vilniaus universitetas, gamtos mokslai, chemija – N 003).

**Nariai:**
**Dr. Guido Bolognesi** (Londono universiteto koledžas, gamtos mokslai, fizika – N 002),
**Dr. Danielis Rutkauskas** Fizinių ir technologijos mokslų centras, gamtos mokslai, fizika – N 002),
**Prof. Dr. Simas Šakirzanovas** (Vilniaus universitetas, gamtos mokslai, gamtos mokslai, chemija – N 003),
**Dr. Marijonas Tutkus** (Fizinių ir technologijos mokslų centras, gamtos mokslai, fizika – N 002).

Disertacija ginama viešame Gynimo tarybos posėdyje 2023 m. rugsėjo mėn. 22 d. 10:00 val. Nacionalinio fizinių ir technologijos mokslų centro A101 auditorijoje. Adresas: Saulėtekio al. 3, NFTMC, A101 aud., Vilnius, Lietuva.
Tel. +370 5 264 8884; el. paštas: office@ftmc.lt.

Disertaciją galima peržiūrėti Vilniaus universiteto bibliotekoje ir VU interneto svetainėje adresu: www.vu.lt/naujienos/ivykiu-kalendorius.

# ACKNOWLEDGEMENTS

My life in physics started with many doubts: the physics teacher did not believe I could pass the national exam, while very close friends told me: "Physics… it's just not you, Karolina". Well, here we are.

Trust those you want to trust. Yourself. Your family. Your significant other. Your inspiration.

Therefore, I thank myself for being strong enough to finish it. My family and my extended family for saying "You are smart". My significant otter Vincas for going down this road together and becoming The Babes*. My inspiration who told me "You need to do a PhD".

I would like to give very special thanks to my PhD supervisor Aurimas, who did what he had to do and has my absolute respect. Further special thanks go to the co-authors of the publications who made this work possible.

Yet everyone I know has motivated me to deliver this thesis. Former and current colleagues, friends, people I met at conferences and internships. I am very glad to have met you all on this undoubtedly interesting scientific journey, which has now lasted a decade, long may it continue!

Cheers,
Karolina

*Should we rebrand to The PhD Babes?

# CONTENTS

ACKNOWLEDGEMENTS 5

CONTENTS 6

INTRODUCTION 8

ACRONYMS IN ALPHABETICAL ORDER 12

1 LITERATURE REVIEW 14

1.1 Environmental properties and microenvironment of the cell . . . . 14

1.2 A brief intro into the luminescence . . . . . 19

1.3 Microenvironment imaging . . . . . 22

1.4 Fluorescent molecular rotors . . . . . 25

1.5 BODIPY probes and their mechanism . . . . . 26

2 EXPERIMENTAL METHODS 30

2.1 Synthesis of compounds . . . . . 30

2.2 Preparation of samples . . . . . 30

2.3 Calibration of viscosity sensors . . . . . 30

2.4 Absorbance. Steady-state and time-resolved fluorescence. Determination of the fluorescence quantum yield. . . . . 32

2.5 Preparation of LUVs . . . . . 32

2.6 Theoretical calculations . . . . . 33

2.7 Cellular imaging . . . . . 34

2.8 Data analysis . . . . . 34

3 TRANSFORMING THE VISCOSITY-SENSITIVE BODIPY MOLECULAR ROTOR INTO A TEMPERATURE SENSOR WITH CYCLOPROPYL SUBSTITUENTS 35

3.1 Probe design . . . . . 35

3.2 Spectroscopic properties . . . . . 36

3.3 Temperature and viscosity sensitivity . . . . . 36

3.4 Polarity sensitivity . . . . . 38

3.5 Rationalisation of temperature-dependence of BODIPY2 and BODIPY3 . . . . . 40

3.6 Cellular imaging . . . . . 41

3.7 Conclusions . . . . . 42

4 RED-EMITTING VISCOSITY SENSITIVE BODIPY FLUOROPHORE FOR INTRACELLULAR IMAGING OF LIPID DROPLETS 44

4.1 Fluorophore design . . . . . 44

4.2 DFT calculations . . . . . 45

4.3 Absorbance and fluorescence spectra . . . . . 46

4.4 Influence of viscosity . . . . . 47
4.5 Cellular imaging . . . . . 49
4.6 Conclusions . . . . . 50
5 THE IMPACT OF ELECTRON-DONATING/-WITHDRAWING GROUPS IN RED-FLUORESCENT BODIPY MOLECULAR ROTORS 52
5.1 The design of probes and motivation . . . . . 52
5.2 Absorbance and fluorescence spectra . . . . . 53
5.3 Theoretical calculations . . . . . 54
5.4 Time-resolved fluorescence and sensitivity to viscosity, temperature and polarity . . . . . 55
5.5 Conclusions . . . . . 58
6 RED-EMITTING MOLECULAR ROTOR FOR HIGH MICROVISCOSITY ENVIRONMENTS 59
6.1 Motivation and probes design . . . . . 59
6.2 Synthesis of the derivatives . . . . . 60
6.3 Absorbance and fluorescence spectra . . . . . 61
6.4 Viscosity sensitivity . . . . . 61
6.5 Polarity and temperature sensitivity . . . . . 64
6.6 Conclusions . . . . . 65
7 A RED-EMITTING THIOPHENE-MODIFIED BODIPY PROBE FOR FLUORESCENCE LIFETIME-BASED POLARITY IMAGING OF LIPID DROPLETS IN LIVING CELLS 66
7.1 Motivation and probe design . . . . . 66
7.2 Absorbance and fluorescence spectra . . . . . 67
7.3 Sensitivity of the fluorescence decay to polarity, viscosity and temperature . . . . . 68
7.4 Fluorescence decays in liquid-ordered/-disordered vesicles . . . . . 70
7.5 Cellular imaging . . . . . 71
7.6 Conclusions . . . . . 73
CONCLUSIONS OF THE THESIS 74
LIST OF PUBLICATIONS 75
CURRICULUM VITAE 79
SANTRAUKA 81
COPIES OF PUBLICATIONS 92
BIBLIOGRAPHY 149

# INTRODUCTION

Many diffusion-controlled processes are taking place in our cells every second. These processes can be affected by changing microenvironment, such as alternations of viscosity [1–3], temperature [4–6], and polarity [7–9]. Moreover, the drastic variations of these properties at the cellular level can indicate serious diseases [10–15]. Therefore, the intracellular research methods that can detect these changes should be developed. Fluorescent probes bring such opportunity for biophysicists to understand changing microenvironment in living cells [16–18]. However, there are different probe types and imaging techniques with their own advantages and drawbacks.

BODIPY-based molecular rotors are a group of fluorescent probes that are mostly used for microviscosity sensing in living cells [1]. They have a handful of attractive properties, like monoexponential fluorescence decay and nontoxicity, making them a great platform for the development of fluorescent probes [19]. The ability to easily modify BODIPY core can provide ways to create fluorophores with longer emission wavelengths and sensitivity to temperature and polarity.

This work highlights a need of red fluorescent probes for a simplified live-cell imaging. Moreover, the development of probes that are sensitive to viscosity, temperature, and polarity are presented.

## Aim, novelty and tasks

The aim of this work was to investigate how substitution with different functional groups alters the photophysical properties of BODIPY molecular rotors and their sensitivity to environmental changes.

The motivation and novelty of this research was to develop new red fluorescent BODIPY microviscosity probes. Moreover, this work focused on the transformation of microviscosity probes into temperature and polarity probes. In addition, it was very important to create environmental probes that can be used *in vitro*.

To achieve these goals several tasks were set:

- Examine if the $\beta$-substitution of the BODIPY core with phenyl and vinyl groups extends the conjugation and creates a red-emitting fluorophore, while preserving sensitivity to viscosity;

- Evaluate how cyclopropyl- and thiophene-substitution in $\alpha$ and $\beta$ positions of the BODIPY core changes spectroscopic and sensitivity properties of the probe depending on the substitute and its position;

- Demonstrate that the most promising compounds can be used for imaging the microenvironment of living cells.

**Statements to be defended**

1. Substitution with a nitro group in the *meso*-phenyl position of the BODIPY core is a universal way to increase the viscosity sensitivity of the probe.

2. Electron donating groups (EDG) substitutes, such as methoxy and thiophene groups, increase polarity sensing in BODIPY molecular rotors when placed at the $\beta$ position of the BODIPY core.

3. The $\beta$-substitution of the BODIPY core by cyclopropyl, phenyl, vinyl and thiophene moieties, increases the conjugation of the derivatives and leads to a red shift of the absorption and fluorescence spectra.

4. Red fluorescent BODIPY probes with $\beta$-phenyl- and $\beta$-thiophene-substitutes can be used for imaging lipid droplets (LDs) in living cells to detect changes in microviscosity and polarity, respectively.

**Layout of the dissertation**

The thesis begins with a literature review, which firstly introduces a microscopic environment of the cell, the importance of lipid-rich cellular organelles called LDs and how cell is affected by fluctuations of viscosity, temperature, and polarity. It is followed by the explanation of the model lipid systems called large unilamellar vesicles (LUVs), also known as liposomes. Moreover, the reader is introduced why the development of the red fluorescent environment-sensitive probes is an important task. The second section briefly overviews the photophysical mechanisms, such as absorbance and fluorescence. It also explains the fluorescence lifetime measuring technique time-correlated single-photon counting (TCSPC). The third section summaries different methods of visualising microenvironment of live cells. In the forth section of the literature review the reader will find a summary of most common types of molecular probes. The literature review is finalised by explication of BODIPY-based molecular probes, their advantages and drawbacks.

In the experimental methods section the reader will find a brief introduction about how samples are prepared and what setups were used for absorbance and fluorescence spectroscopy measurements. Moreover, the calibration of sensors is explained as well as preparation of LUVs. The methodology section is completed with the summary of the data analysis.

The most complex part of thesis – results and discussion – is divided into five sections that all correspond to publications included in this work:

- [**P1**] *Cyclopropyl Substituents Transform the Viscosity-Sensitive BODIPY Molecular Rotor into a Temperature Sensor*
  Explains how cyclopropyl substituents change the properties of the commonly-used BODIPY-$C_{10}$ viscosity probe, turning it a temperature sensor, while maintaining a green emission.

- [**P2**] *Designing a Red-Emitting Viscosity-Sensitive BODIPY Fluorophore for Intracellular Viscosity Imaging*
  Reveals how DFT aids the design of red-emitting microviscosity probe prior to its synthesis. It also explores how phenyl moieties redshift the fluorescence spectrum, while the nitro group helps to lower the energy barrier and preserve viscosity sensitivity. Moreover, the application of the red fluorescent probe in living cells is demonstrated.

- [**P3**] *Give or Take: Effects of Electron-Accepting/-Withdrawing Groups in Red-Fluorescent BODIPY Molecular Rotors*
  Continues a story about phenyl-disubstituted derivatives and explains the impact of electron accepting/donating groups. The publication explores how a red microviscosity sensor can be transformed into a temperature or polarity probe. Moreover, the role of the energy barrier for BODIPY sensitivity to viscosity and temperature is explained in the original publication.

- [**P4**] *Red fluorescent BODIPY molecular rotor for high microviscosity environments*
  A follow-up for a phenyl-modified viscosity sensor explained in [**P2**] that explains the role of methyl position on $\beta$-phenyls. Furthermore, a creation of a red fluorescent viscosity probe with vinyl-substitutes is reported.

- [**P5**] *A red-emitting thiophene-modified BODIPY probe for imaging polarity of lipid droplets in living cells*
  Finalises the main topic of the thesis – red fluorescent probes for live cell imaging. This section presents thiophene-modified disubstituted and tetrasubstituted derivatives that enables the creation of polarity probe and its use for imaging LDs polarity in living cancer cells.

The thesis is finished with the results concluding chapter.

### Contribution of the author

All photophysical characterisation, steady-state, and time-resolved spectroscopy investigations, including sample preparation, were carried out by the author, who also processed and analysed the data. Moreover, the author took part in the development and discussion of all the manuscripts. Furthermore, thesis author was the main writer of publications [**P2, P3, P4**].

The thesis author is exceptionally glad being able to present an interdisciplinary work that would not be possible without contribution from colleagues of Center of Physical Sciences and Technology (FTMC), Vilnius University, National Cancer Institute in Lithuania, Imperial College London and King's College London. Therefore, parts of this work were delegated or conducted in collaboration, which is detailed in the Chapter 2.

## ACRONYMS IN ALPHABETICAL ORDER

| | |
|---|---|
| **CSP** | cisplatin |
| **DCE** | 1,2-dichloroethane |
| **DCM** | dichloromethane |
| **DFT** | density functional theory |
| **DMF** | N,N-dimethylformamide |
| **DMSO** | dimethyl sulfoxide |
| **DOPC** | dioleoylphosphatidylcholine phospholipide |
| **DPPC** | dipalmitoylphosphatidylcholine phospholipide |
| **EDG** | electron donating groups |
| **ER** | endoplasmic reticulum |
| **EWG** | electron withdrawing groups |
| **FCS** | fluorescence correlation spectroscopy |
| **FLAP** | fluorescence localisation after photobleaching |
| **FLIM** | fluorescence lifetime imaging microscopy |
| **FLIP** | fluorescence loss in photobleaching |
| **FMRs** | fluorescent molecular rotors |
| **FRAP** | fluorescence recovery after photobleaching |
| **FRET** | Förster resonance energy transfer |
| **HOMO** | highest occupied molecular orbital |
| **LDs** | lipid droplets |
| **LUMO** | lowest unoccupied molecular orbital |
| **LUVs** | large unilamellar vesicles |
| **MCF-7** | breast cancer cells |
| **PAX** | paclitaxel |
| **PBS** | phosphate-buffered saline |

| | |
|---|---|
| **PES** | potential energy surface |
| **ROI** | region of interest |
| **SdP** | solvent dipolarity parameter |
| **QY** | quantum yield |
| **TCSPC** | time-correlated single-photon counting |
| **THF** | tetrahydrofuran |
| **TDDFT** | time-dependent density functional theory |
| **TS** | transition state |
| **U2OS** | human osteosarcoma (bone cancer) cells |

# 1. LITERATURE REVIEW

## 1.1. Environmental properties and microenvironment of the cell

In this section, the reader is introduced to the basics of the cellular environment, and learns how observing changes within the cell provides important information about the cellular health. The three main environmental properties-viscosity, temperature, and polarity-and the importance of visualising changes in these properties inside the cell are discussed.

### Cells, lipid droplets and the need of red fluorophores

The body contains a wide variety of cell kinds, sizes, and forms. Therefore, the idea of a "generalised eukaryotic cell" is introduced. The cell membrane, the nucleus, and the cytoplasm are the three components that make up this type of cell. Numerous, possibly even thousands, of tiny, unique structures known as organelles are found in the cytoplasm. The mitochondrion, ribosomes, endoplasmic reticulum (ER), Golgi apparatus, and lysosomes are a few examples of cytoplasmic organelles [20, 21].

LDs are important cellular organelles involved in lipid supply and storage, buffering cellular lipid concentrations, and managing their release to satisfy certain cellular needs. As a result, they are considered essential for preserving lipid and energy balance [23]. The core of LDs is composed of non-polar lipids, such as triacylglycerols and sterol esters, while the surface is formed by of polar lipids, such as sterols and phospholipids, and a variety of proteins [24]. Figure 1.1 shows some of the interactions between LDs and other organelles as well as a few aspects of LDs dynamics.

The intracellular environment can be studied using small fluorescent molecules called "fluorophores" (also called fluorescent probes or sensors). Their use allows scientists to detect changes in the environment and understand binding events or chemical reactions as fluorescence emission changes during these processes [25]. Fluorescent probes that emit light in a blue or green spectral region can be used for biomolecular labeling or even for phosgene gas detection, which is used in chemical warfare [26].

Unfortunately, live cell imaging requires red fluorescent fluorophores for easier identification of environmental properties. There are several problems that can be solved by using red fluorescence. First off, autofluorescence of biological samples, which can be thought as a visual noise of various self-fluorescent organelles, is less of a problem in the red part of the visible spectrum [27]. Secondly, the same biological samples can also be imaged more easily when they are combined with additional fluorophores, such as green fluorescent protein (GFP). Third, in order to minimise visible light scattering, imaging of thick

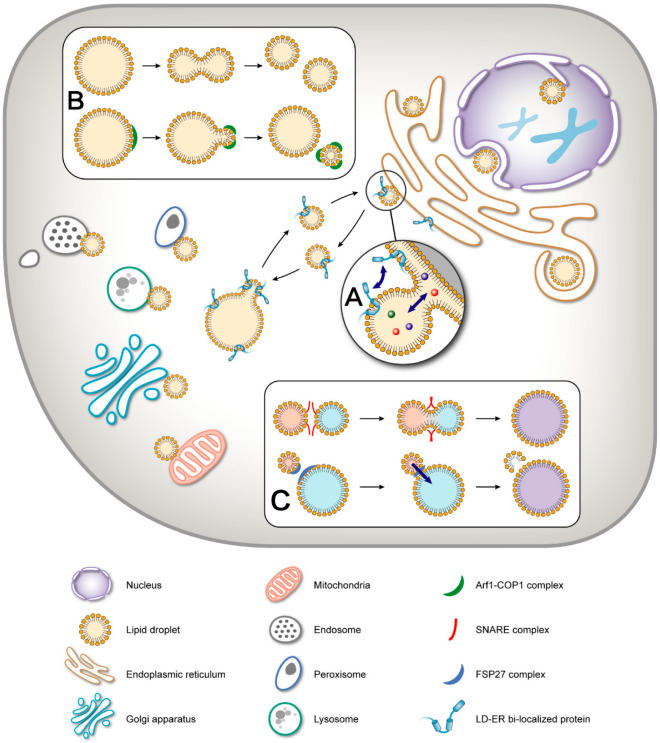


**Figure 1.1:** Various organelles found inside the eukaryotic cells and LDs dynamics. LDs are very active organelles in cells, moving around, interacting with other organelles, and changing in size. (A) LD-ER interaction sites allow LDs to communicate with the ER. The two organelles are exchanging materials and information. (B) Fission and budding are two ways in which a large LD might be split up into smaller LDs. (C) Fusion and neutral lipid transit enable the formation of a big LD from two minor LDs. Figure source: Li *et al.* [22]

.

biological samples must occur within the optical window of deep tissue (650-1350 nm) [28, 29]. For these reasons, one of the main objectives of this work was to develop red-emitting probes.

### Viscosity

There are a lot of diffusion-controlled processes happening in biological systems that can be affected by microviscosity, which is the microscopic equivalent of bulk viscosity. Therefore, imaging changes in microviscosity can reveal biochemical and biophysical mechanisms that take place inside of living cells [1–3]. Microviscosity visualisation is important for researchers studying polymers [30], aerosols [31], live cells [32–34] and their specific organelles [35–37], such as lipid packing in cell membranes [38].

Viscosity plays a crucial role in how apoptosis, autophagy, ferroptosis, oxidative stress, and other cellular processes are carried out [11]. Observing these changes may even be used to diagnose diseases like Alzheimer's [10,39] and diabetes [40]. For example, the increased viscosity of erythrocytes and platelets, inhibits the aggregation of insulin receptors and promotes the development of diabetes [11, 12]. Meanwhile, a decrease in the viscosity of leukocyte membranes encourages $\beta$-amyloid to aggregate, which in turn promotes insoluble plaques to accumulate in the brain and can cause Alzheimer's disease [41].

One of focal points of this thesis is viscosity-sensing of lipid droplets. Although viscosity-sensing in LDs is still an emerging topic, there are already some promising results. In a 2022 study, Yang *et al.* showed that LDs become more viscous in response to ER stress [42]. On the other hand, in the article by Dong *et al.* it was demonstrated that the viscosity of LDs increases during the ferroptosis process [43]. Hence, there is a significant evidence that the viscosity of the LDs should be studied further.

### Temperature

Many intracellular processes, both normal and abnormal, produce heat or are influenced by temperature, e.g. cell division, respiration, and thermogenesis [4–6]. Additionally, some cancer tissues have been observed to generate more heat than normal cells [13]. It is therefore exceedingly desirable to be able to measure temperature, especially at the intracellular level. Additionally, intracellular temperature probes may help in researching and identifying the beginning of a number of disorders that result in a change in body temperature.

Temperature-sensing *in vitro* has been reported in various organelles. For example, studying thermodynamics in mitochondria can help to understand processes related to energy balance and homeostasis [17]. Moreover, heat is generated in the ER, so the specific visualisation of temperature in this organelle is very important [44]. Additionally, Ogle *et al.* has reported that temperature changes in cytosol and the ER be used in studying metabolism, heat shock response, and hyperthermia therapies [45].

### Polarity

Polarity is a physical property of compounds that results from the uneven partial charge distribution between various atoms in a compound. For example, a polar solvent has a partial positive charge on one end and a partial negative charge on the other end, allowing it to dissolve polar solutes and participate in dipole-dipole interactions.

Usually, polar solvents have a tendency to red-shift the fluorescence spectrum. This happens because solvent molecules around the solute reorganise, leading to the lower energy of the relaxed state [46, 47]. Therefore, the more

polar is the solvent, the larger red-shift is observed.

Solvent polarity in literature is described using various methods. One of the most popular is dielectric constant ($\epsilon$). The higher the value of $\epsilon$, the more polar is the solvent. Another polarity parameter is called solvent dipolarity parameter (SdP) and it reflects induced dipole interactions as well as partly permanent dipole forces [48].

In this work, mostly orientation polarisability ($\Delta f$, Equation 1.1) is used as a polarity parameter since it more clearly demonstrates the effects of solvent polarity on the fluorophore than a dielectric constant, because it includes refractive index - a term that accounts for the ability of electron cloud of a solvent molecule to interact with a polar solute.

Orientation polarisation can be evaluated using Lippert-Mataga equation [47]:

$$\Delta f = \frac{\epsilon - 1}{2\epsilon + 1} - \frac{n^2 - 1}{2n^2 + 1} \ , \tag{1.1}$$

where $\Delta f$ - orientation polarisation, $\epsilon$ - dielectric permittivity, $n$ - refractive index.

Polarity in biological systems, particularly at the cellular level, governs the interaction activity of a variety of proteins and enzymes or indicates how permeable membrane compartments are [7]. Polarity sensing has already been implemented in studying in mitochondria [8] and targeting hydrophobic parts of the cell for selective protein detection [9]. Moreover, scientists studying cell cultures have reported that an excessive buildup of partially unfolded or glycosylated proteins, can cause a polarity change in the ER stress environment [49]. Furthermore, an increase in polarity occurs during autophagy as a result of the fusion of the lysosomal membrane with the autophagosome membrane [50]. In addition, unusual polarity changes are closely related to certain diseases and conditions, such as diabetes [12, 14], non-alcoholic fatty liver disease [15] and hepatitis (liver inflammation) [51].

This work includes results about polarity imaging in LDs. Mapping the polarity of LDs is important for a few reasons. Firstly, it has been demonstrated that the polarity of LDs can aid in assessing the lipid arrangement and order [52]. Secondly, the polarity of LDs can reveal the activity of proteins and enzymes that interact with one another [53]). According to Wang *et al.*, it is also believed that the polarity and structure of LDs can change when cells undergo ferroptosis, which is caused by a buildup of lipid peroxides [54]. Finally, it was demonstrated that hunger and oxidative stress alter the local polarity of intracellular membranes and LDs [52]. As a result, it is reasonable to assume that, depending on the many active cellular processes, polarity inside LDs can be diverse and dynamic. Therefore, the polarity inside LDs may provide more details about the condition and function of the cell.

### Liposomes (LUVs)

Unilamellar liposomes are spherical vesicles that contain an aqueous solution and are surrounded by a single bilayer of an amphiphilic lipid or a combination of such lipids [55,56]. The structure of the liposome is presented in Figure 1.2A. These liposomes are used to study biological systems and to mimic cell membranes, and can be classified into groups by their size, composition and even mechanism of delivery. In this work, only LUVs are studied, and their size range from 0.1 to 1 µm.

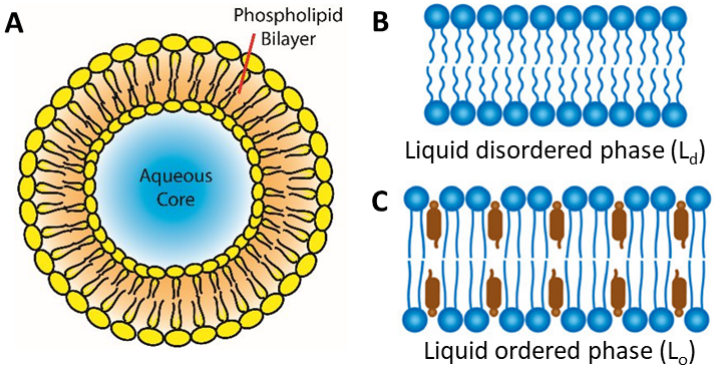


**Figure 1.2:** (A) The composition of a liposome. A phospholipid bilayer and an aqueous center make up a liposome. Figure source: Leung *et al.* [57]. (B-C) Differences between $L_d$ and $L_o$ phases. Brown inserts between phospholipids (in blue) are cholesterol particles. Adapted with permission from Hao *et al.* [58]. Copyright 2022 American Chemical Society.

An easy approach for measuring polarity is based on fluorescent organic molecules, which change their spectroscopic characteristics in response to their physical surroundings. This type of dyes have been employed in the past to detect variations between liquid-ordered ($L_o$) and liquid-disordered ($L_d$) phases in lipid membranes [59]. Both phases are displayed in Figure 1.2B-C. $L_d$ phase is fluid, while the $L_o$ phase is intermediate between $L_d$ and solid (gel) phases [60]. $L_o$ phase compared to $L_d$ is thicker, stiff and, as the name suggests, has an increased order. $L_d$ phase can also be described as unsaturated lipid-rich, while the $L_o$ phase is saturated lipid-rich [61].

Studying both phases can bring a lot of important information because they reflect very well the heterogeneity of biological membranes, since $L_o$ and $L_d$ phases can coexist in cell membranes [60]. Moreover, LUVs having $L_o$ and $L_d$ phases can be used to measure the polarity sensitivity of the probe. $L_o$ phase has fewer water molecules since it is a more compact environment. Because of this, the $L_o$ phase is less polar than the $L_d$ phase, which has a less rigid environment and is consequently more hydrated [62]. Fluorescence techniques can be used to non-destructively observe these domains because of

the difference in hydration between the $L_o$ and $L_d$ phases [59].

### 1.2. A brief intro into the luminescence

The term "luminescence", simply meaning the emission of light by a substance, refers to the phenomenon of light effects brought on by the transition of an electron from an excited state to a lower energy state [46,47,63,64]. Different energy states for a molecule are possible and are depicted in Figure 1.3. The lowest energy level for a molecule is its ground state $S_0$, which is also the most stable state. The molecule can be raised to a higher energy level (an excited state) by absorbing energy.

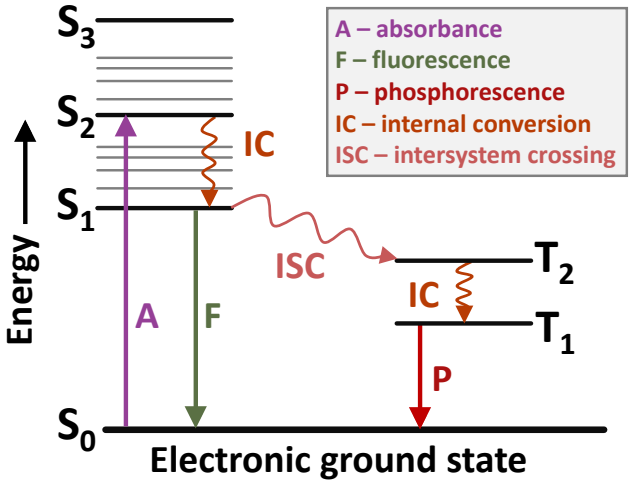


**Figure 1.3:** Jablonski diagram showing electronic states and transitions of the molecule following the excitation.

Absorbance of light is defined by the Beer-Lambert law that in most cases can be expressed as written in Equation 1.2 [46]:

$$A(\lambda) = \log\frac{I_\lambda^0}{I_\lambda} = \varepsilon(\lambda)lc \tag{1.2}$$

where $I_\lambda^0$ is the light intensity of the entering beam, $I_\lambda$ - the light intensity of the leaving absorbing medium beam, $\varepsilon(\lambda)$ - molar absorption coefficient (in L mol$^{-1}$ cm$^{-1}$), $l$ - absorption path length (in cm), $c$ - the concentration of the absorbing species (in mol L$^{-1}$).

The molecule must lose energy when it transitions back to its ground state because the excited state has a higher energy than the ground state. This energy can be emitted as photons, *i.e.* the emission of light is observed.

Depending on how the system is activated, there are several types of luminescence. One of these types is photoluminescence, which results from excitation with photons. Photoluminescence can be divided into two groups: fluorescence and phosphorescence. The main difference between them is the duration of luminescence, which is determined by the state from which the electrons return to the ground state. When the electrons relax from the singlet state, fluorescence occurs, and the relaxation times are from $10^{-10}$ to $10^{-7}$ seconds. Meanwhile, when the electrons relax from the triplet state, phosphorescence is observed, and the lifetimes are in the range of $10^{-6}$–10 s. In this work, only the effects of fluorescence are analysed.

Fluorescence is the photon emission, when excited molecules return from the $S_1$ state to $S_0$ state. It is always followed by the Stokes shift (with a few exceptions) that shows energy losses between excitation and emission, which can be depicted as a red-shift of the fluorescence spectra in contrast to absorbance [47].

### Fluorescence lifetime, quantum yield, radiative and nonradiative rates

Time-resolved fluorescence measurements can let to achieve more accurate information about molecular processes because unlike steady-state measurements (*e.g.* a fluorescence spectrum) it is not averaged [47]. Time-resolved fluorescence can be analysed by looking at fluorescence decays (aka, kinetics). Such kinetics can show how long the radiative state is existing or, in the case of multiexponential decays, it shows the presence of other conformational states, scattering, the presence of impurities, or solvation dynamics [65].

The time a fluorophore remains in the excited state before emitting a photon and going back to the ground state is known as the fluorescence lifetime [46,47]. Depending on the fluorophore, it can range from picoseconds to hundreds of nanoseconds.

Fluorescence lifetime ($\tau$) is expressed in Equation 1.3:

$$\tau = \frac{1}{k_r + k_{nr}} \tag{1.3}$$

where $k_r$ and $k_{nr}$ are radiative and non-radiative rate constants, respectively. $k_r$ defines light-emitting processes, such as fluorescence. Hence, $k_{nr}$ is the sum of all nonradiative processes leading to relaxation to ground state, like internal conversion or intersystem crossing [46].

Unlike fluorescence intensity, fluorescence lifetime is not affected by many properties such as fluorophore concentration, sample thickness, sample absorbance, measurement technique, photobleaching, and/or excitation intensity [66]. In contrast, external influences such as temperature, polarity and

the presence of fluorescence quenchers affect the lifetime making it a very useful feature for environmental sensing.

A competition between $k_r$ and $k_{nr}$ determines not only the fluorescence lifetime, but also fluorescence quantum yield (QY). QY of luminescence is a fundamental characteristic of any photoluminescent species, and its measurement is a crucial step in the characterisation. In this thesis, only molecules in dilute solution are studied. It is typical to take measurements of the fluorescence spectrum in this case and compare them to the integrated intensity of the same quantity for a reference fluorophore with a known QY. Standard absorption and emission spectrometers can be used to make this measurement [67]. Such measurement is called comparative method [68]. The final QY can be calculated using Equation 1.4:

$$\Phi_i = \frac{F_i A_s n_i^2}{F_s A_i n_s^2} \Phi_s \tag{1.4}$$

where $\Phi$ is the fluorescence QY, $F$ - the integrated fluorescence spectrum, $A$ - the integrated absorbance spectrum, $n$ - the refractive index of the solution, subscripts $i$ and $s$ label the sample and the reference, respectively.

The main criteria for choosing the reference is a spectral overlap. Because excitation takes place at the lowest energy absorption band, it should overlap for both the researched dye and the reference compound. That is why several references had to be used for different dyes as their main absorbance band was not consistent among all the dyes.

Experimentally obtained fluorescence lifetime and QY values can be used to calculate $k_r$ and $k_{nr}$ constants. Because fluorescence QY is a relationship of $k_r$ and $k_{nr}$ (Equation 1.5):

$$\phi = \frac{k_r}{k_r + k_{nr}}. \tag{1.5}$$

Combining Equation 1.3 and Equation 1.5 gives:

$$k_r = \frac{\phi}{\tau}, \tag{1.6}$$

$$k_{nr} = \frac{(1-\phi)}{\tau}. \tag{1.7}$$

If there are no other potential quenchers of the system and the molecule remains rigid in both states $S_0$ and $S_1$, which is practically impossible in real systems, $k_r$ can also be expressed by the Strickler-Berg relation [66, 69]:

$$k_r = 2.88 \times 10^{-9} n^2 \upsilon_f^3 (g_l/g_u) \int \varepsilon \cdot d \ln \tilde{\nu} \tag{1.8}$$

where $n$ is the refractive index, $\upsilon_f$ - the fluorescence maximum in $\mathrm{cm}^{-1}$, $g_l/g_u$ - the degeneracies of the lower and upper states (equal to $g_l/g_u = 1$ for the

fluorescence transition), $\varepsilon$ - extinction coefficient, $\tilde{\nu}$ - absorption maximum in wavenumbers (the integration is executed over the entire absorption spectrum).

### Time-Correlated Single Photon Counting

TCSPC is a method for evaluating the lifetime of fluorescence. With picosecond resolution and exceedingly high precision, it is an incredibly sensitive method for capturing low-level light signals [70].

TCSPC works on the basis of detecting single photons and measuring their arrival times in relation to a reference signal, often the light source [47, 71]. Importantly, it is a statistical technique that requires a high repetition rate light source (*e.g.*, a pulsed laser) to collect enough photon events to produce the accurate data. An analogy for TCSPC is a stopwatch with two inputs. The START signal pulse starts the clock, while the STOP signal pulse stops it. The rise of a memory value in a histogram (Figure 1.4, where the channels on the x-axis reflect time, is used to represent the measured duration for a sequence START - STOP. A light source allows rapid measurement of millions of START-STOP sequences, generally detecting 1 photon per 100 excitation pulses. The generated histogram of photon counts *vs.* channels represents fluorescence intensity over time.

Accurate detection of the time delay between the single photon and the reference clock is crucial for a variety of applications of TCSPC including fluorescence lifetime spectroscopy, microscopy, time-of-flight imaging and ranging, and quantum processing [72].

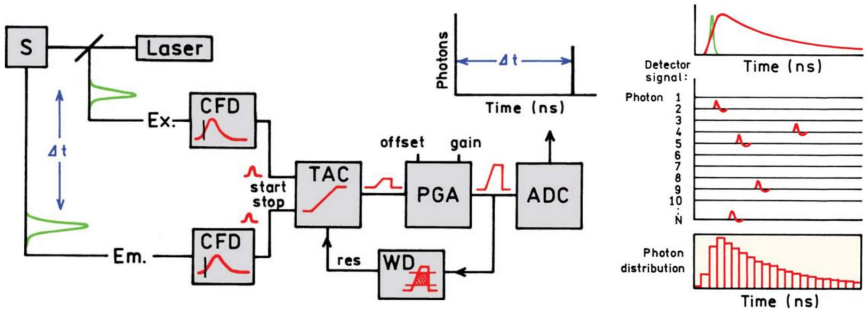


**Figure 1.4:** The principle scheme of TCSPC: the electronic schematic (on the left) and the pulses that create a histogram (on the right). Adapted from Lakowicz [47]. Copyright 2006 Springer US.

## 1.3. Microenvironment imaging

This section provides an overview of some microscopy techniques using fluorescent probes to study molecular dynamics and interactions in living cells.

## Fluorescence Recovery After Photobleaching, Fluorescence Loss in Photobleaching, and Fluorescence Localisation After Photobleaching

Fluorescence recovery after photobleaching (FRAP) is a technique for measuring the kinetics of diffusion through tissue or cells [73, 74]. It has the ability to study individual cells or assess the two-dimensional lateral diffusion of a molecular thin film which includes fluorescent probes. A high-intensity laser beam is used in FRAP to selectively photobleach a region of interest (ROI) within a cell or tissue sample. As unbleached fluorescent molecules diffuse into the bleached area over time, the fluorescence recovery within the ROI is then observed. The diffusion rate of the fluorescent molecules is directly correlated with the rate of fluorescence recovery [75]. The FRAP methodology has been widely utilised in biological research to study membrane dynamics, protein-protein interactions, and intracellular transport [76–78].

Fluorescence loss in photobleaching (FLIP) is frequently applied and closely related to FRAP. The primary distinction between these two microscopy techniques is that while FLIP examines how the loss of fluorescence spreads throughout the cell following numerous photobleaching events, FRAP examines a capacity of the cell to recover after a single photobleaching event [79]. In addition, many photobleaching events take place in FLIP to stop unbleached fluorophores from returning to the bleaching region.

Fluorescence localisation after photobleaching (FLAP) is another method for studying molecular interactions in living cells. Unlike the previously mentioned methods FRAP and FLIP, FLAP employs basic image differencing to follow the distribution of photo-labelled molecules using a reference fluorophore [80]. The ability to discover and follow subpopulations that migrate quickly and have brief residency durations is a key benefit of FLAP [79].

## Fluorescence Correlation Spectroscopy

Fluorescence correlation spectroscopy (FCS) is a technique that is used to study the dynamics of molecules at the single-molecule level [81]. FCS is based on the investigation of time correlations in the fluorescence fluctuation that results from fluorescent molecules diffusing in and out of a very small monitoring volume [82]. In practise, FCS is frequently used together with a confocal system. FCS is used to study the kinetics and dynamics of DNA and proteins [83].

Compared to FRAP/FLIP and FLAP, which all useful for studying the movement and distribution of molecules within a cell, FCS provides more quantitative information about molecular properties. FCS allows researchers to quantitatively evaluate the concentration, diffusion coefficient, and other dynamic properties of molecules [82, 84].

### Fluorescence Lifetime Imaging Microscopy

Fluorescence lifetime imaging microscopy (FLIM) is a method based on monitoring and analysing the fluorescence lifetime distribution and changes in samples, and as a result, has the potential to probe the microenvironment [85]. It is well known that fluorescence lifetime is highly influenced by their surroundings in addition to the molecular structure of the fluorophores.

As it was mentioned in the Section 1.2, changes in the microenvironment can be measured more accurately using fluorescence lifetime because it is not affected by the intensity of stimulated emission, quenching, light scattering and uneven distribution of fluorophores [85, 86]. This makes it possible to employ FLIM as a tool for reliable evaluation of the environment within a cell or tissue, as well as to monitor changes in a wide range of biophysical parameters including oxygen pressure, polarity, pH, ion concentration, and other biochemical parameters [87, 88].

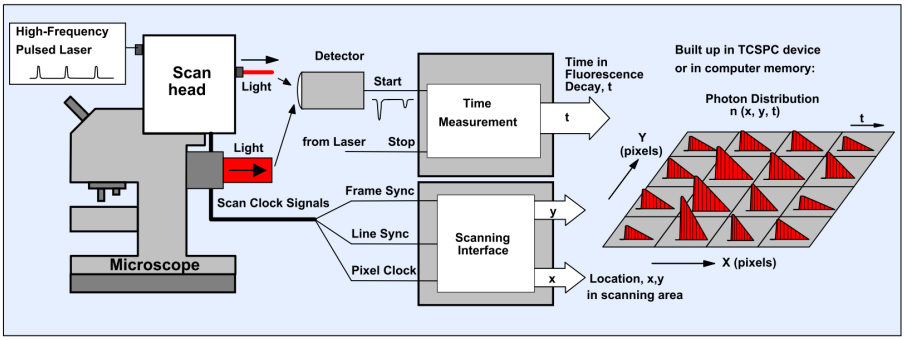


**Figure 1.5:** The principle scheme of FLIM. TCSPC is combined with microscopy. Adapted from Becker *et al.* [70]. Copyright 2010 Becker & Hickl GmbH.

Previously explained TCSPC is very well employed in FLIM to create a multidimensional mechanism - an extension of the traditional TCSPC technique [87]. Figure 1.5 illustrates the principal scheme. The focused beam of a high-frequency pulsed laser scans the sample. To record the data, the individual photons of the fluorescent light must be identified, as well as their relative arrival times with respect to the laser pulses and the position of the laser at the time of photon detection. From these variables, a photon distribution is created over the spatial coordinates $(x, y)$ and the arrival time of the photons $(t)$ after the laser pulses. The final result is a three-dimensional data array representing the pixels of the two-dimensional scan, each pixel having photons in a significant number of time channels that repeatedly follow the excitation pulses.

## 1.4. Fluorescent molecular rotors

Fluorescent molecular rotors (FMRs) have emerged as tools for monitoring changes in cellular and subcellular viscosity [16]. FMRs are generally considered to be microviscosity sensors. FMRs are valued for their high sensitivity, rapid response time, and ability to test targets in biological systems without causing harm.

FMRs work by competing with a nonradiative relaxation, which depends on the viscosity of the environment, and the radiative relaxation (fluorescence) of the molecules [1, 89]. If the excitation takes place in a non-viscous environment, FMRs generally follow a non-radiative path to the ground state using intramolecular rotation. Fluorescence becomes the primary de-excitation pathway when this motion is restricted, as in the case of higher viscosity or intermolecular interactions, leading to an increase in fluorescence intensity and longer decay times (Figure 1.6).

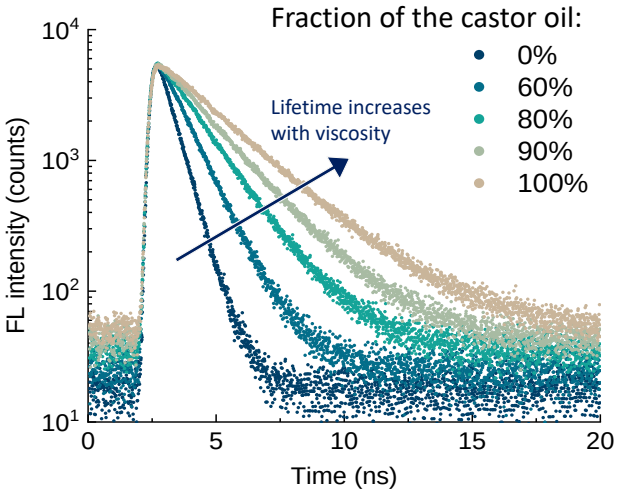


**Figure 1.6:** The example of fluorescence decays in various viscosity mixtures. The arrow shows that the fluorescence lifetime increases with increasing viscosity.

FMRs have become frequently applied for viscosity-sensing of the surrounding environment [1, 90, 91]. Moreover, their environment-sensitive properties were tuned to probe not only viscosity, but also temperature [17, 92, 93] and polarity [18, 94].

### Fluorescence lifetime-based probes

Fluorescent lifetime-based probes are a type that eliminates intensity-related artefacts and uses the fluorescence lifetime as an absolute metric to enable sim-

ple quantification [95]. The changing or even the exact value of the fluorescence lifetime can reflect the properties of the observed environment.

In contrast to fluorescence intensity, lifetime is not affected by fluorophore concentration [1]. This is unquestionably true when the two conditions are present: (1) the lack of excited state self-quenching, which can occur due to aggregation and/or diffusion controlled processes and shorten the observed excited state decay; (2) the absence of excited state aggregation processes, such as excimer formation, when a distinct emission band is observed, characterised by a different fluorescence lifetime.

### FRET-based probes

Förster resonance energy transfer (FRET) involves changes in the electronic interactions between a donor and an acceptor parts of the molecule [47]. FRET is a non-radiative energy transfer mechanism that involves two fluorescent molecules. During this process, a donor molecule uses dipole-dipole coupling to transfer its excitation energy to an acceptor molecule.

As a rule, molecules should meet the following conditions before they can be used in FRET [96, 97]. Firstly, the donor-acceptor pair should be placed closely together (usually 10-100 Å). Secondly, the absorption spectrum of an acceptor and the emission spectrum of the donor need to overlap. Finally, there must be a favourable mutual orientation between the donor emission moment, the acceptor absorption moment, and their separation vector.

FRET-based fluorescent sensors utilize FRET to detect changes in the local environment [98]. Moreover, when the donor and acceptor are both fluorophores, FRET is often referred to "fluorescence resonance energy transfer".

## 1.5. BODIPY probes and their mechanism

The widely used fluorescence lifetime-based probes are formed on the BODIPY-group [16, 90, 92]. BODIPY is an abbreviation for *Fluorinated Boron-Dipyrromethene* (aka *Dipyrrometheneboron difluoride*, or *4,4-difluoro-4-bora-3a,4a-diaza-s-indacene* (IUPAC name)). A widespread BODIPY-based microviscosity sensor is *meso*-phenyl-substituted is BODIPY-$C_{10}$ [99].

Due to the independence of lifetime from local fluorophore's concentration, excitation and detection conditions, BODIPYs are typically utilised as fluorescence lifetime probes rather than simple fluorescence intensity probes [1]. These probes feature a monoexponential fluorescence decay that facilitates data analysis and is perfect for use in FLIM [19].

Furthermore, it has been shown that BODIPY fluorophores can be sensitive to aforementioned environmental parameters: viscosity, temperature, polarity [100]. In fact, there have also been publications on polarity- and temperature-sensitive BODIPY-based fluorophores [45, 101, 102]. This makes BODIPY a

great platform for developing probes designed to sense specific properties.

BODIPY-based probes have been applied for environmental sensing in aerosols [31, 103], living cells [16, 91, 104], various cell organelles [3, 105–110]. Moreover, these derivatives were also utilised in bacteria detection [111] or as photosensitisers in cancer treatment [112].

As mentioned in Section 1.1, the development of red fluorescent probes is of great importance to improve their practical application. However, the majority of BODIPY-based sensors are green fluorescent, which complicates their application in biological samples [113]. This problem arises from the comparatively short excitation wavelength leading to limited penetration depth, photodamage, cellular autofluorescence, and photobleaching [114].

**The importance of the energy barrier**

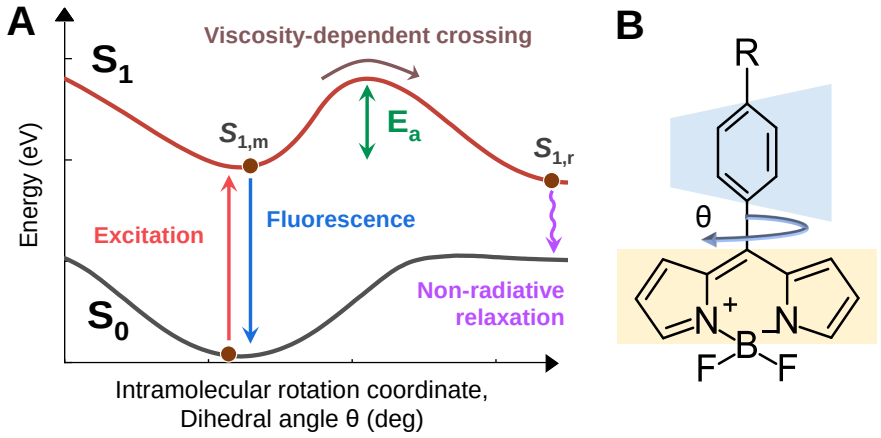


**Figure 1.7:** Photophysical model describing the viscosity sensing mechanism of BODIPY probes. (A) An example of potential energy surface (PES). (B) BODIPY molecular rotor.

To determine the viscosity sensitivity of the molecules, one should calculate how the energy of the $S_1$ state varies with the dihedral angle between the phenyl ring in the *meso* position and the BODIPY core. Such calculations can be represented using PES, which helps to understand the working mechanism of the BODIPY molecular rotor [115–119]. Additionally, PES aids to determine the activation energy barrier ($E_a$), which controls the viscosity and temperature sensitivity of molecular rotors [115, 120].

A basic example of PES is shown in Figure 1.7A. To begin with, it should be mentioned that the $\theta$ angle between the BODIPY core and the *meso*-phenyl is roughly 45° in the ground state ($S_0$), *i.e.* before excitation. Following excitation (red arrow), the BODIPY fluorophore immediately enters the fluorescent

state at the local minimum ($S_{1,m}$), where the rotation angle $\theta$ remains almost the same. From there, the molecule can return to the $S_0$ state by fluorescing (blue arrow). However, the fluorophore can overcome a relatively small energy barrier ($E_a$), reach another minimum at 0° angle (labeled $S_{1,r}$). Following the movement, the BODIPY core loses planarity and becomes V-shaped [115,121]. Eventually, the molecule can quickly relax nonradiatively (pink arrow) to the ground state from $S_{1,r}$.

The rate of the transition from $S_{1,m}$ to $S_{1,r}$ is strongly dependent on viscosity [120]. As a result, if the transition rate is slow due to the high energy barrier, other relaxation pathways will take over, rendering the fluorophore viscosity-insensitive. Therefore, the activation energy barrier which the fluorophore must cross during non-radiative relaxation determines the viscosity sensitivity of BODIPY molecular rotors [115, 120]. Moreover, if the barrier is too high, a fluorophore remains in the fluorescent $S_{1,m}$ state, rendering the QY close to 100%, and making the probe insensitive to environmental properties.

Furthermore, $E_a$ may be extracted using the fluorescence lifetime and temperature dependence [100, 120]:

$$k_{nr}(\eta) \propto exp\left(-\frac{E_a}{k_b T}\right) \tag{1.9}$$

where $E_a$ is the activation energy barrier, $k_b$ – Boltzmann's constant and $T$ is a room temperature in kelvins. This formula can also help to evaluate the reduction in viscosity-dependent relaxation rate $k_{nr}$ caused by the higher barrier.

PES for new derivatives can be obtained by using theoretical models and calculations, such as density functional theory (DFT). It should be mentioned that DFT overestimates electronic transition energies in BODIPYs, which is a well-known issue. Even if the absolute energy values are incorrect, DFT gives accurate relative energies and enables comparison of different fluorophores [122–124].

### Sensitivity of the probe

Visually observed sensitivity trends can be also expressed in numerical values. For this, the sensitivity of the probes can be quantified using the relative sensitivity parameter $S$ (Equation 1.10) [125], which is defined as a lifetime change expressed as a percentage per parameter step:

$$S = -\frac{|\frac{\delta\tau}{\delta x}|}{\tau} \cdot 100\% \ , \tag{1.10}$$

where $\tau$ is a fluorescence lifetime, $\delta x$ is a change of the parameter (viscosity—$\delta\eta$, temperature— $\delta T$, polarity—$\delta\Delta f$). The higher the value, the more sensitive the fluorophore is to that specific environmental parameter.

In addition, the viscosity sensitivity of the probe can be calculated by utilising the Förster-Hoffmann equation [126]. This can be achieved by fitting fluorescence lifetime values:

$$\tau = C\eta^x, \tag{1.11}$$

where $\tau$ is fluorescence lifetime, $\eta$ - viscosity, $C$ and $x$ - constants.

After fitting, linear fits are represented with the constant $x$ which shows an approximate degree of sensitivity to viscosity. Similarly to Equation 1.10, the higher value means a better viscosity sensitivity.

# 2. EXPERIMENTAL METHODS

This chapter describes the measurement equipment and methods used to characterise researched compounds in this work.

## 2.1. Synthesis of compounds

The synthesis of the researched derivatives in publication [**P1**] was performed by Ekaterina M. Budynina and Yulia A. Volkova (Department of Chemistry, Molecular Sciences Research Hub, White City Campus, Imperial College London, UK).

Molecules explored in publications [**P2-P5**] were synthesised by Organic Chemistry Group led by prof. Sigitas Tumkevičius in Institute of Chemistry, Faculty of Chemistry and Geosciences, Vilnius University, Lithuania. Synthesis performed by dr. Jelena Dodonova-Vaitkūnienė with a help of Rokas Žvirblis (for [**P5**]).

The details of molecular synthesis and characterisations are presented in corresponding papers and their supporting information.

## 2.2. Preparation of samples

Stock solutions of all dyes used in [**P1-P5**] were prepared in toluene at the concentration of 0.2-2.5 mM and diluted for further experiments in a solvent or solvent mixtures of interest.

Cyclohexane, toluene, castor oil, chloroform, dichloromethane (DCM), 1,2-dichloroethane (DCE), diethyl ether, dimethyl sulfoxide (DMSO), glycerol, methanol, and tetrahydrofuran (THF) were spectroscopic grade and obtained from Sigma-Aldrich, except for glycerol used in [**P1**], which was obtained from Alfa-Aesar.

Quartz cuvettes (10 mm) were used for absorption, fluorescence, and QY measurements. The concentration of dyes used for the experiments at room temperature and for the temperature-dependent experiments was 2-14 µM.

The concentration of BP-Vinyl-$NO_2$ in cooled glycerol was 95 µM ([**P4**]). For the experiments in cryostat, the 0.5 mm quartz cuvette was used.

## 2.3. Calibration of viscosity sensors

The experiments conducted using a varying viscosity mixtures of toluene-castor oil (nonpolar mixtures) and methanol-glycerol (polar mixtures) were included in this work.

The viscosities of toluene-castor oil mixtures at different temperatures were measured using a vibro viscometer SV-10 (A&D) connected to a thermostat,

except for **[P1]**, where SVM 3000 viscometer (Anton Paar) was used. The viscosities of methanol-glycerol mixtures were obtained from previously measured data [100] and double-checked using the SV-10 (A&D) viscometer. Although castor oil is self-fluorescent (total contribution to fluorescence is only ≈1%), it is the only convenient option as a viscous solvent because of low polarity (dielectric constant is equal to 4.7) and ability to dissolve all new derivatives, which is not possible with glycerol.

The calibration curve (Figure 2.1) is created by measuring the fluorescence lifetime in various viscosity mixtures. A wide range of viscosities can be achieved by mixing similar polarity, but very different viscosity solvents. In this work two types of mixtures were used: toluene-castor oil (nonpolar) and methanol-glycerol (polar). Moreover, glycerol can be cooled in a cryostat to achieve even higher viscosity values. After measuring fluorescence lifetimes, they are plotted as the lifetime dependency on viscosity, and fitted with the theoretically-expected lifetime dependency Equation 2.1 [100]:

$$\tau = \frac{1}{k_{nr}(\eta, T) + k_f} \tag{2.1}$$

where $\tau$ is the fluorescence lifetime, $k_{nr}$ - non-radiative decay rate, $\eta$ - viscosity (in cP), $T$ - temperature (in K), $k_f$ - the radiative rate constant.

This calibration curve can later be used for assigning viscosity values from fluorescence lifetime.

More importantly, this calibration curve must be carried out for every fluorophore separately. Additionally, a similar calibration curve could be made for polarity and temperature determination. It could be achieved by measuring the probe in various polarity or temperature solvents and plotting in a similar fashion as Figure 2.1 (placing temperature or polarity in $x$ axis).

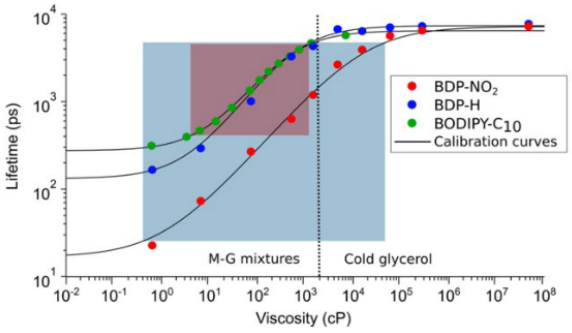


**Figure 2.1:** The principle scheme of calibration curve. Adapted with permission from Toliautas *et al.* [115]. Copyright 2019 John Wiley and Sons.

## 2.4. Absorbance. Steady-state and time-resolved fluorescence. Determination of the fluorescence quantum yield.

Absorption spectra were measured by using a Jasco V-670 spectrophotometer. Fluorescence steady-state and time-resolved measurements were conducted by using a setup of the Edinburgh-F900 (Edinburgh Instruments) fluorimeter and the WhiteLase Micro (Fianium) laser used as an excitation source. The laser was used together with bandpass filters (Thorlabs) with 10 nm bandwidth centred at 520 nm [**P1-P3**], 540 nm [**P1-P2**], 570 nm [**P2-P4**] and 630 nm [**P5**]. Previously reported BODIPY-$C_{10}$ was excited using 1 MHz frequency picosecond pulsed diode laser EPL-470 (Edinburgh Instruments) emitting at 473 nm. Fluorescence decays were measured using the TCSPC technique. Fluorescence decays had 5000 counts at the peak of the decay with 20 ns window being used with 4096 channels, except for BODIPY-$C_{10}$ where 50 ns window was used.

QY were obtained using a previously described comparative method and calculated using Equation 1.4. Table 2.1 shows standards used for determination of QY in this thesis.

**Table 2.1:** Fluorescence QY standards used in this thesis with the solvents used for dilution, their absorption maxima ($\lambda_A$) and fluorescence maxima ($\lambda_F$).

| **Standard and solvent** | **$\lambda_A$, nm $\lambda_F$, nm** | **QY** | **Compounds in comparison** | **Publications** |
|---|---|---|---|---|
| Rhodamine-101 in EtOH + 0.01% HCl [127] | 576 600 | 1 | BODIPY-$C_{10}$, BODIPY2, BODIPY3 | P1 |
| Rhodamine-101 in EtOH [128] | 564 587 | 0.91 | BP-PH, BP-PH-$CF_3$, BP-PH-OMe, BP-PH-m2M, BP-PH-m2M-$NO_2$, BP-Vinyl, BP-Vinyl-$NO_2$ | P2, P3, P4 |
| Rhodamine-6G in EtOH [128] | 530 558 | 0.94 | BP-PH-2M, BP-PH-2M, BP-PH-2M-$NO_2$, BP-PH-8M | P2, P3 |
| Fluorescein in 0.1 M $NaOH_{aq}$ [129] | 491 512 | 0.95 | BODIPY-$C_{10}$ | P2, P3 |
| Nile Blue in EtOH [130] | 636 702 | 0.27 | BP-$OC_{10}$ TP2, BP-$OC_{10}$ TP4, BP-$OC_{16}$ TP2, BP-$OC_{16}$ TP4 | P5 |

## 2.5. Preparation of LUVs

Thesis author prepared LUVs that were used for cellular imaging in the publication [**P2**]. Stock solutions of dipalmitoylphosphatidylcholine phospholipide

(DPPC) used for LUVs were purchased from Avanti Polar Lipids. Phosphate-buffered saline (PBS) buffer (pH 7.4) was prepared using a well-known protocol [131]. NaCl, KCl, $Na_2HPO_4$, and $KH_2PO_4$ had purity of $\geq 99\%$ and were purchased from Carl Roth. LUVs were prepared by the extrusion method. A 222 $\mu$l mixture of DPPC lipid and BP-PH-2M-$NO_2$ dye concentrate in chloroform was blow-dried using nitrogen. The dried solution was put in the desiccator and the remaining solvent evaporated under vacuum for 1 hour. After this, 2.4 ml PBS buffer was used for hydration of the dry lipid sample. The solution was vortexed and sonicated above the phase transition temperature (>41 °C). The solution was extruded 10 times through a polycarbonate membrane with a pore diameter of 0.1 µm using Avanti Polar Lipids Mini-Extruder. It was ensured that the process is carried out above the phase transition temperature.

LUVs that were studied in the publication [**P5**] were prepared in a similar fashion by Rokas Žvirblis (Vilnius University). First, a required amount of lipid concentrate was mixed with an aliquot of dye (400 $\mu$M in chloroform) at a 500:1 lipid to dye ratio, before using a stream of $N_2$ gas and vacuum (1 h) to remove the solvents and to produce a lipid film. For $L_d$ vesicles dioleoylphosphatidylcholine phospholipide (DOPC) was used, whereas $L_o$ membranes were formed from a 5:5:1 molar ratio mixture of DPPC, cholesterol and DOPC. Next, 2 ml of Milli-Q water (18.2 MΩ·cm) was used to hydrate the lipid layer, then the mixtures were vortexed and extruded 20 times through a polycarbonate membrane (pore size 0.1 $\mu$m) with the same mini-extrude. The hydration and extrusion was conducted above the fluid-gel transition temperature of all lipids in the mixture.

### 2.6. Theoretical calculations

Structural and optical properties of the investigated molecular rotors were modelled by performing quantum chemical computations based on DFT [132] for the ground state properties, as well as time-dependent density functional theory (TDDFT) [133] for the excited state properties.

For the first publication [**P1**], DFT calculations were performed by Bethan Cornell and Carla Molteni from Physics Department at King's College London, UK.

Stepas Toliautas from Institute of Chemical Physics, Faculty of Physics, Vilnius University, Lithuania conducted DFT calculations for publications [**P2-P3**].

The corresponding papers and their supplementary information contain the specifics of DFT calculations.

### 2.7. Cellular imaging

Experiments with live cells in **P1** were conducted by Aurimas Vyšniauskas, Markéta Kubánková, Maria Angeles Izquierdo, Thanh Truc Vu from Department of Chemistry, Molecular Sciences Research Hub, White City Campus, Imperial College London, UK.

Further experiments with living cells were performed by Džiugas Jurgutis at Biomedical Physics Laboratory, National Cancer Institute, Lithuania under supervision of Prof. Vitalijus Karabanovas ([**P2, P5**]. Experimental details are reported in corresponding publications.

### 2.8. Data analysis

Fluorescence decays were fitted using Edinburgh-F900 software package F900. Intensity-weighted lifetimes for biexponential fluorescence decays were calculated using Equation 2.2:

$$\bar{\tau} = \frac{\sum\limits_{i} a_i \tau_i^2}{\sum\limits_{i} a_i \tau_i} \tag{2.2}$$

where $a$ is an amplitude value and $\tau$ is the value of the lifetime. The goodness-of-fit parameter ($\chi^2$) was 1.5 or less for single decays.

Data processing of DFT calculations and FLIM images were performed by aforementioned experimenters and are reported in a methods section of corresponding publications.

# 3. TRANSFORMING THE VISCOSITY-SENSITIVE BODIPY MOLECULAR ROTOR INTO A TEMPERATURE SENSOR WITH CYCLOPROPYL SUBSTITUENTS

This chapter is based on the first publication [P1], in which the photophysical properties as well as the environmental sensitivity of $\alpha$- and $\beta$-cyclopropyl-substituted BODIPY-based derivatives were investigated.

## 3.1. Probe design

The earlier research demonstrated that extending the conjugation significantly alters the spectroscopic features of BODIPY-based environmentally sensitive fluorophores, such as BODIPY-$C_{10}$ (Figure 3.1). The parent BODIPY-$C_{10}$ emits green light with a maximum wavelength of 515 nm and exhibits great viscosity sensitivity, but no significant temperature sensitivity [92, 100]. Moreover, adding double and triple bonds to the $\alpha$ position of the fluorophore causes a noticeable red shift in emission. However, it also gives quantum yields that are close to 100% making these dyes unsuitable for environmental sensing because the competition between radiative and nonradiative rates disappear [134]. Nevertheless, adding naphthalene and phenanthrene substituents to the $\alpha$ positions led to the creation of a red-shifted BODIPY sensor that was sensing temperature of the environment and not its viscosity [102]. A cyclopropyl substituent was taken into consideration in the search for a more compact, less substantial moiety that would result in a temperature sensor that is more biocompatible. Despite only having single carbon-carbon bonds, cyclopropane is predicted to have characteristics somewhere between $sp^3$ and $sp^2$ hybridised carbon atoms [135, 136].

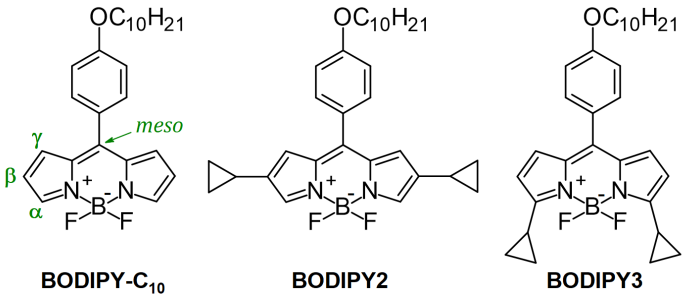


**Figure 3.1:** The chemical structures of the viscosity sensor BODIPY-$C_{10}$ and its $\beta$- (BODIPY2) and $\alpha$- (BODIPY3) cyclopropyl derivatives examined in this work. Green labels indicate the substituted position on the BODIPY core.

### 3.2. Spectroscopic properties

After adding cyclopropyl substituents to $\alpha$ and $\beta$ positions of BODIPY-$C_{10}$, the absorption and emission spectra are altered significantly (Figure 3.2A). To start, the wavelengths for both emission and absorption have a large bathochromic shift. $\alpha$-substituted derivative BODIPY3 showed a moderate shift (≈25 nm), while the $\beta$-substituted BODIPY2 had a more significant shift (≈60 nm). Second, both spectra of BODIPY2 are greatly widened, and the fluorophore has significantly larger Stokes shifts, 1200 $cm^{-1}$ instead of 300 $cm^{-1}$ in the case of BODIPY3 (Table 3.1). Finally, compared to the other two fluorophores, BODIPY2 exhibits a substantially stronger second absorption peak, which is located between 350-400 nm. For BODIPYs with styryl [137] and 2-thienyl [138] substituents in the $\beta$ position, larger Stokes shift and wider bands were also observed. Moreover, these results are supported by TDDFT calculations of absorption and emission spectra of all three fluorophores. The absorption and emission energies of BODIPY fluorophores are frequently overestimated using TDDFT methods, as is the case with these findings. However, the calculated spectra (Figure 3.2B) closely match the trend in maximum absorption and emission wavelengths exhibited in the experimental spectra.

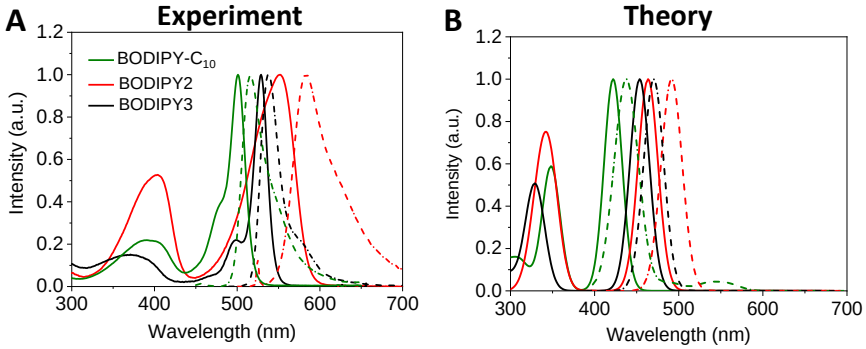


**Figure 3.2:** Spectra of BODIPY-$C_{10}$ (green), BODIPY2 (red), and BODIPY3 (black) in toluene, as measured experimentally (A) and theoretically (B). Solid lines represent the absorption spectra, whereas dashed-dotted lines represent the fluorescence spectra.

### 3.3. Temperature and viscosity sensitivity

Because BODIPY2 and BODIPY3 easily dissolve in a variety of organic solvents, it is possible to examine the sensitivity of their properties to temperature, polarity, and viscosity. By obtaining fluorescence spectra and time-resolved decays in toluene at temperatures ranging from 10 to 70 °C, the temperature dependence of BODIPY2 and BODIPY3 (Figure 3.3) was investigated.

The emission intensity was gradually reduced, while the shape of the emission band at rising temperatures remained constant Figure 3.3A, D). This shows that when temperature rises, non-radiative relaxation of both fluorophores accelerates. The similar result may be drawn from fluorescence decays, which demonstrate that fluorescence lifetimes become noticeably shorter as temperature rises (Figure 3.3B, E).

Following this, the viscosity-dependent properties of the novel probes were next investigated at room temperature in toluene-castor oil mixtures with a range of viscosities from 0.6 to 920 cP. This range of viscosities covers the predicted viscosities in the intracellular environment [139]. Figure 3.3C demonstrates that the fluorescence decays of BODIPY2 exhibit strong viscosity sensitivity, however not to the same extent as the primary fluorophore BODIPY-$C_{10}$. Changing solvents from non-viscous (toluene) to very viscous (castor oil) increased the lifetimes of BODIPY2 and BODIPY3 by 2.5 and 1.3 fold, respectively. These changes are moderate compared to BODIPY-$C_{10}$, where the lifetime increased fivefold. The viscosity sensitivity of BODIPY3 is much weaker than that of BODIPY2 and BODIPY-$C_{10}$ (Figure 3.3F). BODIPY3 can

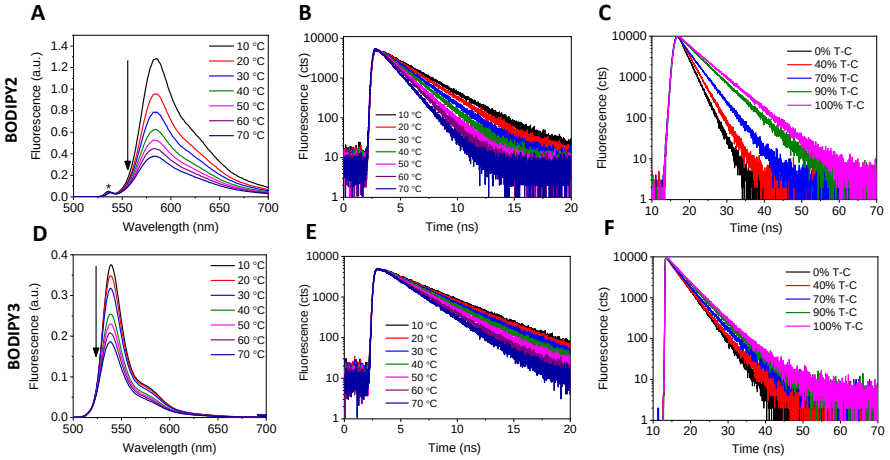


**Figure 3.3:** Sensitivity of BODIPY2 (top panels) and BODIPY3 (bottom panels) to temperature and viscosity. BODIPY2 temperature-dependent fluorescence spectra (A) and fluorescence decays (B) in toluene. C) Fluorescence decays of BODIPY2 in mixtures of toluene and castor oil with various viscosities. D) Temperature-dependent BODIPY3 fluorescence spectra. The excitation source gives rise to the peak denoted by an asterisk (*). The arrows in A) and D) demonstrate how fluorescence intensity decreases as temperature increases. E) BODIPY3 fluorescence decays in toluene at various temperatures. F) Fluorescence decays of BODIPY3 in mixtures of toluene and castor oil with various viscosities. The volume fraction of castor oil in the mixture, with viscosities ranging from 0.6 to 920 cP, is shown in the legends in C) and F).

potentially be utilised as a temperature sensor, at least in non-polar solvents, due to its relatively low sensitivity to viscosity. However, BODIPY2 could be utilised as a viscosity or temperature sensor, but only if one of these parameters is stable throughout the experiment.

Similar to the previously reported naphtyl-substituted BODIPY [102], BODIPY3 appears to have lost its viscosity sensitivity and switched to temperature sensitivity. Nonetheless, in comparison to naphthalene derivatives, the size and hydrophobicity of the fluorophore are decreased, whereas monoexponential fluorescence decay was conserved. This makes BODIPY3 an accurate lifetime-based temperature sensor that should work in biological conditions [140].

**Table 3.1:** Experimental values of the peak maxima of absorption ($\lambda_A$) and fluorescence emission ($\lambda_F$) spectra, Stokes shifts ($\tilde{\nu}_{SS}$), quantum yield (QY) and fluorescence lifetime ($\tau$) values of studied derivatives in cyclohexane (CHX), toluene (Tol.), ditheyl ether (Ether), chloroform ($CHCl_3$), dichloromethane (DCM), ethanol (EtOH), methanol (MeOH), acetonitrile (MeCN) and dimethyl sulfoxide (DMSO).

| | **BODIPY2** | | | | | **BODIPY3** | | | | |
|---|---|---|---|---|---|---|---|---|---|---|
| **Solvent** | $\lambda_A$, **nm** | $\lambda_F$ | $\tilde{\nu}_{SS}$, **cm**$^{-1}$ | **QY, %** | $\tau$, **ns** | $\lambda_A$, **nm** | $\lambda_F$ | $\tilde{\nu}_{SS}$, **cm**$^{-1}$ | **QY, %** | $\tau$, **ns** |
| **CHX** | 547 | 576 | 920 | 0.20 | 1.94 | 526 | 534 | 285 | 0.48 | 3.35 |
| **Tol.** | 552 | 585 | 1022 | 0.20 | 2.23 | 529 | 538 | 316 | 0.56 | 3.48 |
| **Ether** | 545 | 580 | 1107 | 0.16 | 1.7 | 523 | 532 | 324 | 0.43 | 3.14 |
| **$CHCl_3$** | 551 | 586 | 1084 | 0.23 | 2.62 | 529 | 538 | 316 | 0.61 | 3.84 |
| **DCM** | 550 | 584 | 1059 | 0.17 | 1.87 | 527 | 537 | 353 | 0.54 | 3.34 |
| **EtOH** | 546 | 582 | 1133 | 0.15 | 1.56 | 526 | 533 | 250 | 0.47 | 3.02 |
| **MeOH** | 545 | 583 | 1196 | 0.12 | 1.22 | 523 | 532 | 324 | 0.42 | 2.64 |
| **MeCN** | 548 | 585 | 1154 | 0.10 | 1.01 | 523 | 534 | 394 | 0.42 | 2.60 |
| **DMSO** | 555 | 593 | 1155 | 0.12 | 1.32 | 529 | 541 | 419 | 0.54 | 2.91 |

### 3.4. Polarity sensitivity

It has been demonstrated previously that BODIPY fluorophores having substituents in $\alpha$ and $\beta$ position are polarity-sensitive [102, 137, 138]. The impact of solvent polarity on these fluorophores at room temperature were investigated in order to get a full understanding of how different environmental conditions can affect the spectroscopic properties of BODIPY2 and BODIPY3 (Figure 3.4). Both derivatives exhibit minor solvatochromic shifts in fluorescence (Figure 3.4A, B) spectra in various solvents. The absorption and emission peaks in different solvents, Stokes shifts and quantum yields are listed in the Table 3.1. Polarity has little impact on the emission bands, but it has a greater effect on fluorescence decays. The SdP caused a decrease in the fluorescence lifetimes of BODIPY2 and BODIPY3 (Figure 3.4C). These findings show that the influence of polarity is substantial and cannot be disregarded, especially at higher polarities. The non-smooth trend of lifetime values suggests that, in

addition to solvent dipolarity, BODIPY2 and BODIPY3 are influenced by additional properties of the solvents examined. Chloroform (SdP = 0.6) stands out as the remarkable exception to the non-smooth trend, with high lifetime values obtained for both dyes.

Lastly, the effect of different polarity environments for the temperature sensitivity of BODIPY2 and BODIPY3 (Figure 3.4D, E) was examined. Toluene (a non-polar solvent) and methanol (a polar solvent) were selected as two representative solvents. The temperature sensitivity of both BODIPY dyes was similar (the gradients of all plots are roughly the same), while BODIPY3 exhibited higher lifetime values in both solvents, in contrast to BODIPY2. BODIPY2 had relative temperature sensitivities [141] of 0.84 %/°C in toluene and 1.0 %/°C in methanol. BODIPY3 showed sensitivities of 0.63 %/°C in toluene and 0.95 %/°C in methanol.

While the pattern of lifetime decrease with temperature (the gradient of the curve in Figures 3D and E) is comparable for all solvents, the lifetime values themselves differ significantly. Therefore, the sensors must be calibrated in the same polarity environment in order to perform the relevant temperature readings. On the other hand, if the temperature is maintained constant throughout the experiment, these molecules can also be utilised as polarity sensors.

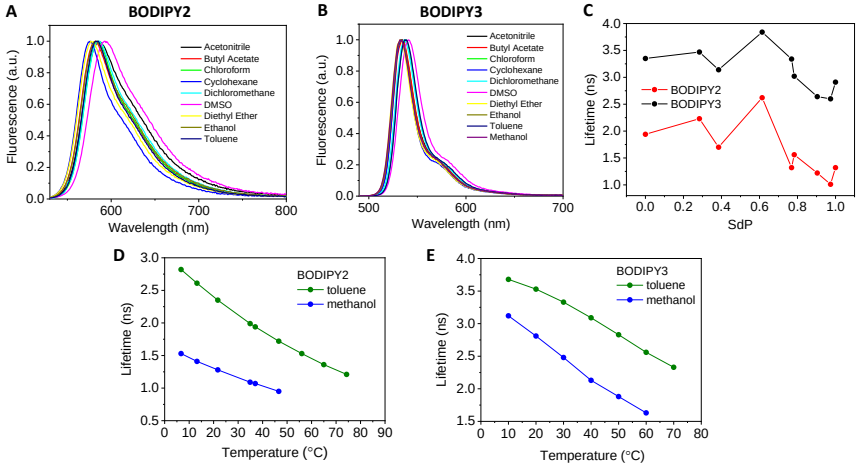


**Figure 3.4:** The impact of solvent polarity on the spectroscopic characteristics of BODIPY2 and BODIPY3. BODIPY2 (A) and BODIPY3 (B) fluorescence spectra in different solvents. C) Dependence of fluorescence lifetime on the SdP of the two fluorophores. BODIPY2 (D) and BODIPY3 (E) fluorescence lifetime dependency on temperature in a non-polar (toluene) and a polar (methanol) solvent.

### 3.5. Rationalisation of temperature-dependence of BODIPY2 and BODIPY3

To find out if cyclopropyl substituents influence the energy barrier for non-radiative relaxation, DFT and TDDFT calculations of BODIPY2, BODIPY3, and the primary viscosity-sensitive rotor BODIPY-$C_{10}$ were performed. Figure 3.5 illustrates the ground and first excited singlet state potential energy surfaces as a function of the dihedral angle between the BODIPY core and the phenyl ring. The three fluorophores have essentially identical energy curves in the ground state, while the differences appear in the first excited state. Figure 3.5B, where the curves are shifted to have a common energy minimum value, provides a detailed comparison of the $S_1$ energy barriers for the three fluorophores. It is evident that the addition of cyclopropanes significantly raises the $S_1$ energy barrier for the phenyl rotation, which is particularly evident for BODIPY3. Figure 3.5B displays the calculated values, that almost match the values obtained from experimentation. The larger steric repulsion of the cyclopropanes in the $\alpha$ position is most likely the cause of the higher barrier for BODIPY3, as the bending of the BODIPY core occurs simultaneously with the reduction of the dihedral angle [115, 117]. Previous research by Liu *et al.* on inserting methyl groups in the same place demonstrated a similar impact [120]. The measured energy barrier height for BODIPY-$C_{10}$ is in good agreement with prior theoretical findings [99] and the experimental value [100].

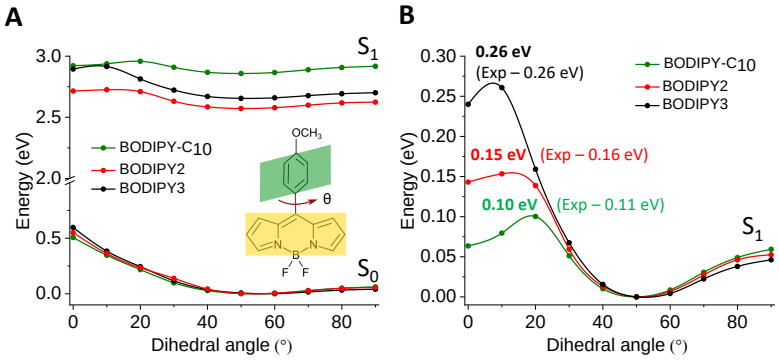


**Figure 3.5:** A) Calculated potential energy surfaces for the ground state in toluene ($S_0$), as well as the first excited state ($S_1$), with regard to the dihedral angle between the BODIPY core and the phenyl ring ($\theta$). The zero of the energy scale is the ground state minimum. B) Different barrier heights for the three fluorophores are shown on the potential energy surfaces of the $S_1$ state in toluene. Additionally, experimentally determined energy barrier values are displayed (for each BODIPY, in colour). $S_1$ surfaces have minima set at 0 eV. To speed up computation, the -$OCH_3$ group in fluorophores was shortened from the -$OC_{10}H_{21}$ group.

These theoretical findings indicate the following explanation for the significantly increased temperature sensitivity and decreased dependence on viscosity of the cyclopropane-BODIPYs. The large rise in $S_1$ barrier heights caused by cyclopropyl substituents must lead to the non-radiative relaxation (via rotation to torsional angle near to 0) to become much slower. Consequently, BODIPY2 and BODIPY3 have fluorescence lifetimes of a few ns even in a low viscosity environment, which is a tenfold increase compared to BODIPY-$C_{10}$. Therefore, a $S_1$ barrier for non-radiative relaxation greater than 0.10 eV causes a reduction in viscosity dependency but an increase in temperature sensitivity.

### 3.6. Cellular imaging

Although both novel fluorophores have successfully internalise into live cells, BODIPY3 showed significantly brighter cellular fluorescence compared to BODIPY2 under the same conditions. Therefore, only the FLIM images with BODIPY3 are analysed in this section.

According to fluorescence intensity images (Figure 3.6, top panel), BODIPY3 localises diffusely throughout the cytoplasm with some punctuated strong staining, most likely of hydrophobic organelles. The fluorophore is likely found in lipid membranes of organelles, such as lysosomes, and in lipid droplets because of its hydrophobicity and resemblance to the parent BODIPY-$C_{10}$.

To determine if the fluorophore is still temperature sensitive in the intracellular environment, FLIM imaging on U2OS live cells containing BODIPY3 at various temperatures was performed (Figure 3.6). The temperature in the live cell chamber was changed from 11 to 37 °C throughout the imaging process, which is within the range required for normal cell function. Images of fluorescence intensity (Figure 3.6, top panel) show that fluorescence intensity decreased as the temperature climbed. Additionally, FLIM images (Figure 3.6, middle panel) demonstrate that the lifetime of the probe inside cells remained temperature-sensitive, as shown by the lifetime histograms in Figure 3.6.

Particularly, BODIPY3 fluorescence decay remained monoexponential even in a complex intracellular environment, as it was published in the Publication [**P1**]. Compared to previously reported temperature probes, which exhibit multiexponential decay kinetics, this is a significant benefit [102,142,143]. Due to this characteristic, BODIPY3 is a more trustworthy probe since undesirable cell behaviour, such as aggregation, would manifest as additional exponential components. Furthermore, monoexponential decay traces can be fitted with a lot fewer counts, enabling much quicker data collection times [140].

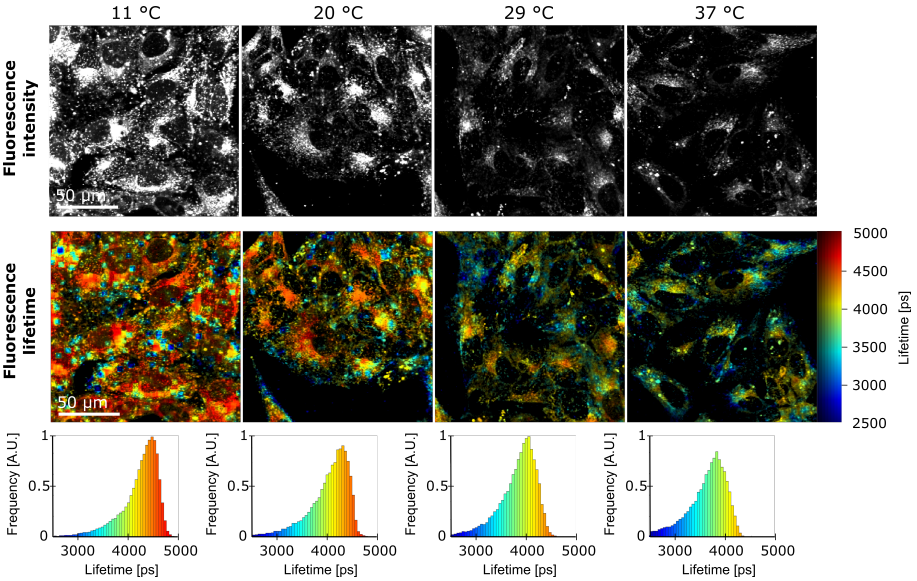


**Figure 3.6:** BODIPY3 fluorescence imaging in human osteosarcoma (bone cancer) cells (U2OS) at temperatures ranging from 11 to 37 °C. Fluorescence intensity images are displayed in the top panels; the intensity scale is consistent throughout the images. In the middle panels, FLIM images are displayed with a constant lifetime range of 2500-5000 ps. The bottom panels depict the corresponding lifetime distribution histograms.

## 3.7. Conclusions

It was demonstrated how to convert a fluorescent lifetime-based viscosity sensor into a temperature sensor by adding an uncommonly utilised substituent - a cyclopropyl group. BODIPY3 is a green fluorescent temperature sensor with $\alpha$-cyclopropyl substituents that can be used in non-polar solvents. It has weak fluorescence-lifetime sensitivity to viscosity and small solvathochromic shifts in fluorescence spectra with increasing polarity. Compared to its counterpart, the $\beta$-substituted BODIPY2, BODIPY3 showed longer lifetimes and comparable relative temperature sensitivities in temperature dependence experiments in solvents of different polarity. Interestingly, both derivatives should be calibrated for the same polarity environment to be used as temperature sensors. Nevertheless, they could be used as polarity sensors if the temperature is constant.

Furthermore, it was showed that BODIPY3 is capable of rapid internalisation into living cells and precise intracellular temperature sensing. The novel BODIPY fluorophore can be used for temperature sensing via FLIM because of its temperature-dependent fluorescence lifetimes. Furthermore, compared to previously reported temperature probes appropriate for lifetime sensing,

the fluorescence decays of the novel sensor was monoexponential. Theoretical calculations showed that cyclopropyl substitution leads to a higher energy barrier, which decreases the sensitivity to viscosity and increases the sensitivity to temperature. Therefore, BODIPY cyclopropyl-substituted probes have a temperature sensitivity that is due to the barrier height.

# 4. RED-EMITTING VISCOSITY SENSITIVE BODIPY FLUOROPHORE FOR INTRACELLULAR IMAGING OF LIPID DROPLETS

After concluding in the previous chapter that *meso*-phenyl-BODIPYs can be easily modified with moieties in $\alpha$ and $\beta$ position of the BODIPY core, it was decided to see whether it is possible to create a red fluorescent viscosity probe for intracellular imaging. Therefore, this chapter discusses the the results of the second publication **[P2]**, which focuses mainly on this goal.

## 4.1. Motivation and fluorophore design

To attain longer absorbance and fluorescence wavelengths than BODIPY-$C_{10}$, the conjugation of the molecular structure must be extended [144–146]. Because of the weak conjugation with the BODIPY core, it is known that changing the substituent in the *meso* position only slightly changes the absorption and emission spectrum. [147]. Furthermore, with one noteworthy exception [148], any substituent in the $\gamma$ position of the BODIPY core, next to the phenyl ring, eliminates viscosity sensitivity [120]. In contrast, introducing substituents into the $\alpha$ position is a more viable option, though methyl groups in the $\alpha$ position have been shown to decrease viscosity sensitivity [120]. As a result, the introduction of conjugated substituents into the $\beta$ position appears to be the best choice for redshifting the spectra of BODIPY-$C_{10}$ while maintaining viscosity sensitivity. In this research it was chosen to use phenyl groups (Figure 4.1).

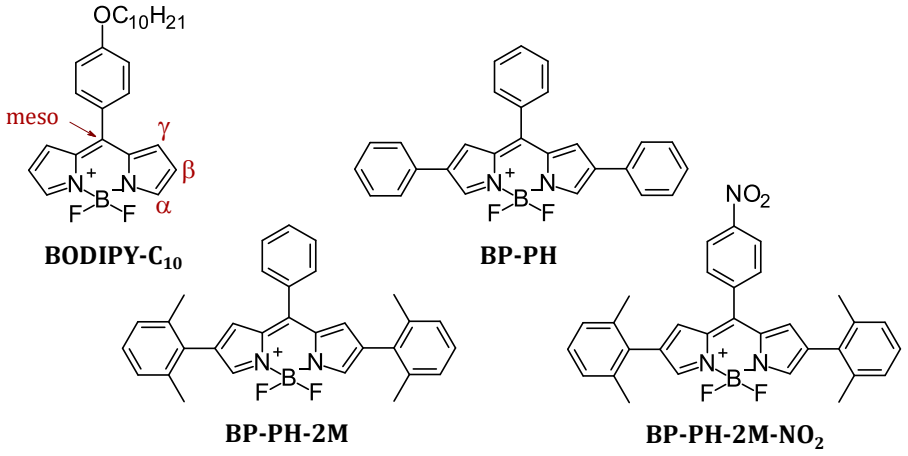


**Figure 4.1:** The structures of new fluorophores explored in this work together with the widely-used molecular rotor BODIPY-$C_{10}$. The substituted position of the BODIPY core is indicated by the red-colored notes.

### 4.2. DFT calculations

The quantum chemical calculations were conducted to predict the absorption, fluorescence wavelengths, and viscosity sensitivity of the proposed molecules (Figure 4.1) and to select the most viable molecules for synthesis. The PES (Figure 4.2A) and geometries of the new fluorophores (Figure 4.2B) are consistent to those of the previously studied *meso*-phenyl-BODIPYs [115–119].

According to the [Equation 1.9], adding only bare phenyl groups (BP-PH) raises the energy barrier by about 70 meV when compared to BODIPY-$C_{10}$. This should result in a 15-fold reduction in the viscosity-sensitive non-radiative

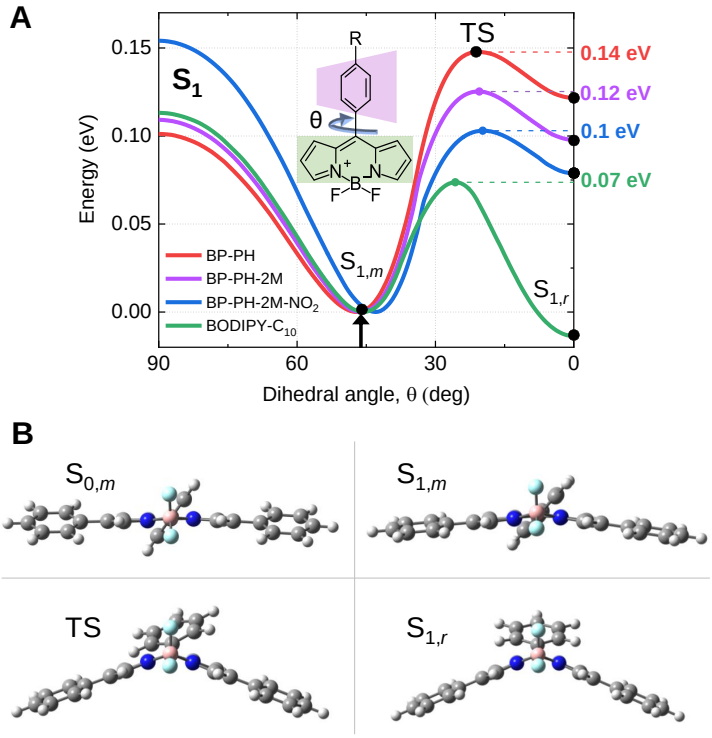


**Figure 4.2:** (A) PES curves of $S_1$ state of BP-PH (red), BP-PH-2M (purple), BP-PH-2M-$NO_2$ (blue), and BODIPY-$C_{10}$ (green) as determined by TDDFT. The dihedral angle $\theta$ between the BODIPY core and the *meso*-phenyl is shown on the X axis. Fluorescence occurs at the minimum denoted as $S_{1,m}$, whereas fast non-radiative relaxation occurs near the minimum $S_{1,r}$. For easier comparison, the energy of the local minimum $S_{1,m}$ at about 45° is set to 0 eV. On the right side of the graph, a value representing the energy barrier for each molecule is displayed. The black arrow shows the dihedral angle right after excitation. (B) Molecular structures of BP-PH at $S_{0,m}$, $S_{1,m}$ and $S_{1,r}$, transition state (TS) between the $S_{1,m}$ and $S_{1,r}$. BP-PH-2M and BP-PH-2M-$NO_2$ showed very similar geometries.

relaxation rate at room temperature. As a consequence, other relaxation pathways will dominate, making BP-PH barely sensitive to viscosity.

Two ways to address this issue were suggested. To begin, steric moieties (methyl groups) to the $\beta$-phenyls were attached, causing the phenyl rings to partly rotate out of the BODIPY plane. This may aid in achieving a compromise where the spectrum red shift is less pronounced but the molecules are more viscosity-sensitive. Second, a nitro group was attached, which has been shown in the past to lower the energy barrier [115]. The results of the quantum chemical calculations shown in Figure 4.2B indicate that the energy barrier is lowered by 0.02 eV when methyl groups are introduced, and by another 0.02 eV when nitro groups are added. One can anticipate that BP-PH-2M-$NO_2$ will be able to detect viscosity effectively and emit at a higher wavelength than BODIPY-$C_{10}$ because the final energy barrier for BP-PH-2M-$NO_2$ is 0.10 eV, which is not far off from the value for BODIPY-$C_{10}$.

### 4.3. Absorbance and fluorescence spectra

The BODIPY fluorophores shown in Figure 4.1 were synthesised to confirm DFT-based predictions. The absorption spectra of all dyes consist of the main absorption band, which is located at 450-630 nm, and the higher energy band, which is located at 300-400 nm, as shown in Figure 4.3A. The experimental spectra closely match the theoretically expected trends (Table 4.1). As expected, the main band of the previously unreported derivatives has 20–90 nm longer wavelengths than the well-researched BODIPY–$C_{10}$ spectrum. The absorption peak for BP-PH is at 590 nm, showing the greatest shift to longer wavelengths. Methyl groups attached in both *ortho* positions on the benzene rings (BP-PH-2M) shift the absorption maximum to 530 nm due to a reduction in conjugation because methyl groups prevent planarisation of the $\beta$-phenyls. The addition of the $NO_2$ group (BP-PH-2M-$NO_2$) results in an absorbance maximum at 545 nm. Previous BODIPY viscosity sensors without substituents in the $\beta$ positions showed a comparable outcome [115].

The fluorescence spectra exhibit similar red-shift trends as well (Figure 4.3B). Due to the increased conjugation, BP-PH exhibits the greatest bathochromic shift, with the fluorescence peak occurring at 630 nm. The steric hindrance causes the fluorescence bands of BP-PH-2M and BP-PH-2M-$NO_2$ to show at shorter wavelengths, with peaks at 585 nm and 620 nm, respectively. The Stokes shift for BP-PH and BP-PH-2M was 1076 $cm^{-1}$ and 1774 $cm^{-1}$, respectively, while it increased to 2220 $cm^{-1}$ for the derivative with a nitro group. Additionally, fluorescence quantum yields in toluene for all new derivatives were determined (Table 4.1). Moreover, the new derivatives with a higher energy barrier exhibit higher quantum yields because the molecule remains in the fluorescent state for a longer period of time before passing through the

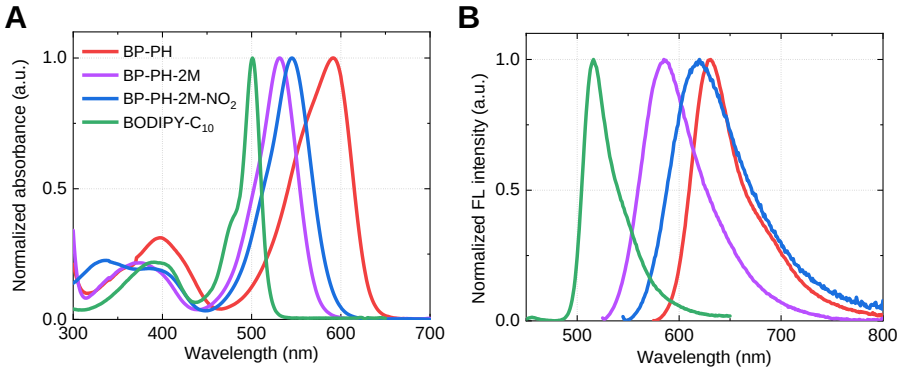


**Figure 4.3:** BP-PH (red), BP-PH-2M (purple), BP-PH-2M-$NO_2$ (blue), and BODIPY-$C_{10}$ (green) absorption (A) and fluorescence (B) spectra in toluene.

potential energy barrier (Figure 4.2A). Despite having a higher barrier, the novel fluorophore BP-PH-2M-$NO_2$ exhibits a lower fluorescence quantum yield than BODIPY-$C_{10}$. This could be because the new fluorophore has additional non-radiative relaxation pathways.

Furthermore, the tests in a variety of polarity solvents (cyclohexane, toluene, chloroform, DCM, DCE, DMSO, and methanol, from non-polar to very polar) were conducted and published in the Publication [**P2**]. When switching from the least polar to the most polar solvents, the compounds do not exhibit strong solvatochromism, resulting in a red-shift of 14, 16 and 19 nm for BP-PH, BP-PH-2M and BP-PH-2M-$NO_2$, respectively.

**Table 4.1:** Theoretical ($_t$) and experimental ($_e$) values of absorption ($\lambda_A$) and fluorescence emission maxima ($\lambda_F$), Stokes shifts ($\tilde{\nu}_{SS}$), fluorescence quantum yields (QY), and molar extinction coefficients ($\epsilon_e$) for BP-PH, BP-PH-2M, BP-PH-2M-$NO_2$, and BODIPY-$C_{10}$ in toluene.

| Derivative | $\lambda_{tA}$, nm | $\lambda_{tF}$, nm | $\lambda_{eA}$, nm | $\lambda_{eF}$, nm | $\tilde{\nu}_{eSS}$, $cm^{-1}$ | $QY_e$, % | $\epsilon_e$, $M^{-1} \cdot cm^{-1}$ |
|---|---|---|---|---|---|---|---|
| BP-PH | 485 | 535 | 590 | 630 | 1076 | 28 | $3.3 \cdot 10^4$ |
| BP-PH-2M | 451 | 511 | 530 | 585 | 1774 | 22 | $3.3 \cdot 10^4$ |
| BP-PH-2M-$NO_2$ | 463 | 544 | 545 | 620 | 2220 | 4 | $6.5 \cdot 10^4$ |
| BODIPY-$C_{10}$ | 423 | 443 | 500 | 515 | 583 | 12 | $6.4 \cdot 10^4$ |

### 4.4. Influence of viscosity

The hydrophobic nature of the novel BODIPY derivatives means that when used for live cell imaging, they are likely to localise in non-polar lipid bilayers. Due to this reason, non-polar toluene-castor oil mixtures were selected to test the viscosity sensitivity of the new fluorophores. Mixtures with viscosi-

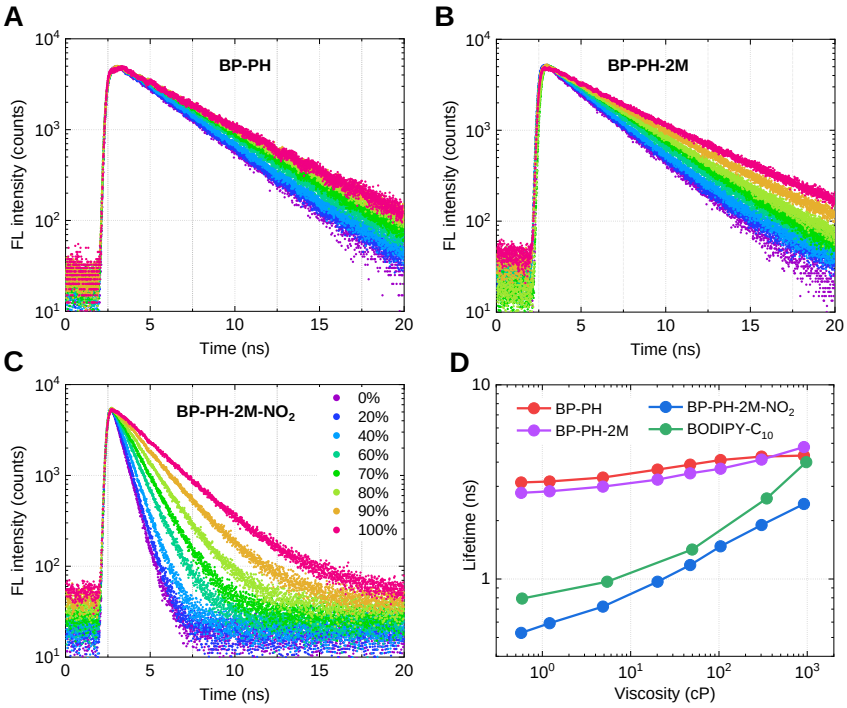


**Figure 4.4:** Fluorescence decays of BP-PH (A), BP-PH-2M (B), BP-PH-2M-$NO_2$ (C) obtained in toluene-castor oil mixtures. The volume fraction of castor oil in the mixture is indicated in the legend. (D) BP-PH (red), BP-PH-2M (purple), BP-PH-2M-$NO_2$ (blue), and BODIPY-$C_{10}$ (green) fluorescence lifetime dependence on viscosity in toluene-castor oil mixtures.

ties varying from 0.5 to 920 cP were used, ranging from pure toluene to pure castor oil. Although some of the decays were biexponential due to the small contribution from fluorescent castor oil, the majority of fluorescence decays in mixtures were monoexponential. The data in Figure 4.4A-C show fluorescence decays at increasing viscosity for all novel derivatives.

The fluorescence lifetime values are shown in Figure 4.4D. Intensity-weighted mean lifetimes for biexponential decays are calculated using Equation 2.2. The experimental findings closely match theoretical predictions; of all the new BODIPY fluorophores, BP-PH has the lowest viscosity sensitivity. The addition of methyl groups (Figure 4.4B) slightly improved viscosity sensitivity, but not to the extent needed for an applicable viscosity sensor. However, the addition of the nitro group led to a very strong viscosity sensitivity that is comparable to the sensitivity of the most used BODIPY molecular rotor BODIPY-$C_{10}$ (Figure 4.4D) because both molecules displayed similar $x$ values (0.21-0.22) for Förster-Hoffmann fits [1, 126]. Furthermore, the dynamic range of the probe increased from 1.4 to 4.6 for the molecules BP-PH and BP-

PH-2M-$NO_2$, respectively, as determined by the lifetime ratio at high and low viscosities (Equation 1.10).

Moreover, it was showed that the nitro-substitution is an effective strategy for improving the viscosity sensitivity of BODIPY viscosity probes as it has now been demonstrated to function with both BODIPYs: with and without $\beta$-phenyl substitutes [115].

This finding is significant for two reasons. First, a greatly extended absorption and emission wavelengths of BODIPY-$C_{10}$, bringing it very close to the visible red spectrum. Second, the trend in viscosity sensitivity of new BODIPY derivatives corresponds to the trend in energy barrier heights (Figure 4.2A). This supports the idea that the height of the energy barrier for non-radiative relaxation determines viscosity sensitivity. This information is essential for being able to predict the viscosity sensitivity of the suggested fluorophores using theoretical calculations.

Temperature and solvent polarity were also examined for their effect on fluorescence lifetime; supporting figures are published in the Publication [**P2**]. Fluorescence lifetimes in cyclohexane decreased with temperature, indicating low temperature sensitivity for all derivatives. The lifetimes for BP-PH and BP-PH-2M were similar as well. Fast non-radiative relaxation in a low viscosity solvent caused BP-PH-2M-$NO_2$ to exhibit much shorter lifetimes. When the polarity of the solvent was altered, a very comparable dependency was observed: lifetimes shorten with increasing polarity. Comparable lifetimes were seen for BP-PH and BP-PH-2M, while the derivative with -$NO_2$ group had shorter lifetimes and exhibited less polarity sensitivity. These findings lead to the conclusion that the addition of the nitro group significantly increased the viscosity sensitivity. This enhancement allows viscosity sensitivity to outweigh temperature and solvent polarity sensitivities.

### 4.5. Cellular imaging

According to the aforementioned findings, BP-PH-2M-$NO_2$ stands out among the new derivatives by exhibiting a strong viscosity sensitivity. This compound was chosen for live cell imaging using FLIM. LUVs with BP-PH-2M-$NO_2$ integrated into the lipid membrane were used to stain breast cancer cells (MCF-7).

After staining, the fluorescence image of the MCF-7 cells (Figure 4.5A) showed that BP-PH-2M-$NO_2$ had effectively internalised into the live cells. The red fluorescence inside MCF-7 cells displays a granular pattern, indicating that BP-PH-2M-$NO_2$ strongly stains spherical organelles. The captured FLIM image (Figure 4.5B) revealed monoexponential fluorescence decays with a mean lifetime of 1532 ps $\pm$74 ps (one standard deviation).

Using this lifetime and toluene-castor oil calibration (Figure 4.4D) enabled us to assign a dynamic viscosity of 123 cP. Similar viscosity values were reported

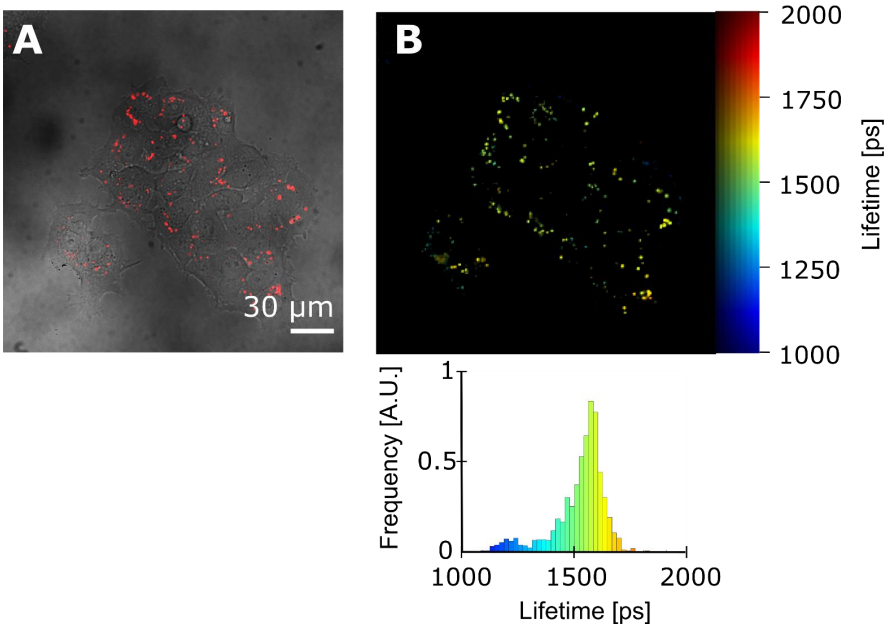


**Figure 4.5:** Live cells (MCF-7) stained with BP-PH-2M-$NO_2$. (A) A bright-field image placed over a BP-PH-2M-$NO_2$ fluorescence image demonstrates the staining of lipid droplets. (B) Image of FLIM with lifetime histogram at the bottom.

in other papers where live cell internal membranes and plasma were stained with BODIPY molecules [104,106,149]. Moreover, the spectral similarity along with monoexponential decays in toluene and live cells proves that the mixtures of toluene and castor oil are appropriate solvents for calibrating the BP-PH-2M-$NO_2$.

## 4.6. Conclusions

To summarize, this chapter described a successfully developed and synthesised red-emitting BODIPY viscosity probe BP-PH-2M-$NO_2$. DFT calculations were extremely helpful in the design of BP-PH-2M-$NO_2$ because they were used to determine the energy barrier height that inhibits viscosity-dependent non-radiative relaxation. The addition of methyl groups to $\beta$-phenylene resulted in lower $E_a$ and slightly improved viscosity sensitivity. Moreover, substitution with the nitro group in *meso*-phenyl position decreased $E_a$ even more and again enhanced the viscosity sensitivity of the probe. In comparison to the commonly used green viscosity probe BODIPY-$C_{10}$/$C_{12}$ and its variants, the new fluorophore emits at a noticeably longer wavelength and has a Stokes shift that is four times larger, while maintaining excellent sensitivity to viscosity. Additionally, the new probe detects viscosity in live MCF-7 cell lipid droplets

and exhibits a monoexponential fluorescence decay in a complicated intracellular environment. This property is highly valued because it allows for accurate viscosity sensing using the FLIM technique.

# 5. THE IMPACT OF ELECTRON-DONATING/-WITHDRAWING GROUPS IN RED-FLUORESCENT BODIPY MOLECULAR ROTORS

This chapter focuses on the modifications of the BP-PH derivative described in an earlier Chapter 4. Since BP-PH is red fluorescent, it was decided to further investigate how the addition of substituents with different electronic effects to $\beta$-phenyls can affect the properties of the fluorophore.

## 5.1. The design of probes and motivation

Substitutes having different electronic effects such as electron donation and withdrawal can affect the properties of the probe. In order to understand these effects, the study was carried out on the previously discussed red fluorescent derivative BP-PH. It was decided to test, how the addition of EDG and electron withdrawing groups (EWG) to $\beta$-phenyls impacts the photophysical properties of the probe. Moreover, the influence of steric moieties (methyl, in this case) on the BODIPY core and $\beta$-phenyls was also a case of interest. Therefore, three new derivatives were introduced: a trifluoromethyl-substituted (EWG) BP-PH-$CF_3$, a methoxy-substituted (EDG) BP-PH-OMe, and a methylated BP-PH-8M.

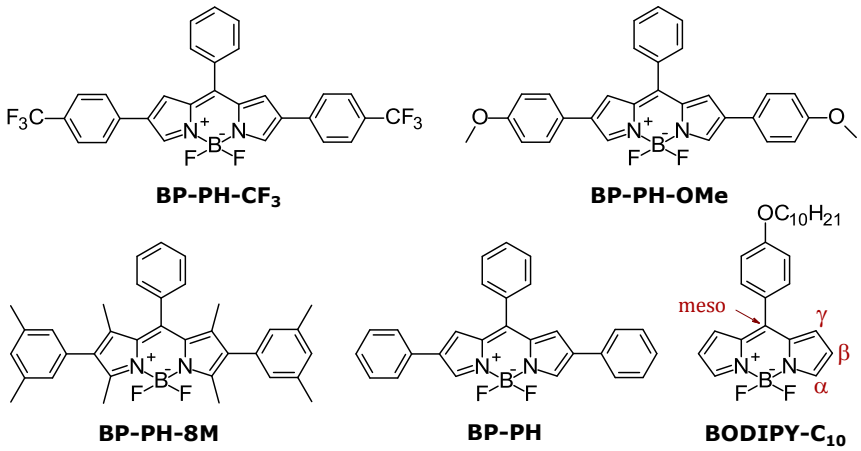


**Figure 5.1:** Molecular structures of derivatives studied in this work: BP-PH-$CF_3$, BP-PH-OMe, and BP-PH-8M, as well as previously discussed BP-PH and BODIPY-$C_{10}$.

### 5.2. Absorbance and fluorescence spectra

In order to better understand the fundamental spectroscopic characteristics of the novel fluorophores, they are contrasted with those of BP-PH and BODIPY-$C_{10}$. Absorbance spectra of all dyes exhibit a higher energy band at 300-450 nm and a main absorption band in the 500-630 nm region (Figure 5.2A). Due to the extension of conjugation, BP-PH exhibits a higher absorption wavelength ($\Delta\lambda$ = 90 nm) than the well-researched BODIPY-$C_{10}$ molecule. EWG in $\beta$-phenyls (BP-PH-$CF_3$) causes a slight blue-shift of the main absorption band in comparison to BP-PH ($\Delta\lambda$ = 15 nm). EDG has the opposite impact when attached to $\beta$-phenyls (BP-PH-OMe), resulting in the highest absorption wavelength of 625 nm. In contrast to previously reported BP-PH, the main absorption band of the new derivative BP-PH-8M is blue-shifted by 60 nm. The conjugation is restricted by the addition of the methyl group in $\beta$-phenyls and the BODIPY core, which causes the blue-shift in BP-PH-8M.

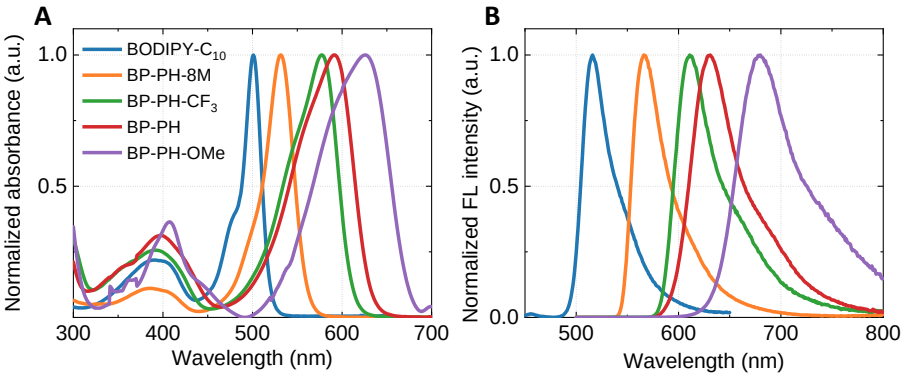


**Figure 5.2:** The absorption (**A**) and fluorescence (**B**) spectra of BODIPY-$C_{10}$ (blue), BP-PH-8M (orange), BP-PH-$CF_3$ (green), BP-PH (red), and BP-PH-OMe (purple).

The fluorescence spectra show very comparable blue- and red-shift tendencies (Figure 5.2B). The fluorescence peaks for BP-PH-8M and BP-PH-$CF_3$ correspond to shorter wavelengths and occur at 565 nm and 610 nm, respectively. As a result of the addition of EDG, BP-PH-OMe has the largest bathochromic shift and has a fluorescence maximum at 680 nm. Derivatives BP-PH-8M, BP-PH-$CF_3$, and BP-PH-OMe had a Stokes shift of 1169, 998, and 1294 $cm^{-1}$, respectively. The findings also demonstrate that EWG at $\beta$-phenyls reduces the Stokes shift, whereas EDG has the opposite effect. Consequently, it was possible to adjust the emission wavelengths of novel BODIPY fluorophores over a 500–700 nm range by altering the substituents on the $\beta$-phenyls. QY measurements in toluene also showed that, compared to previously reported BP-PH without $\beta$-phenyl substitutes [**P2**], attaching EWG to $\beta$-phenyls in-

creases the QY value by 29% (BP-PH-$CF_3$), while attaching EDG reduces it by 16% (BP-PH-OMe). Because of the restricted intramolecular rotation of $\beta$-phenyls, BP-PH-8M displayed the greatest QY of 87%. The values of the examined conjugates' absorption, fluorescence emission, Stokes shift, fluorescence lifetime, QY, and radiative and non-radiative relaxation rates are shown in Table 5.1.

## 5.3. Theoretical calculations

The increase in absorption and fluorescence wavelengths from BODIPY-$C_{10}$ to BP-PH-OMe is accurately predicted by the DFT calculations (Table 5.1). The geometry of BP-PH-8M demonstrates that the $\beta$-phenyls are forced out of plane by the methyl groups on the BODIPY core, which results in weaker conjugation and shorter absorption and fluorescence wavelengths (optimised structures are given in the Publication [**P3**]).

In order to compare the barriers for the novel BODIPY compounds to BODIPY-$C_{10}$ and BP-PH (Figure 5.3), the barriers for each of the new BODIPY compounds were estimated. The biggest barrier is found in BP-PH-8M, where additional methyl groups stop *meso*-phenyl from rotating. This explains why BP-PH-8M exhibits the highest fluorescence QY and the slowest non-radiative decay rate (Table 5.1). The remaining molecules have lower barriers, which causes the non-radiative relaxation to occur more quickly.

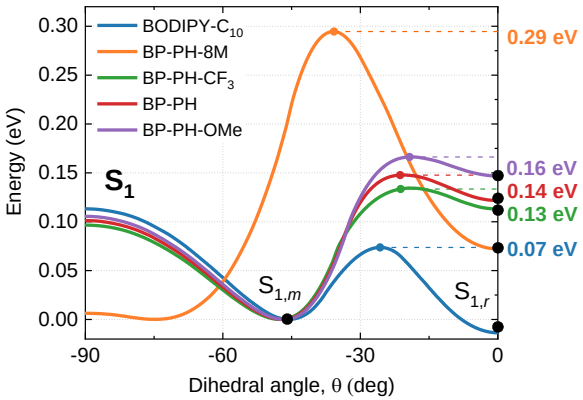


**Figure 5.3:** PES curves of $S_1$ state of BODIPY-$C_{10}$ (blue), BP-PH-8M (orange), BP-PH-$CF_3$ (green), BP-PH (red), and BP-PH-OMe (purple) determined using TDDFT. The BODIPY core and the *meso*-phenyl group have a dihedral angle of $\theta$. For simpler comparison, the $S_{1,m}$ minima of the curves were adjusted to 0.

### 5.4. Time-resolved fluorescence and sensitivity to viscosity, temperature and polarity

The investigation was followed by the evaluation of the viscosity, temperature, and polarity sensing properties of the novel compounds to test their potential as environmental probes. Measurements of viscosity sensitivity were conducted in non-polar toluene/castor oil mixtures with viscosities ranging from 0.5–920 cP. Most of the observed fluorescence decays were monoexponential. Due to the negligible contribution from the self-fluorescent castor oil, the average lifetimes of biexponential decays were determined using Equation (2.2). The viscosity-dependent fluorescence decays of BP-PH-$CF_3$ revealed a small viscosity dependency (Figure 5.4B) but essentially no viscosity dependence for BP-PH-8M or BP-PH-OMe (Figure 5.4A,C). In comparison to BODIPY-$C_{10}$ viscosity sensor, the newly developed derivatives consistently showed significantly reduced viscosity sensitivity (Figure 5.4D). It is no surprise, since the energy barriers for viscosity-sensitive non-radiative relaxation are higher than those for BODIPY-$C_{10}$, according to theoretical calculations. As a result, these findings are consistent with the theory, which states that a high energy barrier predicted by DFT calculations results in little to no viscosity sensitivity [115]. The previously discussed compound without extra moieties (BP-PH) and the conjugates BP-PH-8M and BP-PH-$CF_3$ displayed similar fluorescence lifetimes in the 3–5 ns range. In contrast, the lifetimes of BP-PH-OMe were only 1.5 ns.

All novel fluorophores displayed mild temperature dependence, according to temperature-dependent fluorescence decays measured in toluene (Figure 5.4E–G). Although the novel conjugates BP-PH-8M and BP-PH-$CF_3$ showed longer lifetimes, the extent of temperature dependency was comparable to BP-PH. The least sensitive to temperature was BP-PH-OMe; its modest lifetime values were comparable to the well-studied BODIPY-$C_{10}$, which had short lifetimes in the low viscosity solvent (toluene).

At last, experiments related to polarity dependency were carried out (Figure 5.4I–L). Among all the fluorophores, BP-PH-8M stood out because of the minimal sensitivity to solvent polarity (Figure 5.4I). The main structural distinction between BP-PH-8M and other fluorophores was the presence of methyl groups, which prevented the *meso*-phenyl group from rotating (Figure 5.1). As a result, it is likely that the rotation of the *meso*-phenyl substituent is involved in the non-radiative relaxation route that causes the polarity sensitivity. According to Sazanovich *et al.* [150], this specific intramolecular rotation is known to cause non-radiative relaxation of *meso*-phenyl-BODIPYs. Nonetheless, it leads to in viscosity-sensitivity [1], which BP-PH-OMe does not have. Therefore, the rotation of the *meso*-phenyl group may also be involved in another non-radiative relaxation process as well.

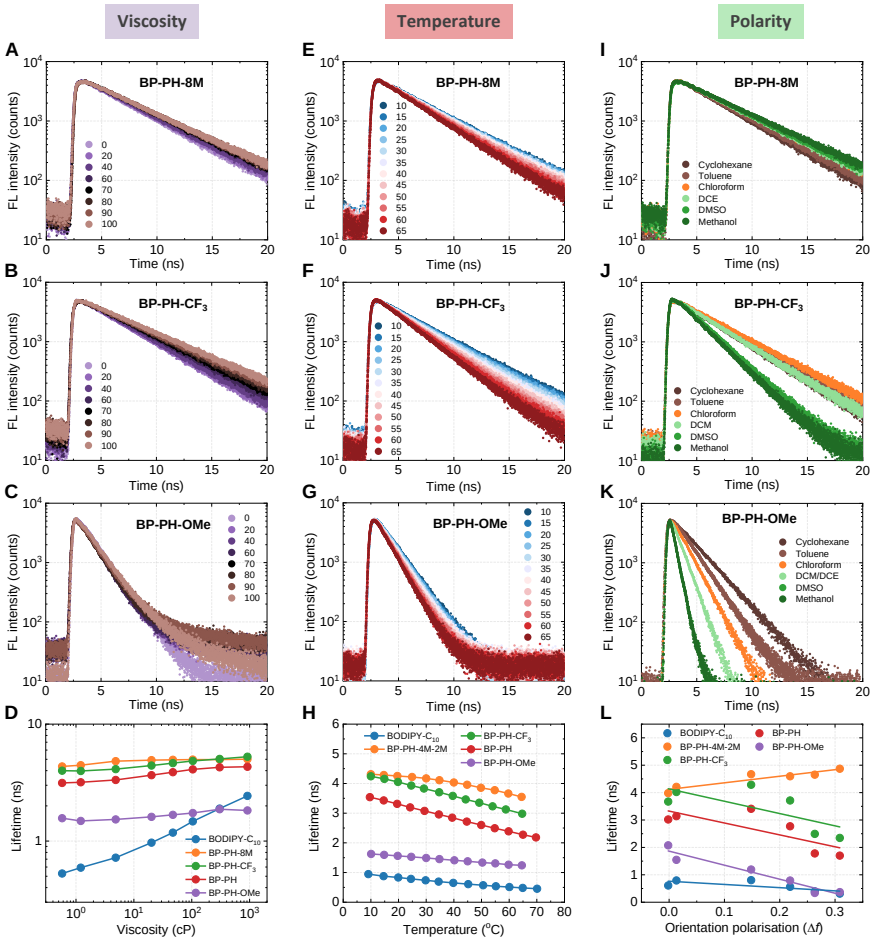


**Figure 5.4:** Fluorescence decays of BP-PH-8M, BP-PH-$CF_3$, BP-PH-OMe, and their sensitivity to viscosity, temperature, and polarity. (**A**–**D**) Viscosity dependence in toluene-castor oil mixtures. (**E**–**H**) Temperature dependence obtained in toluene. (**I**–**L**) Polarity dependence in different polarity solvents. The polarity of solvents is quantified using their orientational polarizability. The data for BP-PH and BODIPY-$C_{10}$ is provided for comparison in (**D**,**H**,**L**).

With the EWG replacement, BP-PH-$CF_3$ displayed considerable polarity-sensitive characteristics. The kinetics of trifluoromethyl-substituted BODIPY (Figure 5.4J) divided into two groups: one contained non-polar and medium-polar solvents (cyclohexane, toluene, chloroform, and DCM), and the other contained very polar solvents (DMSO and methanol). In contrast, EDG-substituted BP-PH-OMe displayed strong polarity dependency and steadily decreasing lifetimes with increasing solvent polarity (Figure 5.4K). This polarity dependence allows for the potential use of the methoxy-substituted con-

jugate as a red-emitting lifetime-based polarity sensor. The solvatochromic shift of BP-PH-OMe (Figure 5.5) was significantly smaller than the most commonly used fluorescent polarity sensors, including the Reichardt's dye [151]. Even so, if the FLIM approach is applied, the constant spectrum position of BP-PH-OMe (Figure 5.5) is advantageous. The spectral detection window can be appropriately set ahead of time without guessing, and the polarity can be determined from the fluorescence lifetime of BP-PH-OMe.

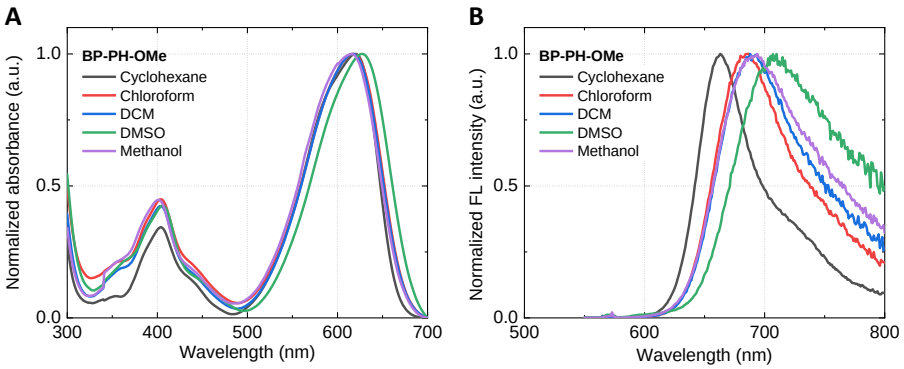


**Figure 5.5:** Absorption (**A**) and fluorescence (**B**) spectra of BP-PH-OMe in various polarity solvents. From non-polar to very polar: cyclohexane (dark grey), chloroform (red), DCM (blue), DMSO (green), and methanol (purple).

**Table 5.1:** Theoretically calculated and experimental values of the peak maxima of absorption ($\lambda_A$) and fluorescence emission ($\lambda_F$) spectra, Stokes shifts ($\tilde{\nu}_{SS}$) of studied molecules in toluene. Experimental values of fluorescence lifetime ($\tau$), quantum yield (QY), radiative ($k_r$), and non-radiative ($k_{nr}$) decay rates in toluene are also displayed.

| | Theoretical | | | Experiment | | | | | | |
|---|---|---|---|---|---|---|---|---|---|---|
| **Derivative** | $\lambda_A$, nm | $\lambda_F$, nm | $\tilde{\nu}_{SS}$, $cm^{-1}$ | $\lambda_A$, nm | $\lambda_F$, nm | $\tilde{\nu}_{SS}$, $cm^{-1}$ | $\tau$, ns | QY, % | $k_r$, $10^8 \times s^{-1}$ | $k_{nr}$, $10^8 \times s^{-1}$ |
| BODIPY-$C_{10}$ | 423 | 443 | 1094 | 500 | 515 | 583 | 0.8 | 12 | 1.5 | 11 |
| BP-PH-8M | 465 | 489 | 1087 | 530 | 565 | 1169 | 4.3 | 87 | 2 | 0.3 |
| BP-PH-$CF_3$ | 476 | 518 | 1703 | 575 | 610 | 998 | 4 | 57 | 1.5 | 1 |
| BP-PH | 485 | 535 | 1959 | 590 | 630 | 1076 | 3.1 | 28 | 0.9 | 2.3 |
| BP-PH-OMe | 510 | 576 | 2258 | 625 | 680 | 1294 | 1.6 | 12 | 0.8 | 5.5 |

Table 5.2 displays the estimated values of relative sensitivity $S$ to temperature and polarity, and $x$ values from the Förster-Hoffmann fits. Needless to say, the most sensitive viscosity sensor was the commonly used BODIPY-$C_{10}$ ($x = 0.21$). The remaining molecules barely showed any viscosity sensitivity ($\leq$0.05). All five conjugates displayed small-to-moderate temperature sensitivity, with lifetime changes per degree Celsius ranging from 0.3% to 1.0%.

Nevertheless, BP-PH-$CF_3$, BP-PH, and BP-PH-OMe exhibited a noteworthy sensitivity to polarity, with the latter having the highest polarity sensitivity (265%). As a result, these findings suggest that BODIPY compounds with $\beta$-phenyl substituents can be tailored to create new temperature and polarity sensors.

**Table 5.2:** The relative sensitivities to temperature, polarity, and values of Förster–Hoffmann constant $x$ showing the viscosity sensitivity of BODIPY-$C_{10}$, BP-PH-8M, BP-PH-$CF_3$, BP-PH, and BP-PH-OMe.

| **Derivative** | **[%/°C]** | **[%/Δf]** | $x$ |
|---|---|---|---|
| BODIPY-$C_{10}$ | 0.9 | 157 | 0.21 |
| BP-PH-8M | 0.3 | 72 | 0.02 |
| BP-PH-$CF_3$ | 0.5 | 116 | 0.04 |
| BP-PH | 0.6 | 141 | 0.05 |
| BP-PH-OMe | 0.4 | 265 | 0.03 |

## 5.5. Conclusions

To conclude, novel $\beta$-phenyl-substituted BODIPY fluorophores with red-shifted emission and absorption were developed. The sensitivity of the molecules to temperature, solvent polarity, and viscosity was investigated. While BP-PH-8M did not demonstrate any appreciable sensitivity, it was demonstrated that EWG-substituted BP-PH-$CF_3$ is a moderate temperature probe. Moreover, the unique combination of appealing qualities that EDG-substituted BP-PH-OMe possesses were showed. The fluorophore has little sensitivity to other parameters, exhibits monoexponential decay kinetics, is a sensitive lifetime-based polarity sensor that absorbs and emits in the red region of the visible spectrum.

# 6. RED-EMITTING MOLECULAR ROTOR FOR HIGH MICROVISCOSITY ENVIRONMENTS

As discussed in Chapter 4, BP-PH-2M-$NO_2$ has very attractive properties: viscosity sensitivity and red fluorescence. Additionally, it was proven that nitro-substitution is a great way to improve viscosity sensitivity. Further development of the probes shows, how the position of methyl groups on $\beta$-phenyls can impact the properties of the fluorophore. Moreover, phenyls in the $\beta$ position of the BODIPY core were swapped for vinyl group and gave appreciable results.

## 6.1. Motivation and probes design

In this investigation four novel BODIPY-based probes are compared with a previously discussed BP-PH-2M-$NO_2$. The new probes can be divided into two groups that have moieties in the $\beta$ position of the main BODIPY core to extend conjugation and create red-fluorescent probes. The first group is phenyl-substituted, and consists of BP-PH-m2M and BP-PH-m2M-$NO_2$, which are very similar to the derivatives presented in a Chapter 4 (BP-PH-2M, BP-PH-2M-$NO_2$), except that the methyl position on the $\beta$-phenyls was changed from *ortho* to *meta*. The second group - vinyl-substituted - consists of BP-Vinyl and BP-Vinyl-$NO_2$, where $\beta$-phenyls are changed to $\beta$-vinyls. As one can observe in a Figure 6.1, both groups consist of unsubstituted and nitro-substituted *meso*-phenyl because it is presumed that -$NO_2$ group should improve viscosity sensitivity [115].

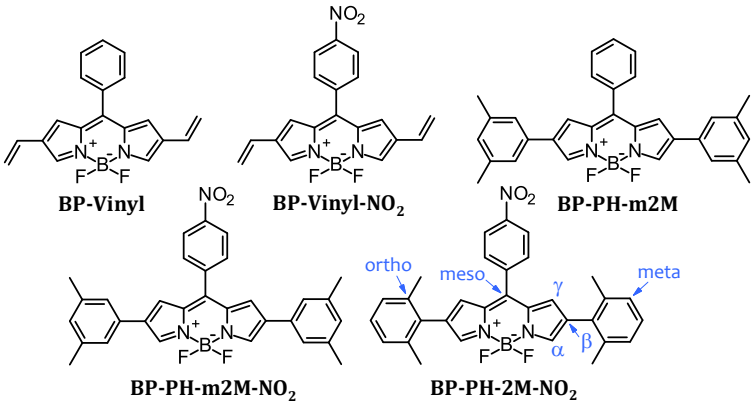


**Figure 6.1:** The molecular structures of conjugates examined in this work together with previously discussed BP-PH-2M-$NO_2$. The substituted position on the molecule is shown by the blue notes.

### 6.2. Synthesis of the derivatives

Synthetic routes of the designed molecules BP-Vinyl, BP-Vinyl-$NO_2$, BP-PH-m2M and BP-PH-m2M-$NO_2$ are outlined in Figure 6.2. Compounds BP1,2 [115] and BP3,4 [**P2**] were synthesized as previously reported in corresponding publications. BP-Vinyl and BP-Vinyl-$NO_2$ were synthesized by the Stille cross-coupling reaction using dibromo-BODIPY (BP3,4) and tri-*n*-butyl(vinyl)tin as starting compounds. Synthesis of BP-PH-m2M and BP-PH-m2M-$NO_2$ was carried out by the Suzuki-Miyaura cross-coupling reaction of BP3,4 and corresponding boronic acids in the present of $Pd_2dba_3$/SPhos catalytic system. The synthetic details, characterization data and spectroscopic analysis data of the synthesized compounds are presented in the Publication [**P4**].

***Reagents and conditions:*** i – NBS, $CH_2Cl_2$/DMF; ii - tri-*n*-butyl(vinyl)tin, $Pd(PPh_3)_4$, toluene, argon, 140 °C, 24h; iii – arylboronic acid, $Pd_2dba_3$, SPhos, $K_3PO_4$, toluene, argon, 140 °C, 24h.

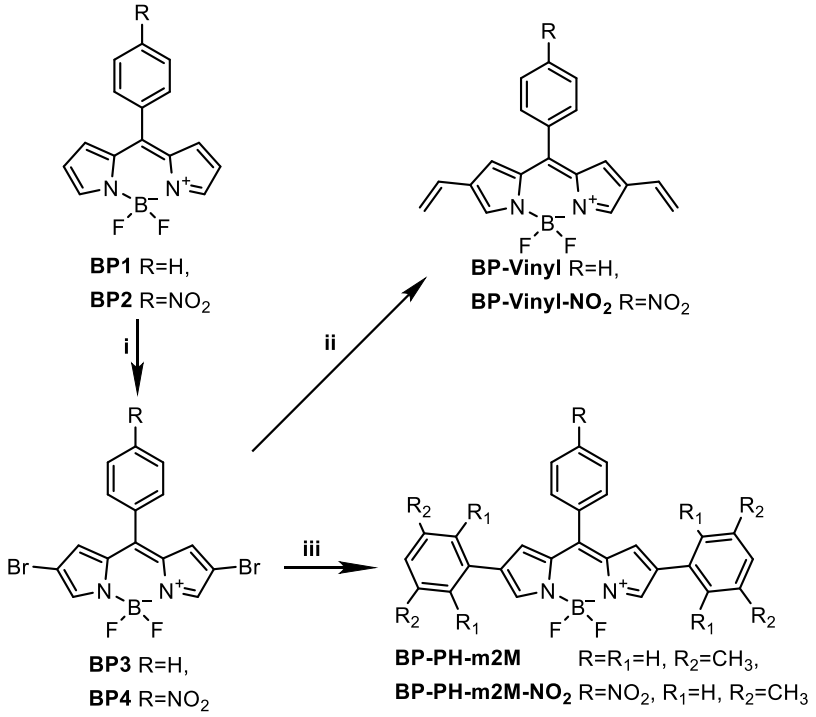


**Figure 6.2:** Synthesis of BP-Vinyl, BP-Vinyl-$NO_2$, BP-PH-m2M and BP-PH-m2M-$NO_2$.

### 6.3. Absorbance and fluorescence spectra

The absorbance and fluorescence spectra of the examined compounds in toluene are shown in Figure 6.3. The absorbance spectra (Figure 6.3A) are composed of a low intensity band in the 300-450 nm range and a main band in the 520-650 nm range. Contrary to a plain BODIPY, which absorbs and fluoresces in the range of 480-550 nm [104], the main absorbance and fluorescence peaks are red-shifted as a result of an increased conjugation length.

Study shows that adding a nitro group to *meso*-phenyl (BP-Vinyl-$NO_2$ and BP-PH-m2M-$NO_2$) increases the wavelengths of absorbance and fluorescence. The absorption peak of the vinyl- and phenyl-substituted conjugates shifted by 17 nm and 15 nm, respectively, when -$NO_2$ was added, while the bathochromic shifts in the fluorescence spectra were 30 nm and 37 nm, respectively. Additionally, the Stokes shift of both molecules was increased by the nitro group. Furthermore, by switching the methyl substituents from the *ortho* to *meta* positions on $\beta$-phenyls (BP-PH-2M-$NO_2$ and BP-PH-m2M-$NO_2$, respectively), the steric hindrance that prevents conjugation between the $\beta$-phenyls and the BODIPY core was reduced. This caused the fluorescence spectra to shift to the red region, from 620 to 679 nm. Table 6.1 provides the exact values for the absorbance, fluorescence maxima, and Stokes shifts. The fluorescence quantum yields of BP-Vinyl and BP-PH-m2M were 13% and 28%, respectively, which were lowered to 2% and 4% by adding of the nitro group. This decrease in values is a result of the nonradiative rate increasing when the nitro group is introduced.

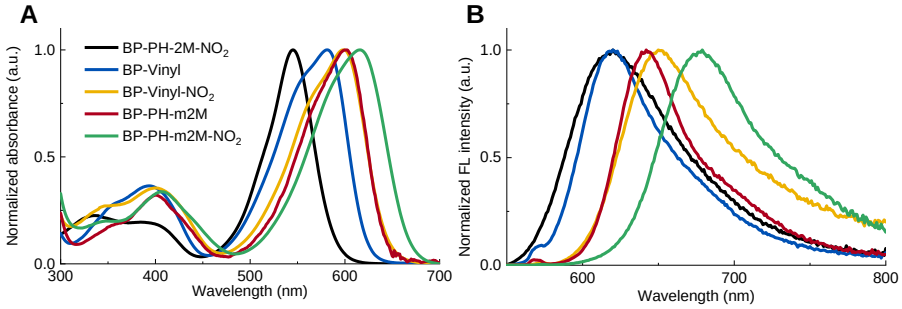


**Figure 6.3:** Absorption (A) and fluorescence (B) spectra of BP-PH-2M-$NO_2$ (black), BP-Vinyl (blue), BP-Vinyl-$NO_2$ (yellow), BP-PH-m2M (red), and BP-PH-m2M-$NO_2$ (green) in toluene.

### 6.4. Viscosity sensitivity

Fluorescence decays in non-polar toluene-castor oil mixtures of different viscosities (0.5-920 cP) were recorded to determine whether the novel derivatives are

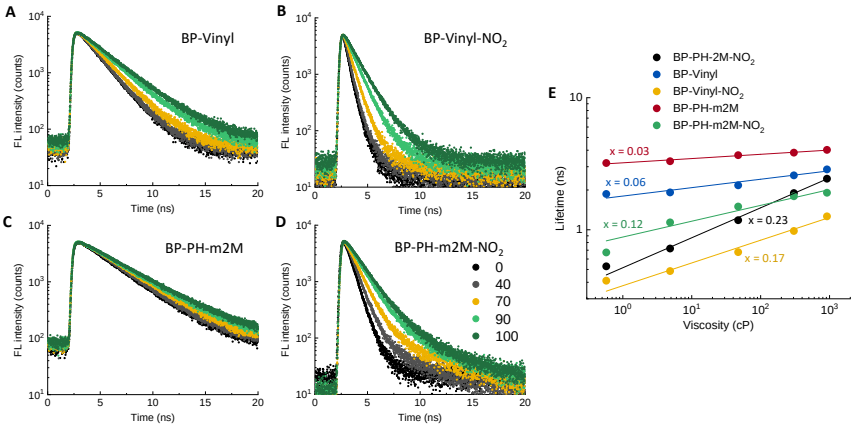


**Figure 6.4:** Fluorescence decays of BP-Vinyl (A), BP-Vinyl-$NO_2$ (B), BP-PH-m2M (C), and BP-PH-m2M-$NO_2$ (D) in toluene-castor oil mixtures. The fraction of castor oil in the solvent is indicated in the legend. (E) Fluorescence lifetime of BP-PH-2M-$NO_2$ (black), BP-Vinyl (blue), BP-Vinyl-$NO_2$ (yellow), BP-PH-m2M (red), and BP-PH-m2M-$NO_2$ (green) dependence on viscosity in non-polar toluene-castor oil mixtures. Fitted using Equation 1.11.

viscosity sensitive. Figure 6.4A-D displays the acquired fluorescence decays. While BP-Vinyl and BP-PH-m2M had monoexponential decays, their nitro-substituted counterparts mainly displayed biexponential decays as a result of the presence of self-fluorescent castor oil, which is apparent when a fluorophore has a shorter fluorescence lifetime. Equation (2.2) was used to calculate the mean fluorescence lifetimes of the biexponential decays. Figure 6.4E compares the lifetimes with the previously discussed BP-PH-2M-$NO_2$. Fluorescence lifetime values were fitted using the Förster-Hoffmann Equation 1.11 [126].

The results showed that BP-Vinyl and BP-PH-m2M exhibit weak sensitivity to viscosity as their lifetimes increase from toluene to viscous castor oil only by 50% (1.9 to 2.9 ns) and 25% (3.2 to 4.0 ns), respectively. Both

**Table 6.1:** Experimental values of absorption ($\lambda_A$), fluorescence emission maxima ($\lambda_F$), Stokes shifts ($\tilde{\nu}_{SS}$), fluorescence quantum yields (QY) and molar extinction coefficients ($\epsilon$) for BP-PH-2M-$NO_2$, BP-Vinyl, BP-Vinyl-$NO_2$, BP-PH-m2M and BP-PH-m2M-$NO_2$ in toluene.

| Derivative | $\lambda_A$, nm | $\lambda_F$, nm | $\tilde{\nu}_{SS}$, $cm^{-1}$ | QY, % | $\epsilon_e$, $M^{-1} \cdot cm^{-1}$ |
|---|---|---|---|---|---|
| BP-PH-2M-$NO_2$ | 545 | 620 | 2220 | 4 | $6.5 \cdot 10^4$ |
| BP-Vinyl | 581 | 620 | 1135 | 13 | $1.4 \cdot 10^4$ |
| BP-Vinyl-$NO_2$ | 598 | 650 | 1408 | 2 | $1.2 \cdot 10^4$ |
| BP-PH-m2M | 600 | 642 | 1139 | 28 | $4.4 \cdot 10^4$ |
| BP-PH-m2M-$NO_2$ | 615 | 679 | 1554 | 4 | $4.0 \cdot 10^4$ |

compounds revealed low $x$ values of 0.06 and 0.03 in Förster-Hoffmann fits, further demonstrating the minimal viscosity sensitivity. The introduction of the nitro group to *meso*-phenyl improved viscosity sensitivity characteristics of both conjugates: the fluorescence decays of BP-Vinyl-$NO_2$ and BP-PH-m2M-$NO_2$ are visually more distinguished (Figure 6.4B and D), with $x$ values of Förster-Hoffmann fits increasing by a factor of 3 and 4, respectively. If the unmodified Förster-Hoffmann equation is used for fitting, the lifetime change of the new vinyl-substituted derivative, which can absorb at longer wavelengths, is comparable to that of the previously discussed BP-PH-2M-$NO_2$ and the green fluorescent BODIPY-$C_{10}$ in toluene-castor oil mixtures [100].

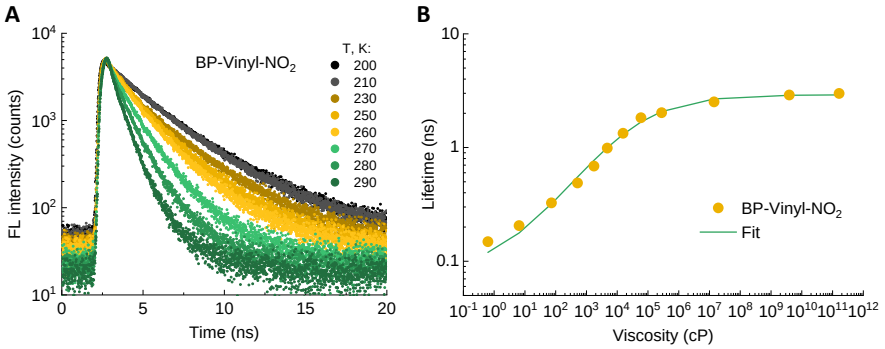


**Figure 6.5:** (A) Fluorescence decays of BP-Vinyl-$NO_2$ in glycerol at different temperatures. Temperature in kelvins in displayed in the legend. (B) Dependence of fluorescence lifetime on viscosity of BP-Vinyl-$NO_2$ in methanol-glycerol mixtures and cooled glycerol. The equation and parameters used for data fitting are published in the Publication **[P4]**.

According to the data presented in Figure 6.4E, the new viscosity probes may have viscosity sensitivity that goes above 1000 cP. Since glycerol has a glass transition temperature of 190 K and can be cooled to a range of viscosities between 1.7 and $1.6{\cdot}10^{11}$ cP, it was decided to test both nitro-substituted probes in this viscous solvent. In order to investigate the viscosity sensitivity, BP-Vinyl-$NO_2$ was dissolved and chilled to 200 K while BP-PH-m2M-$NO_2$ was not soluble in glycerol (Figure 6.5).

Cryostat experiments have demonstrated that BP-Vinyl-$NO_2$ fluorescence lifetime increases significantly at viscosities above 1000 cP and continues to rise up to $10^6$ cP. Furthermore, $\beta$-vinyls broadened the range of viscosity sensitivity by two orders of magnitude (from 0.5 - $5{\cdot}10^4$ cP to 0.5 - $1{\cdot}10^6$ cP) in comparison to earlier reported nitro-substituted BODIPY without moieties in $\beta$ position [115], significantly exceeding the viscosity range of the commonly used BODIPY-$C_{12}$ probe (5-1500 cP) [104]. It should be noted that only a small number of molecules are capable of sensing viscosity at such high viscosities [115, 152]. It is apparent that the maximum lifetime of BP-Vinyl-$NO_2$ is

approximately 3 ns rather than 21 ns as calculated from the radiative decay rate (acquired from fluorescence lifetime and QY) and from absorption spectra using the Strickler-Berg relation (Equation 1.8) [69]. This implies the existence of an extra non-radiative relaxation pathway that is independent of viscosity and temperature.

### 6.5. Polarity and temperature sensitivity

To evaluate the effect of solvent polarity for molecular rotors, the fluorescence lifetime of fluorophores in various solvents was evaluated (Equation 1.1). Fluorescence spectra of the derivatives did not exhibit strong solvatochromism, resulting in red-shifts of 15, 25, 22, and 29 nm for BP-Vinyl, BP-Vinyl-$NO_2$, BP-PH-m2M, and BP-PH-m2M-$NO_2$, respectively, with increasing solvent polarity. Figures supporting these results are published in Publication **[P4]**.

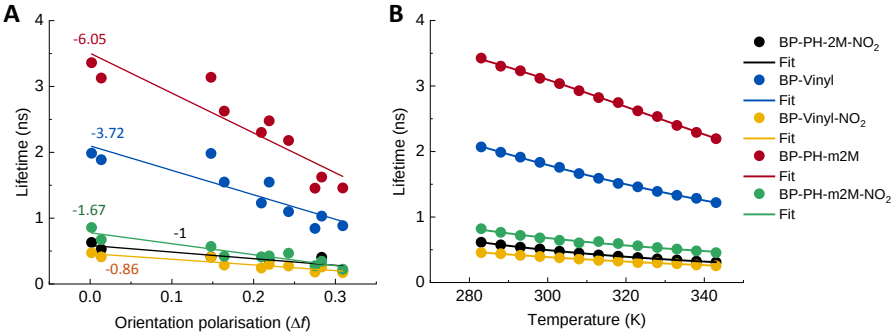


**Figure 6.6:** Fluorescence lifetimes of BP-PH-2M-$NO_2$ (black), BP-Vinyl (blue), BP-Vinyl-$NO_2$ (yellow), BP-PH-m2M (red), and BP-PH-m2M-$NO_2$ (green) obtained in the polarity-varying solvent (A) and in various temperatures in toluene (B). The slopes from the linear fits are shown together.

In addition, how solvent polarity affected the fluorescence lifetime were examined (Figure 6.6A). The measurements were conducted in cyclohexane, toluene, chloroform, diethyl ether, THF, DCM, cyclohexanone, N,N-dimethylformamide (DMF), DMSO, and methanol (listed from non-polar to very polar). The results demonstrate that BP-PH-m2M and BP-Vinyl exhibit substantial solvent polarity sensitivity. Each of nitro-substituted molecules revealed suppressed sensitivity to polarity, in addition to 2-3 times shorter lifetimes due to low viscosity of the solvents. BP-Vinyl-$NO_2$ showed a significantly lower polarity sensitivity than the previously created BP-PH-2M-$NO_2$.

Additionally, temperature-dependent analysis was carried out that allowed to assess the temperature sensitivity of the derivatives. Experiments were performed in toluene at temperatures ranging from 10 to 70 °C (Figure 6.6B). The viscosity of toluene barely changed from 0.65 to 0.3 cP at these tempera-

tures [153], which is insignificant impact on the fluorescence lifetime of the fluorophores alone. As a result, the direct temperature influence on fluorophores as the trend in lifetimes shown in Figure 6.6B. According to the results, BP-Vinyl and BP-PH-m2M display a modest sensitivity to temperature. The temperature sensitivity was reduced by adding the -$NO_2$ group, which is an improvement for a viscosity sensor. The nitro group increased the viscosity-dependent rate of non-radiative relaxation allowing viscosity sensitivity. Temperature has a negligible impact on fluorescence lifetime in low viscosity solvents since the viscosity-dependent relaxation rate is quick. The exact values of radiative and nonradiative rates are reported in the Publication **[P4]**.

## 6.6. Conclusions

In this study, novel $\beta$-substituted BODIPY probes containing phenyl and vinyl moieties were examined. It was demonstrated that the nitro group on a *meso*-phenyl of the BODIPY core is an effective approach for enhancing the probe's sensitivity to viscosity. The novel nitro-substituted compounds also showed red-spectral absorbance and fluorescence, lifetime-based sensitivity to microviscosity, minimal sensitivity to temperature, and solvent polarity. Furthermore, findings showed that BP-Vinyl-$NO_2$ has a remarkable viscosity-sensitive range of seven orders of magnitude. Even samples with extremely high viscosities, like cryopreserved tissues [154], might be appropriate for this probe. Moreover, it was showed that the elimination of steric hindrances causes the $\beta$-phenyl-substituted compound BP-PH-m2M-$NO_2$ to shift its fluorescence spectrum towards red while maintaining viscosity sensitivity. These findings could contribute to the creation of novel red-fluorescent lifetime-based microviscosity probes with a broad range of viscosity sensitivity.

# 7. A RED-EMITTING THIOPHENE-MODIFIED BODIPY PROBE FOR FLUORESCENCE LIFETIME-BASED POLARITY IMAGING OF LIPID DROPLETS IN LIVING CELLS

The final chapter is based on publication [**P5**] and explores how BODIPYs can be transformed into a polarity sensors that can be applied for cellular imaging. EDGs, when used as substitutes in BODIPY derivatives, enables creation of polarity-sensitive probes, as discussed in a Chapter 5. Therefore, the last explored derivatives are substituted with a thiophene group, which is an excellent electron donor.

## 7.1. Motivation and probe design

In this investigation, four BODIPY-based conjugates, modified with 2-thienyl substitutes, resulting in $\beta$,$\beta$'-disubstituted and $\alpha$,$\alpha$',$\beta$,$\beta$'-tetrasubstituted probes are reported (Figure 7.1). This specific aromatic group was chosen because, as previously described in Chapter 5, it has electron-donating properties that can be associated with improved polarity sensitivity of the BODIPY probes. Additionally, it has been shown that the introduction of thienyl groups with a high electron density causes a significant red-shift, which is necessary for producing red emission [138, 155]. In order to ensure an effective fit of probes into the lipid layer, long alkoxy chains (-$C_{10}H_{21}$ and -$C_{16}H_{33}$) were also introduced at the *para*- position of the *meso*-phenyl ring.

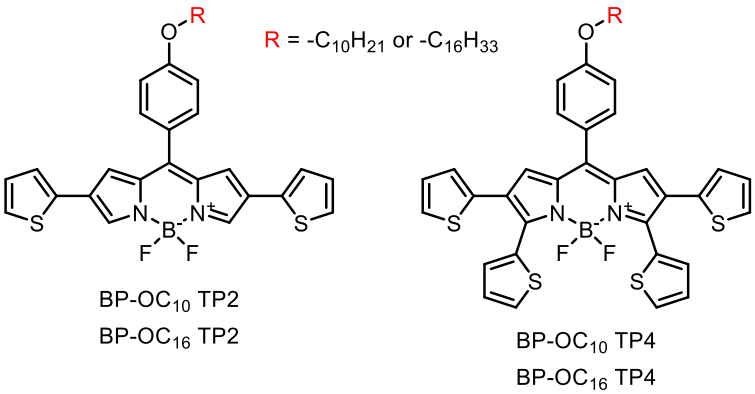


**Figure 7.1:** Molecular structures of thiophene-substituted BODIPY derivatives explored in this section. The substituted position of the BODIPY core is indicated by the red-colored notes. Reproduced from [156] with permission from the Royal Society of Chemistry.

### 7.2. Absorbance and fluorescence spectra

All dyes in toluene had a higher energy band at 300-500 nm and a main absorption band at 620-640 nm (Figure 7.2A)). Tetrasubstituted (TP4) probes displayed a longer absorption wavelength ($\Delta\lambda$ = 10 nm) than disubstituted (TP2) probes, which can be attributed to the two extra groups at the $\alpha$,$\alpha$'-positions that further extended the conjugation.

Similar to that, tetrasubstituted dyes exhibited a red shift ($\lambda_{max}$ = 682 nm) when compared to disubstituted dyes ($\lambda_{max}$ = 671 nm, Figure 7.2B). The position of the absorbance and fluorescence bands was unaffected by the length of the alkoxy chain at the *meso*-phenyl ring. Overall, compared to the unaltered green emitting BODIPY-$C_{10}$ ($\lambda_{max}$ = 515nm) [104], the new probes exhibit a notable change in the spectra. The Stokes shift for TP2 dyes was 1071 $cm^{-1}$, however for BP-$OC_{10}$ TP4 and BP-$OC_{16}$ TP4 it was 1061 $cm^{-1}$ and 1085 $cm^{-1}$, respectively.

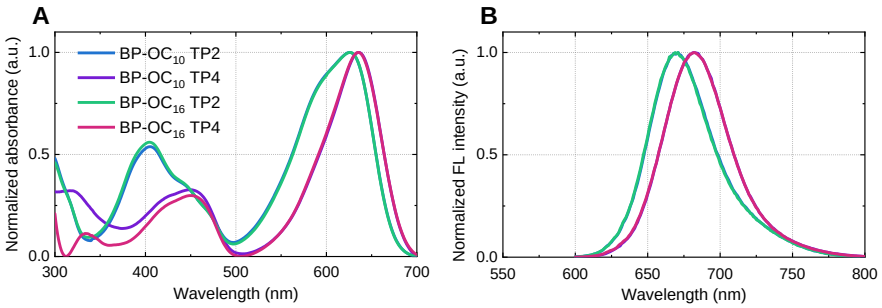


**Figure 7.2:** Absorption (A) and fluorescence (B) spectra of BP-$OC_{10}$ TP2 (blue), BP-$OC_{10}$ TP4 (purple), BP-$OC_{16}$ TP2 (green) and BP-$OC_{16}$ TP4 (magenta) obtained in toluene. The fluorescence spectra of TP2- and TP4-substituted molecules are superimposed. Reproduced from [156] with permission from the Royal Society of Chemistry.

All dyes exhibited modest solvatochromism in normalised absorbance and fluorescence spectra obtained in solvents of varying polarity (from apolar to the most polar: cyclohexane, toluene, chloroform, THF, DMSO, and methanol). The supporting results are presented in Publication [**P5**]. The largest difference among the peaks of the fluorescence spectra was found between cyclohexane and DMSO. The resulting red-shifts for BP-$OC_{10}$ TP2, BP-$OC_{16}$ TP2, BP-$OC_{10}$ TP4 and BP-$OC_{16}$ TP4 were 32, 33, 21, and 23 nm, respectively, indicating that disubstituted probes are more solvatochromic. However, polarity had a smaller impact on absorbance spectra, with the most significant difference between absorbance maxima being only 11–12 nm.

In addition, the fluorescence spectra in non-viscous toluene ($\eta$ = 0.6 cP, $n$ = 1.497, $\epsilon$ = 2.385, $\Delta f$ = 0.0137) and viscous castor oil ($\eta$ = 920 cP,

$n = 1.475$, $\epsilon = 4.478$, $\Delta f = 0.1296$) were examined. Increased viscosity was found to have a negligible effect, shifting spectra slightly to the blue without changing their shape. Similarly, an increase in temperature caused a blue shift in the spectra but had no effect on their shape. The figures containing these results are published in Publication [**P5**].

Moreover, QY measurements were performed in toluene for all compounds. An evaluation of the QY values of di- and tetrasubstituted dyes shows that the QY value increases by around 10% when additional 2-thienyl groups are attached to the BODIPY in $\alpha$,$\alpha$'-positions. QY values are unaffected by the length of the alkoxy chain at the *meso*-phenyl ring. QY values and other spectroscopic characteristics of thiophene-substituted BODIPY derivatives are listed in Table 7.1.

**Table 7.1:** Experimental values of absorption ($\lambda_A$), fluorescence emission maxima ($\lambda_F$), Stokes shifts ($\tilde{\nu}_{SS}$), fluorescence quantum yields (QY), radiative ($k_r$), and non-radiative ($k_{nr}$) decay rates, molar extinction coefficients ($\epsilon_c$) and the relative sensitivites to temperature ($S$) of BP-$OC_{10}$ TP2, BP-$OC_{16}$ TP2, BP-$OC_{10}$ TP4 and BP-$OC_{16}$ TP4 in toluene.

| Derivative | $\lambda_A$, nm | $\lambda_F$, nm | $\tilde{\nu}_{SS}$, $cm^{-1}$ | QY, % | $k_r$, $10^8 \times s^{-1}$ | $k_{nr}$, $10^8 \times s^{-1}$ | $\epsilon_c$, $M^{-1}{\cdot}cm^{-1}$ | $S$, %/°C |
|---|---|---|---|---|---|---|---|---|
| BP-$OC_{10}$ TP2 | 626 | 671 | 1071 | 12 | 0.7 | 5.2 | $4.44 \cdot 10^4$ | 0.4 |
| BP-$OC_{16}$ TP2 | 626 | 671 | 1071 | 13 | 0.8 | 5.2 | $4.38 \cdot 10^4$ | 0.4 |
| BP-$OC_{10}$ TP4 | 636 | 682 | 1061 | 23 | 0.8 | 2.7 | $2.56 \cdot 10^4$ | 0.2 |
| BP-$OC_{16}$ TP4 | 635 | 682 | 1085 | 23 | 0.8 | 2.7 | $3.75 \cdot 10^4$ | 0.2 |

## 7.3. Sensitivity of the fluorescence decay to polarity, viscosity and temperature

To evaluate the photophysical characteristics of new thiophene-modified BODIPY derivatives, their sensitivity to solvent polarity as well as the effect of viscosity and temperature were investigated. Figure 7.3 shows results for -$OC_{16}$ dyes, while -$OC_{10}$ derivatives are discussed in Publication [**P5**].

All probes had monoexponential decays that were polarity-dependent, and they all had longer fluorescence lifetimes in low polarity solvents, according to polarity sensitivity studies carried out in various solvents (Figure 7.3A-B). Additional figures are demonstrated in Publication [**P5**].

The two disubstituted derivatives displayed fluorescence lifetimes between 0.42 and 2.55 ns, whereas tetrasubstituted dyes exhibited a wider range of fluorescence lifetimes between 0.67 and 4.09 ns. This indicates that the dynamic range of polarity sensitivity increases with additional electron-donating 2-thienyl groups. It has been shown that this effect can be produced by adding EDG, as discussed in the Chapter 5. Additionally, Table 7.1 findings show

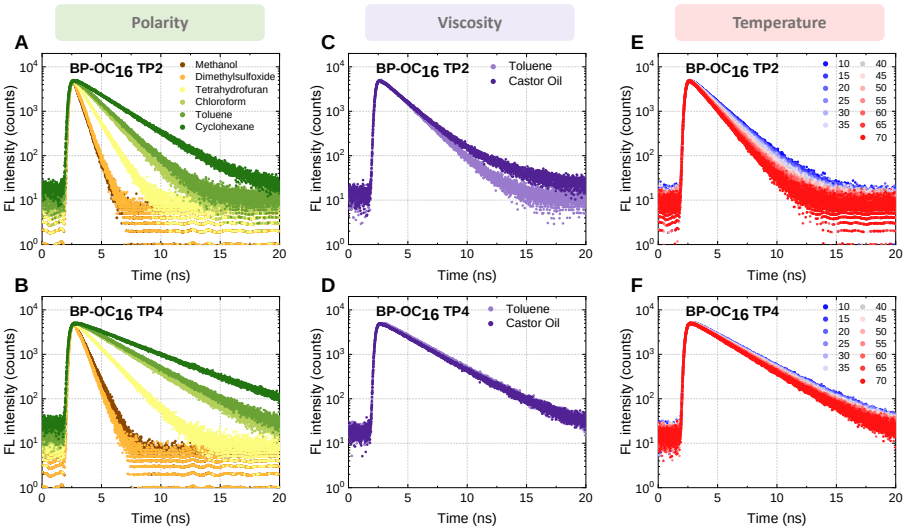


**Figure 7.3:** The fluorescence decays of BP-$OC_{16}$ TP2 (top graphs) and BP-$OC_{16}$ TP4 (bottom graphs), and polarity, viscosity, and temperature sensitivity. Polarity dependence in solvents of various polarity (A-B). Solvent polarity is quantified using their orientational polarisability. Viscosity dependence obtained in nonpolar toluene and castor oil (C-D). Measurements of temperature dependency in toluene, 10 to 70 °C (E-F). Reproduced from [156] with permission from the Royal Society of Chemistry.

that $k_{nr}$ is considerably faster than $k_r$. According to the Strickler-Berg relation (Equation 1.8), none of the thiophene-substituted derivatives in this investigation should show significant changes in $k_r$ because all of the molecules show very minor solvatochromism [69]. Since $k_{nr}$ is 3 to 6 times faster than $k_r$, the former determines most of the fluorescence lifetime. Thus, the polarity sensitivity of the probes is caused by changes in $k_{nr}$ in environments with different polarity.

As mentioned before, BODIPY probes may exhibit sensitivity to a variety of environmental factors, which could influence their readings. Therefore, viscosity and temperature dependence measurements were performed.

Viscosity sensitivity experiments, due to the the strong hydrophobicity of the dyes were performed in non-polar toluene and castor oil mixtures (Figure 7.3C-D). The results showed that all of the probes have a minor dependence on viscosity, which indicates that this environmental parameter has no effect on relaxation pathways of the probes. Although fluorescence decays of TP2 dyes appear to have a modest dependence on viscosity (Figure 7.3C), this is an artefact that can be attributed to the autofluorescence of the castor oil. After subtracting the fluorescence from pure castor oil, which was measured independently under identical experimental conditions, the corrected decay in

castor oil completely overlaps the one in toluene, demonstrating that the TP2 dyes are viscosity independent.

Finally, temperature-dependent fluorescence decays observed in toluene showed a weak temperature sensitivity for all dyes (Figure 7.3E-F). TP2 dyes exhibit lower lifetimes than TP4 fluorophores in the temperature range of 10-70 °C. Furthermore, the temperature sensitivity of the probes was quantified using the relative sensitivity parameter $S$ (Equation 1.10).

The temperature sensitivity of TP2 dyes (0.4%) was twice as high as that of TP4 dyes (0.2%). There have been reports of temperature-sensitive $\alpha$- and $\beta$-substituted BODIPY fluorophores containing aromatic groups in the past [102, 157]. Therefore, it is not unusual that these molecules have a minor temperature sensitivity.

### 7.4. Fluorescence decays in liquid-ordered/-disordered vesicles

After successfully characterising the photophysical properties of the new thiophene-modified BODIPY probes, it was aimed to test them in model lipid membranes to determine their ability to identify different lipid phases. Probes were then incorporated into LUVs representing either $L_d$ phase using DOPC or $L_o$ phase using a mixture of DPPC, cholesterol, and DOPC in a 5:5:1 ratio. Experimental results with LUVs containing -$OC_{16}$ substituted probes are showed in Figure 7.4. Results with -$OC_{10}$ are published in the Publication **[P5]**.

All probes decay monoexponentially in the $L_d$ phase, but as lipid order increases, they become biexponential, as in the $L_o$ phase. This is a common feature of BODIPY probes, explained by the fact that these fluorophores have a preferential orientation only in $L_d$ phase bilayers, but are heterogeneously distributed in $L_o$ phase membranes, leading to biexponential decay [158]. Also, we used Equation 2.2 to determine the difference in average fluorescence lifetimes between the $L_d$ and $L_o$ phases. The difference between the average fluorescence lifetime in the $L_d$ and $L_o$ phases for tetrasubstituted probes with -$OC_{10}$ and -$OC_{16}$ chains was 0.06 ns and 0.12 ns, respectively (Table 7.2). Contrarily, the average lifetimes in the $L_d$ and $L_o$ phases varied significantly for disubstituted dyes. These probes were able to distinguish between lipid phases based on their fluorescence lifetimes, with BP-$OC_{10}$ TP2 showing a difference of 0.30 ns and BP-$OC_{16}$ TP2 having a difference of 0.42 ns (Table 7.2). Furthermore, we concluded that fluorophores with longer alkoxy chains are more effective, as the difference in lifetimes for TP2 and TP4 probes grows with increasing aliphatic chain length. This may indicate that the length of the alkoxy chain enhances the ability of BODIPY probes to bind and ensure their proper insertion into the lipid bilayer.

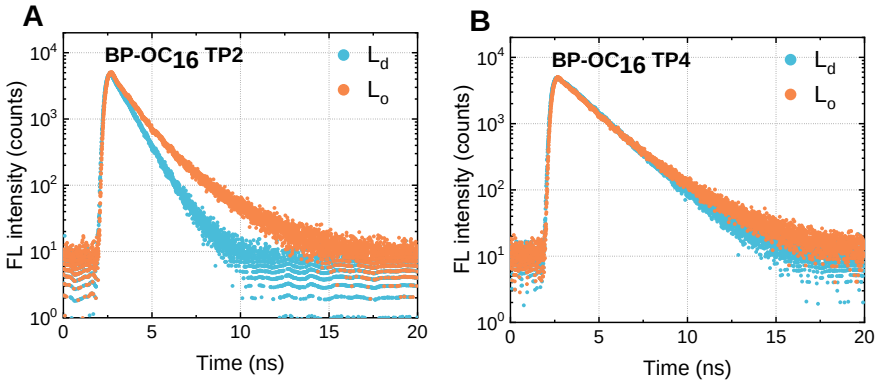


**Figure 7.4:** Fluorescence decays of BP-$OC_{16}$ TP2 and TP4, obtained in $L_d$ phase (composed of DOPC) and $L_o$ phase (composed of DPPC:cholesterol:DOPC at ratio 5:5:1) LUVs. Reproduced from [156] with permission from the Royal Society of Chemistry.

**Table 7.2:** Mean fluorescence lifetimes of molecular probes in different lipid phases ($L_d$ and $L_o$) and difference between these lifetimes ($\Delta\tau_{L_o\text{-}L_d}$). Lifetimes were obtained by mono/biexponential fitting of decays measured in LUVs.

| Derivative | $\tau_{L_d}$, ns | $\tau_{L_o}$, ns | $\Delta\tau_{L_o\text{-}L_d}$, ns |
|---|---|---|---|
| BP-$OC_{10}$ TP2 | 0.86 | 1.16 | 0.30 |
| BP-$OC_{16}$ TP2 | 0.84 | 1.26 | 0.42 |
| BP-$OC_{10}$ TP4 | 1.77 | 1.83 | 0.06 |
| BP-$OC_{16}$ TP4 | 1.71 | 1.83 | 0.12 |

## 7.5. Cellular imaging

The above results show that of all the new derivatives BP-$OC_{16}$ TP2 is the most suitable molecular rotor for distinguishing lipid phases using fluorescence lifetime. Therefore, BP-$OC_{16}$ TP2 was chosen to use in live MCF-7 cells and to see how the internal environment of the cells is affected by different chemotherapeutic agents. The details of cell preparation and imaging are published in the Publication [**P5**].

The intracellular distribution of BP-$OC_{16}$ TP2 was determined using laser-scanning confocal microscopy. According to Figure 7.5A, BP-$OC_{16}$ TP2 acquires punctate-like distribution in vesicular structures. Moreover, a FLIM picture of live MCF-7 cells showed that BP-$OC_{16}$ TP2 exhibits monoexponential fluorescence decay with a mean lifetime of 1487 ps (Figure 7.5B). Thus, it can be concluded that BP-$OC_{16}$ TP2 does not aggregate in the intracellular environment and can be used to measure the polarity of LDs in living cells.

Further investigation of BP-$OC_{16}$ TP2 molecular rotor followed a test of how different chemotherapeutic agents (CSP and PAX) affect the polarity of

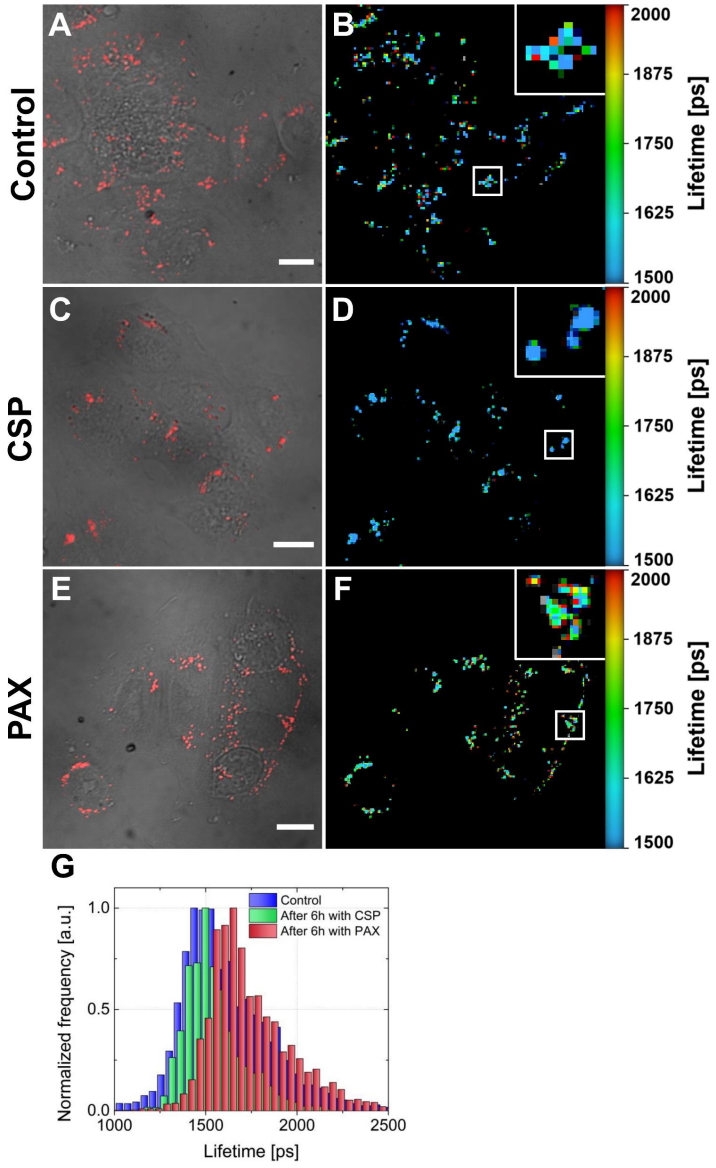


**Figure 7.5:** Application of BP-$OC_{16}$ TP2 in live cells to monitor the polarity of LDs after treatment with cisplatin (CSP) or paclitaxel (PAX). (A, C, E) shows confocal fluorescence images and brightfield images combined with scale bars of 15 $\mu$m. (B, D, F) depicts FLIM images with LDs selected as region of interest. G – lifetime histograms of the displayed FLIM images. Reproduced from [156] with permission from the Royal Society of Chemistry.

LDs in human breast cancer cells. CSP and PAX have different molecular mechanisms of action: CSP mostly targets DNA, while PAX stabilises microtubules [159, 160].

CSP treatment resulted in a mean fluorescence lifetime value of 1483 ps (Figure 7.5D), which is only marginally less than the lifetime of the probe in toluene but nearly comparable to the fluorescence lifetime seen in untreated cells (1487 ps) (Figure 7.5B). This is consistent with earlier research by Wang et al. [54], which showed that treatment with CSP almost had no effect on the polarity of LDs in human fibrosarcoma cells. On the contrary, treatment with PAX led to an increase in fluorescence lifetime (1608 ps) (Figure 7.5F). According to the theory of biophysicists, oxidative stress may potentially be the cause of the changes in LD polarity that were seen in the investigation after treatment with various PAX doses.

## 7.6. Conclusions

Most known fluorescent polarity probes are solvatochromic, which is not suitable for FLIM-based polarity sensing because of the altering spectral position and the multiexponential nature of the fluorescence decays, which complicate measurements and data analysis. In this study, novel polarity-sensitive, red-emitting BODIPY fluorophores that ideal for use as fluorescence lifetime probes to examine the intracellular environment were reported. Novel BODIPY conjugates had 2-thienyl moieties at the $\beta$,$\beta$'-positions or at both $\alpha$,$\alpha$'- and $\beta$,$\beta$'-positions. The probes were additionally modified with-$OC_{10}H_{21}$ and -$OC_{16}H_{33}$ alkoxy chains at the *meso*-phenyl ring to enable their successful insertion into the lipid layer.

The best fluorophore of the group, BP-$OC_{16}$ TP2, also displayed the ability to distinguish between $L_o$ and $L_d$ lipid phases in model lipid membranes. Moreover, it was discovered that it internalised inside LDs when employed for cellular imaging and displayed monoexponential fluorescence degradation lifetimes. Lastly, using BP-$OC_{16}$ TP2 and FLIM, it was possible to show that PAX had a concentration-dependent effect on the polarity of LDs, while CSP had no impact. Thanks to the ability of BP-$OC_{16}$ TP2 to recognise the polarity of LDs, researchers will be able to better understand the cellular response mechanisms to different chemotherapeutic treatments. In conclusion, a new thiophene-modified BODIPY polarity probe, BP-$OC_{16}$ TP2, with remarkable potential for FLIM-based intracellular polarity sensing was presented.

# CONCLUSIONS OF THE THESIS

During this work several conclusions were drawn:

1. The $\alpha$-substitution of the BODIPY core with cyclopropyl moieties increases the activation energy barrier of the molecule. This inhibits viscosity sensitivity and thus increases temperature sensitivity, leading to the creation of the green fluorescent temperature probe.

2. Red fluorescent BODIPY-based probes for the microenvironment can be created by extending the conjugation of derivatives with the $\beta$-substitution of the BODIPY core with cyclopropyl, phenyl, vinyl and thiophene moieties.

3. The use of a nitro group in the *meso*-phenyl position of the BODIPY core increases the viscosity sensitivity of the red fluorescent probes because the -$NO_2$ group lowers the activation energy barrier that determines the viscosity-sensitive properties of the probe.

4. A $\beta$-substituted BODIPY-based probe with phenyl moieties allows the development of a red fluorescent microviscosity probe, while the $\beta$-thiophene substitution transforms the sensor into a polarity probe. In addition, both probes can be used in fluorescence lifetime imaging microscopy to visualise changes in the microenvironment in lipid droplets of living cells.

# LIST OF PUBLICATIONS

### On the dissertation topic

[P1] Cyclopropyl Substituents Transform the Viscosity-Sensitive BODIPY Molecular Rotor into a Temperature Sensor, A. Vyšniauskas, B. Cornell, P. S. Sherin, **K. Maleckaitė**, M. Kubánková, M. A. Izquierdo, T. T. Vu, Y. A. Volkova, E. M. Budynina, C. Molteni, M. K. Kuimova, *ACS Sens.* **6**(6), 2158—2167 (2021)

[P2] Designing a Red-Emitting Viscosity-Sensitive BODIPY Fluorophore for Intracellular Viscosity Imaging, **K. Maleckaitė**, J. Dodonova, S. Toliautas, R. Žilėnaitė, Dž. Jurgutis, V. Karabanovas, S. Tumkevičius, A. Vyšniauskas, *Chem. Eur. J.* **27**(67), 16768—16775 (2021)

[P3] Give or Take: Effects of Electron-Accepting/-Withdrawing Groups in Red-Fluorescent BODIPY Molecular Rotors, **K. Maleckaitė**, D. Narkevičius, R. Žilėnaitė, J. Dodonova-Vaitkūnienė, S. Toliautas, S. Tumkevičius, A. Vyšniauskas, *Molecules* **27**(1), art. n. 23 (2021)

[P4] Red fluorescent BODIPY molecular rotor for high microviscosity environments, **K. Maleckaitė**, J. Dodonova-Vaitkūnienė, R. Žilėnaitė, S. Tumkevičius, A. Vyšniauskas, *Methods Appl. Fluoresc.* **10**(3), art. n. 034008 (2022)

[P5] A red-emitting thiophene-modified BODIPY probe for fluorescence lifetime-based polarity imaging of lipid droplets in living cells, R. Žvirblis, **K. Maleckaitė**, J. Dodonova-Vaitkūnienė, Dž. Jurgutis, R. Žilėnaitė, V. Karabanovas, S. Tumkevičius, A. Vyšniauskas, *J. Mater. Chem. B.* **11**, 3919—3928 (2023)

**Other publications**

[A1] Suppression of benzophenone-induced triplet quenching for enhanced TADF performance, G. Kreiza, D. Banevičius, J. Jovaišaitė, **K. Maleckaitė**, D. Gudeika, D. Volyniuk, J. V. Gražulevičius, S. Juršėnas, K. Kazlauskas, *J. Mater. Chem. C.* **7**(37), 11522—11531 (2019)

[A2] Simple Strategy to Measure the Contact Resistance between Metals and Doped Organic Films, A. Kirch, A. Fischer, R. Werberger, S. M. Aabi Soflaa, **K. Maleckaitė**, P. Imbrasas, J. Benduhn, S. Reineke, *Phys. Rev. Applied.* **18**(3), art. n. 034017 (2022)

**Conference presentations**

[C1] **Karolina Maleckaitė**, Jelena Dodonova-Vaitkūnienė, Sigitas Tumkevičius, Aurimas Vyšniauskas, "Photophysical properties of thiophene-dubstituted BODIPY molecular rotors", Advanced Materials and Technologies, Palanga, Lithuania, 2020.08.24-28, Poster presentation.

[C2] **Karolina Maleckaitė**, Jelena Dodonova-Vaitkūnienė, Stepas Toliautas, Sigitas Tumkevičius, Aurimas Vyšniauskas, "Polarity sensors based on thiophene-substituted BODIPY molecular rotors", APROPOS, Vilnius, Lithuania, 2020.09.29-10.01, Poster presentation.

[C3] **Karolina Maleckaitė**, Jelena Dodonova-Vaitkūnienė, Stepas Toliautas, Sigitas Tumkevičius, Aurimas Vyšniauskas, "Photophysical properties of red fluorescent BODIPY viscosity sensors", Conference of Doctoral Students and Young Researchers *FizTeCh*, Vilnius, Lithuania, 2020.10.22-23, Oral presentation.

[C4] **Karolina Maleckaitė**, Jelena Dodonova-Vaitkūnienė, Stepas Toliautas, Rugilė Žilėnaitė, Džiugas Jurgutis, Vitalijus Karabanovas, Sigitas Tumkevičius, Aurimas Vyšniauskas, "Designing a red viscosity-sensitive BODIPY fluorophore for a live cell imaging", Open Readings, Vilnius, Lithuania (online), 2021.03.16-19, Oral presentation.

[C5] **Karolina Maleckaitė**, Jelena Dodonova-Vaitkūnienė, Rugilė Žilėnaitė, Sigitas Tumkevičius, Aurimas Vyšniauskas, "Red-fluorescing BODIPY-based polarity sensor", Advanced Materials and Technologies, Palanga, Lithuania, 2021.06.23-27, Poster presentation.

[C6] **Karolina Maleckaitė**, Jelena Dodonova-Vaitkūnienė, Stepas Toliautas, Rugilė Žilėnaitė, Džiugas Jurgutis, Vitalijus Karabanovas, Sigitas Tumkevičius, Aurimas Vyšniauskas, "Red fluorescent viscosity sensitive BODIPY fluorophore", Lithuanian National Physics Conference (LNFK), Vilnius, Lithuania, 2021.10.06-08, Oral presentation.

[C7] **Karolina Maleckaitė**, Jelena Dodonova-Vaitkūnienė, Stepas Toliautas, Rugilė Žilėnaitė, Domantas Narkevičius, Džiugas Jurgutis, Vitalijus Karabanovas, Sigitas Tumkevičius, Aurimas Vyšniauskas, "Red fluorescent BODIPY fluorophores for environmental sensing", Conference of Doctoral Students and Young Researchers *FizTeCh*, Vilnius, Lithuania, 2021.10.20-21, Oral presentation.

[C8] **Karolina Maleckaitė**, Domantas Narkevičius, Rugilė Žilėnaitė, Jelena Dodonova-Vaitkūnienė, Stepas Toliautas, Sigitas Tumkevičius, Aurimas Vyšniauskas, "The impact of electron-donating/-withdrawing groups

on red-fluorescent BODIPY molecular rotor", Open Readings, Vilnius, Lithuania (online), 2022.03.15-18, Oral presentation.

[C9] **Karolina Maleckaitė**, Jelena Dodonova-Vaitkūnienė, Stepas Toliautas, Rugilė Žilėnaitė, Džiugas Jurgutis, Vitalijus Karabanovas, Sigitas Tumkevičius, Aurimas Vyšniauskas, "Red-fluorescent BODIPY microviscosity sensor for intracellular imaging", Bio-sensing Technologies, Sitges, Spain, 2022.05.22-25, Poster presentation.

[C10] **Karolina Maleckaitė**, Jelena Dodonova-Vaitkūnienė, Stepas Toliautas, Džiugas Jurgutis, Rugilė Žilėnaitė, Vitalijus Karabanovas, Sigitas Tumkevičius, Aurimas Vyšniauskas, "Red fluorescent BODIPY molecular rotors for lifetime-based sensing of microviscosity", Hanseatic Workshop on Exciton Dynamics and Spectroscopy, Vilnius, Lithuania, 2022.08.24-26, Oral presentation.

[C11] **Karolina Maleckaitė**, Jelena Dodonova-Vaitkūnienė, Stepas Toliautas, Rugilė Žilėnaitė, Sigitas Tumkevičius, Aurimas Vyšniauskas, "Red fluorescent BODIPY microviscosity sensor for investigations of high viscosity", Conference of Doctoral Students and Young Researchers *FizTeCh*, Vilnius, Lithuania, 2022.10.19-20, Oral presentation.

[C12] **Karolina Maleckaitė**, Jelena Dodonova-Vaitkūnienė, Džiugas Jurgutis, Rokas Žvirblis, Rugilė Žilėnaitė, Vitalijus Karabanovas, Sigitas Tumkevičius, Aurimas Vyšniauskas, "Red fluorescent BODIPY molecular rotors for intracellular microenvironment sensing", Conference of Young Researchers (JMK) "Interdisciplinary Research in Physical and Technological Sciences", Vilnius, Lithuania, 2023-03-23, Oral presentation.

[C13] **Karolina Maleckaitė**, Jelena Dodonova-Vaitkūnienė, Stepas Toliautas, Džiugas Jurgutis, Rugilė Žilėnaitė, Vitalijus Karabanovas, Sigitas Tumkevičius, Aurimas Vyšniauskas, "BODIPY-based red fluorescent molecular rotors for microviscosity sensing", Faraday Joint Interest Group Conference, Sheffield, UK, 2023.04.03-05, Oral presentation.

# CURRICULUM VITAE


| | |
|---|---|
| **Name:** | Karolina |
| **Surname:** | Maleckaitė |
| Date of birth: | 1994-09-21 |
| Place of birth: | Kaunas, Lithuania |
| Current town: | Vilnius, Lithuania |
| E-mail: | kmaleckaite@gmail.com |
| | karolina.maleckaite@ftmc.lt |


**Education:**

| | |
|---|---|
| 2019 – 2023 | Center for Physical Sciences and Technology & Vilnius University, Faculty of Physics, *joint Ph.D. studies.* |
| 2017 – 2019 | Vilnius University, Faculty of Physics, *Master's degree in Technology.* |
| 2013 – 2017 | Vilnius University, Faculty of Physics, *Bachelor's degree in Physics.* |

**Work experience:**

| | |
|---|---|
| 2022 – now | Center for Physical Sciences and Technology, *Junior Research Fellow.* |
| 2019 – 2022 | Center for Physical Sciences and Technology, *Engineer.* |
| 2017 – 2019 | Vilnius University, Institute of Photonics and Nanotechnology, *Engineer.* |
| 2016 – 2017 | Vilnius University, Institute of Photonics and Nanotechnology, *Technician.* |

**Internships:**

| | |
|---|---|
| **2022 March – April** | Department of Chemistry, |
| | Molecular Sciences Research Hub, |
| | Imperial College London, UK. |
| Research topic: | *G-quadruplex RNA visualisation with FLIM.* |
| Supervisor: | Prof. Marina K. Kuimova |
| | |
| **2018 April – July** | Dresden Integrated Center for Applied |
| | Physics and Photonic Materials (IAPP), |
| | TU Dresden, Germany |
| Research topic: | *Organic Interlayers for Improving Charge Injection.* |
| Supervisor: | Prof. Sebastian Reineke |

# SANTRAUKA

## Įvadas

Mūsų ląstelėse vyksta daug difuzijos nulemtų procesų. Šiuos procesus gali paveikti besikeičianti mikroaplinka, pavyzdžiui, terpės klampumo, temperatūros ir poliškumo kaita. Be to, drastiški šių savybių pokyčiai ląstelių lygmenyje gali rodyti rimtas ligas. Todėl turėtų būti sukurti viduląsteliniai tyrimo metodai, galintys aptikti šiuos pokyčius. Fluorescuojantys molekuliniai jutikliai suteikia tokią galimybę biofizikams suprasti besikeičiančią mikroaplinką gyvose ląstelėse. Tačiau yra įvairių jutiklių tipų ir vaizdavimo metodų, turinčių savo privalumų ir trūkumų.

Fluorescuojantys molekuliniai jutikliai, naudojami kartu su FLIM, yra patogus būdas vizualizuoti gyvų ląstelių mikroaplinkos pokyčius. Šią techniką minimaliai veikia lazerio svyravimai ir fluoroforo koncentracija, taip pat yra galimybė vienu metu vaizdinti visą mėginį. Nepaisant to, dauguma fluorescuojančių žymeklių, kurie naudojami jutimui, yra žalios spalvos. Tai yra problema, nes daugelis gyvų ląstelių organelių autofluorescuoja toje pačioje – žaliojoje – spektrinėje srityje, todėl jutiklio naudojimas nėra praktiškas. Be to, giliųjų audinių mėginiai dažniausiai būna gana stori, todėl reikėtų naudoti ilgesnius bangos ilgius. Todėl ir kyla poreikis raudonųjų fluorescencinių jutiklių kūrimui.

Šiame darbe daugiausiai dėmesio skiriama raudonųjų fluorescuojančių molekulinų jutiklių kūrimui, nes jie leistų supaprastinti gyvų ląstelių vaizdavimą. Be to, pristatomi klampumui, temperatūrai ir poliškumui jautrūs žymekliai, jų fotofizikinės savybės.

## Darbo tikslas ir naujumas

Šio darbo tikslas buvo ištirti, kaip skirtingos funkcinės grupės keičia BODIPY molekulinių rotorių fotofizikines savybes ir jų jautrumą aplinkos pokyčiams.

Šio tyrimo motyvas ir naujumas buvo sukurti naujus raudonai fluorescuojančius BODIPY mikroklampos jutiklius. Be to, šis darbas buvo skirtas mikroklampumo žymeklių pavertimui į temperatūros ir poliškumo jutiklius. Taip pat, buvo labai svarbu sukurti aplinkos jutiklius, kuriuos būtų galima naudoti *in vitro*.

Norint pasiekti šiuos tikslus, buvo iškeltos kelios užduotys:

- Ištirti, ar BODIPY kamienas su fenilo ir vinilo grupių $\beta$-pakaitais padidina konjugaciją ir leidžai sukurti raudonai spinduliuojantį ir klampumui jautrų fluoroforą;
- Įvertinti, kaip ciklopropilo ir tiofeno grupių prijungimas prie BODIPY kamieno $\alpha$ ir $\beta$ padėčių pakeičia molekulinio jutiklio spektroskopines ir jautrumo savybes, priklausomai nuo pakaito ir jo padėties;
- Pademonstruoti, kad perspektyviausius junginius galima pritaikyti gyvų ląstelių mikroaplinkos vaizdinimui.

### Ginamieji teiginiai

- Nitrogrupės pakaitas ant BODIPY kamieno *meso*-fenilo padėtyje yra universalus būdas padidinti žymeklio jautrumą klampumui.
- BODIPY kamieno $\beta$ pozicijoje esantys elektronus donuojantys (EDG) pakaitalai, tokie kaip metoksi ir tiofeno grupės, padidina BODIPY molekulinių rotorių jautrumą poliškumui.
- $\beta$-BODIPY kamieno pozicijoje pridėti ciklopropilo, fenilo, vinilo ar tiofeno pakaitai, padidina junginių konjugaciją ir lemia raudoną sugerties ir fluorescencijos spektrų poslinkį.
- Raudonai fluorescuojantys BODIPY jutikliai su $\beta$-fenilo ir $\beta$-tiofeno grupių pakaitais gali būti naudojami lipidinių pūslelių vaizdinimui gyvose ląstelėse, atitinkamai siekiant nustatyti mikroklampumo ir poliškumo pokyčius.

### Autoriaus indėlis

Visus fotofizikinių charakteristikų, pastovių ir laike koreliuotų spektroskopijos, tyrimus, įskaitant mėginių paruošimą, atliko autorė, kuri taip pat apdorojo ir išanalizavo duomenis. Be to, autorė dalyvavo rašant ir aptariant visus publikacijų rankraščius. Taip pat, disertacijos autorė buvo pagrindinė publikacijų **P2, P3, P4** rašytoja.

Doktorantūros baigiamojo darbo autorė nepaprastai džiaugiasi galėdama pristatyti tarpdisciplininį darbą, kuris nebūtų įmanomas be Fizinių ir technologijų mokslų centro (FTMC), Vilniaus universiteto, Lietuvos Nacionalinio vėžio instituto, Londono imperatoriškojo koledžo ir Londono karališkojo koledžo kolegų indėlio. Todėl, kai kurios šio darbo dalys buvo deleguotos arba atliekamos bendradarbiaujant, o tai išsamiai aprašyta eksperimentinės metodikos skyriuje.

## Literatūros įvadas

Mūsų kūnuose yra daugybė įvairių tipų, dydžių ir formų ląstelių. Ląstelės membrana, branduolys ir citoplazma yra trys komponentai, sudarantys „apibendrintą eukariotinę ląstelę“. Citoplazmoje randama daugybė, galbūt net tūkstančiai, mažyčių unikalių struktūrų, žinomų kaip organelės. Lipidų pūslelės (angl. *lipid droplets*, LDs) yra svarbios ląstelių organelės, susijusios su lipidų tiekimu ir saugojimu, kaupiančios ląstelių lipidus ir valdančios jų išsiskyrimą, kad patenkintų tam tikrus ląstelių poreikius. Dėl to jos būtinos lipidų ir energijos balanso išsaugojimui [23]. Lipidų pūslelių vidų sudaro nepoliniai lipidai, tokie kaip triacilgliceroliai ir sterolių esteriai, o paviršių sudaro poliniai lipidai, tokie kaip steroliai ir fosfolipidai, bei įvairūs baltymai [24].

Viduląstelinę aplinką galima tirti naudojant mažas fluorescencines molekules, vadinamas „fluoroforais“ (taip pat vadinami fluorescenciniais jutikliais arba žymekliais). Jų naudojimas leidžia mokslininkams aptikti aplinkos pokyčius, suprasti biochemines sąveikas ir chemines reakcijas, nes fluorescencijos emisija keičiasi šių procesų metu [25]. Fluorescenciniai jutikliai, skleidžiantys šviesą mėlynoje arba žalioje spektrinėje srityje, gali būti naudojami biomolekuliniam žymėjimui ar net fosgeno dujų aptikimui, kuris naudojamas kaip cheminis ginklas [26]. Tačiau, gyvųjų audinių vaizdinimui reikalingi raudonieji fluoroforai dėl kelių priežasčių. Visų pirma, biologinių mėginių autofluorescencija, kurią galime laikyti įvairių savaime fluorescuojančių organelių „vizualiniu triukšmu“, yra mažiau matoma raudonojoje matomo spektro dalyje [27]. Antra, tuos pačius biologinius mėginius taip pat galima paprasčiau vaizdinti derinant su papildomais fluoroforais, tokiais kaip žalias fluorescencinis baltymas (angl. *green fluorescent protein*, GFP). Trečia, siekiant sumažinti matomos šviesos sklaidą, storų biologinių mėginių vaizdavimas turi būti atlieka-

mas giliųjų audinių optiniame lange (650–1350 nm) [28, 29]. Dėl šių priežasčių vienas iš pagrindinių šio darbo tikslų buvo sukurti raudoną spinduliuotę skleidžiančius jutikius.

Pagrindiniai mikroaplinkos parametrai yra mikroklampumas, temperatūra ir poliškumas. Biologinėse sistemose vyksta daug difuzijos kontroliuojamų procesų, kuriuos gali paveikti mikroklampumas, kuris yra mikroskopinis tūrinės klampos ekvivalentas. Todėl mikroklampumo pokyčiai gali atskleisti biocheminius ir biofizinius mechanizmus, vykstančius gyvų ląstelių viduje [1–3]. Mikroklampumo vaizdinimas yra svarbus mokslininkams, tyrinėjantiems polimerus [30], aerozolius [31], gyvas ląsteles [32–34] ir jų specifines organeles [35–37], pavyzdžiui, lipidų susikaupimą ląstelių membranose [38]. Daugelis tarpląstelinių procesų, tiek normalių ir neįprastų, gamina šilumą arba yra veikiami temperatūros, pavyzdžiui, ląstelių dalijimasis, kvėpavimas ir termogenezė [4–6]. Be to, pastebėta, kad kai kurie vėžio audiniai generuoja daugiau šilumos nei sveikos ląstelės [13]. Todėl labai norima turėti galimybę matuoti temperatūrą, ypač tarpląsteliniame lygmenyje. Be to, tarpląsteliniai temperatūros jutikliai gali padėti tirti ir nustatyti daugelio sutrikimų, dėl kurių pasikeičia kūno temperatūra, pradžią. Trečiasis iš parametrų - poliškumas - yra fizinė junginių savybė, atsirandanti dėl netolygaus dalinio krūvio pasiskirstymo tarp įvairių junginio atomų [46, 47]. Pavyzdžiui, polinio tirpiklio viename gale yra dalinis teigiamas krūvis, o kitame – dalinis neigiamas krūvis, todėl jis gali ištirpinti polines medžiagas ir dalyvauti dipolio-dipolio sąveikoje.

Vienasluoksnės liposomos yra sferinės pūslelės, viduje turinčios vandeninį tirpalą, kurį supa vienas dvisluoksnis amfifilinis lipidas arba tokių lipidų derinys [55,56]. Šios liposomos naudojamos biologinėms sistemoms tirti ir ląstelių membranoms imituoti, o jas galima suskirstyti į grupes pagal dydį, sudėtį ir net veikimo mechanizmą. Šiame darbe tiriamos tik didelės vienasluoksnės liposomos (angl. *large unilamellar vesicles*, LUVs), o jų dydis svyruoja nuo 0,1 iki 1 µm. Paprastas poliškumo matavimo metodas yra pagrįstas fluorescuojančiomis organinėmis molekulėmis, kurios keičia savo spektroskopines charakteristikas, reaguodamos į aplinkos pokyčius. Šio tipo dažai yra naudojami norint nustatyti lipidų membranų skirtumą tarp skystos tvarkingos (angl. *liquid-ordered*, $L_o$) ir skystos netvarkingos (angl. *liquid-disordered*, $L_d$) fazių [59]. $L_d$ fazė yra skysta, o $L_o$ fazė yra tarpinė tarp $L_d$ ir kietos (gelinės) fazės [60]. $L_o$ fazė, palyginti su $L_d$, yra storesnė, standesnė ir, kaip rodo pava-

dinimas - tvarkingesnė. $L_d$ fazė taip pat gali būti apibūdinta kaip sudaryta iš nesočiųjų lipidų, o $L_o$ fazė – iš sočiųjų lipidų [61].

Sąvoka „liuminescencija“, paprasčiausiai suvokiama kaip šviesos spinduliavimas iš medžiagos, reiškia šviesos efekto reiškinį, atsirandantį elektronui pereinant iš sužadintos būsenos į žemesnės energijos būseną [46, 47, 63, 64]. Priklausomai nuo to, kaip sistema sužadinama, yra keletas liuminescencijos tipų. Vienas iš šių tipų yra fotoliuminescencija, atsirandanti sužadinant fotonais. Fotoliuminescencija gali būti suskirstyta į dvi grupes: fluorescencija ir fosforescencija. Pagrindinis skirtumas tarp jų yra liuminescencijos trukmė, kurią lemia būsena, iš kurios elektronai grįžta į pagrindinę būseną. Elektronams relaksuojant iš singuletinės būsenos yra stebima fluorescencija, jos relaksacijos trukmė yra nuo $10^{-10}$ iki $10^{-7}$ sekundžių. Tuo tarpu, kai elektronai relaksuoja iš tripletinės būsenos, yra stebima fosforescencija, o gyvavimo trukmė yra $10^{-6}$–10 s. Šiame darbe analizuojama tik fluorescencija.

Laike koreliuotos fluorescencijos matavimai gali tiksliau nustatyti informaciją apie molekulinius procesus, nes skirtingai nuo nuostoviosios būsenos matavimų (pavyzdžiui, fluorescencijos spektro), jie nėra vidurkinami [47]. Laike koreliuotos fluorescencijos matavimuose analizuojamas fluorescencijos gesimas (kinetika). Ši kinetika parodo, kiek laiko egzistuoja spinduliuojanti būsena. Be to, daugiaeksponentinio skilimo atveju ji parodo kitų konformacinių būsenų buvimą, sklaidą, priemaišų buvimą arba solvatinių procesų dinamiką [65]. Skirtingai nuo fluorescencijos intensyvumo, fluorescencijos gesimo trukmei įtakos neturi daugelis savybių, tokių kaip fluoroforo koncentracija, bandinio storis ir sugertis, matavimo technika, fotobalinimas ir sužadinimo intensyvumas [66].

Laike koreliuotų pavienių fotonų skaičiavimas (angl. *time-correlated single photon counting*, TCSPC) yra fluorescencijos gesimo trukmės įvertinimo metodas. Jis pasižymi pikosekundine skiriamaja geba ir nepaprastai dideliu tikslumu, kas leidžia užfiksuoti net ypač neintesyvios šviesos signalą. TCSPC veikimas paremtas pavienių fotonų detektavimu ir jų detekcijos laiko matavimu atskaitos signalo atžvilgiu [47, 71]. Atskaitos signalas dažniausiai yra šviesos šaltinis, pavyzdžiui, lazeris. TCSPC yra statistinis metodas, kuriam reikalingas didelį pasikartojimo dažnį turintis šviesos šaltinis (pavyzdžiui, impulsinis lazeris), kad būtų galima surinkti pakankamai fotonų ir gauti tikslius duomenis.

TCSPC yra puikiai pritaikomas fluorescencijos gyvavimo trukmių

mikroskopijoje (angl. *fluorescence lifetime imaging microscopy*, FLIM) kuriant daugiamatį mechanizmą, kas iš esmės yra tradicinės TCSPC technikos išplėtimas [87]. FLIM yra metodas, pagrįstas fluorescencijos gesimo trukmių pasiskirstymo ir pokyčių bandinyje stebėjimu ir analize, todėl gali ištirti mikroaplinką [85]. Kadangi daugelis prieš tai minėtų, su fluorescencijos gyvevimo trukme susijusių, veiksnių neturi įtakos FLIM metodikai, tai puiki priemonė patikimam ląstelės ar audinio aplinkos įvertinimui, taip pat įvairių biofizinių parametrų, įskaitant deguonies slėgio, poliškumo, pH, jonų koncentracijos ir kitų biocheminių parametrų pokyčių stebėjimui [87, 88].

Fluorescenciniai molekuliniai rotoriai (angl. *fluorescent molecular rotors*, FMRs) buvo sukurti kaip priemonė stebėti ląstelių ir tarpląstelinio klampumo pokyčius [16]. FMRs veikimas pagrįstas konkurencija tarp nespindulinės relaksacijos, kuri priklauso nuo aplinkos klampumo, ir spindulinės relaksacijos (fluorescencijos) [1, 89]. Jei sužadinimas vyksta neklampioje aplinkoje, FMRs paprastai relaksuoja nespinduliniu keliu į pagrindinę būseną, vykstant molekulės sukimuisi. Fluorescencija tampa pagrindiniu relaksacijos keliu, kai molekulės rotacija yra apribota, pavyzdžiui, didesnio klampumo arba tarpmolekulinės sąveikos atvejais, kas lemia išaugusį fluorescencijos intensyvumą ir ilgesnį gesimo laiką.

Fluorescencijos gyvavimo trukme paremti jutikliai pašalina su intensyvumu susijusius artefaktus ir naudoja fluorescencijos gesimo trukmę kaip matavimo vienetą kiekybiniam įvertinimui [95]. Kintanti ar net tiksli fluorescencijos trukmės vertė gali atspindėti stebimos aplinkos savybes.

Plačiai naudojami fluorescencijos gyvavimo trukme paremti jutikliai yra paremti BODIPY grupe [16, 90, 92]. Vienas iš dažniausiai naudojamų BODIPY mikroklampumo jutiklių yra BODIPY-$C_{10}$ [99]. BODIPY junginiai paprastai naudojami kaip fluorescencijos gyvavimo trukme, o ne intensyvumu paremti jutikliai [1]. Šie jutikliai pasižymi monoeksponentiniu fluorescencijos gesimu, kuris palengvina duomenų analizę ir puikiai tinka naudoti FLIM [19].

### Eksperimentiniai metodai

Tirtų darinių sintezę publikacijoje **[P1]** atliko Ekaterina M. Budynina ir Yulia A. Volkova (Londono imperatoriškasis koledžas, Jungtinė Karalystė).

**[P2-P5]** publikacijose tyrinėtas molekules susintetino Organinės chemijos

grupė, vadovaujama prof. Sigitas Tumkevičius Vilniaus universiteto Chemijos ir geomokslų fakulteto Chemijos institute. Sintezę atliko dr. Jelena Dodonova-Vaitkūnienė ir Rokas Žvirblis ([**P5**]).

Visi tyrimams naudoti bandiniai buvo 0.2-2.5 mM koncentratai, kurie vėlesniams tyrimams buvo skiedžiami. Tyrimai su tirpalais atlikti kvarcinėse (10 mm) kiuvetėse, kuriose dažo koncentracija buvo 2-14 µM. Eksperimentams kriostate buvo naudojama 0.5 mm kvarcinė kiuvetė.

Tolueno-ricinos aliejaus mišinių klampumas įvairiose temperatūrose nustatytas naudojant SV-10 (AD) viskozimetrą, prijungtą prie termostato, išskyrus [**P1**] ir metanolio-glicerolio mišinius, kuriems naudotas SVM 3000 (Anton Paar) viskozimetras. Iš šių matavimų sudarytos kalibracinės kreivės.

Sugerties spektrai užregistruoti naudojant Jasco V-670 spektrometrą. Fluorescencijos spektrai išmatuoti naudojant Edinburgh-F900 (Edinburgh Instruments) fluorimetrą kartu su balto pluošto WhiteLase Micro (Fianium) lazeriu ir ThorLabs filtrais (520, 540, 570, 630 nm). Fluorescencijos kinetikos turėjo 5000 fotonų kinetikos smailėje ir 20 ns langą. Fluorescencijos kvantinės išeigos (QY) išmatuotos palyginamuoju metodu ir apskaičiuotos naudojant 1.4 lygtį.

Liposomos suformuotos kaip didelės vienasluoksnės pūslelės (LUVs) naudojant Avanti Polar Lipids Mini-Extruder. Liposomų formavimui naudoti cholesterolio, DOPC ir DPPC lipidai.

Teoriniam molekulių modeliavimui naudota tankio funkcionalo teorija (DFT). Pirmajai publikacijai [**P1**] skaičiavimus atliko Bethan Cornell ir Carla Molteni (Londono karališkasis koledžas, Jungtinė Karalystė). Dr. Stepas Toliautas iš Vilniaus universiteto Fizikos fakulteto Cheminės fizikos instituto atliko DFT skaičiavimus publikacijoms [**P2-P3**].

## Rezultatai

### 1. Klampumui jautraus BODIPY molekulinio rotoriaus pavertimas temperatūros jutikliu pridedant ciklopropilo pakaitus

Pirmajame skyriuje aptarta, kaip fluorescencijos gyvavimo trukme pagrįstą klampumo jutiklį paversti temperatūros jutikliu, pridedant retai naudojamą pakaitą – ciklopropilo grupę. BODIPY3 yra žalias fluorescencinis temperatūros jutiklis su $\alpha$-ciklopropilo pakaitalais, kurie gali būti naudojami nepoliniuose tirpikliuose. Jis turi silpną fluorescencijos gyvavimo trukmės jautrumą klam-

pumui ir nedidelius solvatochrominius poslinkius fluorescencijos spektruose didėjant poliškumui. Palyginti su panašiu $\beta$ pozicijoje pakaitus turintį BODIPY2, BODIPY3 parodė ilgesnes fluorescencijos gyvavimo trukmes ir panašų santykinį temperatūros jautrumą. Įdomu tai, kad abu junginiai turėtų būti sukalibruoti pastovaus poliškumo aplinkai, kad būtų naudojami kaip temperatūros jutikliai. Nepaisant to, jie gali būti naudojami kaip poliškumo jutikliai, jei temperatūra yra pastovi.

Be to, buvo įrodyta, kad BODIPY3 gali greitai įsiskverbti į gyvas ląsteles ir tiksliai nustatyti tarpląstelinę temperatūrą. Naujasis BODIPY fluoroforas gali būti naudojamas temperatūros jutimui naudojant FLIM, nes jo fluorescencijos trukmė priklauso nuo temperatūros. Taip pat, kitaip nei anksčiau publikuoti fluorescencijos gyvavimo trukme paremti temperatūros jutikliai, naujasis jutiklis pasižymi monoeksponentinėmis fluorescencijos gesimo kinetikomis. Teoriniai skaičiavimai parodė, kad pridėjus ciklopropilo grupę susidaro didesnis energijos barjeras, dėl kurio sumažėja jautrumas klampumui ir padidėja jautrumas temperatūrai. Todėl BODIPY jutikliai su ciklopropilo pakaitais yra jautrūs temperatūrai, o šią savybę lemia barjero aukštis.

## 2. Raudonai šviečiantis, klampumui jautrus BODIPY fluoroforas, skirtas lipidų pūslelių viduląsteliniam vaizdavimui

Antrajame skyriuje aprašytas raudonai fluorescuojantis BODIPY klampumo žymeklis BP-PH-2M-$NO_2$. DFT skaičiavimai buvo labai naudingi kuriant BP-PH-2M-$NO_2$, nes tai leido apskaičiuoti aktyvacijos energijos barjero aukštį ($E_a$) ir nustatyti nuo klampumo priklausančią nespindulinę relaksaciją. Metilo grupių pridėjimas prie $\beta$-fenilo sumažino $E_a$ ir šiek tiek pagerino klampumo jautrumą. Be to, nitrogrupės pridėjimas *meso*-fenilo padėtyje dar labiau sumažino $E_a$ ir padidino žymeklio jautrumą klampumui. Palyginti su dažniausiai naudojamu žaliu klampumo jutikliu BODIPY-$C_{10}/C_{12}$ ir jo variantais, naujasis fluoroforas spinduliuoja pastebimai raudonesnėje spektro srityje ir turi keturis kartus didesnį Stokso poslinkį, išlaikydamas puikų jautrumą klampumui. Taip pat, naujasis žymeklis tinka vaizdinti gyvų MCF-7 vėžinių ląstelių lipidų pūslelių klampumą ir pasižymi monoeksponentine fluorescencijos gesimo kinetika sudėtingoje tarpląstelinėje aplinkoje. Ši savybė yra labai aktuali, nes leidžia tiksliai nustatyti klampumą naudojant FLIM metodiką.

## 3. Elektronus donuojančių/pritraukiančių grupių poveikis raudonai fluorescuojantiems BODIPY molekuliniams rotoriams

Trečiajame skyriuje aptariami BODIPY fluoroforai su $\beta$-fenilo grupės pakaitais ir papildomomis metilo, metoksi arba trifluorometilo grupėmis. Visi junginiai pasižymėjo raudonos spalvos sugertimi ir fluorescencijos emisija. Ištirtas molekulių jautrumas klampumui, temperatūrai ir tirpiklio poliškumui. Junginys su metilo grupe (BP-PH-8M) neparodė didelio jautrumo nei vienai iš savybių. Tačiau ištirta, kad molekulė su trifluorometilais (BP-PH-$CF_3$) yra vidutiniškas temperatūros jutiklis. Be to, parodyta, kad junginys su metoksi grupe (BP-PH-OMe) turi išskirtinį patrauklių savybių derinį: fluoroforas yra fluorescencijos gyvavimo trukme paremtas poliškumo jutiklis, kuris sugeria ir spinduliuoja raudonoje matomo spektro srityje, turi minimalų jautrumą kitiems parametrams ir pasižymi monoeksponentine fluorescencijos gesimo kinetika.

## 4. Raudonasis molekulinis rotorius didelio mikroklampumo aplinkai

Ketvirtajame skyriuje aprašyti nauji BODIPY junginiai su fenilo ir vinilo grupės pakaitais $\beta$ pozicijoje. Įrodyta, kad nitrogrupės prijungimas prie BODIPY kamieno *mezo*-fenilo yra veiksmingas būdas padidinti žymeklio jautrumą klampumui. Nauji junginiai su nitrogrupe taip pat pasižymėjo sugertimi ir fluorescencija raudonojoje spektro dalyje, fluorescencijos gyvavimo trukme pagrįstu mikroklampumo jutiklio veikimu, minimaliu jautrumu temperatūrai ir tirpiklio poliškumui. Taip pat parodyta, kad BP-Vinyl-$NO_2$ yra jautrus klampumui net septynių eilių diapazone. Šis jutiklis galėtų būti pritaikytas net labai didelio klampumo bandiniuose, pavyzdžiui, užšaldytuose audiniuose [154]. Be to, tyrime atskleista, kad junginiui su $\beta$-fenilu pašalinus sterinius trikdžius (BP-PH-m2M-$NO_2$) yra stebimas raudonasis poslinkis ir išlaikomas jautrumas klampumui. Šie rezultatai galėtų padėti sukurti naujus raudonai fluorescuojančius mikroklampumo jutiklius, turinčius platų klampumo jautrumo diapazoną.

## 5. Raudonai spinduliuojantis, tiofeno grupe modifikuotas BODIPY poliškumo jutiklis lipidų pūslelių gyvose ląstelėse vaizdinimui FLIM metodu

Penktajame skyriuje aptartas raudonai fluorescuojantis, fluorescencijos gyvavimo trukme paremtas poliškumo jutiklis.

Dauguma fluorescuojančių poliškumo žymeklių yra solvatochrominiai, o tokio tipo jutikliai netinka FLIM metodu pagrįstam poliškumo vaizdinimui. Taip yra dėl kintančios spektro padėties ir daugiaeksponentinio fluorescencijos gesimo, kurie apsunkina matavimus ir duomenų analizę. Šiame tyrime pademonstruoti nauji, poliškumui jautrūs, raudonai spinduliuojantys BODIPY fluoroforai, kurie idealiai tinka naudoti kaip fluorescenciniai jutikliai, skirti ištirti viduląstelinę aplinką. Nauji BODIPY junginiai turėjo 2-tienilo fragmentus $\beta$,$\beta$'-padėtyse arba $\alpha$,$\alpha$'- ir $\beta$,$\beta$'-padėtyse. Jutikliai buvo papildomai modifikuoti naudojant -$OC_{10}H_{21}$ ir -$OC_{16}H_{33}$ alkoksigrupės grandines ant *mezo*-fenilo žiedo, kad žymekliai lengviau įsiterptų į lipidų sluoksnį.

Geriausias grupės fluoroforas BP-$OC_{16}$ TP2 pasižymėjo galimybe atskirti $L_o$ ir $L_d$ lipidų fazes lipidų membraną imituojančiose liposomose. Taip pat nustatyta, kad šis fluoroforas lokalizuojasi lipidų pūslelėse, kai yra naudojamas ląstelių vaizdavimui, ir pasižymi monoeksponentiniu fluorescencijos gesimu. Galiausiai, naudojant BP-$OC_{16}$ TP2 ir FLIM, buvo parodyta, kad paklitakselis (PAX) turi nuo koncentracijos priklausomą poveikį lipidinių pūslelių poliškumui, o cisplatina (CSP) - neturi jokio poveikio. Kadangi BP-$OC_{16}$ TP2 geba atpažinti lipidinių pūslelių poliškumą gyvose ląstelėse, tai gali padėti mokslininkams geriau suprasti ląstelių atsaką į skirtingus chemoterapinius gydymo mechanizmus. Apibendrinant, šiame tyrime pristatytas naujas tiofeno grupe modifikuotas BODIPY poliškumo jutiklis BP-$OC_{16}$ TP2, kuris gali būti taikomas su FLIM vaizdinant lipidų pūslelių gyvose ląstelėse poliškumą.

## Išvados

Atliekant darbą buvo padarytos šios išvados:

1. BODIPY kamieno $\alpha$ pozicijoje pridėtas ciklopropilo grupės pakaitas padidina molekulės aktyvacijos energijos barjerą. Tai sumažina jautrumą klampumui ir padidina jautrumą temperatūrai, todėl yra sukuriamas žaliai fluorescuojantis temperatūros jutiklis.

2. Raudonai fluorescuojantys BODIPY jutikliai mikroaplinkos tyrimams gali būti sukurti BODIPY kamieno $\beta$ pozicijoje pridedant ciklopropilo, fenilo, vinilo ir tiofeno grupių pakaitus, taip padidintant junginių konjugaciją.

3. Nitrogrupės panaudojimas BODIPY kamieno *mezo*-fenilo padėtyje padidina raudonų fluorescencinių jutiklių jautrumą klampumui, nes -$NO_2$ grupė sumažina aktyvacijos energijos barjerą, kuris lemia žymeklio jautrumą klampumui.

4. BODIPY kamieno $\beta$ pozicijoje prijungus fenilo grupę yra sukuriamas raudonai fluorescuojantis mikroklampumo jutiklis, o $\beta$-tiofeno grupės pakaitas paverčia žymeklį poliškumo jutikliu. Be to, abu jutikliai gali būti naudojami taikant fluorescencinę vaizdavimo mikroskopiją, taip vizualizuojant mikroaplinkos pokyčius gyvų ląstelių lipidų lašeliuose.

# COPIES OF PUBLICATIONS

# P1

# Cyclopropyl Substituents Transform the Viscosity-Sensitive BODIPY Molecular Rotor into a Temperature Sensor

A. Vyšniauskas, B. Cornell, P. S. Sherin, **K. Maleckaitė**, M. Kubánková, M. A. Izquierdo, T. T. Vu, Y. A. Volkova, E. M. Budynina, C. Molteni, M. K. Kuimova

ACS Sens. **6**(6), 2158—2167 (2021)
DOI: 10.1021/acssensors.0c02275

Reprinted from *ACS Sensors*
with permission from American Chemical Society.

Supporting information: https://pubs.acs.org/doi/suppl/10.1021/acssensors.0c02275/suppl_file/se0c02275_si_001.pdf

ACS SENSORS

pubs.acs.org/acssensors

Article

# Cyclopropyl Substituents Transform the Viscosity-Sensitive BODIPY Molecular Rotor into a Temperature Sensor

Aurimas Vyšniauskas, Bethan Cornell, Peter S. Sherin, Karolina Maleckaitė, Markéta Kubánková, Maria Angeles Izquierdo, Thanh Truc Vu, Yulia A. Volkova, Ekaterina M. Budynina, Carla Molteni, and Marina K. Kuimova*

Cite This: *ACS Sens.* 2021, 6, 2158−2167

Read Online

ACCESS | Metrics & More | Article Recommendations | Supporting Information

**ABSTRACT:** A quantitative fluorescent probe that responds to changes in temperature is highly desirable for studies of biological environments, particularly *in cellulo*. Here, we report new cell-permeable fluorescence probes based on the BODIPY moiety that respond to environmental temperature. The new probes were developed on the basis of a well-established BODIPY-based viscosity probe by functionalization with cyclopropyl substituents at $\alpha$ and $\beta$ positions of the BODIPY core. In contrast to the parent BODIPY fluorophore, $\alpha$-cyclopropyl-substituted fluorophore displays temperature-dependent time-resolved fluorescence decays showing greatly diminished viscosity dependence, making it an attractive sensor to be used with fluorescence lifetime imaging microscopy (FLIM). We performed theoretical calculations that help rationalize the effect of the cyclopropyl substituents on the photophysical behavior of the new BODIPYs. In summary, we designed an attractive new quantitative FLIM-based temperature probe that can be used for temperature sensing in live cells.

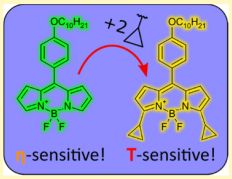


**KEYWORDS:** *fluorescence spectroscopy, temperature sensing, fluorescence microscopy, FLIM, BODIPY fluorophores*

Downloaded via VILNIUS UNIV on July 30, 2021 at 11:39:43 (UTC).
See https://pubs.acs.org/sharingguidelines for options on how to legitimately share published articles.

Numerous normal and abnormal intracellular processes generate heat or are affected by temperature, and examples include respiration, thermogenesis,[1,2] and cell division.[3] Also, some cancer tissues are known to produce more heat than healthy cells.[4] Therefore, the ability to measure temperature, particularly at the intracellular level, is highly sought after. Moreover, intracellular temperature probes could aid in studying and detecting the onset of various diseases that produce a change in temperature.

A number of different spectroscopic temperature probes have been developed in recent years,[5−7] for example, temperature-sensitive nanoparticles, such as quantum dots[8−10] or nanodiamonds.[11] Temperature-sensitive nanogels[12] and polymers[13−15] were also used as temperature sensors. Moreover, lanthanide complexes[16−18] and organic fluorophores[19−24] were used for temperature sensing. The latter have a number of important advantages over other groups of temperature sensors. Their structure can be easily customized to ensure targeting of the organelles of interest, minimizing toxicity and enabling cell permeabilization, which is normally a challenge for temperature-sensitive polymers.[25] Finally, due to their size, small organic fluorophores are attractive temperature probes as they are expected to minimally perturb cellular functions, compared to other groups of temperature sensors reported to date.

At the basis of temperature sensitivity of small-molecule fluorescence is the internal conformational flexibility of such dyes, leading to nonradiative excited-state decay that can be affected by temperature. An efficient excited-state deactivation becomes faster when the temperature is increased, leading to lower emission intensities and faster time-resolved excited-state decays. The most reliable and quantitative way to perform temperature sensing using fluorescence is by exploiting temperature-dependent fluorescence lifetimes derived from their time-resolved decays. Assessing temperature by monitoring fluorescence intensity is also a possibility but fluorescence intensity may be affected by various other factors, such as nonuniform distribution of fluorophores inside the cell, or variations in excitation intensity, *e.g.*, following a change in the refractive index of the inhomogeneous cellular environment. Fluorescence lifetime is not affected by variations in concentration, as long as the aggregation and self-quenching are absent. Furthermore, temperature imaging can be achieved when temperature-sensitive fluorophores are used in combination with fluorescence lifetime imaging microscopy (FLIM).[13]

Previously, we reported temperature-sensitive fluorophores emitting in the orange-to-red region of the visible spectrum.

**Received:** October 30, 2020
**Accepted:** May 14, 2021
**Published:** June 1, 2021






© 2021 American Chemical Society



https://doi.org/10.1021/acssensors.0c02275
*ACS Sens.* 2021, 6, 2158−2167

The probes were based on the boron-dipyrromethene (BODIPY) fluorophore structure, a so-called "molecular rotor."[26] By extending the conjugation *via* aromatic substitution to the viscosity-sensitive BODIPY-$C_{10}$[27−30] (shown in Chart 1), we shifted the absorption/emission spectra of the

**Chart 1. Molecular structures of the viscosity sensor BODIPY-$C_{10}$ and its $\beta$-(BODIPY2) and $\alpha$- (BODIPY3) cyclopropyl derivatives studied in this work**

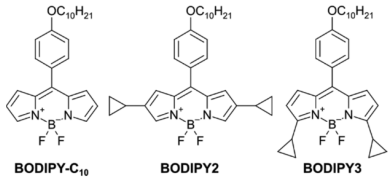


new fluorophores into the red, which should, in principle, allow deeper tissue penetration in biological imaging. Unexpectedly, this substitution also achieved temperature sensitivity of fluorescence, instead of viscosity sensitivity. Unfortunately, these previously reported fluorophores were not able to internalize into biological cells, possibly due to their bulky naphthalene and phenanthrene substituents, limiting their aqueous solubility and, hence, bioavailability. The rationale for the switch between the viscosity and temperature sensitivity was not clear at that time since the viscosity-sensing design (the rotation of the phenyl ring relative to the BODIPY core) was preserved in the temperature sensors.

In this work, we report new BODIPY fluorophores with a unique substituent—cyclopropyl group (Chart 1). We explore the spectroscopic properties of the probes at conditions of varying temperatures, viscosities, and solvent polarities. We demonstrate that these dyes exhibit a significant red shift in fluorescence and good biocompatibility suitable for cellular imaging. We perform cellular imaging using FLIM to produce reliable temperature readings in the intracellular environment. Finally, we rationalize the mechanism of temperature sensing of these new dyes using density functional theory (DFT) and time-dependent density functional theory (TDDFT) calculations.

## RESULTS AND DISCUSSION

**Probe Design.** Our previous experiments established that in BODIPY-based environmentally sensitive fluorophores such as BODIPY-$C_{10}$ (Chart 1), extending the conjugation dramatically changes the spectroscopic properties. The parent BODIPY-$C_{10}$ is a green emitter ($\lambda_{max}$ = 515 nm) and shows excellent sensitivity to viscosity but not to the temperature of its environment.[30,31] However, introducing double and triple bonds at the $\alpha$ positions of the fluorophore (relative to the boron atom) not only results in a marked red shift of emission but also results in quantum yields close to unity, which makes these dyes unsuitable for environmental sensing.[32] Interestingly, introducing naphthalene and phenanthrene substituents at the $\alpha$ positions, produced a red-shifted BODIPY sensor, which was sensitive to the temperature and not to the viscosity of its environment.[26] In the search for a smaller, less bulky substituent that may produce a more biocompatible temperature sensor, we considered a cyclopropyl substituent. Even though cyclopropane contains only single carbon−carbon bonds, it is expected to have an intermediate character between $sp^3$- and $sp^2$-hybridized carbon atoms.[33−35] To our knowledge, the ability of cyclopropyl substituents to tune the properties of fluorophores has been exploited very little. Here, we synthesized and characterized two new FLIM-based BODIPY temperature sensors that readily internalize into cells, with monoexponential time-resolved fluorescence decays that allow easy data interpretation.

The synthesis and characterization of the new BODIPY derivatives BODIPY2 and BODIPY3 (Chart 1) are detailed in the Electronic Supporting information (SI).

**Spectroscopic Properties.** Significant changes occur in the absorption and emission spectra upon introducing cyclopropyl substituents at the $\alpha$ and $\beta$ positions of BODIPY-$C_{10}$ (Figure 1A). First, there is a significant bathochromic shift in both absorption and emission wavelengths. While it is moderate for BODIPY3 in the case of $\alpha$-substitution (∼25 nm), it is more significant in the case of $\beta$-substitution in BODIPY2 (∼60 nm). Second, the spectra of BODIPY2 are significantly broadened and the fluorophore has substantially larger Stokes shifts, 1200 $cm^{-1}$ instead of 300 $cm^{-1}$ in the case of BODIPY3 (Table S2, SI). Last, the second absorption peak situated at 350−400 nm is significantly more intense for BODIPY2 than for the other two fluorophores. A larger Stokes shift and broadened bands were also observed for BODIPYs containing styryl[36] and 2-thienyl[37] substituents at the $\beta$ position.

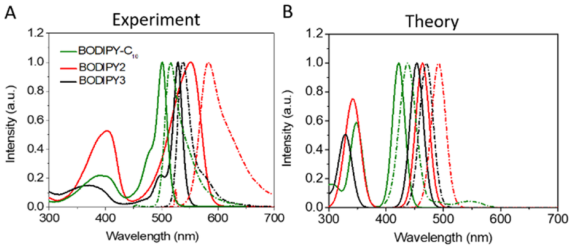


**Figure 1.** Experimental (A) and theoretical (B) spectra of BODIPY-$C_{10}$ (green), BODIPY2 (red), and BODIPY3 (black) in toluene. The absorption spectra are shown as solid lines, while the fluorescence spectra are shown as dash-dotted lines.


https://doi.org/10.1021/acssensors.0c02275
ACS Sens. 2021, 6, 2158−2167

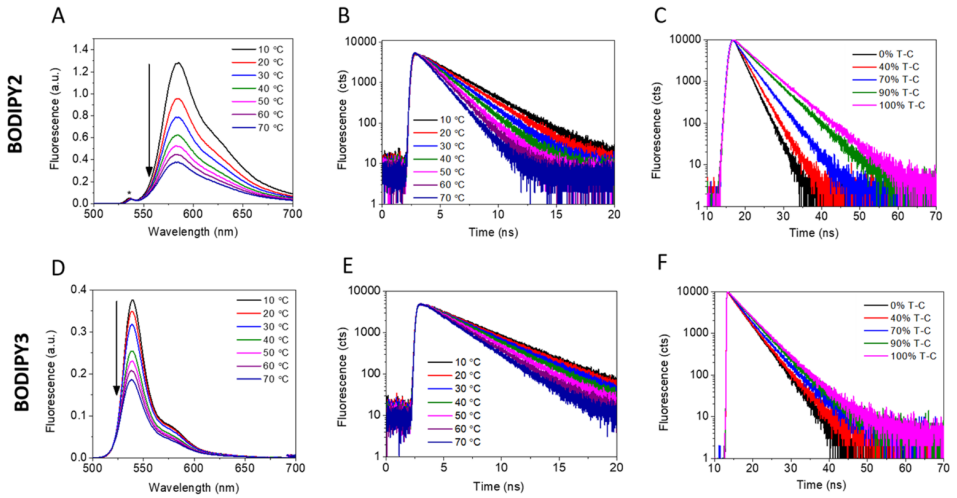


**Figure 2.** Temperature and viscosity sensitivities of BODIPY2 (top panels) and BODIPY3 (bottom panels). Temperature-dependent fluorescence spectra (A) and time-resolved fluorescence decays (B) of BODIPY2 in toluene. The peak marked by asterisk (*) arises from the excitation source. (C) Fluorescence decays of BODIPY2 in toluene−castor oil mixtures of different viscosities. (D) Temperature-dependent fluorescence spectra of BODIPY3. The arrows in (A) and (D) show the decrease in fluorescence intensity with increasing temperature. (E) Fluorescence decays of BODIPY3 at different temperatures in toluene. (F) Fluorescence decays of BODIPY3 in toluene−castor oil mixtures of different viscosities. The fitted lifetime values (monoexponential fit) are shown in Figure S2, SI. The legends in (C) and (F) show the volume fraction of castor oil in the mixture, with viscosities in the range 0.6−920 cP.

We further rationalize these observations by performing TDDFT calculations of absorption and emission spectra of all three fluorophores. For computational efficiency, the $-OC_{10}H_{21}$ group was truncated to a $-OCH_3$ group in all calculations. It is well known that TDDFT methods usually overestimate the absorption and emission energies of BODIPY fluorophores,[38,39] as is the case with our results. Nevertheless, the calculated spectra (Figure 1B) accurately reproduce the trend in maximum absorption and emission wavelengths seen in the experimental spectra. The bathochromic shift observed in cyclopropane-containing BODIPYs is caused by a smaller highest occupied molecular orbital−lowest unoccupied molecular orbital (HOMO−LUMO) gap due to the delocalization of frontier HOMO and LUMO over the cyclopropyl substituents (Figure S1, SI). The oscillator strengths for the $S_0$−$S_1$ transition are shown in Table S1, SI.

**Temperature and Viscosity Sensitivities of BODIPY2 and BODIPY3.** BODIPY2 and BODIPY3 readily dissolve in a wide range of organic solvents, which allows for testing their temperature, polarity, and viscosity-dependent properties. We tested the temperature sensitivity of BODIPY2 and BODIPY3 by recording the fluorescence spectra and time-resolved decays in toluene at temperatures between 10 and 70 °C (Figure 2). While the shape of the emission band at increasing temperature remained the same, the emission intensity progressively decreased (Figure 2A,D). This suggests that the nonradiative relaxation of both fluorophores is faster at increasing temperatures. The same conclusion follows from fluorescence decays, which show considerably shorter fluorescence lifetimes at increasing temperatures (Figure 2B,E).

Next, we have explored the viscosity-dependent properties of the new probes in toluene−castor oil mixtures of different viscosities, ranging from 0.6 to 920 cP, at room temperature. Such viscosity range sufficiently covers viscosities that could be expected in the intracellular environment.[40] Figure 2C shows that the fluorescence decays of BODIPY2 show significant sensitivity to viscosity, although not as high as the one of the parent fluorophore BODIPY-$C_{10}$. The viscosity dependence of fluorescence lifetimes of all three fluorophores is compared in Figure S2, SI. In contrast to BODIPY2 and BODIPY-$C_{10}$, the viscosity sensitivity of BODIPY3 is very weak (Figure 2F). Due to its very low sensitivity to viscosity, BODIPY3 can be used as a temperature sensor, at least in nonpolar solvents (*vide infra*). In comparison, BODIPY2 could be used as a viscosity or as a temperature sensor, but only on the condition that one of these parameters is fixed during the course of the experiment.

Similar to the naphthyl-substituted BODIPY previously reported by us,[26] BODIPY3 appeared to have lost its sensitivity to viscosity and, instead, became sensitive to temperature. However, the size of the fluorophore and its hydrophobicity are reduced compared to naphthalene derivatives, while the monoexponential fluorescence decay remained preserved in BODIPY3. This makes this probe a reliable sensor of temperature *via* lifetime,[41] hopefully suitable for biological environments.

**Polarity Sensitivities of BODIPY2 and BODIPY3.** The previously synthesized BODIPY fluorophores with substituents at $\alpha$ and $\beta$ positions were shown to be polarity-sensitive.[26,36,37] In order to have the full picture of how various environmental parameters can affect the spectroscopic properties of BODIPY2 and BODIPY3, we have examined the effect of


https://doi.org/10.1021/acssensors.0c02275
ACS Sens. 2021, 6, 2158−2167

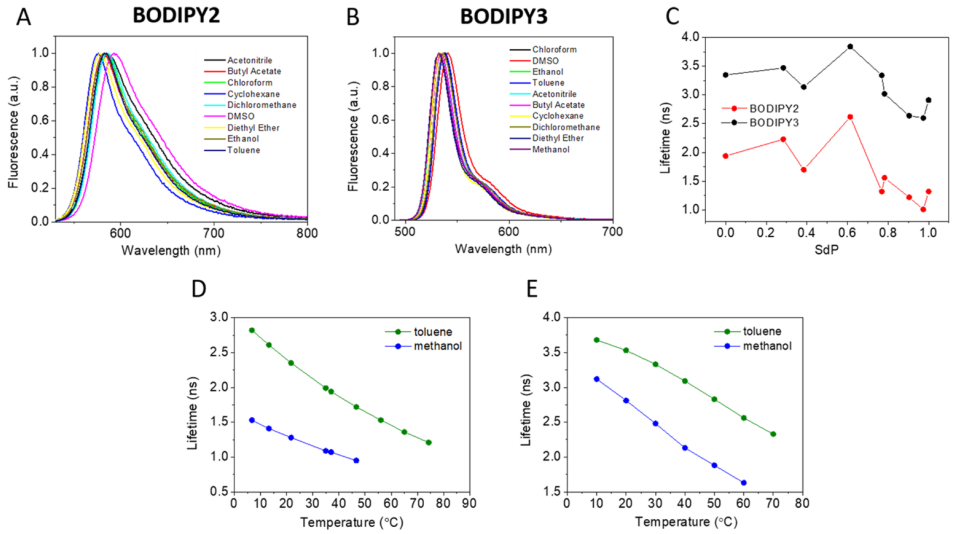


**Figure 3.** Effect of solvent polarity on the spectroscopic properties of BODIPY2 and BODIPY3. Fluorescence spectra of BODIPY2 (A) and BODIPY3 (B) in various solvents. (C) Fluorescence lifetimes of both fluorophores with respect to the solvent dipolarity parameter (SdP). Fluorescence lifetime dependence on temperature for BODIPY2 (D) and BODIPY3 (E) in a nonpolar solvent (toluene) and a polar solvent (methanol).

solvent polarity on these fluorophores at room temperature (Figure 3). Both molecules demonstrate slight solvatochromic shifts of their absorption (Figure S3, SI) and fluorescence (Figure 3A,B) in different solvents. The peaks of absorption and emission together with the values of Stokes shifts in various solvents are given in Table S2 (SI), and the quantum yields of fluorescence are shown in Table S3, SI. While the emission bands are not significantly affected by polarity, time-resolved fluorescence decays demonstrate stronger dependence (lifetime values are shown in Table S4, SI). Fluorescence lifetimes of BODIPY2 and BODIPY3 decreased with increasing the solvent dipolarity parameter (SdP)[42] (Figure 3C). These data demonstrate that the influence of polarity is significant and cannot be ignored, particularly at higher polarities. The uncertainty in lifetime estimation from monoexponential decays that have >1000 photons at the peak is <5%,[41] which is far less than the variation in lifetime values seen in Figure 3C as a function of SdP. The nonsmooth trend of lifetime values likely signifies that BODIPY2 and BODIPY3 are additionally affected by other properties of the solvents tested, besides solvent dipolarity. The notable exception from the nonsmooth trend is chloroform (SdP = 0.6), with high lifetime values observed for both dyes.

Finally, we have examined how the temperature sensitivity of BODIPY2 and BODIPY3 is affected in environments of different polarities (Figure 3D,E). Two representative solvents were chosen, a nonpolar solvent toluene and a polar solvent methanol. Both BODIPY dyes showed similar temperature sensitivity (the gradients of all graphs are approximately the same), although BODIPY3 had higher lifetime values than BODIPY2 in both solvents. The relative sensitivities[43] of BODIPY2 to temperature were 0.84%/°C (toluene) and 1.0%/°C (methanol). The sensitivities of BODIPY3 were 0.63%/°C (toluene) and 0.95%/°C (methanol).

Overall, these data are consistent with what was previously observed for naphthalene-BODIPY dyes, which possessed polarity-sensitive fluorescence lifetimes at high polarity (SdP > 0.6) but showed no polarity sensitivity for solvents with SdP <0.5.[26] Regarding different solvents, while the magnitude of lifetime decrease with increasing temperature (the gradient of the graph in Figure 3D,E) is similar in all solvents, the lifetime values themselves are significantly different. Therefore, care must be taken to make sure that the sensors are calibrated in the same polarity environment when performing the temperature measurements of interest. On the other hand, these molecules may be also used as polarity sensors, as long as the temperature is kept constant during the experiment.

**Rationalization of Temperature Dependence of BODIPY2 and BODIPY3.** Judging by the structure alone, the temperature sensitivity and the lack of viscosity sensitivity in cyclopropyl-derivatives BODIPY2 and BODIPY3 is surprising, when compared to the parent viscosity sensor BODIPY-$C_{10}$, which shows only weak temperature sensitivity.[30] Both new cyclopropyl-functionalized dyes have the rotatable phenyl group identical to the parent BODIPY-$C_{10}$ with no hindrance to rotation. However, these new dyes follow the same trend previously observed for naphthalene and phenanthrene BODIPY derivatives.[26]

The temperature sensitivity of fluorescent dyes is caused by the thermal activation of a nonradiative relaxation pathway. It usually has the following dependence on temperature

$$k_{nr}(T) = Ae^{-E_a/kT} \quad (1)$$



https://doi.org/10.1021/acssensors.0c02275
ACS Sens. 2021, 6, 2158−2167

where $k_{nr}$ is a nonradiative relaxation rate, $E_a$ is the activation energy barrier, $k$ is the Boltzmann's constant, $A$ is a constant, and $T$ is the temperature. Consequently, the fluorescence lifetime is expressed as

$$\tau = \frac{1}{k_f + k_{nr} + k_{nr}(T)} = \frac{1}{k_f + k_{nr} + Ae^{-E_a/kT}} \quad (2)$$

where $k_f$ is the rate constant of fluorescence and $k_{nr}$ is the rate constant of any nonradiative relaxation that is not temperature-dependent. We used this equation to fit temperature-dependent fluorescence lifetimes of BODIPY2 and BODIPY3 (Figure 3D,E) to obtain energy barrier heights for nonradiative relaxation (Figure S7). The values we obtained were 0.14−0.16 eV for BODIPY2 and 0.21−0.26 eV for BODIPY3.

It has been shown theoretically that phenyl-BODIPYs can nonradiatively relax at the geometry with a torsional angle close to 0°.[44,45] To reach this point, the fluorophore needs to overcome the energy barrier in the $S_1$ state. To determine if cyclopropyl substituents affect the energy barrier for nonradiative relaxation, we performed DFT and TDDFT calculations of BODIPY2, BODIPY3, and the parent viscosity-sensitive rotor BODIPY-$C_{10}$. The ground and the first excited singlet-state potential energy surfaces as a function of the dihedral angle between the BODIPY core and the phenyl ring are shown in Figure 4. In the ground state, the

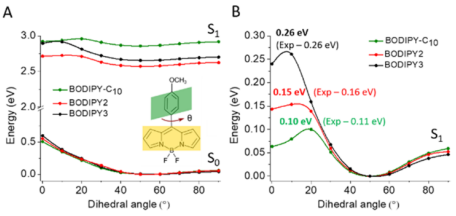


**Figure 4.** (A) Calculated potential energy surfaces for the ground ($S_0$) and the first excited ($S_1$) states with respect to the dihedral angle between the BODIPY core and the phenyl ring ($\theta$) in toluene; the zero of the energy scale corresponds to the ground state minimum. (B) Potential energy surfaces of the $S_1$ state in toluene showing different barrier heights for all three fluorophores. Experimentally obtained energy barrier values (color-coded for each BODIPY) are also shown. The minima of the $S_1$ surfaces are set to 0 eV. The $-OC_{10}H_{21}$ group in fluorophores was truncated to the $-OCH_3$ group for computational effieciency.

energy curves are nearly identical for the three fluorophores; the differences arise in the first excited state. A detailed comparison of the $S_1$ energy barriers for the three fluorophores is shown in Figure 4B, where the curves are shifted to have a common minimum energy value. It is clear that the introduction of cyclopropanes significantly increases the $S_1$ energy barrier for the phenyl rotation, especially noticeable for BODIPY3. The calculated values are shown in Figures 4B and S7 and they closely match the experimentally determined values. Most likely, the higher barrier for BODIPY3 is observed due to the stronger steric repulsion of the cyclopropanes at the $\alpha$ position, as the decrease of the dihedral angle is accompanied by the bending of the BODIPY core.[44,46] A similar effect has been shown previously by Liu et al. upon introducing methyl groups in the same position.[47] The obtained energy barrier height for BODIPY-$C_{10}$ also closely matches previous theoretical results[48] and its experimental estimate.[30]

Our theoretical results suggest the following explanation for the significant reduction of viscosity dependence and the gain in temperature sensitivity of cyclopropane-BODIPYs. The significant increase in $S_1$ barrier heights upon adding cyclopropyl substituents must cause the nonradiative relaxation (through rotation to torsional angle close to 0°) to become much slower. Therefore, even in a low-viscosity environment, BODIPY2 and BODIPY3 have fluorescence lifetimes of a few nanoseconds, a tenfold increase compared to BODIPY-$C_{10}$. Thus, an increasing viscosity makes a much weaker impact on the fluorescence lifetime, as the nonradiative relaxation is already insignificant, even in low-viscosity solvents. As the energy barrier for the phenyl group rotation in BODIPY2 is not as high as that in BODIPY3, BODIPY2 preserves a fraction of its viscosity sensitivity (characteristic of the parent compound BODIPY-$C_{10}$), while the viscosity sensitivity of BODIPY3 is greatly diminished. However, increasing the temperature increases the nonradiative relaxation in both new dyes, BODIPY2 and BODIPY3, particularly since the barrier height is larger, as the nonradiative relaxation rate is proportional to $e^{-Ea/kT}$. As a result, an $S_1$ barrier larger than 0.10 eV for the nonradiative relaxation leads to diminished viscosity dependence but amplified temperature sensitivity.

**Application of BODIPY3 in Lipid Vesicles and Live Cells.** Having rationalized the sensing behavior of the new dyes and characterized their temperature responses, we attempted to use BODIPY2 and BODIPY3 for temperature sensing in an intracellular environment.

Both fluorophores readily internalized into live cells following 12 h incubation at 37 °C. This is a significant improvement on our previously reported temperature-sensitive BODIPY probes containing naphthyl substituents, which failed to interact with live cells at any tested conditions, possibly due to a bulky nature of substituents and poor aqueous solubility.[26] It should be noted that even though BODIPY2 and BODIPY3 have very similar structures, the incubation with BODIPY3 resulted in noticeably brighter cellular fluorescence, as compared to BODIPY2 at identical conditions (Figure S4, SI). Furthermore, biexponential decay kinetics were recorded for BODIPY2 in FLIM of live cells (Figure S5), consistent with the aggregation of this dye.[29] No aggregation-like features were observed in the time-resolved decays of BODIPY3 in cells, at least at the conditions used in our experiments. As a result, we used BODIPY3 for all further cellular experiments.

Judging from the fluorescence intensity images (Figure 5, top panel), the fluorophore appears to localize diffusely in the cytoplasm, with some punctate bright staining, presumably of hydrophobic organelles. Given the hydrophobicity of the fluorophore, and its similarity to the parent BODIPY-$C_{10}$, it is most likely that it resides in the lipid membranes of organelles (*e.g.*, in lysosomes) and in lipid droplets. This staining pattern is similar to what was previously observed for BODIPY-$C_{10}$[27] (Figure S12).

Next, we performed FLIM imaging of U2OS cells containing BODIPY3 at a variable temperature to check if the fluorophore remains temperature-sensitive in the intracellular environment (Figure 5). During the imaging, the temperature in the chamber containing live cells was varied from 11 to 37 °C, which is in the range compatible with normal cell function. The brightfield images of cultured cells are shown in Figure S9,


https://doi.org/10.1021/acssensors.0c02275
ACS Sens. 2021, 6, 2158−2167

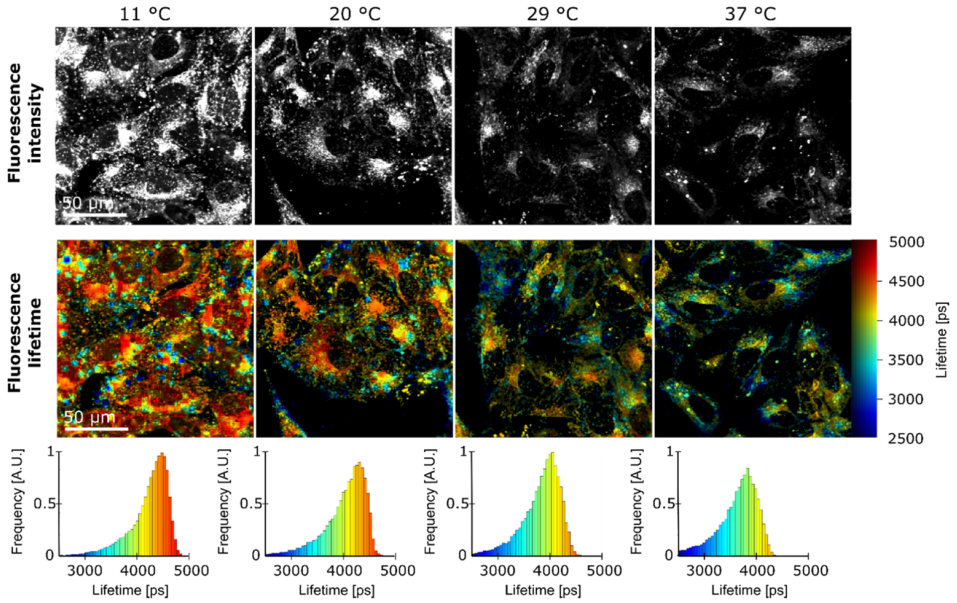


**Figure 5.** Fluorescence imaging of BODIPY3 in U2OS cells at a variable temperature between 11 and 37 °C. The top panels show fluorescence intensity images (the same intensity scale is kept between the images). FLIM images are shown in the middle panels; the lifetime range of 2500−5000 ps is kept constant between images. The corresponding lifetime histograms are shown in the bottom panels. The lifetime of BODIPY3 shows a clear decrease with increasing temperature.

SI, confirming their normal morphology, while the fluorescence intensity images before and after FLIM measurements are shown in Figure S10, SI. Fluorescence intensity images (Figure 5, top panel) demonstrate that fluorescence intensity decreased with increasing temperature. Furthermore, FLIM images (Figure 5, middle panel) show that the lifetime of BODIPY3 inside the cells remained temperature sensitive, as can be seen in the lifetime histograms in Figure 5. The lifetime−intensity correlation plots for each image are shown in Figure S11, SI, and confirm there is no significant correlation.

Notably, even in a complex intracellular environment, the BODIPY3 fluorescence decays remained monoexponential (Figure S6, SI). This is an important advantage over previously reported temperature probes, which show multiexponential decay kinetics.[13,22,26] This property makes BODIPY3 a more reliable probe since undesired behavior inside cells such as aggregation would reveal itself as additional exponential component(s) (as observed, for example, for BODIPY2, Figure S5). Additionally, significantly lower counts are required to fit monoexponential decay traces, allowing much faster data collection times.[41]

We also attempted to incubate cells with a tenfold lower concentration of BODIPY3 (0.5 $\mu$M) to verify whether lower concentration may affect the detected lifetime (Figure S8, SI). The decays remained monoexponential, and the lifetime values obtained in both cases (0.5 and 5 $\mu$M) were nearly identical (Figure 6). These data indicate that the dye's behavior in cells is not altered upon 10-fold dilution in the incubation medium

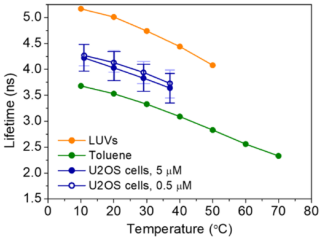


**Figure 6.** Temperature-dependent fluorescence lifetimes of BODIPY3 in U2OS cells (blue) at two concentrations of BODIPY3 in the incubation medium. The error bars are equal to one standard deviation from the mean lifetime values. Fluorescence lifetimes in toluene (green) and 1,2-dioleoyl-*sn*-glycero-3-phosphocholine (DOPC) large unilamellar vesicles (LUVs) are provided for comparison.

and gives evidence that the lifetime of BODIPY3 is not likely to be impacted by aggregation in cells. The temperature-dependent slope of fluorescence lifetimes recorded for BODIPY3 in cells closely matches the trend obtained in toluene, confirming that the temperature sensitivity was retained, with 20 ps/°C (Figure 6). However, the lifetime values in cells are higher compared to the values seen in toluene, which could be caused by a mild viscosity sensitivity of BODIPY3 (Figure 2F).



https://doi.org/10.1021/acssensors.0c02275
ACS Sens. 2021, 6, 2158−2167

For comparison, we also recorded FLIM images of BODIPY-$C_{10}$, which displays a similar intracellular localization pattern to BODIPY3 (Figure S12). The temperature was varied between 14 and 37 °C, and we recorded a significant lifetime variation in the images, from 2.01 ± 0.13 to 1.67 ± 0.13 ns (the values with errors correspond to histogram maxima and full widths at half-maximum (FWHM) of the distributions; Figure S12). However, in the case of BODIPY-$C_{10}$, this change in lifetime is almost entirely due to a viscosity change. Using a calibration graph (Figure S2), we can assign this difference in lifetime to a viscosity change from 140 cP (14 °C) to 80 cP (37 °C). According to our calibration data (Figure S2), such a change in viscosity will induce a lifetime reduction of less than 0.05 ns (1%) in BODIPY3. This could be contrasted to the 13% change (0.55 ns) seen in our cell data. Thus, our data indicate that viscosity change contributes insignificantly to the temperature-induced changes seen with BODIPY3 in live cells. We formed large unilamellar vesicles (LUVs) composed of unsaturated lipid 1,2-dioleoyl-*sn*-glycero-3-phosphocholine (DOPC) with BODIPY3 incorporated at a 1:200 dye/lipid ratio. The lifetimes of BODIPY3 were measured in LUVs at different temperatures (Figures 6 and S13, SI). As expected, the fluorescence decays of BODIPY3 remained monoexponential in these model membranes (Figure S13A), which are expected to have a viscosity range of 30−400 cP at this temperature range.[49] However, unexpectedly, the lifetimes were slightly higher than those recorded in live cells or in toluene at similar temperatures. We do not believe that viscosity is likely to play a role in this lifetime increase since we expect cellular lipid bilayers to be more viscous compared to DOPC bilayers that do not contain cholesterol or sphingomyelin and do not have any ordered domains.[50] Previously, we extensively characterized the position of the parent BODIPY-$C_{10}$ in model membranes[29,49] experimentally and through molecular dynamics simulations. Based on the spectroscopic and FLIM data, we can assume that due to a similar structure and an identical $C_{10}H_{21}$ substituent, the new dyes (at least BODIPY3) display a similar localization.

Notably, the lifetimes obtained in cells are lower than those in DOPC LUVs, which we expect to have very similar (or even slightly lower) viscosity values to lipid-rich organelles of cells, where BODIPYs are likely to localize.[49] We hypothesize that the reduction in lifetime observed in cells, as compared to nonpolar DOPC LUVs, might be caused by a more polar lipid environment in cells, which is likely to have a significant percentage of proteins and other components, as well as lipids. Our calibration data indicate that increased polarity can significantly reduce the lifetime of BODIPY3 (Figure 3C) while preserving its temperature sensitivity (*e.g.*, compare sensitivity in methanol and toluene, Figure 3E). In summary, our FLIM data in cells are in agreement with the fact that BODIPY3 resides in a lipid bilayer-like environment inside cells, where the lipid tail region is known to create a viscous environment, which is likely to be more polar than pure DOPC bilayer in model LUVs.[51]

## ■ CONCLUSIONS

We have shown that by introducing a unique and rarely used substituent—a cyclopropyl group—we were able to transform a fluorescent lifetime-based viscosity sensor into temperature sensor, BODIPY3, and suggested a mechanism for its temperature sensitivity. Additionally, we have demonstrated that BODIPY3 was able to easily internalize into live cells and accurately sense temperature in the intracellular environment. Even though more temperature-sensitive fluorophores have been reported previously,[20,21] our developed probes have important advantages. The new BODIPY fluorophores have temperature-dependent fluorescence lifetimes, which makes them suitable for temperature sensing *via* FLIM. Furthermore, the fluorescence decays of the new sensors were monoexponential, which is a significant improvement over previously reported temperature probes suitable for lifetime sensing. We have also performed theoretical calculations to explain why the addition of cyclopropyl substituents diminished viscosity sensitivity and caused temperature sensitivity of the fluorophores. We found that, as a result of the cyclopropyl substitution, a higher energy barrier for the rotation of the phenyl group in the excited singlet state, which is the motion thought to be responsible for the nonradiative deactivation of BODIPY-phenyl based sensors, has emerged. We interpret the barrier height as the reason for the new temperature sensitivity of our BODIPY-cyclopropyl substituted probes. Further development of the cyclopropyl-BODIPY probes and the enhancement of their temperature sensitivity is a subject of our ongoing work.

## ■ MATERIALS AND METHODS

**Materials.** Common reagents and organic solvents of spectroscopic grade were obtained from Sigma-Aldrich, except glycerol, which was obtained from Alfa-Aesar. SVM 3000 viscometer (Anton Paar) was used for measuring the viscosities of toluene−castor oil mixtures. The synthesis and characterization of BODIPY2 and BODIPY3 are described in the SI.

**Absorption and Fluorescence Spectra, and Quantum Yield Measurements.** Quartz cuvettes (10 mm) were used for all spectroscopic measurements. Absorption and fluorescence spectra were recorded using an Agilent 8453 UV−vis spectrophotometer and a Fluoromax-4 spectrofluorometer (Jobin-Yvon, Horiba), respectively. To calculate fluorescence quantum yields, Rhodamine 101 in ethanol containing 0.01% HCl was used as a standard ($\varphi_f$ = 1).[52] The temperature during fluorescence measurements was controlled using a Peltier thermostat F3004 (F3004, Jobin-Yvon; Horiba). The solution temperature was additionally verified by a thermocouple 2006T (Digitron).

**Fluorescence Decay Measurements.** Time-resolved fluorescence decays were measured using three different time-correlated single-photon counting (TCSPC) setups. The first one is based on the DeltaFlex TCSPC device (Horiba). The excitation sources were 404 and 571 nm NanoLEDs (Horiba). We used a 100 ns time window containing 4096 time bins. The fluorescence decays had 10 000 counts at the maximum. A circulating thermostat (RE104, Lauda Technology Ltd.) was used for controlling the temperature, which was verified by a 2006T thermocouple (Digitron). Time-resolved fluorescence decays were fitted using a monoexponential decay function. The resulting goodness-of-fit parameter $\chi^2$ was between 1.0 and 1.3. The second TCSPC setup was home-built and consisted of an SPC-830 photon counting card (Becker & Hickl), a BDL-488 SMN ps pulsed diode laser (Becker & Hickl), which was operated at 20 MHz frequency, a PMC-100-1 photomultiplier tube (Hamamatsu), a DCC-100 detector control module (Becker & Hickl), Omni-$\lambda$ grating monochromator (LOT-Quantum Design), and a cuvette holder (qpod) combined with TC125 Peltier thermostat (Quantum Northwest). The time window for acquiring fluorescence decays was 50 ns containing 4096 time bins. The third setup was based on an Edinburgh F-900 (Edinburgh Instruments) fluorimeter and excited using the WhiteLase Micro (Fianium) laser with 520 ± 5 and 540 ± 5 nm bandpass filters (Thorlabs). The instrument response function (IRF) for all setups was measured using a Ludox solution.


https://doi.org/10.1021/acssensors.0c02275
ACS Sens. 2021, 6, 2158−2167

**Large Unilamellar Vesicles (LUVs).** 1,2-Dioleoyl-*sn*-glycero-3-phosphocholine (DOPC, Avanti Polar Lipids) was used for making LUVs by extrusion. First, a chloroform solution containing DOPC and BODIPY3 was evaporated, which resulted in a dry film at a 200:1 lipid/dye ratio. The dry lipid film was suspended in 400 mM aqueous solution of sucrose, and the concentration of DOPC was 1 mM. The suspension was then extruded 11 times through a polycarbonate membrane containing 200 nm pores using an Avanti Mini-Extruder. Time-resolved fluorescence decays of fluorophores in DOPC LUVs were recorded using the aforementioned home-built TCSPC setup. The fluorescence was detected at 540 ± 5 nm. The time window was 50 ns containing 1024 channels.

**Cellular Imaging.** SK-OV-3 and U2OS cell lines were used, both of which were obtained from ECACC. Dulbecco's modified Eagle's medium (DMEM) containing 10% fetal bovine serum (FBS) was used for growing cells at 37 °C with 5% $CO_2$. Eight-well chamber slides (Lab-Tek) were used for seeding cells at 50 000 cells per well. The cells were then grown for 24 h and incubated in the growth medium, which contained 0.5 or 5 $\mu$M of the fluorophore, for 12 h. The cells were washed three times in Hank's balanced salt solution (HBSS) prior to imaging, also in HBSS. The cells were imaged in a chamber that was heated by a circulating thermostat (Lauda). Leica SP5-II microscope was used for imaging. FLIM imaging was performed using the microscope with an SPC-830 photon counting card (Becker & Hickl). Coherent Chameleon Ti:sapphire laser was used for two-photon excitation at 800 nm; 20× (HCX PL APO CS, N.A. = 0.7, Leica) objective was used. The fluorescence was detected over the 500−650 nm range. The size of FLIM images was 256 pixels × 256 pixels, with 256 time bins used for fluorescence decays. The IRF was obtained by measuring the second-harmonic generation (SHG) signal from urea. The FLIM data were analyzed using the FLIMfit software tool developed at Imperial College London[53] and SPCImage software (Becker & Hickl).

**Theoretical Calculations.** DFT and linear-response time-dependent DFT (TDDFT) calculations were carried out with the Gaussian 09 code,[54] for the molecules shown in Chart 1; however, the $C_{10}H_{21}$ group was substituted by a methyl group (as shown in Figure S1). This modification simplifies the calculation but does not alter the excited-state properties.[48] The CAM-b3lyp exchange and correlation functional and a 6-311++G(1d,2p) basis set were used.[55,56] Potential energy surfaces in the ground ($S_0$) and the first excited singlet state ($S_1$, which has predominantly a HOMO−LUMO character) were calculated as a function of the dihedral angle between the BODIPY core and the phenyl ring (Figure 4A). Toluene was added implicitly by the polarizable continuum model (PCM).[57−59] The linear response solvent formalism was employed. Toluene was chosen since it is a nonpolar solvent and is not expected to have a significant impact on the energy levels of the fluorophore. Additionally, toluene was extensively used during the experimental characterization of the fluorophores. Structures were relaxed with the dihedral angle constrained between 0 and 90° in 10° steps, and the zero of the energy scale was set to the ground-state energy minimum. The absorption spectra included 12 vertical excited states calculated for the ground-state minimal energy structure, with the dihedral angle at 50°, and a spectral Gaussian broadening of 13 nm. The emission spectra were calculated at the S1 minimal energy structure with the same broadening.

## ■ ASSOCIATED CONTENT

### Supporting Information

The Supporting Information is available free of charge at https://pubs.acs.org/doi/10.1021/acssensors.0c02275.

Additional spectroscopic data; organic synthesis and characterization (PDF)

The computational data that support the findings of this study are openly available in King's College London research data archive (http://doi.org/doi:10.18742/RDM01-731).

## ■ AUTHOR INFORMATION


### Corresponding Author

**Marina K. Kuimova** − *Department of Chemistry, Molecular Sciences Research Hub, White City Campus, Imperial College London, London W12 0BZ, U.K.*; orcid.org/0000-0003-2383-6014; Email: m.kuimova@imperial.ac.uk

### Authors

**Aurimas Vyšniauskas** − *Department of Chemistry, Molecular Sciences Research Hub, White City Campus, Imperial College London, London W12 0BZ, U.K.; Center of Physical Sciences and Technology, Vilnius 10257, Lithuania*; orcid.org/0000-0002-4750-8149

**Bethan Cornell** − *Physics Department, King's College London, London WC2R 2LS, U.K.*

**Peter S. Sherin** − *Department of Chemistry, Molecular Sciences Research Hub, White City Campus, Imperial College London, London W12 0BZ, U.K.*

**Karolina Maleckaitė** − *Center of Physical Sciences and Technology, Vilnius 10257, Lithuania*; orcid.org/0000-0002-4992-9158

**Markéta Kubánková** − *Department of Chemistry, Molecular Sciences Research Hub, White City Campus, Imperial College London, London W12 0BZ, U.K.*; orcid.org/0000-0001-7086-8938

**Maria Angeles Izquierdo** − *Department of Chemistry, Molecular Sciences Research Hub, White City Campus, Imperial College London, London W12 0BZ, U.K.*

**Thanh Truc Vu** − *Department of Chemistry, Molecular Sciences Research Hub, White City Campus, Imperial College London, London W12 0BZ, U.K.*

**Yulia A. Volkova** − *Department of Chemistry, Molecular Sciences Research Hub, White City Campus, Imperial College London, London W12 0BZ, U.K.; Zelinsky Institute of Organic Chemistry, Russian Academy of Sciences, Moscow 119991, Russia*; orcid.org/0000-0001-8554-838X

**Ekaterina M. Budynina** − *Department of Chemistry, Molecular Sciences Research Hub, White City Campus, Imperial College London, London W12 0BZ, U.K.; Department of Chemistry, Lomonosov Moscow State University, Moscow 119991, Russia*

**Carla Molteni** − *Physics Department, King's College London, London WC2R 2LS, U.K.*; orcid.org/0000-0002-0402-2376

Complete contact information is available at: https://pubs.acs.org/10.1021/acssensors.0c02275


### Author Contributions

All authors have given approval to the final version of the manuscript.

### Notes

The authors declare no competing financial interest.

## ■ ACKNOWLEDGMENTS

A.V. is thankful to the Research Council of Lithuania for a grant no. S-MIP-19-6. B.C. and C.M. thank the U.K. Engineering and Physical Science Research Council for computational support through the UKCP consortium (EP/P022472/1) and the Materials and Molecular Modelling Hub (partially funded by EP/P020194/1). This work was partially supported by the European Commission in the form of Marie Curie individual Fellowships to T.T.V., P.S.S. and M.A.I., M.K.

was supported by an EPSRC Doctoral Prize fellowship. M.K.K. is grateful to the EPSRC for a Career Acceleration Fellowship (EP/I003983/1).

## REFERENCES

(1) Bal, N. C.; Maurya, S. K.; Sopariwala, D. H.; Sahoo, S. K.; Gupta, S. C.; Shaikh, S. A.; Pant, M.; Rowland, L. A.; Bombardier, E.; Goonasekera, S. A.; Tupling, A. R.; Molkentin, J. D.; Periasamy, M. Sarcolipin Is a Newly Identified Regulator of Muscle-Based Thermogenesis in Mammals. *Nat. Med.* **2012**, *18*, 1575−1579.
(2) Tseng, Y.-H.; Cypess, A. M.; Kahn, C. R. Cellular Bioenergetics as a Target for Obesity Therapy. *Nat. Rev. Drug Discovery* **2010**, *9*, 465−482.
(3) Francis, D.; Barlow, P. W. In *Temperature and the Cell Cycle*, Symposia of the Society for Experimental Biology, 1988; pp 181−201.
(4) Stark, A. M.; Way, S. The Use of Thermovision in the Detection of Early Breast. *Cancer* **1974**, *33*, 1664−1670.
(5) Bai, T.; Gu, N. Micro/Nanoscale Thermometry for Cellular Thermal Sensing. *Small* **2016**, *12*, 4590−4610.
(6) Jaque, D.; Vetrone, F. Luminescence Nanothermometry. *Nanoscale* **2012**, *4*, 4301−4326.
(7) Quintanilla, M.; Liz-Marzán, L. M. Guiding Rules for Selecting a Nanothermometer. *Nano Today* **2018**, *19*, 126−145.
(8) Maestro, L. M.; Rodríguez, E. M.; Rodríguez, F. S.; La Cruz, M. C. I.; Juarranz, A.; Naccache, R.; Vetrone, F.; Jaque, D.; Capobianco, J. A.; Solé, J. G. CdSe Quantum Dots for Two-Photon Fluorescence Thermal Imaging. *Nano Lett.* **2010**, *10*, 5109−5115.
(9) Yang, J.-M.; Yang, H.; Lin, L. Quantum Dot Nano Thermometers Reveal Heterogeneous Local Thermogenesis in Living Cells. *ACS Nano* **2011**, *5*, 5067−5071.
(10) Qiu, X.; Zhou, Q.; Zhu, X.; Wu, Z.; Feng, W.; Li, F. Ratiometric Upconversion Nanothermometry with Dual Emission at the Same Wavelength Decoded via a Time-Resolved Technique. *Nat. Commun.* **2020**, *11*, No. 4.
(11) Kucsko, G.; Maurer, P. C.; Yao, N. Y.; Kubo, M.; Noh, H. J.; Lo, P. K.; Park, H.; Lukin, M. D. Nanometre-Scale Thermometry in a Living Cell. *Nature* **2013**, *500*, 54−58.
(12) Gota, C.; Okabe, K.; Funatsu, T.; Harada, Y.; Uchiyama, S. Hydrophilic Fluorescent Nanogel Thermometer for Intracellular Thermometry. *J. Am. Chem. Soc.* **2009**, *131*, 2766−2767.
(13) Okabe, K.; Inada, N.; Gota, C.; Harada, Y.; Funatsu, T.; Uchiyama, S. Intracellular Temperature Mapping with a Fluorescent Polymeric Thermometer and Fluorescence Lifetime Imaging Microscopy. *Nat. Commun.* **2012**, 3, No. 705.
(14) Qiao, J.; Qi, L.; Shen, Y.; Zhao, L.; Qi, C.; Shangguan, D.; Mao, L.; Chen, Y. Thermal Responsive Fluorescent Block Copolymer for Intracellular Temperature Sensing. *J. Mater. Chem.* **2012**, *22*, 11543−11549.
(15) Uchiyama, S.; Gota, C.; Tsuji, T.; Inada, N. Intracellular Temperature Measurements with Fluorescent Polymeric Thermometers. *Chem. Commun.* **2017**, *53*, 10976−10992.
(16) Zohar, O.; Ikeda, M.; Shinagawa, H.; Inoue, H.; Nakamura, H.; Elbaum, D.; Alkon, D. L.; Yoshioka, T. Thermal Imaging of Receptor-Activated Heat Production in Single Cells. *Biophys. J.* **1998**, *74*, 82−89.
(17) Vetrone, F.; Naccache, R.; Zamarron, A.; De La Fuente, A. J.; Sanz-Rodriguez, F.; Maestro, L. M.; Rodriguez, E. M.; Jaque, D.; Sole, J. G.; Capobianco, J. A. Temperature Sensing Using Fluorescent Nanothermometers. *ACS Nano* **2010**, *4*, 3254−3258.
(18) Mi, C.; Zhou, J.; Wang, F.; Lin, G.; Jin, D. Ultrasensitive Ratiometric Nanothermometer with Large Dynamic Range and Photostability. *Chem. Mater.* **2019**, *31*, 9480−9487.
(19) Homma, M.; Takei, Y.; Murata, A.; Inoue, T.; Takeoka, S. A Ratiometric Fluorescent Molecular Probe for Visualization of Mitochondrial Temperature in Living Cells. *Chem. Commun.* **2015**, *51*, 6194−6197.
(20) Arai, S.; Lee, S.-C.; Zhai, D.; Suzuki, M.; Chang, Y. T. A Molecular Fluorescent Probe for Targeted Visualization of Temperature at the Endoplasmic Reticulum. *Sci. Rep.* **2014**, *4*, No. 6701.
(21) Arai, S.; Suzuki, M.; Park, S.-J.; Yoo, J. S.; Wang, L.; Kang, N.-Y.; Ha, H.-H.; Chang, Y.-T. Mitochondria-Targeted Fluorescent Thermometer Monitors Intracellular Temperature Gradient. *Chem. Commun.* **2015**, *51*, 8044−8047.
(22) Itoh, H.; Arai, S.; Sudhaharan, T.; Lee, S.-C.; Chang, Y.-T.; Ishiwata, S.; Suzuki, M.; Lane, E. B. Direct Organelle Thermometry with Fluorescence Lifetime Imaging Microscopy in Single Myotubes. *Chem. Commun.* **2016**, *52*, 4458−4461.
(23) Hammerer, F.; Garcia, G.; Charles, P.; Sourdon, A.; Achelle, S.; Teulade-Fichou, M.-P.; Maillard, P. Glycoconjugated Porphyrin Dimers as Robust Ratiometric Temperature Sensors. *Chem. Commun.* **2014**, *50*, 9529−9532.
(24) Feng, J.; Tian, K.; Hu, D.; Wang, S.; Li, S.; Zeng, Y.; Li, Y.; Yang, G. A Triarylboron-Based Fluorescent Thermometer: Sensitive over a Wide Temperature Range. *Angew. Chem., Int. Ed.* **2011**, *50*, 8072−8076.
(25) Tsuji, T.; Yoshida, S.; Yoshida, A.; Uchiyama, S. Cationic Fluorescent Polymeric Thermometers with the Ability to Enter Yeast and Mammalian Cells for Practical Intracellular Temperature Measurements. *Anal. Chem.* **2013**, *85*, 9815−9823.
(26) Vu, T. T.; Méallet-Renault, R.; Clavier, G.; Trofimov, B. A.; Kuimova, M. K. Tuning BODIPY Molecular Rotors into the Red: Sensitivity to Viscosity vs. Temperature. *J. Mater. Chem. C* **2016**, *4*, 2828−2833.
(27) Kuimova, M. K.; Yahioglu, G.; Levitt, J. A.; Suhling, K. Molecular Rotor Measures Viscosity of Live Cells via Fluorescence Lifetime Imaging. *J. Am. Chem. Soc.* **2008**, *130*, 6672−6673.
(28) Sherin, P. S.; Lopez Duarte, I.; Dent, M. R.; Kubánková, M.; Vysniauskas, A.; Bull, J. A.; Reshetnikova, E. S.; Klymchenko, A. S.; Tsentalovich, Y. P.; Kuimova, M. K. Visualising Membrane Viscosity of Porcine Eye Lens Cells Using Molecular Rotors. *Chem. Sci.* **2017**, *8*, 3523−3528.
(29) Wu, Y.; Stefl, M.; Olzyńska, A.; Hof, M.; Yahioglu, G.; Yip, P.; Casey, D. R.; Ces, O.; Humpolíčková, J.; Kuimova, M. K. Molecular Rheometry: Direct Determination of Viscosity in Lo and Ld Lipid Phases via Fluorescence Lifetime Imaging. *Phys. Chem. Chem. Phys.* **2013**, *15*, 14986−14993.
(30) Vyšniauskas, A.; López-Duarte, I.; Duchemin, N.; Vu, T.-T.; Wu, Y.; Budynina, E. M.; Volkova, Y. A.; Peña Cabrera, E.; Ramírez-Ornelas, D. E.; Kuimova, M. K. Exploring Viscosity, Polarity and Temperature Sensitivity of BODIPY-Based Molecular Rotors. *Phys. Chem. Chem. Phys.* **2017**, *19*, 25252−25259.
(31) Vyšniauskas, A.; Kuimova, M. K. A Twisted Tale: Measuring Viscosity and Temperature of Microenvironments Using Molecular Rotors. *Int. Rev. Phys. Chem.* **2018**, *37*, 259−285.
(32) Qin, W.; Rohand, T.; Dehaen, W.; Clifford, J. N.; Driesen, K.; Beljonne, D.; Van Averbeke, B.; Van Auweraer, M. Der.; Boens, N. Boron Dipyrromethene Analogs with Phenyl, Styryl, and Ethynylphenyl Substituents: Synthesis, Photophysics, Electrochemistry, and Quantum-Chemical Calculations. *J. Phys. Chem. A* **2007**, *111*, 8588−8597.
(33) de Meijere, A. Bonding Properties of Cyclopropane and Their Chemical Consequences. *Angew. Chem., Int. Ed.* **1979**, *18*, 809−826.
(34) *The Chemistry of the Cyclopropyl Group*; Rappoport, Z., Ed.; Wiley: New York, 1987; Vol. *1*.
(35) *The Chemistry of the Cyclopropyl Group*; Rappoport, Z., Ed.; Wiley: New York, 1995; Vol. *2*.
(36) Gai, L.; Mack, J.; Lu, H.; Yamada, H.; Kuzuhara, D.; Lai, G.; Li, Z.; Shen, Z. New 2,6-Distyryl-Substituted BODIPY Isomers: Synthesis, Photophysical Properties, and Theoretical Calculations. *Chem. - Eur. J.* **2014**, *20*, 1091−1102.
(37) Chen, Y.; Zhao, J.; Guo, H.; Xie, L. Geometry Relaxation-Induced Large Stokes Shift in Red-Emitting Borondipyrromethenes (BODIPY) and Applications in Fluorescent Thiol Probes. *J. Org. Chem.* **2012**, *77*, 2192−2206.


https://doi.org/10.1021/acssensors.0c02275
*ACS Sens.* 2021, 6, 2158−2167

(38) Momeni, M. R.; Brown, A. Why Do TD-DFT Excitation Energies of BODIPY/Aza-BODIPY Families Largely Deviate from Experiment? Answers from Electron Correlated and Multireference Methods. *J. Chem. Theory Comput.* **2015**, *11*, 2619−2632.
(39) Schlachter, A.; Fleury, A.; Tanner, K.; Soldera, A.; Habermeyer, B.; Guilard, R.; Harvey, P. D. The TDDFT Excitation Energies of the BODIPYs; The DFT and TDDFT Challenge Continues. *Molecules* **2021**, *26*, No. 1780.
(40) Xiao, H.; Li, P.; Tang, B. Small Molecular Fluorescent Probes for Imaging of Viscosity in Living Biosystems. *Chem. - Eur. J.* **2020**, 6880−6898.
(41) Köllner, M.; Wolfrum, J. How Many Photons Are Necessary for Fluorescence-Lifetime Measurements? *Chem. Phys. Lett.* **1992**, *200*, 199−204.
(42) Catalán, J. Toward a Generalized Treatment of the Solvent Effect Based on Four Empirical Scales: Dipolarity (SdP, a New Scale), Polarizability (SP), Acidity (SA), and Basicity (SB) of the Medium. *J. Phys. Chem. B* **2009**, *113*, 5951−5960.
(43) Brites, C. D. S.; Lima, P. P.; Silva, N. J. O.; Millán, A.; Amaral, V. S.; Palacio, F.; Carlos, L. D. Thermometry at the Nanoscale. *Nanoscale* **2012**, *4*, 4799−4829.
(44) Prlj, A.; Vannay, L.; Corminboeuf, C. Fluorescence Quenching in BODIPY Dyes: The Role of Intramolecular Interactions and Charge Transfer. *Helv. Chim. Acta* **2017**, *100*, No. e1700093.
(45) Lin, Z.; Kohn, A. W.; Van Voorhis, T. Toward Prediction of Nonradiative Decay Pathways in Organic Compounds II: Two Internal Conversion Channels in BODIPYs. *J. Phys. Chem. C* **2020**, *124*, 3925−3938.
(46) Toliautas, S.; Dodonova, J.; Žvirblis, A.; Čiplys, I.; Polita, A.; Devižis, A.; Tumkevičius, S.; Šulskus, J.; Vyšniauskas, A. Enhancing the Viscosity-Sensitive Range of a BODIPY Molecular Rotor by Two Orders of Magnitude. *Chem. - Eur. J.* **2019**, *25*, 10342−10349.
(47) Liu, X.; Chi, W.; Qiao, Q.; Kokate, S. V.; Cabrera, E. P.; Xu, Z.; Liu, X.; Chang, Y. T. Molecular Mechanism of Viscosity Sensitivity in BODIPY Rotors and Application to Motion-Based Fluorescent Sensors. *ACS Sens.* **2020**, *5*, 731−739.
(48) Polita, A.; Toliautas, S.; Žvirblis, R.; Vyšniauskas, A. The Effect of Solvent Polarity and Macromolecular Crowding on the Viscosity Sensitivity of a Molecular Rotor BODIPY-C10. *Phys. Chem. Chem. Phys.* **2020**, *22*, 8296−8303.
(49) Dent, M. R.; Lopez Duarte, I.; Dickson, C. J.; Geoghegan, N. D.; Cooper, J. M.; Gould, I. R.; Krams, R.; Bull, J. A.; Brooks, N. J.; Kuimova, M. K. Imaging Phase Separation in Model Lipid Membranes Through the Use of BODIPY Based Molecular Rotors. *Phys. Chem. Chem. Phys.* **2015**, *17*, 18393−18402.
(50) Dent, M. R.; López-Duarte, I.; Dickson, C. J.; Chairatana, P.; Anderson, H. L.; Gould, I. R.; Wylie, D.; Vyšniauskas, A.; Brooks, N. J.; Kuimova, M. K. Imaging Plasma Membrane Phase Behaviour in Live Cells Using a Thiophene-Based Molecular Rotor. *Chem. Commun.* **2016**, *52*, 13269−13272.
(51) Marsh, D. Polarity and Permeation Profiles in Lipid Membranes. *Proc. Natl. Acad. Sci. U.S.A.* **2001**, *98*, 7777−7782.
(52) Karstens, T.; Kobs, K. Rhodamine B and Rhodamine 101 as Reference Substances for Fluorescence Quantum Yield Measurements. *J. Phys. Chem. A* **1980**, *84*, 1871−1872.
(53) Frisch, M. J.; Trucks, G. W.; Schlegel, H. B.; Scuseria, G. E.; Robb, M. A.; Cheeseman, J. R.; Scalmani, G.; Barone, V.; Petersson, G. A.; Nakatsuji, H.; Li, X.; Caricato, M.; Marenich, A.; Bloino, J.; Janesko, B. G.; Gomperts, R.; Mennucci, B.; Hratchian, H. P.; Ortiz, J. V.; Izmaylov, A. F.; Sonnenberg, J. L.; Williams-Young, D.; Ding, F.; Lipparini, F.; Egidi, F.; Goings, J.; Peng, B.; Petrone, A.; Henderson, T.; Ranasinghe, D.; Zakrzewski, V. G.; Gao, J.; Rega, N.; Zheng, G.; Liang, W.; Hada, M.; Ehara, M.; Toyota, K.; Fukuda, R.; Hasegawa, J.; Ishida, M.; Nakajima, T.; Honda, Y.; Kitao, O.; Nakai, H.; Vreven, T.; Throssell, K.; Montgomery, J. A., Jr.; Peralta, J. E.; Ogliaro, F.; Bearpark, M.; Heyd, J. J.; Brothers, E.; Kudin, K. N.; Staroverov, V. N.; Keith, T.; Kobayashi, R.; Normand, J.; Raghavachari, K.; Rendell, A.; Burant, J. C.; Iyengar, S. S.; Tomasi, J.; Cossi, M.; Millam, J. M.; Klene, M.; Adamo, C.; Cammi, R.; Ochterski, J. W.; Martin, R. L.; Morokuma, K.; Farkas, O.; Foresman, J. B.; Fox, D. J. *Gaussian 09*, revision A.02; Gaussian, Inc.: Wallingford CT, 2016.
(54) Frisch, M. J.; Trucks, G. W.; Schlegel, H. B.; Scuseria, G. E.; Robb, M. A.; Cheeseman, J. R.; Scalmani, G.; Barone, V.; Petersson, G. A.; Nakatsuji, H.; Li, X.; Caricato, M.; Marenich, A.; Bloino, J.; Janesko, B. G.; Gomperts, R.; Mennucci, B.; Hratchian, H. P.; Ort, J. V.; J, D.. *Gaussian 09*, revision D.01; Gaussian, Inc., 2016.
(55) Yanai, T.; Tew, D. P.; Handy, N. C. A New Hybrid Exchange−Correlation Functional Using the Coulomb-Attenuating Method (CAM-B3LYP). *Chem. Phys. Lett.* **2004**, *393*, 51−57.
(56) Hehre, W. J. Ab Initio Molecular Orbital Theory. *Acc. Chem. Res.* **1976**, *9*, 399−406.
(57) Miertuš, S.; Scrocco, E.; Tomasi, J. Electrostatic Interaction of a Solute with a Continuum. A Direct Utilizaion of AB Initio Molecular Potentials for the Prevision of Solvent Effects. *Chem. Phys.* **1981**, *55*, 117−129.
(58) Miertuš, S.; Tomasi, J. Approximate Evaluations of the Electrostatic Free Energy and Internal Energy Changes in Solution Processes. *Chem. Phys.* **1982**, *65*, 239−245.
(59) Pascual-Ahuir, J. L.; Silla, E.; Tuñon, I. GEPOL: An Improved Description of Molecular Surfaces. III. A New Algorithm for the Computation of a Solvent-Excluding Surface. *J. Comput. Chem.* **1994**, *15*, 1127−1138.


https://doi.org/10.1021/acssensors.0c02275
*ACS Sens.* 2021, 6, 2158−2167

# P2

# Designing a Red-Emitting Viscosity-Sensitive BODIPY Fluorophore for Intracellular Viscosity Imaging

**K. Maleckaitė**, J. Dodonova, S. Toliautas, R. Žilėnaitė, Dž. Jurgutis, V. Karabanovas, S. Tumkevičius, A. Vyšniauskas

*Chem. Eur. J.* **27**(67), 16768—16775 (2021)
DOI: 10.1002/chem.202102743

Reprinted from *Chemistry - A European Journal*
with permission from John Wiley and Sons.

Supporting information: https://shorturl.at/rtIR6

Chemistry–A European Journal
Full Paper
doi.org/10.1002/chem.202102743
Chemistry Europe
European Chemical Societies Publishing

# Designing a Red-Emitting Viscosity-Sensitive BODIPY Fluorophore for Intracellular Viscosity Imaging

Karolina Maleckaitė,[a] Jelena Dodonova,[b] Stepas Toliautas,[c] Rugilė Žilėnaitė,[a] Džiugas Jurgutis,[d] Vitalijus Karabanovas,[d, e] Sigitas Tumkevičius,[b] and Aurimas Vyšniauskas*[a]

**Abstract:** Viscosity imaging at a microscopic scale can provide important information about biosystems, including the development of serious illnesses. Microviscosity imaging is achievable with viscosity-sensitive fluorophores, the most popular of which are based on the BODIPY group. However, most of the BODIPY probes fluoresce green light, whereas the red luminescence is desired for the imaging of biological samples. Designing a new viscosity probe with suitable spectroscopic properties is a challenging task because it is difficult to preserve viscosity sensitivity after modifying the molecular structure. Here we describe how we developed a new red-emitting, viscosity-sensitive, BODIPY fluorophore BP-PH-2M-$NO_2$ that is suitable for reliable intracellular viscosity imaging of lipid droplets in MCF-7 breast cancer cells. The design of BP-PH-2M-$NO_2$ was aided by DFT calculations that allowed a successful prediction of the viscosity sensitivity of fluorophores before synthesis. In summary, we report a new red viscosity probe possessing monoexponential fluorescence decay that makes it attractive for lifetime-based viscosity imaging.

## Introduction

Imaging microviscosity, a bulk viscosity equivalent on a microscopic scale, can provide important information about the diffusion-controlled processes in biosystems. Determination of microviscosity can help to indicate the development of atherosclerosis,[1] diabetes,[2] and Alzheimer's disease.[3] Viscosity-sensitive fluorophores, called 'molecular rotors', provide one of the easiest methods to image microviscosity.[4] The mechanism of molecular rotors is based on a change in fluorescence signal that arises from the competition between fluorescence and intramolecular rotation, with the latter leading to faster non-radiative relaxation.[5–8] A high-viscosity environment restricts the rotation and results in the long stay of the molecule in a fluorescent state, leading to higher fluorescence intensity and longer fluorescence lifetime.[5,9,10] The fluorescence lifetime is not affected by the fluorophore concentration, which makes the lifetime-based molecular rotors more advantageous than simple fluorescence intensity probes.[11–13] Lifetime-based molecular rotors are compatible with Fluorescence Lifetime Imaging Microscopy (FLIM) which can record a time-resolved fluorescence decay in every pixel of the image, providing a convenient method for viscosity-imaging.[12–15]

The most widely used viscosity-sensitive molecular rotors are BODIPY-$C_{10}$ and BODIPY-$C_{12}$ (Figure 1) which differ only in the length of the hydrocarbon chain and have otherwise identical photophysical properties.[12,16] BODIPY-$C_{10}$ and other closely related fluorophores have been used to measure microviscosity in live cells,[12,17] plasma membranes,[18–20] collagen in tumor tissues,[21] eye lens cell membranes,[22] mitochondria,[13] model lipid membranes,[23–26] lipid microbubbles,[27] polymers[28]

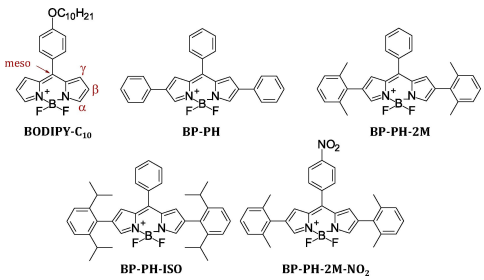


**Figure 1.** The structures of the most widely used molecular rotor BODIPY-$C_{10}$ together with new fluorophores explored in this work. The red-coloured notes indicate the substituted position of the BODIPY core.

[a] K. Maleckaitė, R. Žilėnaitė, Dr. A. Vyšniauskas
Center of Physical Sciences and Technology Saulėtekio av. 3, Vilnius, LT-10257, Lithuania
E-mail: aurimas.vysniauskas@ftmc.lt
[b] Dr. J. Dodonova, Prof. S. Tumkevičius
Institute of Chemistry, Faculty of Chemistry and Geosciences, Vilnius University Naugarduko str. 24, Vilnius, LT-03225, Lithuania
[c] Dr. S. Toliautas
Institute of Chemical Physics, Faculty of Physics, Vilnius University Saulėtekio av. 9-III, Vilnius, LT-10222, Lithuania
[d] D. Jurgutis, Prof. V. Karabanovas
Biomedical Physics Laboratory, National Cancer Institute
P. Baublio str. 3b, Vilnius, LT-08406, Lithuania
[e] Prof. V. Karabanovas
Department of Chemistry and Bioengineering,
Vilnius Gediminas Technical University
Saulėtekio av. 11, Vilnius, LT-10223, Lithuania
Supporting information for this article is available on the WWW under https://doi.org/10.1002/chem.202102743


© 2021 Wiley-VCH GmbH

and aerosols.[29] The main advantage of BODIPY-$C_{10}$/$C_{12}$ is a monoexponential fluorescence decay, which simplifies the data analysis and enables a quicker recording of the lifetime-based viscosity map using FLIM.[30] The greatest drawback of BODIPY-$C_{10}$/$C_{12}$ is green-light absorbance and fluorescence wavelengths, around 500 nm, which are rather short if imaging of the biological sample is desired. One must red-shift the fluorophore's spectra to fall into the tissue optical window (650–1350 nm), where the light penetration is deeper and there is a minimal overlap with autofluorescence and fluorescence of widely used probes, such as green fluorescent protein (GFP).[31] Red fluorescence wavelengths can be achieved simply by introducing conjugated substituents and extending the conjugation length within the fluorophore.[32,33] However, the difficult part is to ensure that the new modified red-emitting BODIPY probe remains sensitive to viscosity. There is little known about how fluorophore's structure is related to its viscosity sensitivity[4] and therefore it is extremely difficult to predict if a proposed fluorophore will be a molecular rotor. In such case, the only remaining option is a synthesis of a large number of fluorophores with various modifications, which is a time-consuming endeavour with a low probability of success. In this research, we show how quantum chemical calculations can help to determine viscosity-sensitive properties of the conjugate before its synthesis and then use them for developing a red BODIPY viscosity probe. First, we predict that a BODIPY molecular rotor with merely extended conjugation is unlikely to be viscosity-sensitive but then we show how this can be counteracted by further modifications. Second, we proceed to synthesise and characterise new BODIPY fluorophores (Figure 1) that we previously examined theoretically and demonstrate that our predictions made using density functional theory (DFT) results are largely correct. As a result, we have a new BODIPY viscosity probe with a significantly red-shifted emission that is capable of reliable intracellular viscosity imaging.

## Results and Discussion

### Fluorophore design

To achieve longer absorbance and fluorescence wavelengths than the ones of BODIPY-$C_{10}$, the conjugation of the molecular structure has to be extended.[34–36] It is known that the modification of the substituent in the *meso* position barely changes the absorption and emission spectrum due to a weak conjugation with the BODIPY core.[37] Moreover, any substituent in the $\gamma$ position of the BODIPY core, next to the phenyl ring, eliminates the viscosity sensitivity[38] with one notable exception.[39] In contrast, the introduction of substituents into the $\alpha$ position is a more viable option, although it has been shown that methyl groups in the $\alpha$ position reduce the viscosity sensitivity.[38]

Therefore, the best option to redshift the spectra of BODIPY-$C_{10}$ while preserving viscosity sensitivity seems to be the introduction of conjugated substituents into the $\beta$ position. We chose to use phenyl groups (Figure 1).

### DFT calculations

To predict the absorption, fluorescence wavelengths, the viscosity sensitivity of the proposed molecules (Figure 1) and to select the most promising molecules for synthesis, the quantum chemical calculations were performed. Theoretical calculations showed that the extension of the conjugated system should successfully shift absorption and fluorescence spectra to the longer wavelengths (Table 1). The overestimation of electronic transition energies in BODIPYs by DFT is a well-known problem. Nevertheless, DFT provides accurate relative energies and allows comparison between different fluorophores even if the absolute energy values are incorrect.[40–42]

The previous work by Toliautas et al.[43] and Liu et al.[38] has demonstrated that the viscosity sensitivity of BODIPY molecular rotors is determined by the activation energy barrier the fluorophore needs to cross during the non-radiative relaxation (Figure 2A). Immediately upon excitation the BODIPY fluorophore reaches the fluorescent state at local minimum ($S_{1,m}$, Figure 2B), where the rotation angle $\theta$ is approximately 45 . However, the fluorophore can cross a relatively small energy barrier, go through a transition state (TS, Figure 2B), and reach another minimum at 0 angle (labeled $S_{1,r}$, Figure 2B). The rotation is followed by the loss of planarity, with the BODIPY core becoming V-shaped (Figure 2C).[43,44] From $S_{1,r}$ the molecule can rapidly relax to the ground state non-radiatively.[43,45–48] The $S_{1,m}$ to $S_{1,r}$ transition rate is heavily viscosity-dependent.[38] Therefore, if the transition rate is slow due to the high energy barrier, other relaxation pathways will dominate, which will render the fluorophore viscosity-insensitive.

To estimate the viscosity sensitivity of the proposed molecules, we have calculated how the energy of the $S_1$ state depends on the dihedral angle between the phenyl ring in the *meso* position and the BODIPY core. Figure 2B compares the potential energy surface (PES) of the fluorophores in the excited

**Table 1.** Theoretical ($_t$) and experimental ($_e$) values of absorption ($\lambda_A$) and fluorescence emission maxima ($\lambda_F$), Stokes shifts ($\bar{\nu}_{SS}$), fluorescence quantum yields (QY), and molar extinction coefficients ($\varepsilon_e$) for BP-PH, BP-PH-2M, BP-PH-2M-$NO_2$, BP-PH-ISO and BODIPY-$C_{10}$ in toluene.

| Derivative | $\lambda_{tA}$ [nm] | $\lambda_{tF}$ [nm] | $\lambda_{eA}$ [nm] | $\lambda_{eF}$ [nm] | $\bar{\nu}_{eSS}$ [$cm^{-1}$] | $QY_e$ [%] | $\varepsilon_e$ [$M^{-1}\cdot cm^{-1}$] |
|---|---|---|---|---|---|---|---|
| BP-PH | 485 | 535 | 590 | 630 | 1076 | 28 | $3.3\times10^4$ |
| BP-PH-2M | 451 | 511 | 530 | 585 | 1774 | 22 | $3.3\times10^4$ |
| BP-PH-2M-$NO_2$ | 463 | 544 | 545 | 620 | 2220 | 4 | $6.5\times10^4$ |
| BP-PH-ISO | 448 | 490 | 535 | 575 | 1300 | 36 | $8\times10^4$ |
| BODIPY-$C_{10}$ | 423 | 443 | 500 | 515 | 583 | 12 | $6.4\times10^4$ |

 © 2021 Wiley-VCH GmbH

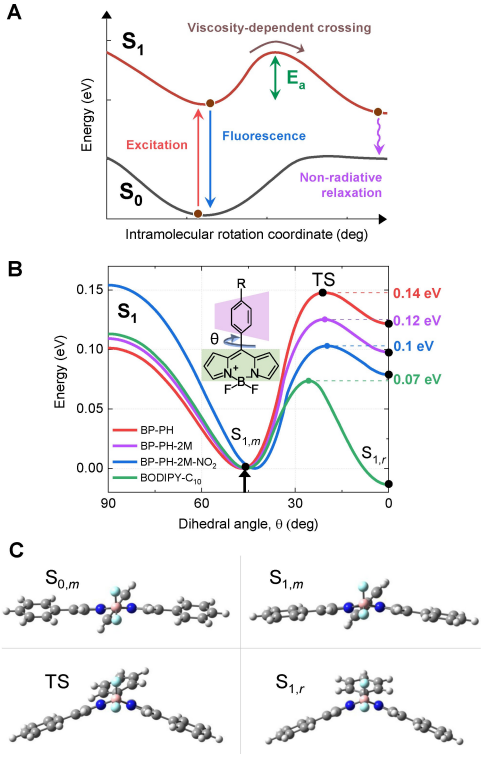


**Figure 2.** (A) Photophysical model explaining the viscosity-sensing mechanism of BODIPY probes. Upon excitation (red arrow) the molecule can return to the $S_0$ state through fluorescence (blue arrow) or by overcoming an activation energy barrier ($E_a$) followed by a non-radiative relaxation (pink arrow). (B) Potential energy surface (PES) curves of the first excited electronic state ($S_1$) of BP-PH (red), BP-PH-2M (purple), BP-PH-2M-$NO_2$ (blue), and BODIPY-$C_{10}$ (green) calculated by TD-DFT. The PES curve of BP-PH-ISO is shown in Figure S3, Supporting Information due to the similarity to BP-PH-2M. The x-axis shows the dihedral angle θ between the BODIPY core and the *meso*-phenyl (inset). Fluorescence takes place in the vicinity of the minimum denoted $S_{1,m}$, whereas a fast non-radiative relaxation occurs via the minimum $S_{1,r}$ . The energy of the local minimum $S_{1,m}$ at approximately 45 is set to 0 eV as a reference point for easier comparison. A value of the energy barrier for each molecule is shown on the right side of the graph. The black arrow indicates the dihedral angle immediately upon excitation. (C) Molecular structures of BP-PH at ground-state minimum $S_{0,m}$, excited-state minima $S_{1,m}$ and $S_{1,r}$, a transition state (TS) between the $S_{1,m}$ and $S_{1,r}$ .The geometries of BP-PH-2M and BP-PH-2M-$NO_2$ are closely similar to the ones of BP-PH.

state and reveals differences between the new molecules and the well studied BODIPY-$C_{10}$. The PES and the geometries of the new fluorophores (Figure 2C, the coordinates are provided in the Supporting Information) are consistent with the PES and geometries of the previously investigated *meso*-phenyl-BODIPYs.[43,45–48] Therefore, we consider that the main non-radiative relaxation pathway remains the same and involves the V-bending of the BODIPY core, as reported previously.[45–47]

The results show that attaching bare phenyl groups only (BP-PH) increases the energy barrier compared to BODIPY-$C_{10}$ by approximately 70 meV. To estimate the decrease of viscosity-dependent relaxation rate due to the barrier increase, we used the following relationship [Eq. (1)]:

$$k_{nr}(\eta) \propto \exp\left(-\frac{E_a}{k_b T}\right) \quad (1)$$

where $E_a$ is the activation energy barrier, $k_b$ – Boltzmann's constant and $T$ is a room temperature in kelvins. The Equation (1) shows that the estimated barrier increase (70 meV) should make the viscosity-sensitive non-radiative relaxation rate slower by a factor of 15 at room temperature. As a result, other relaxation pathways will dominate, making BP-PH barely sensitive to viscosity.

To investigate the reason behind the barrier increase upon introducing the phenyl groups, we have calculated the corresponding energy values of the artificial compound when the β-phenyls are rotated 90 out of conjugation. Upon the loss of conjugation, the energy barrier for non-radiative relaxation located between $S_{1,r}$ and $S_{1,m}$ greatly diminishes (Figure S1, Supporting Information) and becomes more similar to the one for BODIPY-$C_{10}$. This means that the higher barrier is caused by the conjugation of the new phenyl groups with the BODIPY core. Furthermore, this finding implies that shifting the spectra of BODIPY-$C_{10}$ by extending its conjugation unavoidably leads to the loss of viscosity-sensitivity.

To deal with this problem, we have proposed two solutions. Firstly, we have attached steric moieties (methyl or isopropyl groups) to the β-phenyls, which forces the phenyl rings to partially rotate out of the BODIPY plane. This may help to reach the middle ground, where the spectral red shift is not as strong but the molecules are more sensitive to viscosity. Secondly, we have attached a nitro group, which has been previously shown to reduce the energy barrier.[43] The quantum chemical calculation results shown in Figure 2B demonstrate that introducing methyl groups reduces the energy barrier by 0.02 eV, whereas the nitro group leads to the reduction by yet another 0.02 eV. The final value of the energy barrier for BP-PH-2M-$NO_2$ (0.10 eV) is not far off the value for BODIPY-$C_{10}$, which allows us to expect that BP-PH-2M-$NO_2$ will be able to effectively sense the viscosity and at the same time emit at the higher wavelength than BODIPY-$C_{10}$. The shapes of the highest occupied (HOMO) and the lowest unoccupied molecular orbitals (LUMO) (Figure S2) reveal that the nitro group increases the electron density on the *meso*-phenyl ring and on the bond connecting the ring to the BODIPY core. Therefore, a better overlap of *p* orbitals is achieved upon intramolecular rotation, which leads to the reduction of the energy barrier.

### Absorbance and fluorescence spectra

To verify our DFT-based predictions, we have synthesised the BODIPY fluorophores shown in Figure 1. As shown in Figure 3A, the absorption spectra of all dyes consist of the higher energy


© 2021 Wiley-VCH GmbH

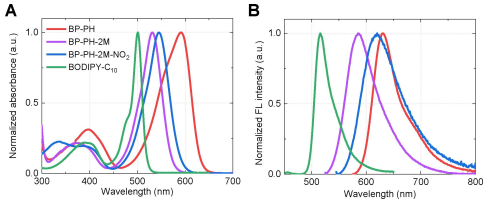


**Figure 3.** The absorption (A) and fluorescence (B) spectra of BP-PH (red), BP-PH-2M (purple), BP-PH-2M-$NO_2$ (blue), and BODIPY-$C_{10}$ (green) obtained in toluene.

band at 300–400 nm and the main absorption band, which is located at 450–630 nm. The experimental spectra follow the trends predicted by theoretical calculations (Table 1) quite closely. As expected, the position of the main band of previously unreported derivatives has 20–90 nm longer wavelengths in contrast to well investigated BODIPY-$C_{10}$. BP-PH shows the largest shift to the longer wavelengths with the absorption peak at 590 nm. Methyl groups attached in both *ortho* positions on the benzene rings (BP-PH-2M) shift the absorption maximum to 530 nm due to the decrease in conjugation because methyl groups prohibit planarization of the β-phenyls. Increasing the steric hindrance by replacing the methyl groups with isopropyl groups (BP-PH-ISO) does not drastically shift the spectra (Figure S3A–B). The introduction of the $NO_2$ group (BP-PH-2M-$NO_2$) results in the absorption maximum at 545 nm. A similar effect was observed previously for BODIPY viscosity sensors with no substituents in the β positions.[43]

Similar red-shift tendencies are also seen in the fluorescence spectra (Figure 3B). BP-PH shows the largest bathochromic shift with the fluorescence peak at 630 nm due to the increased conjugation. Because of the steric hindrance, the fluorescence bands of BP-PH-2M and BP-PH-2M-$NO_2$ appear at shorter wavelengths, with the peaks at 585 nm and 620 nm, respectively. A Stokes shift for BP-PH and BP-PH-2M was 1076 $cm^{-1}$ and 1774 $cm^{-1}$, respectively, while for the derivative with a nitro group it increased to 2220 $cm^{-1}$. Furthermore, we have determined the fluorescence quantum yields in toluene for all new derivatives (Table 1). As expected, the new derivatives with the higher energy barrier show larger quantum yields because the molecule stays longer in the fluorescent state before overcoming the potential energy barrier (Figure 2A). The fact that BP-PH-2M-$NO_2$ shows a smaller fluorescence quantum yield than BODIPY-$C_{10}$ despite having the higher barrier may be the result of additional non-radiative relaxation pathways that are present in the new fluorophore.

Additionally, we performed the experiments in different polarity solvents (from non-polar to very polar: cyclohexane, toluene, chloroform, dichloromethane (DCM), dichloroethane (DCE), dimethyl sulfoxide (DMSO), methanol). The derivatives show no strong solvatochromism, resulting in the red-shift of 14, 16, 8 and 19 nm for BP-PH, BP-PH-2M, BP-PH-ISO, and BP-PH-2M-$NO_2$, respectively, when going from the least polar to the most polar solvents (Figure S4).

### Influence of viscosity

Since our new BODIPY derivatives are hydrophobic, they are likely to localize in non-polar lipid bilayers during their application in live cell imaging. Due to this reason, non-polar toluene-castor oil mixtures were chosen for determining the viscosity sensitivity of the new fluorophores. Mixtures ranging from pure toluene to pure castor oil covering 0.5-920 cP viscosity range were used. The majority of fluorescence decays in mixtures were monoexponential, although some of the decays were biexponential owing to the small contribution from castor oil, which is itself fluorescent. Data shown in Figure 4A–C demonstrate time-resolved fluorescence decays at increasing viscosity for all new derivatives. The fluorescence lifetime values are shown in Figure 4D, exact lifetimes and amplitudes are shown in Table S2, Supporting Information. In the case of biexponential decays, intensity-weighted mean lifetimes are shown [Eq. (1)]. The experimental results closely follow our theoretical predictions; BP-PH has the weakest viscosity sensitivity out of all new BODIPY fluorophores. The introduction of methyl groups (Figure 4B) or isopropyl groups (Figure S3D) slightly increased viscosity sensitivity but to a lesser degree than required for an applicable viscosity sensor. However, the addition of the nitro group has resulted in a very

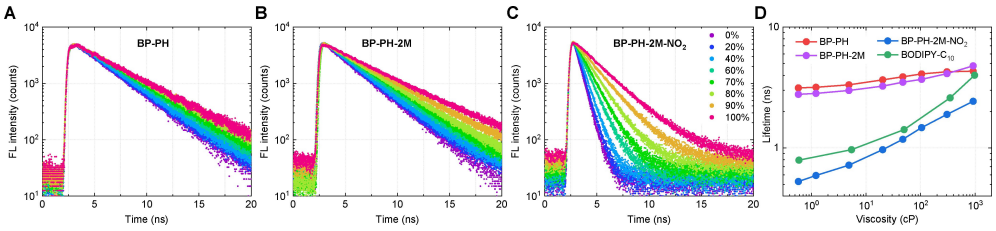


**Figure 4.** Time-resolved fluorescence decays of BP-PH (A), BP-PH-2M (B), BP-PH-2M-$NO_2$ (C) obtained in toluene-castor oil mixtures. The colours in the legend indicate the volume fraction of castor oil in the mixture. (D) Fluorescence lifetimes of BP-PH (red), BP-PH-2M (purple), BP-PH-2M-$NO_2$ (blue), and BODIPY-$C_{10}$ (green) obtained in toluene-castor oil mixtures.


© 2021 Wiley-VCH GmbH

strong viscosity sensitivity, which is comparable to the sensitivity of the most applied BODIPY molecular rotor BODIPY-$C_{10}$ (Figure 4D) as both molecules displayed similar *x* values for Förster-Hoffmann fits[5,49] (Figure S5). Additionally, the dynamic range of the probe, which can be calculated from the lifetime ratio at high and low viscosities, increased from 1.4 to 4.6, for the molecules BP-PH and BP-PH-2M-$NO_2$, respectively. This is supplemented by fluorescence intensities at low and high viscosities shown in Figure S6. The quantum yields of fluorescence of BP-PH-2M-$NO_2$ in toluene-castor oil mixtures are shown in Table S3, Supporting Information.

Furthermore, we proved that the nitro-substitution is a universal strategy for increasing the viscosity-sensitivity of BODIPY viscosity probes as it has now been shown to work with β-phenyl-substituted BODIPYs in addition to BODIPYs without substituents in the β position[43] (Figure S7).

The importance of this result is twofold. First, we managed to significantly increase the absorption and emission wavelength of BODIPY-$C_{10}$, which now is very close to the red region of the visible spectrum. Second, our discovered trend in viscosity sensitivity of new BODIPY derivatives matches the trend in the energy barrier heights (Figure 2A). This further supports the hypothesis that viscosity sensitivity is determined by the height of the energy barrier for non-radiative relaxation. This knowledge is crucial for being able to make predictions about viscosity sensitivity of proposed fluorophores by theoretical calculations.

The influence of temperature and solvent polarity on fluorescence lifetime was also investigated (Figure S8). All derivatives showed weak temperature sensitivity as demonstrated by decreasing fluorescence lifetimes in cyclohexane with increasing temperature (Figure S8A). Also, the values of the lifetimes for BP-PH and BP-PH-2M are comparable, while BP-PH-ISO showed around 1 ns longer lifetimes in cyclohexane. BP-PH-2M-$NO_2$ has much lower lifetimes due to fast non-radiative relaxation in a solvent of low viscosity. Very similar dependency is seen when the polarity of solvent is changed: lifetimes decrease with increasing polarity. BP-PH, BP-PH-2M and BP-PH-ISO demonstrate comparable lifetimes, while derivative with $-NO_2$ group showed lower lifetimes and less sensitivity to polarity (Figure S8B). These observations let us state that the viscosity sensitivity was drastically increased with an attachment of the $-NO_2$ group. This improvement lets viscosity sensitivity dominate over the observed sensitivities to temperature and solvent polarity.

### Cellular imaging

The above-described results show that BP-PH-2M-$NO_2$ stands out of all the new derivatives, demonstrating strong viscosity sensitivity. We decided to use this conjugate for live cell imaging. MCF-7 breast cancer cells were stained using large unilamellar vesicles (LUV) containing BP-PH-2M-$NO_2$ incorporated into the lipid membrane of LUVs.

The fluorescence image of MCF-7 cells after staining (Figure 4A) revealed that BP-PH-2M-$NO_2$ successfully internalizes into the live cells. The granulated pattern of red fluorescence inside MCF-7 cells indicates that BP-PH-2M-$NO_2$ intensely stains spherical organelles. Further intracellular colocalisation analysis (Figures S10 and S11) showed accumulation of BP-PH-2M-$NO_2$ in lipid droplets. Recorded FLIM image (Figure 5B) showed monoexponential fluorescence decays (Figure S9A) with the mean lifetime of 1532 ps. Using this lifetime, toluene-castor oil calibration (Figure 4D) allowed us to assign a dynamic viscosity of 123 cP. Similar viscosity values were published in other articles, where BODIPY molecules were used to stain plasma and internal membranes of the live cells.[12,20,21]

The fluorescence spectrum of BP-PH-2M-$NO_2$ in live cells closely matched the spectrum in toluene both in terms of position and shape (Figure S9). Such spectral resemblance in addition to monoexponential decays demonstrated that the photophysical properties of the probe did not change when moving from toluene-castor oil mixtures to the complex intracellular environment. Therefore, toluene-castor oil mixtures are suitable solvents for calibrating BP-PH-2M-$NO_2$. Additionally, BP-PH-2M-$NO_2$ shows no signs of aggregation or degradation in the intracellular environment, as this would lead to change in the fluorescence spectrum and the emergence of an additional exponential component in the fluorescence decay. As a result, BP-PH-2M-$NO_2$ is suitable for staining live MCF-7 cells and reporting intracellular viscosity in lipid droplets. In the future work, we plan to modify the structure of BP-PH-2M-$NO_2$, so it could be directed to other cellular organelles besides lipid droplets.

## Conclusions

To conclude, we have successfully designed and synthesised a red-emitting BODIPY viscosity probe BP-PH-2M-$NO_2$. The design process of BP-PH-2M-$NO_2$ was greatly aided by DFT calculations,

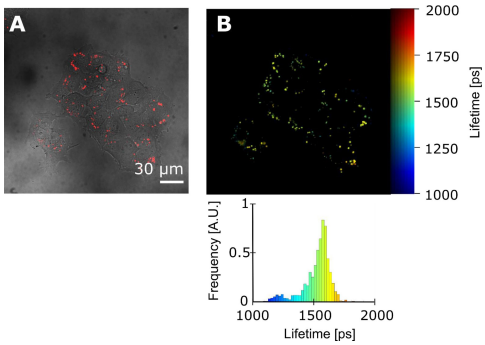


**Figure 5.** Live MCF-7 cells stained with BP-PH-2M-$NO_2$. (A) Brightfield image superimposed with a fluorescence image of BP-PH-2M-$NO_2$ showing the staining of lipid droplets. (B) FLIM image with the lifetime histogram at the bottom. The mean lifetime is 1532 ± 74 ps (one standard deviation). The fluorescence was excited at 560 ± 5 nm and detected over the range 621–755 nm.


© 2021 Wiley-VCH GmbH

which were used to obtain an energy barrier height that prevents viscosity-dependent non-radiative relaxation. This was used to predict the viscosity sensitivity of the target molecular structures before synthesis. To our knowledge, this is the first example in the literature where such an approach was used. The new fluorophore emits at a significantly longer wavelength and has a Stokes shift that is four times larger than the one of widely used green viscosity probe BODIPY-$C_{10}$/$C_{12}$ and its variants. Furthermore, the new probe successfully senses viscosity in lipid droplets of live MCF-7 cells and shows a monoexponential fluorescence decay in a complex intracellular environment. Such a property is a highly desired feature as it enables reliable viscosity sensing via the FLIM technique. Overall, our work shows how DFT calculations can be exploited for the development of a new red fluorescent viscosity sensor with attractive properties.

## Experimental Section

### Dyes, reagents, and solvents

BODIPY-$C_{10}$ was synthesised as previously reported.[1,2] The synthesis of novel BODIPY derivatives BP-PH, BP-PH-2M, BP-PH-ISO and BP-PH-2M-$NO_2$ was accomplished using Suzuki reaction of corresponding β-dibromo BODIPY derivatives with arylboronic acids in the presence of $Pd(OAc)_2$/SPhos as a catalyst system. The synthetic details and characterization data of the synthesized compounds are presented in Supporting Information. Stock solutions of all dyes were prepared in toluene at the concentration of 2–2.5 mM and diluted for further experiments in a solvent or solvent mixtures of interest. Toluene, castor oil, cyclohexane, chloroform, DCM, DCE, DMSO, ethanol (EtOH) and methanol (MeOH) were obtained from Sigma-Aldrich. The viscosities of toluene/castor oil mixtures at a variable temperature were measured by using a vibro viscometer (SV10, A&D).

### Absorption, steady-state, time-resolved fluorescence, and quantum yield measurements

Absorption spectra were measured by using a Jasco V-670 spectrophotometer. Fluorescence spectra and time-resolved fluorescence were recorded with the Edinburgh-F900 (Edinburgh Instruments) fluorimeter. Excitation of the new molecules was performed by using the WhiteLase Micro (Fianium) laser together with bandpass filters (Thorlabs) with 10 nm bandwidth centred at 520 nm (BP-PH-2M and BP-PH-ISO), 540 nm (BP-PH-2M-$NO_2$), 570 nm (BP-PH), while previously reported BODIPY-$C_{10}$ was excited using 1 MHz frequency picosecond pulsed diode laser EPL-470 (Edinburgh Instruments) emitting at 473 nm. Fluorescence decays were measured using the time-correlated singlephoton counting technique. Fluorescence decays had 5000 counts at the peak of the decay with 20 ns (BP-PH, BP-PH-2M, BP-PH- ISO and BP-PH-2M-$NO_2$) and 50 ns (BODIPY-$C_{10}$) window being used with 4096 channels. Quantum yields (QY) were determined by comparative method using Rhodamine-101 ($QY_F$ = 0.91 in EtOH; used for BP-PH),[50] Rhodamine-6G ($QY_F$ = 0.94 in EtOH; used for BP-PH-2M, BP-PH-2M, BP-PH-2M-$NO_2$, BP-PH-ISO),[50] and fluorescein ($QY_F$ = 0.95 in 0.1 M $NaOH_{aq}$; used for BODIPY-$C_{10}$)[51] as a standard. Quartz cuvettes (10 mm) were used for absorption, fluorescence, and QY measurements. The concentration of dyes was 2–8 μM.

### Theoretical calculations

Structural and optical properties of the investigated molecular rotors were modelled by performing quantum chemical computations based on DFT,[52] as well as time-dependent DFT[53] for the excited state properties. M06-2X hybrid functional[54] and cc-pVDZ basis set for the electronic wave-function[55] were used in all stages of computations. The choice was based on the internal benchmarks and the findings of Momeni et al.[56] Coordinate scans of the potential energy surfaces (PES) of the first excited molecular state $S_1$ were constructed by performing relaxed geometry optimizations at the various fixed values of the rotation angle (*meso* position in Figure 1). The inclusion of zero-point vibrational energy (ZPVE) in estimation of the $S_1$ energy had an insignificant effect, changing relative shape of the surfaces by 6–7 meV (Table S1, Supporting Information). Bulk solvent effects on the solute molecules were taken into account by the conductor-like polarizable continuum model (C-PCM)[57] with solvent parameters of toluene. Even though PCM might have been sufficient, we used C-PCM in order to be consistent with our previous calculations.[16,43] Calculations were carried out using electronic structure modelling package Gaussian09.[58] Properties of BODIPY-$C_{10}$ variant were obtained substituting its molecular structure with alkyl group shortened to a single carbon atom; this change was shown earlier to have no effect on the photophysical results,[16] while significantly reducing numerical calculation times.

### Imaging of live cancer cells

Stock solutions of 1,2-dipalmitoyl-*sn*-glycero-3-phosphocholine (DPPC) used for LUVs were purchased from Avanti Polar Lipids. Phosphate-buffered saline (PBS) buffer was prepared using a well-known protocol.[59] NaCl, KCl, $Na_2HPO_4$ an $KH_2PO_4$ were purchased from CARL-ROTH. LUVs were prepared by the extrusion method. A 222 μL mixture of DPPC lipid and BP-PH-2M-$NO_2$ dye concentrate in chloroform was blow-dried using nitrogen. The dried solution was put in the desiccator and the remaining solvent evaporated under vacuum for 1 hour. After this, 2.4 mL PBS buffer was used for hydration of the dry lipid sample. The solution was vortexed and sonicated above the phase transition temperature (>41 C). The solution was extruded 10 times through a polycarbonate membrane with a pore diameter of 0.1 μm using Avanti Polar Lipids Mini-Extruder. It was ensured that the process is carried out above the phase transition temperature.

Human breast cancer cell line MCF-7 was purchased from European Collection of Cell Cultures and cultured in cell growth medium (Dulbecco's modified Eagle's medium – DMEM), supplemented with 10% fetal bovine serum, 100 μg /mL penicillin and 100 μg/mL streptomycin (Gibco). Cells were maintained at 37 C in 5% $CO_2$ and routinely subcultured 2–3 times a week in 25 $cm^2$ culture dishes. For live cell imaging, cells were seeded into an 8-chambered cover glass plate (Nunc, Lab-Tek) with a density of $3\times10^4$ cells/chamber and subsequently incubated at 37 C in 5% $CO_2$ for 24 h. MCF-7 cells were treated with BP-PH-2M-$NO_2$ encapsulated in lipid vesicles in PBS for 15 min at 37 C. After incubation, the cells were washed with Dulbecco's phosphate-buffered saline with $Ca^{2+}$ and $Mg^{2+}$, w/o Phenol Red (DPBS) (Cegrogen Biotech). For BODIPY-h and Nile Red (Invitrogen) localisation, cells were stained with 9 μM BODIPY-h (stock solution prepared in DMSO and diluted with DPBS) for 60 min at 37 C. Afterwards, cells were treated with 314 nM Nile Red (stock solution prepared in DMSO and diluted with DPBS) for 10 min at room temperature. For localisation of BP-PH-2M-$NO_2$ and BODIPY-h, MCF-7 cells were treated with BP-PH-2M-$NO_2$ encapsulated in lipid vesicles in PBS for 15 min at 37 C. Afterwards, cells were incubated with 9 μM BODIPY-h for 60 min 37 C. After each staining step, cells were washed 3 times with warm DPBS. During

 © 2021 Wiley-VCH GmbH

the imaging, cells were maintained at 37 C in the Microscope Stage Incubation System (OkoLab) in a humidified atmosphere containing 5% of $CO_2$ (0.80 Nl/min $O_2$ and 0.04 Nl/min $CO_2$). For localisation experiments, control samples were prepared for finding the detection parameters that eliminate emission bleed-through from Nile Red and BP-PH-2M-$NO_2$ in the green channel (501-590 nm), where the fluorescence of BODIPY-h was detected.

Samples were imaged using Nikon Eclipse Te2000-S, C1si confocal laser scanning microscope (Nikon) equipped with Fianium White-Lase Micro supercontinuum laser (NKT Photonics) with a pulse repetition rate of 30 MHz and filtered using 480/10 nm or 560/10 nm band-pass filters (Thorlabs Inc.). Imaging was performed using 60×/1.4 NA oil immersion objective (Nikon). The 32-channel spectral detector was applied to measure the fluorescence spectra of BP-PH-2M-$NO_2$ and BODIPY-h in live MCF-7 cells. FLIM imaging was performed using a Lifetime and Fluorescence Correlation Spectroscopy Upgrade for Nikon C1si (PicoQuant GmbH) microscope. The fluorescence-signal was detected through a 620 nm long-pass filter (Thorlabs Inc.) using a single-photon-counting avalanche photodiode (SPAD) (Micro Photon Devices) and counted by a time-correlated singlephoton counter PicoHarp 300 (PicoQuant GmbH). The resolution of FLIM images was 512×512 pixels.

#### Data analysis

Fluorescence decays were fitted using Edinburgh-F900 software package F900. For biexponential fluorescence decays, intensity-weighted lifetimes were calculated [Eq. (2)]:

$$\bar{\tau} = \frac{\sum_i a_i \tau_i^2}{\sum_i a_i \tau_i} \quad (2)$$

where $a$ is an amplitude value and $\tau$ is the value of the lifetime. The goodness-of-fit parameter ($\chi^2$) was 1.5 or less for single decays. Brightfield and fluorescence microscopy images were done using the Nikon EZ–C1 Bronze version 3.80 and ImageJ 1.52a software. FLIM image analysis was performed using the FLIMfit software tool developed at Imperial College London.[60] Further data processing and analysis were done with Origin 2018.

## *Acknowledgement*

Quantum chemical computations were carried out using resources at the High-Performance Computing Center "HPC Saulėtekis" (Vilnius University, Faculty of Physics). This research was funded by a grant (no. S-MIP-19-6) from the Research Council of Lithuania.

## Conflict of Interest

The authors declare no conflict of interest.

**Keywords:** Density functional calculations · Fluorescence spectroscopy · Molecular rotors · Viscosity sensing

[1] G. Deliconstantinos, V. Villiotou, J. C. Stavrides, *Biochem. Pharmacol.* **1995**, *49*, 1589–1600.
[2] O. Nadiv, M. Shinitzky, H. Manu, D. Hecht, C. T. Roberts, D. LeRoith, Y. Zick, *Biochem. J.* **1994**, *298*, 443–450.
[3] G. S. Zubenko, U. Kopp, T. Seto, L. L. Firestone, *Psychopharmacology* **1999**, *145*, 175–180.
[4] H. Xiao, P. Li, B. Tang, *Chem. A Eur. J.* **2020**.
[5] M. K. Kuimova, *Phys. Chem. Chem. Phys.* **2012**, *14*, 12671–12686.
[6] M. A. Haidekker, E. A. Theodorakis, *Org. Biomol. Chem.* **2007**, *5*, 1669–1678.
[7] A. Vyšniauskas, M. K. Kuimova, *Int. Rev. Phys. Chem.* **2018**, *37*, 259–285.
[8] D. Su, C. L. Teoh, L. Wang, X. Liu, Y. T. Chang, *Chem. Soc. Rev.* **2017**, *46*, 4833–4844.
[9] M. A. Haidekker, M. Nipper, A. Mustafic, D. Lichlyter, M. Dakanali, E. A. Theodorakis in *Adv. Fluoresc. Reporters Chem. Biol. I*, Springer, Berlin, Heidelberg, **2010**, pp. 267–308.
[10] S. C. Lee, J. Heo, H. C. Woo, J. A. Lee, Y. H. Seo, C. L. Lee, S. Kim, O. P. Kwon, *Chem. A Eur. J.* **2018**, *24*, 13706–13718.
[11] J. E. Chambers, M. Kubánková, R. G. Huber, I. López-Duarte, E. Avezov, P. J. Bond, S. J. Marciniak, M. K. Kuimova, *ACS Nano* **2018**, *12*, 4398–4407.
[12] M. K. Kuimova, G. Yahioglu, J. A. Levitt, K. Suhling, *J. Am. Chem. Soc.* **2008**, *130*, 6672–6673.
[13] I. E. Steinmark, A. L. James, P. H. Chung, P. E. Morton, M. Parsons, C. A. Dreiss, C. D. Lorenz, G. Yahioglu, K. Suhling, *PLoS One* **2019**, *14*, 1–20.
[14] A. Vyšniauskas, I. López-Duarte, N. Duchemin, T.-T. Vu, Y. Wu, E. M. Budynina, Y. A. Volkova, E. Peña Cabrera, D. E. Ramírez-Ornelas, M. K. Kuimova, *Phys. Chem. Chem. Phys.* **2017**, *19*, 25252–25259.
[15] A. S. Klymchenko, *Acc. Chem. Res.* **2017**, *50*, 366–375.
[16] A. Polita, S. Toliautas, R. Žvirblis, A. Vyšniauskas, *Phys. Chem. Chem. Phys.* **2020**, *22*, 8296–8303.
[17] W. Miao, C. Yu, E. Hao, L. Jiao, *Front. Chem.* **2019**, *7*, 1–6.
[18] M. Kubánková, I. López-Duarte, D. Kiryushko, M. K. Kuimova, *Soft Matter* **2018**, *14*, 9466–9474.
[19] M. Kubánková, P. A. Summers, I. López-Duarte, D. Kiryushko, M. K. Kuimova, *ACS Appl. Mater. Interfaces* **2019**, *11*, 36307–36315.
[20] I. López-Duarte, T. Truc Vu, M. A. Izquierdo, J. A. Bull, M. K. Kuimova, *Chem. Commun.* **2014**, *50*, 5282–5284.
[21] L. E. Shimolina, M. A. Izquierdo, I. López-Duarte, J. A. Bull, M. V. Shirmanova, L. G. Klapshina, E. V. Zagaynova, M. K. Kuimova, *Sci. Rep.* **2017**, *7*, 1–11.
[22] P. S. Sherin, I. López-Duarte, M. R. Dent, M. Kubánková, A. Vyšniauskas, J. A. Bull, E. S. Reshetnikova, A. S. Klymchenko, Y. P. Tsentalovich, M. K. Kuimova, *Chem. Sci.* **2017**, *8*, 3523–3528.
[23] M. Olšinová, P. Jurkiewicz, M. Pozník, R. Šachl, T. Prausová, M. Hof, V. Kozmík, F. Teplý, J. Svoboda, M. Cebecauer, *Phys. Chem. Chem. Phys.* **2014**, *16*, 10688–10697.
[24] M. R. Dent, I. López-Duarte, C. J. Dickson, N. D. Geoghegan, J. M. Cooper, I. R. Gould, R. Krams, J. A. Bull, N. J. Brooks, M. K. Kuimova, *Phys. Chem. Chem. Phys.* **2015**, *17*, 18393–18402.
[25] Y. Wu, M. Štefl, A. Olzyńska, M. Hof, G. Yahioglu, P. Yip, D. R. Casey, O. Ces, J. Humpolíčková, M. K. Kuimova, *Phys. Chem. Chem. Phys.* **2013**, *15*, 14986–14993.
[26] A. Vyšniauskas, M. Qurashi, M. K. Kuimova, *Chem. A Eur. J.* **2016**, *22*, 13210–13217.
[27] N. A. Hosny, G. Mohamedi, P. Rademeyer, J. Owen, Y. Wu, M. X. Tang, R. J. Eckersley, E. Stride, M. K. Kuimova, *Proc. Natl. Acad. Sci. USA* **2013**, *110*, 9225–9230.
[28] J. M. Nölle, C. Jüngst, A. Zumbusch, D. Wöll, *Polym. Chem.* **2014**, *5*, 2700–2703.
[29] N. A. Hosny, C. Fitzgerald, A. Vyšniauskas, A. Athanasiadis, T. Berkemeier, N. Uygur, U. Pöschl, M. Shiraiwa, M. Kalberer, F. D. Pope, M. K. Kuimova, *Chem. Sci.* **2016**, *7*, 1357–1367.
[30] J. A. Levitt, P. H. Chung, M. K. Kuimova, G. Yahioglu, Y. Wang, J. Qu, K. Suhling, *ChemPhysChem* **2011**, *12*, 662–672.
[31] R. Weissleder, *Nat. Biotechnol.* **2001**, *19*, 316–317.
[32] D. Zhang, V. Martín, I. García-Moreno, A. Costela, M. E. Pérez-Ojeda, Y. Xiao, *Phys. Chem. Chem. Phys.* **2011**, *13*, 13026–13033.
[33] J. R. Lakowicz, *Principles of Fluorescence Spectroscopy* 3rd ed., Springer, Boston, **2006**.
[34] V. J. Pansare, S. Hejazi, W. J. Faenza, R. K. Prud'Homme, *Chem. Mater.* **2012**, *24*, 812–827.
[35] Y. Ni, J. Wu, *Org. Biomol. Chem.* **2014**, *12*, 3774–3791.
[36] C. S. Kue, S. Y. Ng, S. H. Voon, A. Kamkaew, L. Y. Chung, L. V. Kiew, H. B. Lee, *Photochem. Photobiol. Sci.* **2018**, *17*, 1691–1708.
[37] E. Lager, J. Liu, A. Aguilar-Aguilar, B. Z. Tang, E. Peña-Cabrera, *J. Org. Chem.* **2009**, *74*, 2053–2058.

 © 2021 Wiley-VCH GmbH

[38] X. Liu, W. Chi, Q. Qiao, S. V. Kokate, E. P. Cabrera, Z. Xu, X. Liu, Y.-T. Chang, *ACS Sens.* **2020**, *5*, 731–739.
[39] J. Cui, H. Nie, S. Zang, S. Su, M. Gao, J. Jing, X. Zhang, *Sens. Actuators B* **2021**, *331*, 129432.
[40] B. Le Guennic, D. Jacquemin, *Acc. Chem. Res.* **2015**, *48*, 530–537.
[41] R. Berraud-Pache, F. Neese, G. Bistoni, R. Izsák, *J. Chem. Theory Comput.* **2020**, *16*, 564–575.
[42] M. R. Momeni, A. Brown, *J. Chem. Theory Comput.* **2015**, *11*, 2619–2632.
[43] S. Toliautas, J. Dodonova, A. Žvirblis, I. Čiplys, A. Polita, A. Devižis, S. Tumkevičius, J. Šulskus, A. Vyšniauskas, *Chem. A Eur. J.* **2019**, *25*, 10342–10349.
[44] F. Li, S. I. Yang, Y. Ciringh, J. Seth, C. H. Martin, D. L. Singh, D. Kim, R. R. Birge, D. F. Bocian, D. Holten, J. S. Lindsey, *J. Am. Chem. Soc.* **1998**, *120*, 10001–10017.
[45] Q. Ou, Q. Peng, Z. Shuai, *J. Phys. Chem. Lett.* **2020**, *11*, 7790–7797.
[46] A. Prlj, L. Vannay, C. Corminboeuf, *Helv. Chim. Acta* **2017**, *100*, 1–9.
[47] Z. Lin, A. W. Kohn, T. Van Voorhis, *J. Phys. Chem. C* **2020**, *124*, 3925–3938.
[48] T. Suhina, S. Amirjalayer, S. Woutersen, D. Bonn, A. M. Brouwer, *Phys. Chem. Chem. Phys.* **2017**, *19*, 19998–20007.
[49] T. Förster, G. Hoffmann, *Zeitschrift für Phys. Chemie* **1971**, *75*, 63–76.
[50] K. P. Wall, R. Dillon, M. K. Knowles, *Biochem. Mol. Biol. Educ.* **2015**, *43*, 52–59.
[51] J. H. Brannon, D. Magde, *J. Phys. Chem.* **1978**, *82*, 705–709.
[52] R. G. Parr, *Density Functional Theory of Atoms and Molecules*, Oxford University Press, Oxford, **1989**.
[53] R. E. Stratmann, G. E. Scuseria, M. J. Frisch, *J. Chem. Phys.* **1998**, *109*, 8218–8224.
[54] Y. Zhao, D. G. Truhlar, *Theor. Chem. Acc.* **2008**, *120*, 215–241.
[55] R. A. Kendall, T. H. Dunning, R. J. Harrison, *J. Chem. Phys.* **1992**, *96*, 6796–6806.
[56] M. R. Momeni, A. Brown, *J. Phys. Chem. A* **2016**, *120*, 2550–2560.
[57] M. Cossi, N. Rega, G. Scalmani, V. Barone, *J. Comput. Chem.* **2003**, *24*, 669–681.
[58] M. J. Frisch, G. W. Trucks, H. B. Schlegel, G. E. Scuseria, M. A. Robb, J. R. Cheeseman, G. Scalmani, V. Barone, G. A. Petersson, H. Nakatsuji, X. Li, M. Caricato, A. V. Marenich, J. Bloino, B. G. Janesko, R. Gomperts, B. Mennucci, H. P. Hratchian, J. V. Ortiz, A. F. Izmaylov, J. L. Sonnenberg, D. Williams-Young, F. Ding, F. Lipparini, F. Egidi, J. Goings, B. Peng, A. Petrone, T. Henderson, D. Ranasinghe, V. G. Zakrzewski, J. Gao, N. Rega, G. Zheng, W. Liang, M. Hada, M. Ehara, K. Toyota, R. Fukuda, J. Hasegawa, M. Ishida, T. Nakajima, Y. Honda, O. Kitao, H. Nakai, T. Vreven, K. Throssell, J. A. Montgomery, Jr., J. E. Peralta, F. Ogliaro, M. J. Bearpark, J. J. Heyd, E. N. Brothers, K. N. Kudin, V. N. Staroverov, T. A. Keith, R. Kobayashi, J. Normand, K. Raghavachari, A. P. Rendell, J. C. Burant, S. S. Iyengar, J. Tomasi, M. Cossi, J. M. Millam, M. Klene, C. Adamo, R. Cammi, J. W. Ochterski, R. L. Martin, K. Morokuma, O. Farkas, J. B. Foresman, D. J. Fox, Gaussian09, Revision D.01, Gaussian, Inc., Wallingford CT, **2013**.
[59] Cold Spring Harbor Laboratory Press, *PBS (pH 7.4) recipe*, 2018.
[60] S. C. Warren, A. Margineanu, D. Alibhai, D. J. Kelly, C. Talbot, Y. Alexandrov, I. Munro, M. Katan, C. Dunsby, P. M. W. French, *PLoS One* **2013**, *8*, e70687.

Manuscript received: July 29, 2021
Accepted manuscript online: September 22, 2021
Version of record online: November 3, 2021

 © 2021 Wiley-VCH GmbH

P3

# Give or Take: Effects of Electron-Accepting/-Withdrawing Groups in Red-Fluorescent BODIPY Molecular Rotors

**K. Maleckaitė**, D. Narkevičius, R. Žilėnaitė, J. Dodonova-Vaitkūnienė, S. Toliautas, S. Tumkevičius, A. Vyšniauskas

*Molecules* **27**(1), art. n. 23 (2021)
DOI: 10.3390/molecules27010023

Reprinted from *Molecules*
with permission from Multidisciplinary Digital Publishing Institute.

Supporting information: https://www.mdpi.com/1420-3049/27/1/23/s1?version=1640094214

*molecules*

MDPI

*Article*

# Give or Take: Effects of Electron-Accepting/-Withdrawing Groups in Red-Fluorescent BODIPY Molecular Rotors

**Karolina Maleckaitė [1], Domantas Narkevičius [2], Rugilė Žilėnaitė [2], Jelena Dodonova-Vaitkūnienė [2], Stepas Toliautas [3], Sigitas Tumkevičius [2] and Aurimas Vyšniauskas [1,2,*]**

[1] Center of Physical Sciences and Technology, Saulėtekio av. 3, LT-10257 Vilnius, Lithuania; karolina.maleckaite@ftmc.lt
[2] Institute of Chemistry, Faculty of Chemistry and Geosciences, Vilnius University, Naugarduko str. 24, LT-03225 Vilnius, Lithuania; domantas.narkevicius@chgf.stud.vu.lt (D.N.); rzilenaitei@gmail.com (R.Ž.); jelena.dodonova@gmail.com (J.D.-V.); sigitas.tumkevicius@chf.vu.lt (S.T.)
[3] Institute of Chemical Physics, Faculty of Physics, Vilnius University, Saulėtekio av. 9-III, LT-10222 Vilnius, Lithuania; stepas.toliautas@ff.vu.lt
* Correspondence: aurimas.vysniauskas@ftmc.lt

**Abstract:** Mapping microviscosity, temperature, and polarity in biosystems is an important capability that can aid in disease detection. This can be achieved using fluorescent sensors based on a green-emitting BODIPY group. However, red fluorescent sensors are desired for convenient imaging of biological samples. It is known that phenyl substituents in the $\beta$ position of the BODIPY core can shift the fluorescence spectra to longer wavelengths. In this research, we report how electron-withdrawing (EWG) and -donating (EDG) groups can change the spectral and sensory properties of $\beta$-phenyl-substituted BODIPYs. We present a trifluoromethyl-substituted (EWG) conjugate with moderate temperature sensing properties and a methoxy-substituted (EDG) molecule that could be used as a lifetime-based polarity probe. In this study, we utilise experimental results of steady-state and time-resolved fluorescence, as well as quantum chemical calculations using density functional theory (DFT). We also explain how the energy barrier height ($E_a$) for non-radiative relaxation affects the probe's sensitivity to temperature and viscosity and provide appropriate $E_a$ ranges for the best possible sensitivity to viscosity and temperature.

**Keywords:** fluorescent probes; photophysics; molecular rotors; microviscosity; polarity sensing

check for updates

**Citation:** Maleckaitė, K.; Narkevičius, D.; Žilėnaitė, R.; Dodonova-Vaitkūnienė, J.; Toliautas, S.; Tumkevičius, S.; Vyšniauskas, A. Give or Take: Effects of Electron-Accepting/-Withdrawing Groups in Red-Fluorescent BODIPY Molecular Rotors. *Molecules* **2022**, *27*, 23. https://doi.org/10.3390/molecules27010023

Academic Editors: Barbara Panunzi and Yuriy S. Marfin

Received: 25 November 2021
Accepted: 16 December 2021
Published: 21 December 2021

**Publisher's Note:** MDPI stays neutral with regard to jurisdictional claims in published maps and institutional affiliations.

**Copyright:** © 2021 by the authors. Licensee MDPI, Basel, Switzerland. This article is an open access article distributed under the terms and conditions of the Creative Commons Attribution (CC BY) license (https://creativecommons.org/licenses/by/4.0/).

## 1. Introduction

Fluorophores that are sensitive to environmental properties are very useful in biological studies and help to understand changes in the intracellular environment. Fluorescent molecular probes are widely used for imaging polarity [1,2], temperature [3,4], and microviscosity [5–7]. Fluorescent sensors have already been utilised in experimental objects, such as live cells [8–10], various organelles [3,11,12], polymers [13,14], aerosols [15,16], and lipid membranes [17–19]. The working principle of the majority of such sensors is based on the competition between fluorescence and non-radiative relaxation, where the rate of the latter is heavily affected by either viscosity, temperature, or polarity [20]. Together with fluorescence microscopy or fluorescence lifetime imaging microscopy (FLIM), fluorescent probes provide a non-invasive method for imaging changes in the medium [11,21,22].

Some of the most popular microviscosity probes are based on the BODIPY group [8,23,24], such as BODIPY-$C_{10}$ (Figure 1). They are generally used as fluorescence lifetime probes rather than simple fluorescence intensity probes due to the independence of lifetime on local concentration of fluorophores and the conditions of excitation and detection [25]. These probes stand out for having a monoexponential fluorescence decay, which simplifies data analysis [26]. Studies about polarity- and temperature-sensitive BODIPY-based fluorophores have also been published [9,27,28]. Furthermore, it has already been shown that

a single BODIPY fluorophore can be partially sensitive to all three parameters: polarity, temperature, and microviscosity [29]. All this indicates that the BODIPY group is a perfect platform for the development of all mentioned types of environmental sensors.

However, since a bare BODIPY fluorophore absorbs and emits close to 500 nm [21], the majority of BODIPY-based sensors are not red absorbers or emitters. Creating a red-fluorescent sensor is an important task because such a sensor would prevent the light scattering in deep tissue imaging and avoid an overlap with autofluorescence [30,31]. Moreover, it would enable scientists to use a red BODIPY probe together with other fluorophores for various markings in live cells [32] that often tend to be green, such as green fluorescent protein (GFP). Recently, we published an article on a red fluorescent $\beta$-phenyl-substituted BODIPY microviscosity sensor [33]. We decided to explore this group of BODIPY derivatives with $\beta$-phenyls more thoroughly (Figure 1) and to continue aiming for better microviscosity, temperature, and polarity probes.

In this research, we present how the addition of an electron-withdrawing group (EWG) or an electron-donating group (EDG) to $\beta$-phenyls allows the tuning of the absorption and fluorescence spectra of the fluorophores. Furthermore, we investigate the sensitivity of the new probes to viscosity, temperature, and solvent polarity. The results show that attaching EDG to $\beta$-phenyls can suppress the temperature and viscosity sensitivity but enhance the polarity sensitivity, leading to a reliable red polarity probe. Finally, by performing theoretical calculations, we demonstrate that the extent of viscosity or temperature sensitivity is heavily determined by the energy barrier for non-radiative relaxation. We suggest that the acceptable barrier height for a viscosity sensor should not exceed 100 meV, whereas, for a temperature probe, it should fall within 100–200 meV.

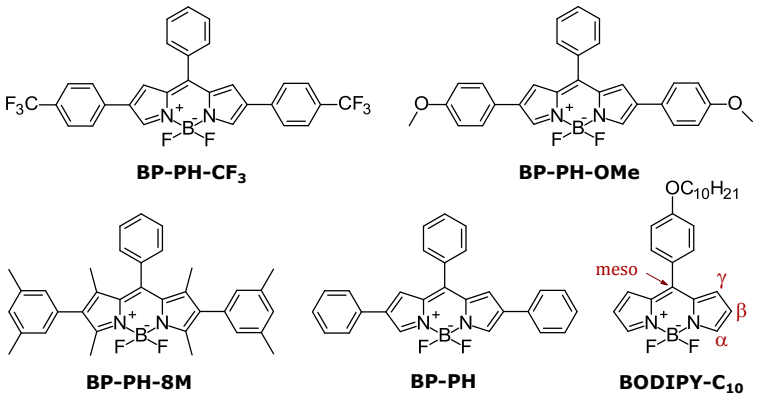


**Figure 1.** Molecular structures of BODIPYs investigated in this research (BP-PH-$CF_3$, BP-PH-OMe, BP-PH-8M) together with previously reported BP-PH [33] and a well-known viscosity probe BODIPY-$C_{10}$.

## 2. Results and Discussion

### *2.1. Absorbance and Fluorescence Spectra*

We begin by investigating basic spectroscopic properties of the new fluorophores and compare them to those of BP-PH and BODIPY-$C_{10}$. The absorbance spectra (Figure 2A) of all dyes show a higher energy band at 300–450 nm and the main absorption band in the 500–630 nm region. BP-PH shows an increased absorption wavelength ($\Delta\lambda$ = 90 nm) compared to the well-studied BODIPY-$C_{10}$ due to the extension of conjugation. The addition of EWG in $\beta$-phenyls (BP-PH-$CF_3$) results in a small blue-shift of the main absorption band compared to BP-PH ($\Delta\lambda$ = 15 nm). An opposite effect is observed when the EDG is attached to $\beta$-phenyls (BP-PH-OMe), resulting in the highest absorption wavelength of 625 nm. The position of the main absorption band of the new derivative BP-PH-8M

is blueshifted by 60 nm in contrast to previously reported BP-PH. The shift is caused by the addition of the methyl group in $\beta$-phenyls and the BODIPY core, which restricts the conjugation in BP-PH-8M.

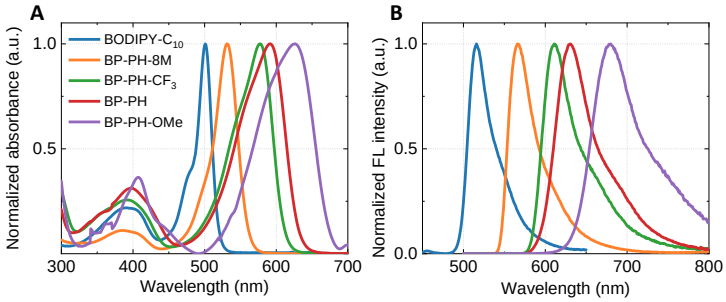


**Figure 2.** Absorbance (**A**) and fluorescence emission (**B**) spectra of BODIPY-$C_{10}$ (blue), BP-PH-8M (orange), BP-PH-$CF_3$ (green), BP-PH (red), and BP-PH-OMe (purple).

Very similar blue- and red-shift tendencies are observed in the fluorescence spectra (Figure 2B). BP-PH-8M and BP-PH-$CF_3$ correspond to the shorter wavelengths with the fluorescence maximum at 565 nm and 610 nm, respectively. In contrast, BP-PH-OMe shows the largest bathochromic shift, with the fluorescence peak at 680 nm due to an introduction of the EDG. A Stokes shift for unreported derivatives BP-PH-8M, BP-PH-$CF_3$, and BP-PH-OMe was 1169 $cm^{-1}$, 998 $cm^{-1}$, and 1294 $cm^{-1}$, respectively. The results also show that EWG at $\beta$-phenyls decreases the Stokes shift, while the opposite happens when EDG is introduced. As a result, by varying substituents on the $\beta$-phenyls, we were able to tune the emission wavelengths of new BODIPY fluorophores over a 500–700 nm range. In addition, quantum yield (QY) measurements in toluene demonstrated that attaching EWG to $\beta$-phenyls increases the QY value by 29% (BP-PH-$CF_3$), while EDG reduces it by 16% (BP-PH-OMe), with respect to previously reported BP-PH without $\beta$-phenyl substitutes [33]. BP-PH-8M showed the highest QY of 87% due to restricted intramolecular rotation of $\beta$-phenyls. The absorption, fluorescence emission, Stokes shift, fluorescence lifetime, QY, and radiative and non-radiative relaxation values of the investigated conjugates are displayed in Table 1. Normalised absorbance and fluorescence spectra of BP-PH-8M and BP-PH-$CF_3$ in solvents of various polarities are shown in Figure S1, ESI.

**Table 1.** Theoretically calculated and experimental values of the peak maxima of absorption ($\lambda_A$) and fluorescence emission ($\lambda_F$) spectra, as well as Stokes shifts ($\tilde{\nu}_{SS}$) for investigated derivatives in toluene. Experimental values of fluorescence lifetime ($\tau$), quantum yield (QY), radiative ($k_r$), and non-radiative ($k_{nr}$) decay rates in toluene are also displayed.

| | **Theoretical** | | | **Experiment** | | | | | | |
|---|---|---|---|---|---|---|---|---|---|---|
| **Derivative** | $\lambda_A$, **nm** | $\lambda_F$, **nm** | $\tilde{\nu}_{SS}$, $cm^{-1}$ | $\lambda_A$, **nm** | $\lambda_F$, **nm** | $\tilde{\nu}_{SS}$, $cm^{-1}$ | $\tau$, **ns** | **QY, %** | $k_r$, $10^8 \times s^{-1}$ | $k_{nr}$, $10^8 \times s^{-1}$ |
| BODIPY-$C_{10}$ | 423 | 443 | 1094 | 500 | 515 | 583 | 0.8 | 12 | 1.5 | 11 |
| BP-PH-8M | 465 | 489 | 1087 | 530 | 565 | 1169 | 4.3 | 87 | 2 | 0.3 |
| BP-PH-$CF_3$ | 476 | 518 | 1703 | 575 | 610 | 998 | 4 | 57 | 1.5 | 1 |
| BP-PH | 485 | 535 | 1959 | 590 | 630 | 1076 | 3.1 | 28 | 0.9 | 2.3 |
| BP-PH-OMe | 510 | 576 | 2258 | 625 | 680 | 1294 | 1.6 | 12 | 0.8 | 5.5 |

### *2.2. Theoretical Calculations*

The DFT calculations correctly predict the trend of increasing absorption and fluorescence wavelengths from BODIPY-$C_{10}$ to BP-PH-OMe (Table 1). The geometry of BP-PH-8M

shows that the methyl groups on the BODIPY core force $\beta$-phenyls out of plane (Figure S2, ESI), leading to weaker conjugation and shorter absorption and fluorescence wavelengths. Furthermore, the DFT calculations reveal that increasing absorption and fluorescence wavelengths, going from BP-PH-$CF_3$, to BP-PH, to BP-PH-OMe, are the result of a closer energy match between HOMO of BODIPY and $\beta$-phenyls (Figure S3, ESI). As a result, the HOMO of the resulting molecule is higher in energy, leading to a smaller HOMO-LUMO gap and higher absorption and fluorescence wavelengths. We note that theoretical wavelengths are shorter than experimental wavelengths by approximately 100 nm. This is a result of a well-known weakness of DFT, resulting in the overestimation of electronic transition energies in BODIPY fluorophores [34–36].

*Meso*-phenyl BODIPYs are known for their viscosity and temperature sensitivity, which arises due to the competition between fluorescence and non-radiative relaxation [25]. The key factor affecting the rate of non-radiative relaxation is the height of energy barrier that the molecule needs to cross during the rotation of *meso*-phenyl in order to relax non-radiatively (Figure 3A) [37–40]. Therefore, we calculated the barriers for the new BODIPY compounds and contrasted them with the barriers for BODIPY-$C_{10}$ and BP-PH (Figure 3B) [33]. BP-PH-8M has by far the highest barrier due to extra methyl groups that prevent the rotation of *meso*-phenyl. This explains why BP-PH-8M has the highest quantum yield of fluorescence and the slowest non-radiative decay rate (Table 1). The remaining molecules have smaller barriers, resulting in a faster non-radiative relaxation.

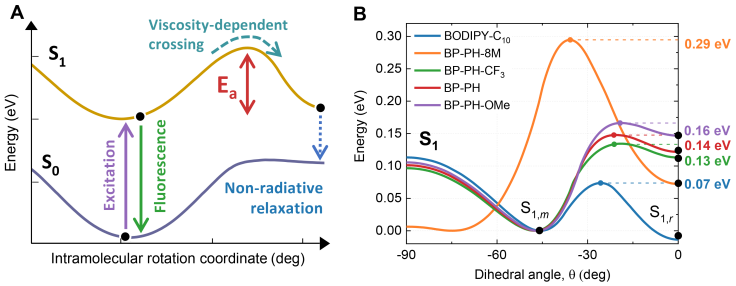


**Figure 3.** (**A**) Theoretical model of deexcitation pathways in BODIPY-based molecular rotors. (**B**) Potential energy surface curves of the first excited electronic state ($S_1$) of BODIPY-$C_{10}$ (blue), BP-PH-8M (orange), BP-PH-$CF_3$ (green), BP-PH (red), and BP-PH-OMe (purple) calculated using DFT. $\theta$ is a dihedral angle between the BODIPY core and the *meso*-phenyl group. The $S_{1,m}$ minima of curves were set to 0 for easier comparison.

### *2.3. Time-Resolved Fluorescence and Its Sensitivity to Viscosity, Temperature and Polarity*

In order to test if the new molecules could be used as probes of their environment, we explored their viscosity, temperature, and polarity sensing capabilities. Viscosity sensitivity measurements were performed in non-polar toluene/castor oil mixtures, covering the viscosity range of 0.5–920 cP. The majority of the observed fluorescence decays were monoexponential. The average lifetimes of biexponential decays were calculated using Equation (7) (Materials and Methods section), owing to the small contribution from the self-fluorescent castor oil. The viscosity-dependent fluorescence decays showed a slight viscosity dependence for BP-PH-$CF_3$ (Figure 4B) and almost no viscosity dependence for BP-PH-8M or BP-PH-OMe (Figure 4A,C). Overall, the new derivatives showed much lower viscosity sensitivity compared to the viscosity sensor BODIPY-$C_{10}$ (Figure 4D). This is expected, as theoretically calculated energy barriers for viscosity-sensitive non-radiative relaxation are larger than those for BODIPY-$C_{10}$. Thus, these results support the hypothesis that a large energy barrier predicted by the DFT calculations leads to little to no viscosity sensitivity [33,41]. Conjugates BP-PH-8M and BP-PH-$CF_3$ showed very similar

fluorescence lifetimes, in a 3–5 ns range, to the previously reported conjugate without additional moieties (BP-PH). Meanwhile, BP-PH-OMe showed much shorter lifetimes, around 1.5 ns.

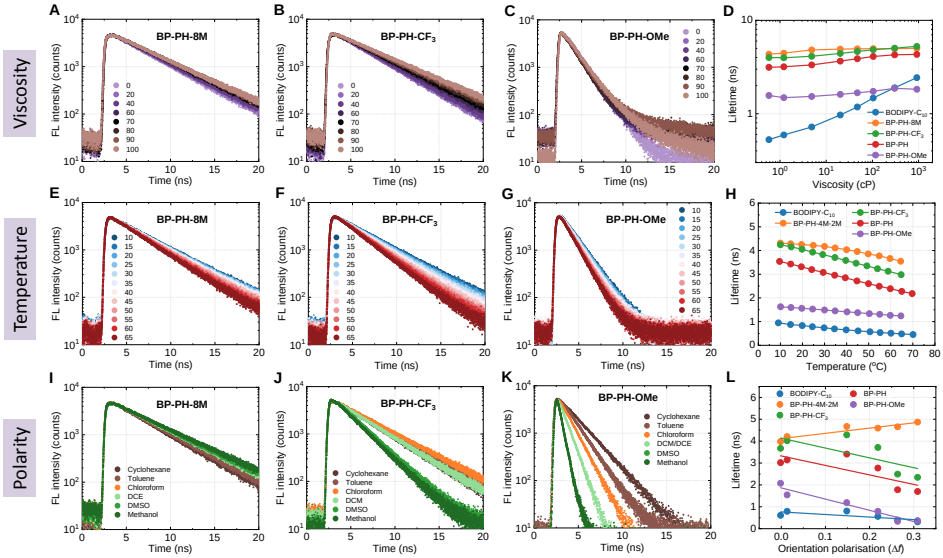


**Figure 4.** Time-resolved fluorescence decays of BP-PH-8M, BP-PH-$CF_3$, BP-PH-OMe, and their sensitivity to viscosity, temperature, and polarity. (**A**–**D**) Viscosity dependence in toluene-castor oil mixtures. (**E**–**H**) Temperature dependence obtained in toluene. (**I**–**L**) Polarity dependence in different polarity solvents. The polarity of solvents is quantified using their orientational polarizability. The data for BP-PH and BODIPY-$C_{10}$ is provided for comparison in (**D**,**H**,**L**).

Temperature-dependent fluorescence decays recorded in toluene reveal that all new fluorophores exhibited moderate temperature dependence (Figure 4E–G). The extent of temperature dependence was similar to BP-PH, although new conjugates BP-PH-8M and BP-PH-$CF_3$ showed longer lifetimes. BP-PH-OMe showed the weakest temperature sensitivity; its small lifetime values were more comparable to the widely studied BODIPY-$C_{10}$, which showed low lifetimes in the low viscosity solvent (toluene). Fits of Figure 4H are shown in Figure S4, ESI.

Lastly, the polarity dependence experiments were performed (Figure 4I–L). BP-PH-8M stood out among all the fluorophores; its sensitivity to solvent polarity was minimal (Figure 4I). The key structural difference of BP-PH-8M compared to other fluorophores was the existence of the methyl groups that prevented the rotation of the *meso*-phenyl group (Figure 1). Therefore, it is likely that the non-radiative relaxation pathway responsible for the polarity sensitivity involves the rotation of the *meso*-phenyl substituent. This particular intramolecular rotation is known to result in non-radiative relaxation of *meso*-phenyl-BODIPYs [42]. However, it also causes viscosity-sensitivity [25], which BP-PH-OMe does not possess. Therefore, another non-radiative relaxation pathway is likely to also involve the rotation of the *meso*-phenyl group.

BP-PH-$CF_3$ with the EWG substitute showed moderate polarity-sensitive properties. The kinetics of trifluoromethyl-substituted BODIPY (Figure 4J) was split into two groups: one consisted of non-polar and medium-polar solvents (cyclohexane, toluene, chloroform, and DCM) and the other had very polar solvents (DMSO and methanol). Meanwhile, EDG-substituted BP-PH-OMe showed strong polarity dependence and gradually decreasing

lifetimes with increasing solvent polarity (Figure 4K). Thanks to this polarity dependence, the methoxy-substituted conjugate could be used as a red-emitting lifetime-based polarity sensor. Compared to the absolute majority of other known fluorescent polarity sensors, such as the Reichardt's dye [43], BP-PH-OMe showed a far smaller solvatochromic shift (Figure 5). However, the constant spectral position of BP-PH-OMe (Figure 5) is an advantage if the FLIM technique is used. The spectral detection window can be correctly chosen beforehand without the need to guess, while the polarity can be determined from the fluorescence lifetime of BP-PH-OMe.

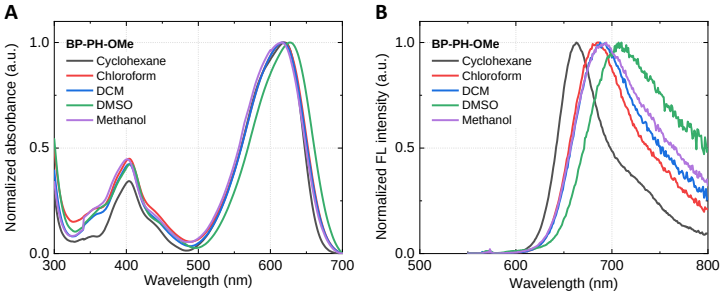


**Figure 5.** Absorbance (**A**) and fluorescence emission (**B**) spectra of BP-PH-OMe in various polarity solvents. From non-polar to very polar: cyclohexane (dark grey), chloroform (red), dichloromethane (DCM; blue), dimethyl sulfoxide (DMSO; green), and methanol (purple).

The visually observed trends (Figure 4D,H,L) can be quantified using the relative sensitivity $S$ [44]:

$$S = -\frac{\left|\frac{\delta\tau}{\delta x}\right|}{\tau} \cdot 100\% \,, \tag{1}$$

where $\tau$ is a fluorescence lifetime, $\delta x$ is a change of the parameter (temperature—°C, polarity—$\Delta f$). The $S$ is expressed as a percentage change of lifetime per step change of the parameter. The calculated values of relative sensitivity to temperature and polarity are shown in Table 2. The higher the value, the stronger the sensitivity of the fluorophore to the particular environmental parameter. The sensitivity to viscosity is usually quantified using the $x$ value from the Förster-Hoffmann equation [45]:

$$\tau = C\eta^x \,, \tag{2}$$

where $\tau$ is fluorescence lifetime, $\eta$ is viscosity, and $C$, $x$ are constants. Unsurprisingly, a widely used viscosity sensor BODIPY-$C_{10}$ showed the highest value of the viscosity sensitivity ($x$ = 0.21, Figure S5, ESI). The remaining molecules displayed very minor viscosity sensitivity ($\leq$0.05). All five conjugates showed small-to-moderate temperature sensitivity as a percentage change in lifetime per one degree Celsius, which was in the 0.3–1.0% range. However, a significant polarity sensitivity was observed for BP-PH-$CF_3$, BP-PH, and BP-PH-OMe, the latter showing the strongest sensitivity to polarity (265%). Therefore, our results show that BODIPY compounds with $\beta$-phenyl substituents can be tuned for making new temperature and polarity sensors.

**Table 2.** The relative sensitivities to temperature, polarity, and Förster–Hoffmann constant $x$ showing the extent of viscosity sensitivity of BODIPY-$C_{10}$, BP-PH-8M, BP-PH-$CF_3$, BP-PH, and BP-PH-OMe.

| Derivative | [%/°C] | [%/Δf] | $x$ |
|---|---|---|---|
| BODIPY-$C_{10}$ | 0.9 | 157 | 0.21 |
| BP-PH-8M | 0.3 | 72 | 0.02 |
| BP-PH-$CF_3$ | 0.5 | 116 | 0.04 |
| BP-PH | 0.6 | 141 | 0.05 |
| BP-PH-OMe | 0.4 | 265 | 0.03 |

### *2.4. The Role of Energy Barrier for Determining Sensitivity to Viscosity and Temperature*

In addition to the BODIPY fluorophores investigated in this work, there are a number of other known BODIPY probes that are sensitive to viscosity and temperature [9,10,21,28]. It is already known that the energy barrier for non-radiative relaxation is the key parameter affecting viscosity and temperature sensitivity [10,40,41]. Therefore, we set out to find optimal values that the energy barrier must have in order for the molecule to be the best sensor of viscosity or temperature. We started first with the viscosity probes.

The fluorescence lifetime and intensity of viscosity-sensitive fluorophores typically show a sigmoidal dependence on viscosity on a double logarithmic plot, as shown in Figure 6, when the fluorophore is characterised over a sufficiently large viscosity range [29,41]. If the fluorophore is characterised only at intermediate viscosities, a linear viscosity-fluorescence lifetime (or intensity) dependence is observed on a logarithmic plot [24,46], which conforms to the Förster–Hoffmann equation (Equation (2)). Deviations from linearity occur due to the fact that a fluorophore cannot have a fluorescence lifetime equal to zero or infinity. The maximum possible fluorescence lifetime is set by a radiative decay constant, while the minimum possible lifetime is limited by the time required for the molecule to change its geometry and relax to ground state at zero viscosity and infinite temperature. The full sigmoidal viscosity-lifetime dependence is described by Equation (3), which was derived using the Förster–Hoffmann equation (Equation (2)) as a starting point [29]:

$$\tau = \frac{1}{\frac{1}{C\eta^x + \frac{1}{k_{nr,max}}} \cdot e^{-\frac{E_a}{kT}} + k_r + k_x} \approx \frac{1}{\frac{1}{C\eta^x + \tau_{min}} \cdot e^{-\frac{E_a}{kT}} + \frac{1}{\tau_{max}}}, \quad (3)$$

where $\tau$ is a fluorescence lifetime, $\eta$ is the dynamic viscosity, $C$ and $x$ are constants, $E_a$ is the activation energy for non-radiative relaxation, $k_{nr,max}$ is the non-radiative decay constant at zero viscosity and infinite temperature, $k$ is the Boltzmann's constant, $T$ is the temperature in Kelvin, $k_r$ is the radiative decay constant, $k_x$ is the the sum of any other viscosity- and temperature-independent rate constants that lead to the population loss from the fluorescent state, and $\tau_{min}$ and $\tau_{max}$ are the minimum and maximum fluorescence lifetimes of the probe, respectively.

Usually, it is assumed that the parameter $x$, which comes from the Förster–Hoffman equation, is the most important parameter that shows sensitivity of the molecule to viscosity [25,26,29,46,47]. However, a high parameter $x$ has disadvantages. For instance, increasing it from 0.5 to 0.9 (Figure 6) shortens the viscosity sensitivity range. This creates a viscosity probe that can only be used for a limited range of viscosities. In our opinion, a parameter that better reveals the applicability of the viscosity sensor is its dynamic range, which is equal to the ratio of fluorescence lifetimes at infinite and zero viscosity at room temperature ($\tau_{\eta=\infty}/\tau_{\eta=0}$). As shown by simulated time-resolved fluorescence decays in Figure S6 (ESI), if the ratio is not sufficiently high, the sensor shows similar response at both high and low viscosities. Therefore, its applicability suffers and a high constant $x$ would not make this sensor a useful viscosity probe. Since our goal is to determine the values of the energy

barrier that are suitable for a viscosity sensor, we derived how $\tau_{\eta=\infty}/\tau_{\eta=0}$ depends on the energy barrier:

$$\frac{\tau_{\eta=\infty}}{\tau_{\eta=0}} = \tau_{max} \cdot \left( \frac{1}{\tau_{min}} \cdot e^{-\frac{E_a}{kT}} + \frac{1}{\tau_{max}} \right) = \frac{\tau_{max}}{\tau_{min}} \cdot e^{-\frac{E_a}{kT}} + 1. \quad (4)$$

Full derivation of Equation (4) is provided in the ESI. Equation (4) shows that the dynamic range of the probe depends on two parameters: the ratio $\tau_{max}/\tau_{min}$ and the height of the energy barrier ($E_a$). The lifetimes $\tau_{min}$ and $\tau_{max}$ correspond to zero viscosity, infinite temperature, and infinite viscosity, 0 K temperature, respectively.

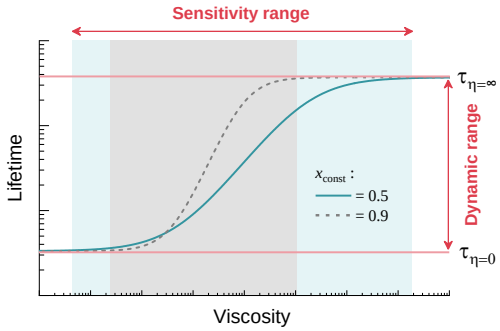


**Figure 6.** Fluorescence lifetime as a function of viscosity when the Förster–Hoffmann constant $x = 0.5$ (solid blue line) is at room temperature. If $x$ is increased ($x = 0.9$, dashed grey line), the viscosity sensitivity becomes greater but the sensitivity range is decreased. Red lines indicate lifetime limits when the viscosity is 0 (bottom line, $\tau_{\eta=0}$) and infinity (top line, $\tau_{\eta=\infty}$).

The $\tau_{max}/\tau_{min}$ ratio for the derivatives examined in this research can be obtained from the fitting parameters in Table S1, ESI, and is approximately equal to 500. Figure 7A displays how the dynamic range of viscosity probe depends on the $E_a$ when the $\tau_{max}/\tau_{min}$ ratio is equal to this value. The blue colored region shows dynamic range values between 5 and 50 and is considered a good dynamic range for a moderate-viscosity sensor. The upper bound ($\tau_{\eta=\infty}/\tau_{\eta=0} > 50$, the red colored area) is set by the typical time resolution of TCSPC or FLIM [48]. A viscosity sensor with $\tau_{\eta=\infty}/\tau_{\eta=0} > 50$ could only be used for imaging high-viscosity environments, as its fluorescence lifetime at moderate viscosities would be too fast for the usual TCSPC or FLIM setups.

The calculations show that acceptable values of $E_a$ for a viscosity sensor with similar molecular structure to our investigated compounds (Figure 1) are 0.05–0.12 eV, preferably closer to 0.05 eV. These values depend slightly on $\tau_{max}$ and $\tau_{min}$, which are set by the radiative decay constant and the degree of geometrical change occurring during non-radiative relaxation, respectively. The dependencies when the ratio $\tau_{max}/\tau_{min}$ equals 100 and 2500 are shown in Figure S7 (ESI).

Next, we proceeded to theoretically estimate the optimal energy barrier height $E_a$ for a fluorescent temperature sensor. The key parameter for a temperature sensor is its temperature sensitivity, which has the following expression:

$$s = -\frac{\partial\tau/\partial T}{\tau} \cdot 100\%\,, \quad (5)$$

where $s$ is sensitivity, $T$ is temperature, and $\tau$ is fluorescence lifetime. Starting with Equation (S1) (ESI), the following dependence of sensitivity on $E_a$ can be obtained:

$$s = \frac{E_a}{T^2 k\left(1 + \frac{\tau_{T=\infty}}{\tau_{T=0}} e^{\frac{E_a}{kT}}\right)} \cdot 100\% \,, \tag{6}$$

where $\tau_{T=\infty}$ and $\tau_{T=0}$ are fluorescence lifetimes at infinite and 0 K temperature, respectively, $k$ is Boltzmann's constant, and $T$ is temperature. The full derivation of Equation (6) can be found in the ESI. Using this equation, we calculated how sensitivity to temperature depends on the energy barrier for non-radiative relaxation (Figure 7B) for three different $\tau_{T=0}/\tau_{T=\infty}$ ratios. The results show that the optimal values of $E_a$ (0.10–0.20 eV) are slightly higher than those for a viscosity probe. The ratio $\tau_{T=0}/\tau_{T=\infty}$ is also important, as, for instance, if it is equal to 100, it will not be possible to reach a sensitivity of 1% at any $E_a$ value. As the value of the ratio increases (500 or 2500), it becomes easier to develop a temperature probe with good sensitivity. To get a high ratio, a molecule needs to be able to relax fast at high temperatures, thus giving a low $\tau_{T=\infty}$ value. This would be the case if the molecular geometry needs to change as little as possible during temperature-dependent non-radiative relaxation. Furthermore, our calculations show that it may be very challenging to obtain a fluorescent temperature probe with sensitivity exceeding 2%. Fluorescent temperature sensors based on a completely different mechanism may be required to reach sensitivities higher than that, as in the work of Xue et al. [49] and Pietsch et al. [50].

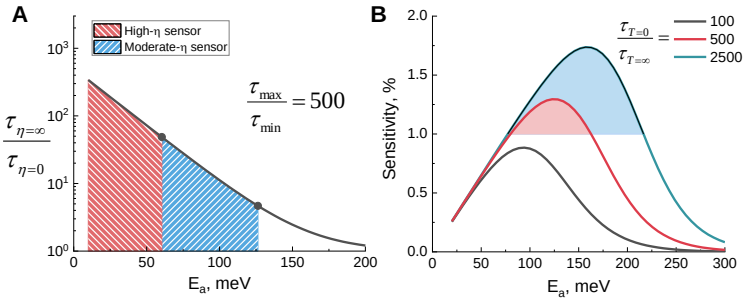


**Figure 7.** (**A**) Dynamic range of a viscosity sensor, expressed as a ratio of fluorescence lifetimes at zero and infinite viscosities, with respect to the energy barrier height for non-radiative viscosity-dependent relaxation. $\tau_{max}/\tau_{min}$ was set to 500 and T was set to 298 K. The shaded areas correspond to energy barrier values that would be appropriate for a moderate-viscosity sensor and a sensor suitable for high viscosities only. (**B**) Sensitivity to the temperature of the fluorescent temperature sensor with respect to the height of the energy barrier for non-radiative relaxation, which is temperature-dependent. The curves were calculated for three different $\tau_{T=0}/\tau_{T=\infty}$ ratios: 100 (black), 500 (red), and 2500 (blue). The shaded areas correspond to energy barrier values resulting in sensitivity above 1%.

In Figure 8, we show guidelines for energy barrier values required to obtain a fluorescent viscosity sensor or a temperature sensor. We also show $E_a$ values of BODIPY molecules investigated in this research, together with some previously reported $E_a$ values of BODIPY probes [9,10,33,41]. The scale represents which kind of sensor a BODIPY-based fluorophore is likely to be, depending on the value of the activation energy barrier, when the ratio $\tau_{max}/\tau_{min}$ is equal to 500, which is an approximate value for BODIPY probes investigated in this work. Two alternative scales for the ratios of 100 and 2500 are shown in Figure S8, ESI. The results show that viscosity probe requires a relatively small energy barrier of < 120 meV and ideally below 100 meV. Otherwise, the probe may also have substantial sensitivity to temperature, which is not generally desired. The most popular BODIPY viscosity probe BODIPY-$C_{10}$ satisfies this condition. The optimal barrier height

for a temperature probe is above 120 meV, where the viscosity-sensitivity is unlikely to be strong. This is where probes BP-PH, BP-PH-$CF_3$, and BP-PH-OMe are located, although the temperature sensitivity of the latter is overshadowed by the strong polarity sensitivity. If the energy barrier exceeds 200 meV, as is the case with BP-PH-8M, the fluorophore is unlikely to show strong sensitivity to either viscosity or temperature. Knowing these guidelines makes it possible to estimate viscosity or temperature sensitivities of new probes before synthesis by calculating energy barrier values using DFT.

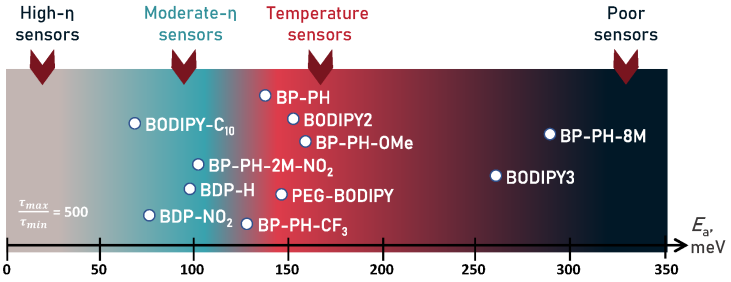


**Figure 8.** Visual scale demonstrating which energy barrier values are required for different types of sensors. From left: light grey—high-viscosity sensors, sky blue—moderate-viscosity sensors, red—temperature sensors, dark grey—poor sensors. White dots show energy barrier values of BODIPY derivatives reported in this paper (BP-PH-$CF_3$, BP-PH-OMe, BP-PH-8M), together with the barriers for other derivatives reported by Toliautas et al. (BDP-H, BDP-$NO_2$) [41], Polita et al. (BODIPY-$C_{10}$) [47], Ogle et al. (PEG-BODIPY) [9], Maleckaite et al. (BP-PH, BP-PH-2M-$NO_2$) [33], and Vysniauskas et al. (BODIPY2, BODIPY3) [10].

## 3. Materials and Methods

### *3.1. Dyes, Reagents, and Solvents*

BODIPY-$C_{10}$ and BP-PH were synthesised as previously reported [21]. The synthesis of previously unreported derivatives, BP-PH-$CF_3$, BP-PH-OMe, and BP-PH-8M, was accomplished using Suzuki reaction and is described in the ESI. Reagents and solvents for the organic synthesis of the BODIPY molecules were purchased directly from commercial suppliers; solvents were purified by known procedures. Thin layer chromatography was performed using TLC-aluminum sheets with silica gel (Merck 60 F254). Visualization was accomplished by UV light. Column chromatography was performed using silica gel 60 (0.040–0.063 mm) (Merck). NMR spectra were recorded on a Bruker Ascend 400 spectrometer (400 MHz for $^{1}$H, 100 MHz for $^{13}$C, 128.4 MHz for $^{11}$B, 376.5 MHz for $^{19}$F). NMR spectra were referenced to residual solvent peaks. Melting points were determined in open capillaries with a digital melting point IA9100 series apparatus (Thermo Fischer Scientific) and were not corrected. Stock solutions for all dyes were prepared in toluene at a concentration of 2 mM and diluted for further experiments in solvents or their mixtures. Cyclohexane, toluene, castor oil, chloroform, dichloromethane (DCM), dichloroethane (DCE), dimethyl sulfoxide (DMSO), and methanol were obtained from Sigma–Aldrich. The viscosities of toluene/castor oil mixtures were measured by using a vibrational viscometer (SV10, A&D) at temperatures of interest.

### *3.2. Absorption, Steady-State, Time-Resolved Fluorescence, and Quantum Yields*

Absorption spectra were measured by using a Jasco V-670 spectrophotometer. Fluorescence spectra and time-resolved fluorescence were recorded with a Edinburgh-F900 (Edinburgh Instruments) fluorimeter. A WhiteLase Micro (Fianium) laser was used as an excitation source together with bandpass filters (Thorlabs), with 10 nm bandwidth centred at 520 nm (BP-PH-8M) and 570 nm (BP-PH, BP-PH-$CF_3$, BP-PH-OMe). Excitation of the previously reported BODIPY-$C_{10}$ was performed by using a picosecond pulsed diode laser

EPL-470 (Edinburgh Instruments), emitting at 473 nm at 1 MHz frequency. Fluorescence decays were measured using the time-correlated single-photon counting technique. Fluorescence decays had 5000 counts at the peak of the decay, with 20 ns (BP-PH, BP-PH-$CF_3$, BP-PH-OMe, BP-PH-8M) and 50 ns (BODIPY-$C_{10}$) windows being used with 4096 channels. Absorption and fluorescence measurements were performed using quartz cuvettes (10 mm). QY measurements were obtained by a comparative method using fluorescein ($QY_F$ = 0.95 in 0.1 M $NaOH_{aq}$; used for BODIPY-$C_{10}$) [51], Rhodamine-6G ($QY_F$ = 0.94 in EtOH; used for BP-PH-8M) [52], and Rhodamine-101 ($QY_F$ = 0.91 in EtOH; used for BP-PH-$CF_3$, BP-PH, BP-PH-OMe) [52] as a standard. The concentration of dyes was 2–6 μM.

### *3.3. Theoretical Calculations*

Quantum chemical calculations of the studied molecular rotors were performed using the electronic structure modeling package Gaussian09. [53] The calculations were based on density functional theory (DFT) [54] (for ground state properties) and time-dependent DFT (TD-DFT) [55] (for the excited state properties). M06-2X hybrid functional [56] and cc-pVDZ basis sets [57] were used at all stages of the calculations; this use was previously validated by functional benchmarks by Momeni et al. [58]. The conductor-like polarizable continuum model (C-PCM) [59] with solvent parameters of toluene was used to account for bulk solvent effects on the solute molecules.

### *3.4. Data Analysis*

An Edinburgh-F900 software package was used for fitting fluorescence decays. For biexponential fluorescence decays, intensity-weighted lifetimes were calculated (Equation (7)):

$$\bar{\tau} = \frac{\sum\limits_i a_i \tau_i^2}{\sum\limits_i a_i \tau_i}, \quad (7)$$

where $a$ is an amplitude value and $\tau$ is the value of the lifetime.

The goodness-of-fit parameter ($\chi^2$) was 1.5 or less for single decays. Further data processing and analysis were done with Origin 2018.

## 4. Conclusions

In conclusion, we reported new $\beta$-phenyl-substituted BODIPY fluorophores showing red-shifted absorption and emission. We investigated the sensitivity of the molecules to viscosity, temperature, and solvent polarity. While BP-PH-8M did not show significant sensitivity, we showed that BP-PH-$CF_3$ is a moderate temperature probe. Furthermore, we showed that BP-PH-OMe has an exceptional combination of attractive properties. The fluorophore is a sensitive lifetime-based polarity sensor, it absorbs and emits in the red region of the visible spectrum, it has minimal sensitivity to other parameters, and it exhibits monoexponential decay kinetics.

Additionally, we analysed photophysical parameters that determine the viscosity or temperature sensitivity. Our theoretical results demonstrate that the sensitivity to viscosity and temperature strongly depends on the energy barrier for non-radiative relaxation. The optimal values of the barrier for a temperature probe are in the range of 100–200 meV, while a microviscosity probe should have a smaller barrier of 120 meV or less. We hope that these guidelines will help to develop new viscosity and temperature sensors as they make it easier to estimate the degree of viscosity or temperature sensitivity of probes before synthesis using theoretically calculated energy barrier values.

**Supplementary Materials:** Supplementary materials are available online. Figure S1: Absorbance and fluorescence spectra, Figure S2: Quantum chemical calculations, Figure S3: HOMO and LUMO orbitals, Figure S4: Temperature sensitivity in toluene, Figure S5: Viscosity-lifetime dependencies in toluene-castor oil mixtures, Figure S6: Simulated time-resolved fluorescence decays for different $\tau_{\eta=\infty}/\tau_{\eta=0} > 50$ ratios, Figure S7: $\tau_{\eta=\infty}/\tau_{\eta=0} > 50$ dependency on the energy barrier for non-

radiative relaxation, Figure S8: Visual scale for BODIPY-based rotors when the ratio $\tau_{max}/\tau_{min}$ is equal to 100 (A) and 2500 (B), Figures S9–S24: NMR spectra of derivatives studied in this research, Derivation: Equation (4), Derivation: Equation (6), DFT data: The Cartesian (XYZ) coordinates of the optimized ground and excited states for BP-PH-$CF_3$, BP-PH-OMe, and BP-PH-8M, Synthesis: Reaction scheme and procedure. Table S1: Obtained fitting parameters from the fits in Figure S1.

**Author Contributions:** K.M., spectroscopic characterisation, data analysis, and writing—original draft preparation; D.N., spectroscopic characterisation, data analysis, and theoretical derivations; R.Ž., spectroscopic characterisation and data analysis; J.D.-V., synthesis and characterisation of new compounds; S.T., (Stepas Toliautas) DFT calculations and data analysis; S.T., (Sigitas Tumkevičius) supervision of organic synthesis; A.V., conceptualization, writing—review and editing, supervision, and funding acquisition. All authors have read and agreed to the published version of the manuscript.

**Funding:** This research was funded by a grant (No. S-MIP-19-6) from the Research Council of Lithuania.

**Institutional Review Board Statement:** Not applicable.

**Informed Consent Statement:** Not applicable.

**Data Availability Statement:** Raw data available upon reasonable request.

**Acknowledgments:** Quantum chemical computations were carried out using resources at the High Performance Computing Center "HPC Saulėtekis" (Vilnius University, Faculty of Physics).

**Conflicts of Interest:** The authors declare no conflict of interest.

## References

1. Sunahara, H.; Urano, Y.; Kojima, H.; Nagano, T. Design and synthesis of a library of BODIPY-based environmental polarity sensors utilizing photoinduced electron-transfer-controlled fluorescence ON/OFF switching. *J. Am. Chem. Soc.* **2007**, *129*, 5597–5604. doi: 10.1021/ja068551y. [CrossRef] [PubMed]
2. Xiao, H.; Li, P.; Tang, B. Recent progresses in fluorescent probes for detection of polarity. *Coord. Chem. Rev.* **2021**, *427*, 213582. doi: 10.1016/j.ccr.2020.213582. [CrossRef]
3. Homma, M.; Takei, Y.; Murata, A.; Inoue, T.; Takeoka, S. A ratiometric fluorescent molecular probe for visualization of mitochondrial temperature in living cells. *Chem. Commun.* **2015**, *51*, 6194–6197. doi: 10.1039/c4cc10349a. [CrossRef] [PubMed]
4. Ogle, M.M.; Smith McWilliams, A.D.; Jiang, B.; Martí, A.A. Latest Trends in Temperature Sensing by Molecular Probes. *ChemPhotoChem* **2020**, *4*, 255–270. doi: 10.1002/cptc.201900255. [CrossRef]
5. Kubánková, M.; López-Duarte, I.; Kiryushko, D.; Kuimova, M.K. Molecular rotors report on changes in live cell plasma membrane microviscosity upon interaction with beta-amyloid aggregates. *Soft Matter* **2018**, *14*, 9466–9474. doi: 10.1039/c8sm01633j. [CrossRef]
6. Chambers, J.E.; Kubánková, M.; Huber, R.G.; López-Duarte, I.; Avezov, E.; Bond, P.J.; Marciniak, S.J.; Kuimova, M.K. An Optical Technique for Mapping Microviscosity Dynamics in Cellular Organelles. *ACS Nano* **2018**, *12*, 4398–4407. doi: 10.1021/acsnano.8b00177. [CrossRef]
7. Xiao, H.; Li, P.; Tang, B. Small Molecular Fluorescent Probes for Imaging of Viscosity in Living Biosystems. *Chem. A Eur. J.* **2021**, *27*, 6880–6898. doi: 10.1002/chem.202004888. [CrossRef]
8. Miao, W.; Yu, C.; Hao, E.; Jiao, L. Functionalized BODIPYs as Fluorescent Molecular Rotors for Viscosity Detection. *Front. Chem.* **2019**, *7*, 1–6. doi: 10.3389/fchem.2019.00825. [CrossRef]
9. Ogle, M.M.; Smith McWilliams, A.D.; Ware, M.J.; Curley, S.A.; Corr, S.J.; Martí, A.A. Sensing Temperature in Vitro and in Cells Using a BODIPY Molecular Probe. *J. Phys. Chem. B* **2019**, *123*, 7282–7289. doi: 10.1021/acs.jpcb.9b04384. [CrossRef]
10. Vyšniauskas, A.; Cornell, B.; Sherin, P.S.; Maleckaitė, K.; Kubánková, M.; Izquierdo, M.A.; Vu, T.T.; Volkova, Y.A.; Budynina, E.M.; Molteni, C.; Kuimova, M.K. Cyclopropyl Substituents Transform the Viscosity-Sensitive BODIPY Molecular Rotor into a Temperature Sensor. *ACS Sens.* **2021**, *6*, 2158–2167. doi: 10.1021/acssensors.0c02275. [CrossRef]
11. Steinmark, I.E.; James, A.L.; Chung, P.H.; Morton, P.E.; Parsons, M.; Dreiss, C.A.; Lorenz, C.D.; Yahioglu, G.; Suhling, K. Targeted fluorescence lifetime probes reveal responsive organelle viscosity and membrane fluidity. *PLoS ONE* **2019**, *14*, e0211165. doi: 10.1371/journal.pone.0211165. [CrossRef]
12. Arai, S.; Lee, S.C.; Zhai, D.; Suzuki, M.; Chang, Y.T. A molecular fluorescent probe for targeted visualization of temperature at the endoplasmic reticulum. *Sci. Rep.* **2014**, *4*, 2–7. doi: 10.1038/srep06701. [CrossRef]
13. Nölle, J.M.; Jüngst, C.; Zumbusch, A.; Wöll, D. Monitoring of viscosity changes during free radical polymerization using fluorescence lifetime measurements. *Polym. Chem.* **2014**, *5*, 2700–2703. doi: 10.1039/c3py01684f. [CrossRef]
14. Barja, B.C.; Chesta, C.A.; Atvars, T.D.; Aramendía, P.F. Fluorescent polymer coatings with tuneable sensitive range for remote temperature sensing. *Spectrochim. Acta Part A Mol. Biomol. Spectrosc.* **2013**, *116*, 13–16. doi: 10.1016/j.saa.2013.07.003. [CrossRef]

15. Hosny, N.A.; Fitzgerald, C.; Vyšniauskas, A.; Athanasiadis, A.; Berkemeier, T.; Uygur, N.; Pöschl, U.; Shiraiwa, M.; Kalberer, M.; Pope, F.D.; et al. Direct imaging of changes in aerosol particle viscosity upon hydration and chemical aging. *Chem. Sci.* **2016**, *7*, 1357–1367. doi: 10.1039/c5sc02959g. [CrossRef]
16. Munson, C.A.; Baker, G.A.; Baker, S.N.; Bright, F.V. Effects of subzero temperatures on fluorescent probes sequestered within aerosol-OT reverse micelles. *Langmuir* **2004**, *20*, 1551–1557. doi: 10.1021/la0302753. [CrossRef]
17. Olšinová, M.; Jurkiewicz, P.; Pozník, M.; Šachl, R.; Prausová, T.; Hof, M.; Kozmík, V.; Teplý, F.; Svoboda, J.; Cebecauer, M. Di- and tri-oxalkyl derivatives of a boron dipyrromethene (BODIPY) rotor dye in lipid bilayers. *Phys. Chem. Chem. Phys.* **2014**, *16*, 10688–10697. doi: 10.1039/c4cp00888j. [CrossRef]
18. Colom, A.; Derivery, E.; Soleimanpour, S.; Tomba, C.; Molin, M.D.; Sakai, N.; González-Gaitán, M.; Matile, S.; Roux, A. A fluorescent membrane tension probe. *Nat. Chem.* **2018**, *10*, 1118–1125. doi: 10.1038/s41557-018-0127-3. [CrossRef]
19. Hassoun, S.; Karam, P. Fluorescent-Based Thermal Sensing in Lipid Membranes. *Langmuir* **2020**, *36*, 1221–1226. doi: 10.1021/acs.langmuir.9b03128. [CrossRef]
20. Berezin, M.Y.; Achilefu, S. Fluorescence lifetime measurements and biological imaging. *Chem. Rev.* **2010**, *110*, 2641–2684. doi: 10.1021/cr900343z. [CrossRef]
21. Kuimova, M.K.; Yahioglu, G.; Levitt, J.A.; Suhling, K. Molecular rotor measures viscosity of live cells via fluorescence lifetime imaging. *J. Am. Chem. Soc.* **2008**, *130*, 6672–6673. doi: 10.1021/ja800570d. [CrossRef]
22. Klymchenko, A.S. Solvatochromic and Fluorogenic Dyes as Environment-Sensitive Probes: Design and Biological Applications. *Acc. Chem. Res.* **2017**, *50*, 366–375. doi: 10.1021/acs.accounts.6b00517. [CrossRef]
23. Lee, S.C.; Heo, J.; Woo, H.C.; Lee, J.A.; Seo, Y.H.; Lee, C.L.; Kim, S.; Kwon, O.P. Fluorescent Molecular Rotors for Viscosity Sensors. *Chem. A Eur. J.* **2018**, *24*, 13706–13718. doi: 10.1002/chem.201801389. [CrossRef]
24. Vyšniauskas, A.; Kuimova, M.K. A twisted tale: Measuring viscosity and temperature of microenvironments using molecular rotors. *Int. Rev. Phys. Chem.* **2018**, *37*, 259–285. doi: 10.1080/0144235X.2018.1510461. [CrossRef]
25. Kuimova, M.K. Mapping viscosity in cells using molecular rotors. *Phys. Chem. Chem. Phys.* **2012**, *14*, 12671–12686. doi: 10.1039/c2cp41674c. [CrossRef]
26. Levitt, J.A.; Chung, P.H.; Kuimova, M.K.; Yahioglu, G.; Wang, Y.; Qu, J.; Suhling, K. Fluorescence anisotropy of molecular rotors. *Chemphyschem* **2011**, *12*, 662–672. doi: 10.1002/cphc.201000782. [CrossRef]
27. Zhu, H.; Fan, J.; Mu, H.; Zhu, T.; Zhang, Z.; Du, J.; Peng, X. D-PET-controlled "off-on" Polarity-sensitive Probes for Reporting Local Hydrophilicity within Lysosomes. *Sci. Rep.* **2016**, *6*, 1–10. doi: 10.1038/srep35627. [CrossRef]
28. Vu, T.T.; Méallet-Renault, R.; Clavier, G.; Trofimov, B.A.; Kuimova, M.K. Tuning BODIPY molecular rotors into the red: Sensitivity to viscosity: Vs. temperature. *J. Mater. Chem. C* **2016**, *4*, 2828–2833. doi: 10.1039/c5tc02954f. [CrossRef]
29. Vyšniauskas, A.; López-Duarte, I.; Duchemin, N.; Vu, T.T.; Wu, Y.; Budynina, E.M.; Volkova, Y.A.; Peña Cabrera, E.; Ramírez-Ornelas, D.E.; Kuimova, M.K. Exploring viscosity, polarity and temperature sensitivity of BODIPY-based molecular rotors. *Phys. Chem. Chem. Phys.* **2017**, *19*, 25252–25259. doi: 10.1039/C7CP03571C. [CrossRef] [PubMed]
30. Eichler, J.; Knof, J.; Lenz, H. Measurements on the depth of penetration of light (0.35–1.0 μm) in tissue. *Radiat. Environ. Biophys.* **1977**, *14*, 239–242. doi: 10.1007/BF01323942. [CrossRef] [PubMed]
31. Weissleder, R. A clearer vision for in vivo imaging: Progress continues in the development of smaller, more penetrable probes for biological imaging. *Nat. Biotechnol.* **2001**, *19*, 316–317. doi: 10.1038/86684. [CrossRef]
32. Alamudi, S.H.; Su, D.; Lee, K.J.; Lee, J.Y.; Belmonte-Vázquez, J.L.; Park, H.S.; Peña-Cabrera, E.; Chang, Y.T. A palette of background-free tame fluorescent probes for intracellular multi-color labelling in live cells. *Chem. Sci.* **2018**, *9*, 2376–2383. doi: 10.1039/c7sc04716a. [CrossRef]
33. Maleckaite, K.; Dodonova, J.; Toliautas, S.; Zilenaite, R.; Jurgutis, D.; Karabanovas, V.; Tumkevicius, S.; Vysniauskas, A. Designing a Red-Emitting Viscosity Sensitive BODIPY Fluorophore for Intracellular Viscosity Imaging. *Chem. A Eur. J.* **2021**. doi: 10.1002/chem.202102743. [CrossRef]
34. Le Guennic, B.; Jacquemin, D. Taking Up the Cyanine Challenge with Quantum Tools. *Acc. Chem. Res.* **2015**, *48*, 530–537. doi: 10.1021/ar500447q. [CrossRef]
35. Berraud-Pache, R.; Neese, F.; Bistoni, G.; Izsák, R. Unveiling the Photophysical Properties of Boron-dipyrromethene Dyes Using a New Accurate Excited State Coupled Cluster Method. *J. Chem. Theory Comput.* **2020**, *16*, 564–575. doi: 10.1021/acs.jctc.9b00559. [CrossRef]
36. Momeni, M.R.; Brown, A. Why do TD-DFT excitation energies of BODIPY/aza-BODIPY families largely deviate from experiment? Answers from electron correlated and multireference methods. *J. Chem. Theory Comput.* **2015**, *11*, 2619–2632. doi: 10.1021/ct500775r. [CrossRef]
37. Prlj, A.; Vannay, L.; Corminboeuf, C. Fluorescence Quenching in BODIPY Dyes: The Role of Intramolecular Interactions and Charge Transfer. *Helv. Chim. Acta* **2017**, *100*, 1–9. doi: 10.1002/hlca.201700093. [CrossRef]
38. Eshuis, H.; Van Voorhis, T. The influence of initial conditions on charge transfer dynamics. *Phys. Chem. Chem. Phys.* **2009**, *11*, 10293–10298. doi: 10.1039/b912085h. [CrossRef]
39. Lin, Z.; Kohn, A.W.; Van Voorhis, T. Toward Prediction of Nonradiative Decay Pathways in Organic Compounds II: Two Internal Conversion Channels in BODIPYs. *J. Phys. Chem. C* **2020**, *124*, 3925–3938. doi: 10.1021/acs.jpcc.9b08292. [CrossRef]

40. Liu, X.; Chi, W.; Qiao, Q.; Kokate, S.V.; Cabrera, E.P.; Xu, Z.; Liu, X.; Chang, Y.T. Molecular Mechanism of Viscosity Sensitivity in BODIPY Rotors and Application to Motion-Based Fluorescent Sensors. *ACS Sens.* **2020**, *5*, 731–739. doi: 10.1021/acssensors.9b01951. [CrossRef]
41. Toliautas, S.; Dodonova, J.; Žvirblis, A.; Čiplys, I.; Polita, A.; Devižis, A.; Tumkevičius, S.; Šulskus, J.; Vyšniauskas, A. Enhancing the Viscosity-Sensitive Range of a BODIPY Molecular Rotor by Two Orders of Magnitude. *Chem. A Eur. J.* **2019**, *25*, 10342–10349. doi: 10.1002/chem.201901315. [CrossRef]
42. Sazanovich, I.V.; Kirmaier, C.; Hindin, E.; Yu, L.; Bocian, D.F.; Lindsey, J.S.; Holten, D. Structural Control of the Excited-State Dynamics of Bis (dipyrrinato) zinc Complexes: Self-Assembling Chromophores for Light-Harvesting Architectures. *J. Am. Chem. Soc.* **2004**, *1*, 2664–2665. [CrossRef]
43. Reichardt, C. *Solvent and Solvent Effects in Organic Chemistry*; Wiley-VCH: Weinheim, Germany, 2003; pp. 1–599.
44. Zhou, J.; del Rosal, B.; Jaque, D.; Uchiyama, S.; Jin, D. Advances and challenges for fluorescence nanothermometry. *Nat. Methods* **2020**, *17*, 967–980. doi: 10.1038/s41592-020-0957-y. [CrossRef]
45. Förster, T.; Hoffmann, G. Effect of viscosity on the fluorescence quantum yield of some dye systems. *Z. Fur Phys. Chem.* **1971**, *75*, 63–76. [CrossRef]
46. Chung, P.H.; Levitt, J.A.; Kuimova, M.K.; Yahioglu, G.; Suhling, K. Mapping intracellular viscosity by advanced fluorescence imaging of molecular rotors in living cells. *Multiphot. Microsc. Biomed. Sci. XI* **2011**, *7903*, 790323. doi: 10.1117/12.876257. [CrossRef]
47. Polita, A.; Toliautas, S.; Žvirblis, R.; Vyšniauskas, A. The effect of solvent polarity and macromolecular crowding on the viscosity sensitivity of a molecular rotor BODIPY-C10. *Phys. Chem. Chem. Phys.* **2020**, *22*, 8296–8303. doi: 10.1039/c9cp06865a. [CrossRef]
48. Becker, W. *The bh TCSPC Handbook*; Becker et Hickl: Berlin, Germany, 2010; pp. 1–566.
49. Xue, K.; Wang, C.; Wang, J.; Lv, S.; Hao, B.; Zhu, C.; Tang, B.Z. A Sensitive and Reliable Organic Fluorescent Nanothermometer for Noninvasive Temperature Sensing. *J. Am. Chem. Soc.* **2021**, *143*, 14147–14157. doi: 10.1021/jacs.1c04597. [CrossRef] [PubMed]
50. Pietsch, C.; Schubert, U.S.; Hoogenboom, R. Aqueous polymeric sensors based on temperature-induced polymer phase transitions and solvatochromic dyes. *Chem. Commun.* **2011**, *47*, 8750–8765. doi: 10.1039/c1cc11940k. [CrossRef]
51. Brannon, J.H.; Magde, D. Absolute quantum yield determination by thermal blooming. Fluorescein. *J. Phys. Chem.* **1978**, *82*, 705–709. doi: 10.1021/j100495a018. [CrossRef]
52. Wall, K.P.; Dillon, R.; Knowles, M.K. Fluorescence quantum yield measurements of fluorescent proteins: A laboratory experiment for a biochemistry or molecular biophysics laboratory course. *Biochem. Mol. Biol. Educ.* **2015**, *43*, 52–59. doi: 10.1002/bmb.20837. [CrossRef]
53. Frisch, M.J.; Trucks, G.W.; Schlegel, H.B.; Scuseria, G.E.; Robb, M.A.; Cheeseman, J.R.; Scalmani, G.; Barone, V.; Petersson, G.A.; Nakatsuji, H.; et al. *Gaussian09, Revision D.01*; Gaussian, Inc.: Wallingford, CT, USA, 2013.
54. Parr, R.G. *Density Functional Theory of Atoms and Molecules*; Oxford University Press: Oxford, UK, 1989.
55. Stratmann, R.E.; Scuseria, G.E.; Frisch, M.J. An efficient implementation of time-dependent density-functional theory for the calculation of excitation energies of large molecules. *J. Chem. Phys.* **1998**, *109*, 8218–8224. doi: 10.1063/1.477483. [CrossRef]
56. Zhao, Y.; Truhlar, D.G. The M06 suite of density functionals for main group thermochemistry, thermochemical kinetics, noncovalent interactions, excited states, and transition elements: Two new functionals and systematic testing of four M06-class functionals and 12 other function. *Theor. Chem. Acc.* **2008**, *120*, 215–241. doi: 10.1007/s00214-007-0310-x. [CrossRef]
57. Kendall, R.A.; Dunning, T.H.; Harrison, R.J. Electron affinities of the first-row atoms revisited. Systematic basis sets and wave functions. *J. Chem. Phys.* **1992**, *96*, 6796–6806. [CrossRef]
58. Momeni, M.R.; Brown, A. A Local CC2 and TDA-DFT Double Hybrid Study on BODIPY/aza-BODIPY Dimers as Heavy Atom Free Triplet Photosensitizers for Photodynamic Therapy Applications. *J. Phys. Chem. A* **2016**, *120*, 2550–2560. doi: 10.1021/acs.jpca.6b02883. [CrossRef]
59. Cossi, M.; Rega, N.; Scalmani, G.; Barone, V. Energies, structures, and electronic properties of molecules in solution with the C-PCM solvation model. *J. Comput. Chem.* **2003**, *24*, 669–681. doi: 10.1002/jcc.10189. [CrossRef]

# P4

# Red fluorescent BODIPY molecular rotor for high microviscosity environments

**K. Maleckaitė**, J. Dodonova-Vaitkūnienė, R. Žilėnaitė, S. Tumkevičius, A. Vyšniauskas

*Methods Appl. Fluoresc.* **10**(3), art. n. 034008 (2022)
DOI: 10.1088/2050-6120/ac7943

Reprinted from *Methods and Applicationsin Fluorescence*
with permission from IOP Publishing, Ltd.

Supporting information: https://doi.org/10.1088/2050-6120/ac7943

IOP Publishing Methods Appl. Fluoresc. 10 (2022) 034008 https://doi.org/10.1088/2050-6120/ac7943

Methods and Applications in Fluorescence



PAPER

RECEIVED
25 January 2022

REVISED
31 May 2022

ACCEPTED FOR PUBLICATION
15 June 2022

PUBLISHED
27 June 2022

# Red fluorescent BODIPY molecular rotor for high microviscosity environments

**Karolina Maleckaitė[1], Jelena Dodonova-Vaitkūnienė[2], Rugilė Žilėnaitė[1,2], Sigitas Tumkevičius[2] and Aurimas Vyšniauskas[1,2,*]**

[1] Center of Physical Sciences and Technology, Saulėtekio av. 3, Vilnius, LT-10257, Lithuania
[2] Institute of Chemistry, Faculty of Chemistry and Geosciences, Vilnius University, Naugarduko str. 24, Vilnius, LT-03225, Lithuania
[*] Author to whom any correspondence should be addressed.

**E-mail:** aurimas.vysniauskas@ftmc.lt

**Keywords:** fluorescence spectroscopy, microviscosity, BODIPY fluorophores

Supplementary material for this article is available online

## Abstract

Microviscosity has a strong impact for diffusion-controlled processes in biological environments. BODIPY molecular rotors are viscosity-sensitive fluorophores that provide a simple and non-invasive way to visualise microviscosity. Although green fluorescent probes are already well developed for imaging, thick biological samples require longer wavelengths for investigation. This work focuses on the examination of novel $\beta$-substituted *meso*-phenyl-BODIPYs possessing a red emission. We report a new red fluorescent BODIPY-based probe BP-Vinyl-$NO_2$ suitable for sensing microviscosity in rigid environments of over 100 000 cP viscosities. Furthermore, we demonstrate that changing the methyl position from *ortho* to *meta* on the $\beta$-phenyl-substituted conjugate BP-PH-m2M-$NO_2$ redshifts absorbance and fluorescence spectra while maintaining viscosity sensitivity. Finally, we show that nitro-substitution of *meso*-phenyl is a versatile approach to improve the sensitivity to viscosity while suppressing sensitivity to polarity and temperature of such derivatives. In summary, we present two nitro-substituted red fluorescent probes that could be used as lifetime-based microviscosity sensors.

## 1. Introduction

Microviscosity imaging is an important capability that can reveal key properties of a biological system. Changes in microviscosity can show biochemical and biophysical processes that occur inside live-cells [1–3], and can even help identify diseases such as Alzheimer's [4, 5] and atherosclerosis [6]. Visualisation of microviscosity is relevant for scientists studying polymers [7], live cells [8–10] and their specific organelles [11–13], lipid packing in cell membranes [14] and aerosols [15].

One of the simplest methods of visualising microviscosity is to use fluorescent probes called 'molecular rotors' [16, 17]. Their mechanism is based on the competition between the non-radiative transition involving intramolecular rotation and the radiative transition to the electronic ground state [1]. The less viscous the medium, the faster the molecular rotation resulting in a shorter lifetime and a lower quantum yield of fluorescence [18]. Molecular rotors can be separated into a few groups by their working principle. There are simple intensity-based probes that show stronger fluorescence in viscous environments [18], but suffer from the dependence of fluorescence intensity on the local concentration of the probes. Fortunately, there are two other groups of molecular rotors without this disadvantage. In the first group are ratiometric probes, which show a viscosity-dependent ratio of two peaks in the fluorescence spectra [19, 20]. Some of these probes have been reported not to respond to polarity, which is a common problem with molecular rotors [21, 22]. The second group are fluorescence lifetime-based probes. Microviscosity can be measured with these probes by fluorescence lifetime imaging microscopy (FLIM), a non-invasive method that visualises the microscopic sample [1, 23]. If a viscosity-sensitive fluorophore is used, a microviscosity map of the sample can be constructed.

BODIPY-based molecular rotors are among the most popular fluorophores used for microviscosity imaging [24]. These molecules stand-out for their

© 2022 IOP Publishing Ltd

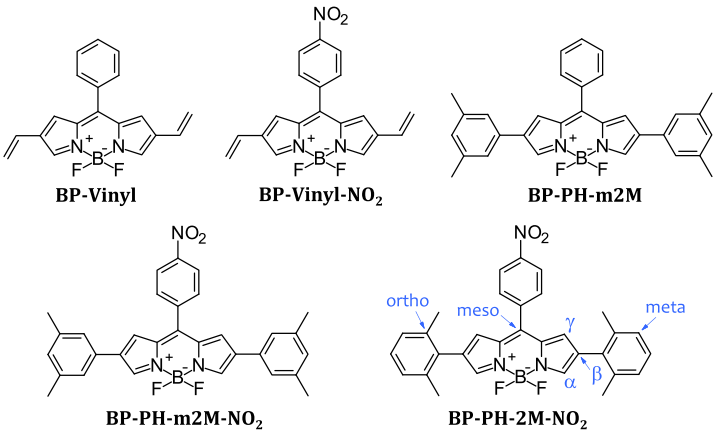


**Figure 1.** The molecular structures of BODIPY derivatives studied in this work (BP-Vinyl, BP-Vinyl-$NO_2$, BP-PH-m2M, BP-PH-m2M-$NO_2$) and a previously reported microviscosity sensor BP-PH-2M-$NO_2$ [43]. The blue-coloured notes indicate the substituted position on the molecule.

monoexponential fluorescence decay, which simplifies the acquisition of reliable fluorescence kinetics during a FLIM measurement [25]. BODIPYs have been used in aerosols [15, 26], live cells [24, 27, 28], and in various cell organelles [3, 29–36]. BODIPY-based molecules can also be used to detect bacteria [37] or as photosensitizers in cancer treatment [38]. Unfortunately, most BODIPY-based probes are green fluorescent, which complicates the application of fluorophores in biological samples [39].

The development of a red fluorescent, microviscosity-sensitive BODIPY rotor is a crucial task that could allow scientists to more easily image microviscosity in various samples for several reasons. First, autofluorescence of biological samples is less of an issue in the red region of the visible spectrum [40]. Second, it is more convenient to image the same biological samples together with other fluorophores (e.g. green fluorescent protein, GFP). Third, imaging of thick biological samples must fall within the optical window of deep tissue (650-1350nm) to minimise visible light scattering [41, 42]. Previously, we developed a red fluorescent BODIPY-based microviscosity probe BP-PH-2M-$NO_2$ [43] (figure 1). The design of this derivative was based on the extension of conjugation by $\beta$-phenyls and the lowering of a viscosity-sensitivity determining activation energy barrier by the introduction of a nitro group on the *meso*-phenyl. However, despite the red emission, BP-PH-2M-$NO_2$ requires excitation at around 550 nm, which is still far from red.

Here we report two new BODIPY probes possessing significantly longer absorption and emission wavelengths compared to BP-PH-2M-$NO_2$ with negligible dependence on solvent polarity and temperature. We demonstrate that one of the probes could also be utilised in high viscosity environments exceeding 100 000 cP. Finally, we show that the addition of -$NO_2$ is a universal way to increase the viscosity sensitivity of *meso*-phenyl-BODIPY probes.

## 2. Methods

### 2.1. Dyes, reagents, solvents

Reagents and solvents for the organic synthesis of the BODIPY molecules were purchased directly from commercial suppliers; solvents were purified by known procedures. Thin layer chromatography was performed using TLC-aluminium sheets with silica gel (Merck 60 F254). Visualization was accomplished by UV light. Column chromatography was performed using Silica gel 60 (0.040–0.063 mm) (Merck). NMR spectra were recorded on a Bruker Ascend 400 (400 MHz for $^{1}$H, 100 MHz for $^{13}$C, 128.4 MHz for $^{11}$B, 376.5 MHz for $^{19}$F). NMR spectra were referenced to residual solvent peaks. Melting points were determined in open capillaries with a digital melting point IA9100 series apparatus (Thermo Fischer Scientific) and were not corrected. High Resolution Mass Spectrometry (HRMS) analyses were carried out on a Dual-ESI Q-TOF 6520 (Agilent Technologies) mass spectrometer.

Stock solutions for all dyes were prepared in toluene at concentrations of 0.2–2 mM and diluted in solutions or solution mixtures for further experiments. The stock solution for the cryostat experiments was diluted in methanol. Cyclohexane, toluene, castor oil, chloroform, diethyl ether, tetrahydrofuran (THF), dichloromethane (DCM), cyclohexanone,

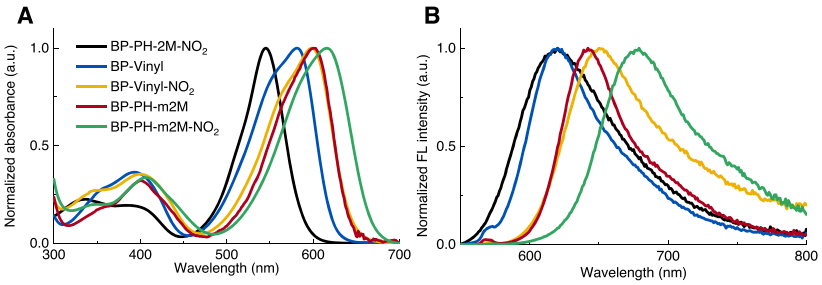


**Figure 2.** Absorbance (A) and fluorescence emission (B) spectra of BP-PH-2M-$NO_2$ (black), BP-Vinyl (blue), BP-Vinyl-$NO_2$ (yellow), BP-PH-m2M (red), and BP-PH-m2M-$NO_2$ (green) in toluene. Data of BP-PH-2M-$NO_2$ is reproduced with permission from [43].

dimethylformamide (DMF), dimethyl sulfoxide (DMSO), methanol, glycerol were purchased at Sigma-Aldrich. The viscosities of toluene-castor oil mixtures at different temperatures were measured using a vibro viscometer (SV10, A&D) connected to a thermostat. The viscosities of methanol-glycerol mixtures were obtained from previously measured data [44] and doublechecked using the aforementioned viscometer. Although castor oil is self-fluorescent (total contribution to fluorescence is only ≈1%), it is the only convenient option as a viscous solvent because of low polarity (dielectric constant is equal to 4.7) and ability to dissolve all new derivatives, which is not possible with glycerol.

### 2.2. Absorption, steady-state and time-resolved fluorescence, and quantum yields

The concentration of dyes used for the experiments at room temperature and for the temperature-dependent experiments was 9–14 $\mu$M. The concentration of BP-Vinyl-$NO_2$ in cooled glycerol was 95 $\mu$M. All spectroscopic measurements were performed using quartz cuvettes (10 mm) except for the experiments in cryostat, where the 0.5 mm quartz cuvette was used. Absorption spectra were measured using a Jasco V-670 spectrophotometer. Fluorescence spectra and time-resolved fluorescence decays were recorded with the Edinburgh-F900 (Edinburgh Instruments) fluorimeter. Excitation of the derivatives was performed using the WhiteLase Micro (Fianium) laser together with bandpass filters (Thorlabs) with a bandwidth of 10 nm centered at 570 nm. Fluorescence decays were measured using time-correlated single-photon counting (TCSPC). Fluorescence decays had 5000 counts at the fluorescence peak in the 20 ns acquisition time window with 4096 collection channels. Quantum yields (QY) were measured by comparative method [45] using Rhodamine-101 ($QY_F$= 0.91 in ethanol) [46] as a standard.

### 2.3. Data analysis

Fluorescence decays were fitted using Edinburgh-F900 software. Intensity-weighted lifetimes were calculated for biexponential fluorescence decays:

$$\bar{\tau} = \frac{\sum_i a_i \tau_i^2}{\sum_i a_i \tau_i}, \quad (1)$$

where $a$ is an amplitude value and $\tau$ is the lifetime value. The goodness-of-fit parameter ($\chi^2$) was 1.5 or less for single decays. Data processing and analysis were performed using Origin 2018.

## 3. Results and discussion

### 3.1. Synthesis of derivatives

Synthetic routes of the designed molecules BP-Vinyl, BP-Vinyl-$NO_2$, BP-PH-m2M and BP-PH-m2M-$NO_2$ are outlined in scheme 1. Compounds BP1,2 [47] and BP3,4 [43] were synthesized as previously reported. BP-Vinyl and BP-Vinyl-$NO_2$ were synthesized by the Stille cross-coupling reaction using dibromo-BODIPY (BP3,4) and tri-*n*-butyl(vinyl)tin as starting compounds. Synthesis of BP-PH-m2M and BP-PH-m2M-$NO_2$ was carried out by the Suzuki-Miyaura cross-coupling reaction of BP3,4 and corresponding boronic acids in the present of $Pd_2dba_3$/SPhos catalytic system. The synthetic details, characterization data and spectroscopic analysis data of the synthesized compounds are presented in the Electronic Supplementary Information (ESI) available online at stacks.iop.org/MAF/10/034008/mmedia, figures S4–S19. HRMS analysis data of BP-PH-m2M and BP-PH-m2M-$NO_2$ are presented in figures S20-S21, ESI. Mass spectroscopy data of BP-Vinyl and BP-Vinyl-$NO_2$ are not available due to a poor solubility of conjugates.

*Reagents and conditions*:i—NBS, $CH_2Cl_2$/DMF; ii—tri-*n*-butyl(vinyl)tin, $Pd(PPh_3)_4$, toluene, argon, 140 °C, 24h; iii—arylboronic acid, $Pd_2dba_3$, SPhos, $K_3PO_4$, toluene, argon, 140 °C, 24h.

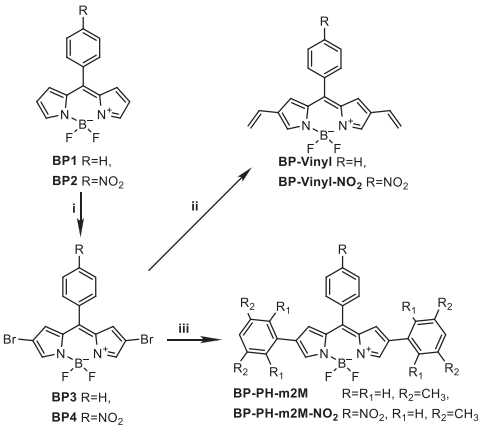


**Scheme 1.** Synthesis of BP-Vinyl, BP-Vinyl-$NO_2$, BP-PH-m2M and BP-PH-m2M-$NO_2$.

**Table 1.** Experimental values of absorption ($\lambda_A$), fluorescence emission maxima ($\lambda_F$), Stokes shifts ($\tilde{\nu}_{SS}$), fluorescence quantum yields (QY) and molar extinction coefficients ($\epsilon$) for BP-PH-2M-$NO_2$, BP-Vinyl, BP-Vinyl-$NO_2$, BP-PH-m2M and BP-PH-m2M-$NO_2$ in toluene.

| Derivative | $\lambda_A$, nm | $\lambda_F$, nm | $\tilde{\nu}_{SS}$, $cm^{-1}$ | QY, % | $\epsilon$, $M^{-1}\cdot cm^{-1}$ |
|---|---|---|---|---|---|
| BP-PH-2M-$NO_2$ | 545 | 620 | 2220 | 4 | $6.5\cdot10^4$ |
| BP-Vinyl | 581 | 620 | 1135 | 13 | $1.4\cdot10^4$ |
| BP-Vinyl-$NO_2$ | 598 | 650 | 1408 | 2 | $1.2\cdot10^4$ |
| BP-PH-m2M | 600 | 642 | 1139 | 28 | $4.4\cdot10^4$ |
| BP-PH-m2M-$NO_2$ | 615 | 679 | 1554 | 4 | $4.0\cdot10^4$ |

### 3.2. Absorbance and fluorescence

Figure 2 shows absorbance and fluorescence spectra of the investigated molecules in toluene. The absorbance spectra (figure 2(A)) consist of the low intensity band in the range of 300-450 nm and the main band in the 520-650 nm region. Due to an increased conjugation length, the main absorbance and fluorescence peaks are red-shifted in contrast to a plain BODIPY, which absorbs and fluoresces in the range of 480–550 nm [27].

Experiments show that a nitro group in *meso*-phenyl (BP-Vinyl-$NO_2$ and BP-PH-m2M-$NO_2$) increases the absorbance and fluorescence wavelengths. The addition of -$NO_2$ to the vinyl- and phenyl-substituted conjugates shifted the absorption peak by 17 nm and 15 nm, while the fluorescence spectra showed bathochromic shifts of 30 nm and 37 nm, respectively. Furthermore, the nitro group increased the Stokes shift for both molecules. Moreover, changing the position of the methyl substituents on the $\beta$-phenyls from *ortho* to *meta* (BP-PH-2M-$NO_2$ and BP-PH-m2M-$NO_2$, respectively) reduced the steric hindrance that prevents conjugation between the $\beta$-phenyls and the BODIPY core. This contributed to a red-shift of the fluorescence spectrum from 620 nm to 679 nm. The exact values of the absorbance, fluorescence maxima and Stokes shifts are given in table 1. Fluorescence quantum yields of BP-Vinyl and BP-PH-m2M were 13% and 28%, respectively, which were reduced to 2% and 4% by the addition of the nitro group. This reduction in the values is a consequence of the increase in the nonradiative rate when the nitro group is present. A similar reduction in quantum yield was also reported for BP-PH-2M-$NO_2$ [43]. The exact values of the quantum yield, radiative and nonradiative rates in toluene and castor oil are shown in table S1, ESI.

### 3.3. Viscosity sensitivity

To find out whether the new derivatives are sensitive to viscosity, we recorded time-resolved fluorescence decays in non-polar toluene-castor oil mixtures of varying viscosity (0.5-920 cP). The obtained fluorescence decays are shown in figures 3(A)–(D). BP-Vinyl and BP-PH-m2M showed monoexponential decays, while their nitro-substituted counterparts demonstrated mostly biexponential decays due to the presence of self-fluorescent castor oil, which becomes visible when a fluorophore has a shorter fluorescence lifetime. Mean fluorescence lifetimes of the biexponential decays were calculated using equation (1) in the Methods section. Exact lifetimes and amplitudes of

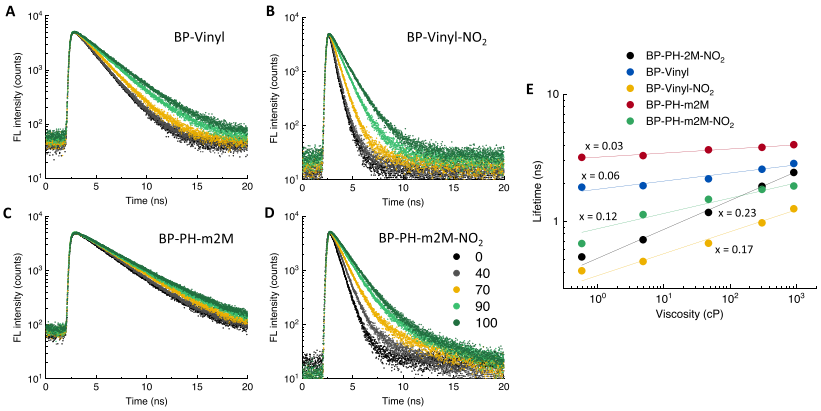


**Figure 3.** Time-resolved fluorescence decays of BP-Vinyl (A), BP-Vinyl-$NO_2$ (B), BP-PH-m2M (C), and BP-PH-m2M-$NO_2$ (D) in toluene-castor oil mixtures. The legend shows the volume fraction of castor oil (%) in the solvent mixture. (E) Fluorescence lifetimes of BP-PH-2M-$NO_2$ (black), BP-Vinyl (blue), BP-Vinyl-$NO_2$ (yellow), BP-PH-m2M (red), and BP-PH-m2M-$NO_2$ (green), obtained in non-polar toluene-castor oil mixtures, with respect to the viscosity of solvent mixtures. The fit was performed using the Förster-Hoffmann equation. Data of BP-PH-2M-$NO_2$ is reproduced with permission from [43].

individual exponential components in toluene-castor oil mixtures are given in table S2, ESI. A comparison of the lifetimes is shown in figure 3(E) together with the previously reported BP-PH-2M-$NO_2$ [43]. Fluorescence lifetime values were fitted using the Förster-Hoffmann equation [48]:

$$\tau = C\eta^x, \qquad (2)$$

where $\tau$ is fluorescence lifetime, $\eta$ - viscosity, $C$ and $x$ - constants. Linear fits are represented with the constant $x$ which shows an approximate degree of sensitivity to viscosity.

The experiments have demonstrated that BP-Vinyl and BP-PH-m2M show weak sensitivity to viscosity as their lifetimes increases only by 50% (1.9 to 2.9 ns) and 25% (3.2 to 4.0 ns), respectively when changing from toluene to viscous castor oil. The low viscosity sensitivity is also evident in Förster-Hoffmann fits as both molecules showed low $x$ values of 0.06 and 0.03. The addition of the nitro group to *meso*-phenyl improved viscosity sensitivity properties of both conjugates: the fluorescence decays of BP-Vinyl-$NO_2$ and BP-PH-m2M-$NO_2$ are visually more separated (figures 3(B) and (D)), with $x$ values of Förster-Hoffmann fits increasing by a factor of 3 and 4, respectively. The lifetime change of BP-Vinyl-$NO_2$ is comparable to the one of previously reported BP-PH-2M-$NO_2$ [43] ($x = 0.23$) and green fluorescent BODIPY-$C_{10}$ in toluene-castor oil mixtures [44] ($x = 0.29$) if unmodified Förster-Hoffmann equation is used for fitting, noting that the new vinyl-substituted derivative can absorb at longer wavelengths. Moreover, we do not see any evidence of excimers because no additional bands are seen in fluorescence spectra of nitro-substituted derivatives in toluene-castor oil mixtures (figure S1, ESI) with increasing fraction of castor oil.

The data in figure 3(E) indicate that viscosity sensitivity of the new viscosity probes might extend further beyond 1000 cP. Therefore, we decided to test both probes in cold glycerol, a viscous solvent with a glass transition temperature of 190 K and allows us to cover a viscosity range of $1.7{\cdot}10^3$ –$1.6{\cdot}10^{11}$ cP by cooling it. While BP-PH-m2M-$NO_2$ was not soluble in glycerol, we dissolved BP-Vinyl-$NO_2$ and cooled it to 200 K to test viscosity sensitivity (figure 4). Fluorescence lifetimes and amplitudes of biexponential fluorescence decays in cooled glycerol are given in table S3, ESI. Viscosity-dependent lifetimes shown in figure 4(B) were fitted using equation (S3), ESI. Obtained fitting parameters are given in table S4, ESI. Experiments in a cryostat have shown that a fluorescence lifetime of BP-Vinyl-$NO_2$ increases much further at viscosities above 1000 cP and continue rising up to $10^6$ cP. Moreover, $\beta$-vinyls expanded the range of viscosity sensitivity by two orders of magnitude (from $0.5\text{-}5{\cdot}10^4$ cP to $0.5\text{-}1{\cdot}10^6$ cP) in contrast to previously reported nitro-substituted BODIPY without moieties in $\beta$ position [47], far exceeding the viscosity range of the commonly used BODIPY-$C_{12}$ probe (5-1500 cP) [27]. To our knowledge, there are only few molecules capable of viscosity sensing at such high viscosities [47, 49]. We note that the maximum lifetime of BP-Vinyl-$NO_2$ reaches approximately 3 ns instead of 21 ns as calculated from the radiative decay rate obtained from fluorescence lifetime and quantum yield and from absorption spectra using Strickler-Berg relation [50]. This suggests that there is additional non-radiative relaxation pathway that is independent of temperature and viscosity.

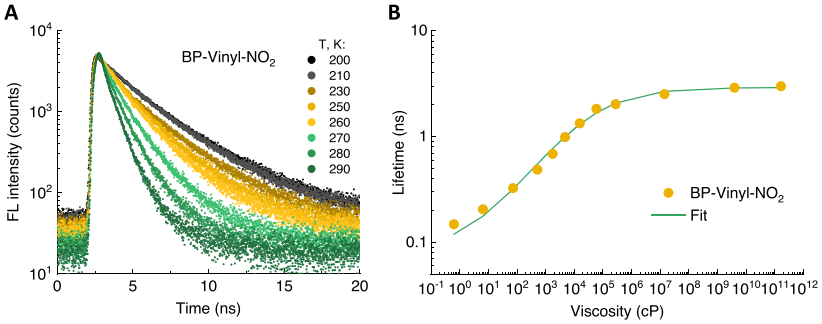


**Figure 4.** (A) Time-resolved fluorescence decays of BP-Vinyl-$NO_2$ in cooled and room temperature glycerol. The legend shows temperature in kelvins. (B) The corresponding fluorescence lifetimes of BP-Vinyl-$NO_2$ in room temperature methanol-glycerol mixtures and cooled glycerol with respect to the viscosity of solvents. Lifetime data is fitted (green curve) using equation (S3), ESI. Fitting parameters are shown in table S3, ESI.

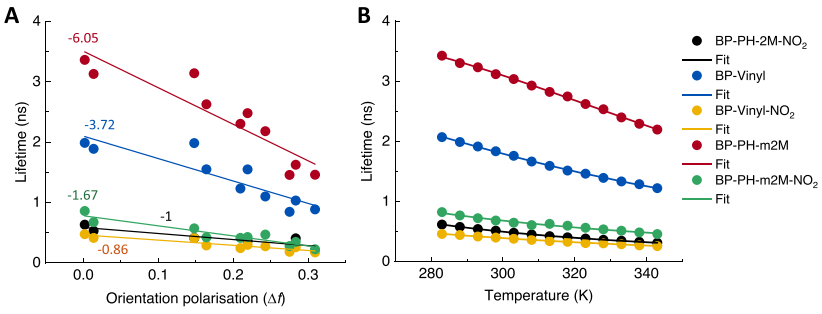


**Figure 5.** Fluorescence lifetimes of BP-PH-2M-$NO_2$ (black), BP-Vinyl (blue), BP-Vinyl-$NO_2$ (yellow), BP-PH-m2M (red), and BP-PH-m2M-$NO_2$ (green) obtained in the solvents of varying polarity (A) and at varying temperature in toluene (B). Slopes of the linear fits are displayed together. Data of BP-PH-2M-$NO_2$ is reproduced with permission from [43].

### 3.4. Polarity and temperature sensitivity

Molecular rotors are often sensitive to the polarity of the solvent [44, 51], which may influence their viscosity readings. Therefore, we measured the fluorescence lifetime of our fluorophores in solvents of various polarity. Polarity is defined here as orientation polarisation used in Lippert's equation [52]:

$$\Delta f = \frac{\epsilon - 1}{2\epsilon + 1} - \frac{n^2 - 1}{2n^2 + 1}, \qquad (3)$$

where $\Delta f$ - orientation polarisation, $\epsilon$ - dielectric permittivity, $n$ - refractive index.

Figure S2 (ESI) shows absorbance and fluorescence spectra in different polarity solvents (from non-polar to very polar: cyclohexane, chloroform, THF, DMSO, methanol). The derivatives did not show strong solvatochromism, resulting in a red-shift of 15, 25, 22 and 29 nm for BP-Vinyl, BP-Vinyl-$NO_2$, BP-PH-m2M, and BP-PH-m2M-$NO_2$, respectively, from the least polar cyclohexane to a very polar DMSO. Interestingly, fluorescence spectra of all fluorophores were red-shifted only by 6-12 nm when the solvent was changed from cyclohexane to a very polar alcohol (methanol). Figure S2I (ESI) shows a Lippert plot, depicting the Stokes shifts in wavenumbers versus orientation polarisation. Such small slopes of the Lippert plot, which are the result of small differences between dipole moments of ground and excited states were also observed for a green fluorescent BODIPY rotor BODIPY-$C_{12}$ [25].

Additionally, we investigated the dependence of fluorescence lifetime on solvent polarity (figure 5(A)) These experiments were performed in cyclohexane, toluene, chloroform, diethyl ether, THF, DCM, cyclohexanone, DMF, DMSO and methanol (listed from non-polar to very polar). The results show that BP-PH-m2M and BP-Vinyl show significant sensitivity to solvent polarity. Both nitro-substituted derivatives showed suppressed sensitivity to polarity, as well as 2-3 times shorter lifetimes due to low viscosity of the solvents. BP-Vinyl-$NO_2$ demonstrated even lower

polarity-sensitivity than the previously reported BP-PH-2M-$NO_2$.

Next, we performed temperature-dependent experiments, which let us to evaluate temperature sensitivity of the derivatives. Moreover, fluorescence lifetime-temperature dependence can be used for extracting values of an activation energy barrier for non-radiative relaxation that determines viscosity and temperature-sensitivity of molecular rotors [44, 53, 54]. Experiments were conducted in toluene, at 10 °C–70 °C temperature range (figure 5(B)). The viscosity of toluene only changed from 0.65 to 0.3 cP at these temperatures [55], which is too small a change to significantly affect the fluorescence lifetime of the fluorophores alone. Therefore the trend in lifetimes in figure 5(B) were the result of direct temperature effect on fluorophores. The data showed that BP-Vinyl and BP-PH-m2M show moderate temperature sensitivity. By adding the -$NO_2$ group, the temperature sensitivity was suppressed, which is a positive development for a viscosity sensor. The -$NO_2$ group enables viscosity-sensitivity by increasing the viscosity-dependent rate of non-radiative relaxation (table S1, ESI). In a low viscosity solvent viscosity-dependent relaxation rate is fast and, as a result, it is the main factor determining fluorescence lifetime with temperature having only a minor effect. Fluorescence decays of all derivatives are shown in figure S3, ESI.

It is known that viscosity probes based on BODIPY group possess an energy barrier for non-radiative relaxation, the height of which heavily influences the viscosity sensitivity [43, 53, 54]. Using equation (S4) (ESI), we were able to extract values of an activation energy barrier for all new fluorophores (table S5, ESI). A nitro group on a *meso*-phenyl lowered the barrier of vinyl- and phenyl-substituted derivatives BP-Vinyl-$NO_2$ and BP-PH-m2M-$NO_2$, which led to an improved viscosity sensitivity.

## 4. Conclusions

In this study, we investigated new $\beta$-substituted BODIPYs with phenyl and vinyl moieties. We showed that the nitro group on a *meso*-phenyl of the BODIPY core is a universal way to improve the viscosity sensitivity of the probe. Moreover, the new nitro-substituted derivatives exhibited absorbance and fluorescence in a red spectral region, lifetime-based sensitivity to microviscosity and low sensitivity to temperature as well as solvent polarity. Additionally, our results demonstrated that BP-Vinyl-$NO_2$ has an outstanding viscosity-sensitive range of seven orders of magnitude. Such probe would be potentially suitable even for samples with very high viscosity, such as cryopreserved tissues [56]. Furthermore, we showed that the removal of steric hindrances in the $\beta$-phenyl-substituted conjugate BP-PH-m2M-$NO_2$ shifts the fluorescence spectrum towards red and preserves the viscosity sensitivity. We believe that these results will help to develop new red fluorescent lifetime-based microviscosity probes with a wide range of sensitivity to viscosity.

## Acknowledgments

This research was funded by a grant (No. S-MIP-19-6) from the Research Council of Lithuania. The authors have declared that no conflicting interests exist.

## Data availability statement

The data that support the findings of this study are available upon reasonable request from the authors.

## ORCID iDs

Karolina Maleckaitė https://orcid.org/0000-0002-4992-9158
Rugilė Žilėnaitė https://orcid.org/0000-0002-4544-1964
Sigitas Tumkevičius https://orcid.org/0000-0002-3279-1770
Aurimas Vyšniauskas https://orcid.org/0000-0002-4750-8149

## References

[1] Kuimova M K 2012 *Phys. Chem. Chem. Phys.* **14** 12671
[2] Clayton K N, Berglund G D, Linnes J C, Kinzer-Ursem T L and Wereley S T 2017 *Anal. Chem.* **89** 13334–41
[3] Kubánková M, López-Duarte I, Kiryushko D and Kuimova M K 2018 *Soft Matter* **14** 9466–74
[4] Zubenko G S, Kopp U, Seto T and Firestone L L 1999 *Psychopharmacology* **145** 175–80
[5] Dzyuba S V 2020 *Biosensors* **10** 192
[6] Deliconstantinos G, Villiotou V and Stavrides J C 1995 *Biochem. Pharmacol.* **49** 1589–600
[7] Nölle J M, Jüngst C, Zumbusch A and Wöll D 2014 *Polym. Chem.* **5** 2700–3
[8] Lee S C, Heo J, Ryu J W, Lee C L, Kim S, Tae J S, Rhee B O, Kim S W and Kwon O P 2016 *Chem. Commun.* **52** 13695–8
[9] Li D, Tian X, Wang A, Guan L, Zheng J, Li F, Li S, Zhou H, Wu J and Tian Y 2016 *Chem. Sci.* **7** 2257–63
[10] Gao M, Hong Y, Chen B, Wang Y, Zhou W, Wong W W H, Zhou J, Smith T A and Zhao Z 2017 *Polym. Chem.* **8** 3862–6
[11] Ghosh P K, Vasanji A, Murugesan G, Eppell S J, Graham L M and Fox P L 2002 *Nat. Cell Biol.* **4** 894–900
[12] Nipper M E, Majd S, Mayer M, Lee J C, Theodorakis E A and Haidekker M A 2008 *Biochimica et Biophysica Acta (BBA) - Biomembranes* **1778** 1148–53
[13] Michels L, Gorelova V, Harnvanichvech Y, Borst J W, Albada B, Weijers D and Sprakel J 2020 *Proc. Natl Acad. Sci.* **117** 18110–8
[14] Páez-Pérez M, López-Duarte I, Vyšniauskas A, Brooks N J and Kuimova M K 2021 *Chem. Sci.* **12** 2604–13
[15] Hosny N A *et al* 2016 *Chem. Sci.* **7** 1357–67
[16] Vyšniauskas A and Kuimova M K 2018 *Int. Rev. Phys. Chem.* **37** 259–85
[17] Lee S C, Heo J, Woo H C, Lee J A, Seo Y H, Lee C L, Kim S and Kwon O P 2018 *Chem. Eur. J.* **24** 13706–18
[18] Haidekker M A and Theodorakis E A 2007 *Org. Biomol. Chem.* **5** 1669–78

[19] Haidekker M A, Brady T P, Lichlyter D and Theodorakis E A 2006 JACS **128** 398–9
[20] Xochitiotzi-Flores E, Jiménez-Sánchez A, García-Ortega H, Sánchez-Puig N, Romero-Ávila M, Santillan R and Farfán N 2016 *New J. Chem.* **40** 4500–12
[21] Kotani R *et al* 2017 *J. Mater. Chem.* C **5** 5248–56
[22] Wu C H, Chen Y, Pyrshev K A, Chen Y T, Zhang Z, Chang K H, Yesylevskyy S O, Demchenko A P and Chou P T 2020 *ACS Chem. Biol.* **15** 1862–73
[23] Klymchenko A S 2017 *Acc. Chem. Res.* **50** 366–75
[24] Miao W, Yu C, Hao E and Jiao L 2019 *Frontiers in Chemistry* **7** 1–6
[25] Levitt J A, Chung P, Kuimova M K, Yahioglu G, Wang Y, Qu J and Suhling K 2011 ChemPhysChem **12** 662–72
[26] Athanasiadis A, Fitzgerald C, Davidson N M, Giorio C, Botchway S W, Ward A D, Kalberer M, Pope F D and Kuimova M K 2016 *Phys. Chem. Chem. Phys.* **18** 30385–93
[27] Kuimova M K, Yahioglu G, Levitt J A and Suhling K 2008 JACS **130** 6672–3
[28] Chambers J E, Kubánková M, Huber R G, López-Duarte I, Avezov E, Bond P J, Marciniak S J and Kuimova M K 2018 *ACS Nano* **12** 4398–407
[29] Wang L, Xiao Y, Tian W and Deng L 2013 JACS **135** 2903–6
[30] López-Duarte I, Vu T T, Izquierdo M A, Bull J A and Kuimova M K 2014 *Chem. Commun.* **50** 5282–4
[31] Su D, Teoh C, Gao N, Xu Q H and Chang Y T 2016 *Sensors* **16** 1397
[32] Mika J T, Thompson A J, Dent M R, Brooks N J, Michiels J, Hofkens J and Kuimova M K 2016 *Biophys. J.* **111** 1528–40
[33] Sherin P S, López-Duarte I, Dent M R, Kubánková M, Vyšniauskas A, Bull J A, Reshetnikova E S, Klymchenko A S, Tsentalovich Y P and Kuimova M K 2017 *Chem. Sci.* **8** 3523–8
[34] Steinmark I E, James A L, Chung P H, Morton P E, Parsons M, Dreiss C A, Lorenz C D, Yahioglu G and Suhling K 2019 *PLoS One* **14** e0211165
[35] Pal S, Chakraborty H, Bandari S, Yahioglu G, Suhling K and Chattopadhyay A 2016 *Chem. Phys. Lipids* **196** 69–75
[36] Rao B D, Shrivastava S, Pal S and Chattopadhyay A 2019 *The Journal of Physical Chemistry* B **123** 639–47
[37] Chen X, Liu Y C, Cui J J, Wu F Y and Xiao Q 2021 *Molecules* **26** 6072
[38] Awuah S G and You Y 2012 *RSC Adv.* **2** 11169
[39] Durantini A M, Heredia D A, Durantini J E and Durantini E N 2018 *Eur. J. Med. Chem.* **144** 651–61
[40] Jun Y W, Kim H R, Reo Y J, Dai M and Ahn K H 2017 *Chem. Sci.* **8** 7696–704
[41] Weissleder R 2001 *Nat. Biotechnol.* **19** 316–7
[42] Wang S, Li B and Zhang F 2020 *ACS Central Science* **6** 1302–16
[43] Maleckaitė K, Dodonova J, Toliautas S, Žilėnaitė R, Jurgutis D, Karabanovas V, Tumkevičius S and Vyšniauskas A 2021 *Chem. Eur. J.* **27** 16768–75
[44] Vyšniauskas A, López-Duarte I, Duchemin N, Vu T T, Wu Y, Budynina E M, Volkova Y A, Peña Cabrera E, Ramírez-Ornelas D E and Kuimova M K 2017 *Phys. Chem. Chem. Phys.* **19** 25252–9
[45] Levitus M 2020 *Methods and Applications in Fluorescence* **8** 033001
[46] Wall K P, Dillon R and Knowles M K 2015 *Biochem. Mol. Biol. Educ.* **43** 52–9
[47] Toliautas S, Dodonova J, Žvirblis A, Čiplys I, Polita A, Devižis A, Tumkevičius S, Šulskus J and Vyšniauskas A 2019 *Chem. Eur. J.* **25** 10342–9
[48] Förster T and Hoffmann G 1971 *Z. Phys. Chem.* **75** 63–76
[49] Jee A Y, Bae E and Lee M 2010 *J. Chem. Phys.* **133** 014507
[50] Strickler S J and Berg R A 1962 *J. Chem. Phys.* **37** 814–22
[51] Xiao H, Li P and Tang B 2021 *Coord. Chem. Rev.* **427** 213582
[52] Lakowicz Joseph R. 2006 *Principles of Fluorescence Spectroscopy* 3 (New York, NY: Springer) 978-0-387-46312-4 (https://doi.org/10.1007/978-0-387-46312-4)
[53] Maleckaitė K, Narkevičius D, Žilėnaitė R, Dodonova-Vaitkūnienė J, Toliautas S, Tumkevičius S and Vyšniauskas A 2021 *Molecules* **27** 23
[54] Liu X, Chi W, Qiao Q, Kokate S V, Cabrera E P, Xu Z, Liu X and Chang Y T 2020 *ACS Sensors* **5** 731–9
[55] Santos F J V, Nieto de Castro C A, Dymond J H, Dalaouti N K, Assael M J and Nagashima A 2006 *J. Phys. Chem. Ref. Data* **35** 1–8
[56] Steif P S, Palastro M C and Rabin Y 2007 *Medical Engineering and Physics* **29** 661–70

# P5

# A red-emitting thiophene-modified BODIPY probe for fluorescence lifetime-based polarity imaging of lipid droplets in living cells

R. Žvirblis, **K. Maleckaitė**, J. Dodonova-Vaitkūnienė, Dž. Jurgutis, R. Žilėnaitė, V. Karabanovas, S. Tumkevičius, A. Vyšniauskas

*J. Mater. Chem. B.* **11**, 3919—3928 (2023)
DOI: 10.1039/d3tb00305a

Reprinted from *Journal of Materials Chemistry B*
with permission from The Royal Society of Chemistry.

Supporting information: https://www.rsc.org/suppdata/d3/tb/d3tb00305a/d3tb00305a1.pdf

Journal of Materials Chemistry B

ROYAL SOCIETY OF CHEMISTRY

PAPER

View Article Online
View Journal | View Issue

Check for updates

Cite this: J. Mater. Chem. B, 2023, 11, 3919

# A red-emitting thiophene-modified BODIPY probe for fluorescence lifetime-based polarity imaging of lipid droplets in living cells†

Rokas Žvirblis,[ab] Karolina Maleckaitė,[a] Jelena Dodonova-Vaitkūnienė,[b] Džiugas Jurgutis,[cd] Rugilė Žilėnaitė,[a] Vitalijus Karabanovas,[ce] Sigitas Tumkevičius[b] and Aurimas Vyšniauskas*[a]

Intracellular polarity in lipid droplets as well as other organelles may provide useful knowledge about various processes taking place in live cells. Therefore, small fluorophores capable of visualising polarity are undergoing rapid development. In this paper, we report new red-emitting polarity sensitive BODIPY probes that can distinguish between liquid-ordered and liquid-disordered phases and can internalise into lipid droplets of live cells. Our reported probes sense lipid environment not through solvatochromic shift of the fluorescence spectra but through the change in the fluorescence lifetime of their monoexponential decays. This makes them convenient for fluorescence lifetime imaging microscopy. The probes were synthesised by modifying viscosity-sensitive *meso*-phenyl BODIPY with electron-donating 2-thienyl moieties at the α- and β-positions, significantly red-shifting absorption and fluorescence spectra of the dyes and improving sensitivity to polarity, while suppressing viscosity dependence. Finally, a novel probe – BP $OC_{16}$ TP2 was suitable for sensing polarity in lipid droplets of live MCF-7 human breast cancer cells. We demonstrated that different chemotherapeutics affected lipid droplet polarity differently: cisplatin had no effect on lipid droplet polarity, whereas paclitaxel, depending on its concentration, either decreased or increased lipid droplet polarity.

Received 13th February 2023,
Accepted 3rd April 2023

DOI: 10.1039/d3tb00305a

rsc.li/materials-b

Published on 06 April 2023. Downloaded on 5/3/2023 1:03:14 PM.

## 1 Introduction

Lipid droplets (LDs) are lipid-enriched organelles found in most eukaryotic cells and produced mainly in the endoplasmic reticulum.[1,2] LDs serve as energy reserves, are responsible for signaling inflammation and are involved in various processes in cancer formation, including lipid metabolism and proliferation.[3–7] In addition, LDs provide protection against lipotoxicity.[8] In 2020, Cruz *et al.* stated that LDs could be potentially targeted for drug development used in cancer treatment or even as a new biomarker for various diseases.[1] Moreover, metabolic disorders, such as obesity, atherosclerosis and fatty liver disease show accumulation of LDs.[9,10]

Overall, LDs and their functionality as a research subject is quite novel and already became a high-importance topic.[7,8,10] It is not surprising that targeted studies, such as polarity within LDs, are just emerging. Nonetheless, it has already been shown that polarity of LDs can help to evaluate the lipid organisation and order.[11] Moreover, polarity inside LDs can show activity of interacting enzymes and proteins.[8] It is also thought that LDs structure and polarity can also change during the ferroptosis (accumulation of lipid peroxides causing cell death).[12] Recently, it has been shown by Ashoka *et al.* that a local polarity inside intracellular membranes and LDs increases when organelles undergo starvation and oxidative stress.[11] The surface of LDs consists of polar lipids (*e.g.*, sterols and phospholipids) and various proteins, while the core is formed by non-polar lipids (*e.g.*, triacylglycerols and sterol esters).[9] Therefore, it can be expected that polarity within LDs can be diverse and dynamic depending on various cellular processes taking place. Consequently, the polarity inside LDs may reveal more information about the state and the behaviour of the cell.

A convenient method for polarity sensing is based on fluorescent organic molecules that alter their spectroscopic

[a] Center of Physical Sciences and Technology, Saulėtekio av. 3, Vilnius, LT-10257, Lithuania. E-mail: aurimas.vysniauskas@ftmc.lt
[b] Institute of Chemistry, Faculty of Chemistry and Geosciences, Vilnius University, Naugarduko str. 24, Vilnius, LT-03225, Lithuania
[c] Biomedical Physics Laboratory, National Cancer Institute, P. Baublio str. 3b, Vilnius, LT-08406, Lithuania
[d] Life Sciences Center, Vilnius University, Saulėtekio av. 7, Vilnius, LT-10257, Lithuania
[e] Department of Chemistry and Bioengineering, Vilnius Gediminas Technical University, Saulėtekio av. 11, Vilnius, LT-10223, Lithuania

† Electronic supplementary information (ESI) available: Additional spectroscopic information and synthesis and characterization details for novel compounds. See DOI: https://doi.org/10.1039/d3tb00305a

Published on 06 April 2023. Downloaded on 5/3/2023 1:03:14 PM.

properties according to their physical environment. Such dyes have been previously used for sensing differences between liquid-ordered ($L_o$) and liquid-disordered ($L_d$) phases in lipid membranes.[13] Because $L_o$ phase is a tightly packed environment, it contains a lower number of water molecules. For this reason, the $L_o$ phase is less polar than the $L_d$ phase that has a less rigid environment and thus is more hydrated.[14] The difference in hydration between $L_o$ and $L_d$ phases makes it possible to visualise these domains in a non-destructive manner using fluorescence techniques.[13]

Most of the polarity-sensitive probes are solvatochromic dyes, which are impacted by the solvent polarity due to the large dipole moment present in the excited state.[15] As a result, their fluorescence wavelength increases in media of higher polarity. Well known fluorophores belonging to this group are Reichardt's dye, Laurdan, Prodan, FR0.[16,17] Solvatochromic polarity sensors for lipid rafts have been widely explored and extensively tested in model and living systems,[13] but fluorescence lifetime-based polarity probes have seen little attention. This is unsatisfactory because fluorescence lifetime-based probes have important advantages. When used together with fluorescence lifetime imaging microscopy (FLIM), aggregation or other unwanted environmental effects will likely cause an appearance of a new fluorescence decay component exposing the problem. Although standard solvatochromic polarity probes can be used with FLIM (*e.g.* Nile red),[18] this is impractical due to an inconsistent emission spectrum and multi-exponential fluorescence decay. To fill in the gap, we sought to create a red-emitting polarity probe that would stain lipid rafts. For this purpose we had chosen BODIPY architecture that offers attractive photophysical properties and freedom of synthetic modification.[19]

BODIPY probes have often been used to measure viscosity rather than intracellular polarity.[20–23] These fluorophores exhibit green emission, and their applicability in living systems is enhanced by the fact that their fluorescence decay is mono-exponential, which is favourable for use in FLIM. It was noticed that attempts to produce red-emitting BODIPY probes for more efficient imaging of biological samples had produced curious outcomes. Modifying α- and β-positions with aromatic moieties to red-shift the fluorescence wavelength, extinguished the sensitivity to viscosity, whilst increasing responsiveness to polarity.[24] The latter observation was taken in practice by Maleckaitė *et al.* who synthesised and explored a red-emitting BODIPY polarity probe BP-PH-OMe modified with electron-donating 4-methoxyphenyl groups at the β,β′-positions of the BODIPY core. These results were the basis of this work, where we aimed to synthesise red-emitting polarity probes for sensing in lipid environment.

In this research we report four red-emitting BODIPY-based probes that are modified with 2-thienyl moieties, producing β,β′-disubstituted and α,α′,β,β′-tetrasubstituted probes (Fig. 1). This particular aromatic group was chosen because it offers electron-donating capabilities that seem to be connected with increased polarity sensitivity of the BODIPY probes as previously reported.[24] Furthermore, it has been noticed that

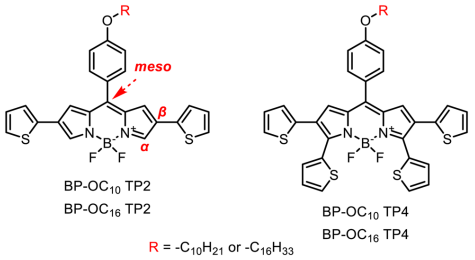


Fig. 1 Molecular structures of thiophene-modified disubstituted (TP2) and tetrasubstituted (TP4) BODIPY fluorophores with the unbranched alkoxy chains of alternating length ($-OC_{10}H_{21}$ or $-OC_{16}H_{33}$) at the *meso*-phenyl ring. The red-coloured notes indicate the substituted position of the BODIPY core.

introduction of electron-rich thienyl groups leads to a large red-shift that is crucial for achieving red emission.[25,26] Additionally, long alkoxy chains ($-C_{10}H_{21}$ and $-C_{16}H_{33}$) were introduced at the *para*-position of the *meso*-phenyl ring of our probes that should ensure efficient fit of the probes into the lipid layer.[27] We demonstrate that one of the new fluorophores – BP-$OC_{16}$ TP2, accumulates in LDs of live MCF-7 human breast cancer cells and exhibits monoexponential fluorescence decay. To utilise BP-$OC_{16}$ TP2, we tested how LD polarity is affected by different chemotherapeutics: platinum-based agent – cisplatin (CSP), and agent that stabilizes microtubules – paclitaxel (PAX). Our findings indicate that polarity of LDs remains unaltered after treatment with CSP. However, chemotherapy with PAX resulted in either decreased or increased LD polarity, depending on the concentration of PAX.

## 2 Methods and materials

### 2.1 Dyes, reagents, solvents

The synthesis of previously unreported derivatives, BP-$OC_{10}$ TP2, BP-$OC_{10}$ TP4, BP-$OC_{16}$ TP2 and BP-$OC_{16}$ TP4 was accomplished by Stille cross-coupling reaction of corresponding β,β′-dibromo or α,α′,β,β′-tetrabromo BODIPY derivatives with 2-(tributylstannyl)thiophene in the presence of $Pd(PPh_3)_4$ catalyst. The synthesis and characterisation data of obtained compounds are presented in the ESI.† Reagents and solvents for the organic synthesis of the BODIPY compounds were purchased directly from commercial suppliers; solvents were purified by known procedures. Thin layer chromatography (TLC) was performed using TLC-aluminium sheets with silica gel (Merck 60 F254). Visualisation was accomplished by UV light. Column chromatography was performed using silica gel 60 (0.040–0.063 mm) (Merck). Nuclear magnetic resonance (NMR) spectra (Fig. S15–S18, S20–S23, S25–S28, S30–S33, S35–S38, S40–S43, S45–S48, S50–S53, ESI†) were recorded on a Bruker Ascend 400 spectrometer (400 MHz for $^1$H, 100 MHz for $^{13}$C, 128.4 MHz for $^{11}$B, 376.5 MHz for $^{19}$F). NMR spectra were referenced to residual solvent peaks. Mass spectra (MS) were

 This journal is © The Royal Society of Chemistry 2023

Published on 06 April 2023. Downloaded on 5/3/2023 1:03:14 PM.

recorded on a Bruker Autoflex Speed mass spectrometer (Fig. S19, S24, S29, S34, S39, S44, S49, S54, ESI†). Melting points were determined in open capillaries with a digital melting point IA9100 series apparatus (Thermo Fisher Scientific) and were not corrected. Stock solutions for all dyes were prepared in toluene at a concentration of 2 mM and diluted for further experiments in solvents or their mixtures. Methanol, dimethyl sulfoxide, tetrahydrofuran, chloroform, toluene, cyclohexane, and castor oil were obtained from Sigma-Aldrich. Lipids 1,2-dioleoyl-*sn-glycero*-3-phosphocholine (DOPC), 1,2-dipalmitoyl-*sn-glycero*-3-phosphocholine (DPPC) and cholesterol were purchased in powder form from Avanti Polar Lipids and resuspended in chloroform prior to use at concentrations of 25 mg ml$^{-1}$ (DPPC and DOPC) and 10 mg ml$^{-1}$ (cholesterol).

### 2.2 Absorption, steady-state, time-resolved fluorescence, and quantum-yield measurements

Absorption spectra were measured by using Jasco V-670 spectrophotometer. Fluorescence spectra and time-resolved fluorescence were recorded with Edinburgh-F900 (Edinburgh Instruments) fluorimeter. Excitation of synthesised molecules was achieved by using WhiteLase Micro (Fianium) laser together with bandpass filters (ThorLabs) with bandwidth of 10 nm centred at 630 nm. Fluorescence decays were measured by using the time-correlated single-photon counting technique. Fluorescence decays had 5000 counts at the peak of the decay, with 20 ns windows being used with 4096 channels. Quartz cuvettes (10 mm) were used for absorption, fluorescence, and quantum yield (QY) measurements. QYs where obtained by a comparative method using Nile Blue (QY = 27% in ethanol) as a standard.[28] The concentration of dyes was 2–3 μM.

### 2.3 Preparation of model lipid membranes

Large unilamellar vesicles (LUVs) were prepared by the extrusion method. First, a required amount of lipid concentrate was mixed with an aliquot of dye (400 μM in chloroform) at a 500 : 1 lipid to dye ratio, before using a stream of $N_2$ gas and vacuum (1 h) to remove the solvents and to produce a lipid film. For $L_d$ vesicles DOPC was used, whereas $L_o$ membranes were formed from a 5 : 5 : 1 molar ratio mixture of DPPC, cholesterol and DOPC. Next, 2 ml of Milli-Q water (18.2 MΩ cm) was used to hydrate the lipid layer, then the mixtures were vortexed and extruded 20 times through a polycarbonate membrane (pore size 0.1 μm) with a mini-extruder (Avanti Polar Lipids). The hydration and extrusion was conducted above the fluid-gel transition temperature of all lipids in the mixture.

### 2.4 Culturing and imaging of live cancer cells

Human breast cancer cell line MCF-7 was purchased from the European Collection of Cell Cultures and cultured in Dulbecco's Modified Eagles Medium (DMEM) (Capricorn Scientific), supplemented with 10% fetal bovine serum, 100 U per mL penicillin and 100 μg per mL streptomycin (all from Gibco). The cells were maintained in a 37 °C incubator with a humidified atmosphere containing 5% $CO_2$ and routinely subcultured 2–3 times a week in 25 cm$^2$ culture dishes.

For live cell imaging, cells were seeded into an 8-chambered cover glass plate (Nunc, Lab-Tek) with a density of $3 \times 10^4$ cells per chamber and subsequently incubated at 37 °C in 5% $CO_2$ for 24 h. MCF-7 cells were treated with 1.2 μM BP-$OC_{16}$ TP2 (0.5% dimethyl sulfoxide) in Dulbecco's phosphate-buffered saline (DPBS) (Cegrogen Biotech) containing $Ca^{2+}$ and $Mg^{2+}$, w/o Phenol Red for 30 min at 37 °C. Afterwards, the cells were washed three times with DPBS.

For the colocalisation experiments, cells were incubated with 32.5 μM Hoechst 33342 nuclei stain (Invitrogen) for 30 min at 37 °C. Afterwards, the cells were washed three times with DPBS and incubated with a mixture of 2 μM BODIPY 493/503 (0.16% dimethyl sulfoxide) (Invitrogen) and 1.2 μM BP-$OC_{16}$ TP2 (0.5% dimethyl sulfoxide) for 15 min at 37 °C. Following this, the cells were washed three times with DPBS.

Chemotherapy was conducted with 93 μM CSP or 7.2 nM PAX (both from Accord). We chose CSP and PAX concentrations, as previously measured by Czarnomysy *et al.* and Nakayama *et al.*, respectively, for the MCF-7 cells as the 50% inhibitory concentrations.[29,30] After 6 h of incubation with chemotherapeutics, the cells were washed three times with DPBS and incubated with BP-$OC_{16}$ TP2 for 30 min at 37 °C. Following this, the cells were washed three times with DPBS.

Imaging was performed using Nikon Eclipse Te2000-U microscope with a C1si confocal laser-scanning confocal system. 60×/1.4 NA oil immersion objective (Nikon) was used. The microscope was equipped with Fianium WhiteLase Micro supercontinuum laser (NKT Photonics) with a pulse repetition rate of 30 MHz and filtered using 400 ± 5 nm (for Hoechst 33342), 480 ± 5 nm (for BODIPY 493/503), 410 ± 5 nm or 600 ± 5 nm (for BP-$OC_{16}$ TP2 FLIM and colocalisation experiments, respectively) band-pass filters (all from ThorLabs). The cells were kept at 37 °C in the Microscope Stage Incubation System (OkoLab) in a humidified atmosphere containing 5% of $CO_2$ (0.80 Nl per min $O_2$ and 0.04 Nl per min $CO_2$) during the imaging process. The fluorescence of BP-$OC_{16}$ TP2 in MCF-7 cells was measured using the 32-channel spectral detector. The brightfield mode of Nikon Eclipse Te2000-U and the three-channel RGB detector with band-pass filters of 450 ± 17 nm, 546 ± 45 nm and 688 ± 67 nm for blue, green and red channels, respectively, were used.

FLIM images were recorded using the aforementioned setup combined with a Lifetime and Fluorescence Correlation Spectroscopy Upgrade for Nikon C1si (PicoQuant GmbH) confocal laser-scanning microscope and time-correlated single photon counter PicoHarp 300 (PicoQuant GmbH). The detection was done through a 620 nm long-pass filter (ThorLabs) using a single-photon-counting avalanche photodiode (Micro Photon Devices). FLIM images were reconstructed using SymPhoTime 64 software (v.2.4.4874, PicoQuant GmbH). The images had 512 × 512 pixels and were binned until a sufficient signal-to-noise ratio was achieved before analysis.

### 2.5 Cytotoxicity assay

Cytotoxicity of BP-$OC_{16}$ TP2 towards MCF-7 cell line was determined using CyQUANT lactate dehydrogenase (LDH)

Published on 06 April 2023. Downloaded on 5/3/2023 1:03:14 PM.

Cytotoxicity Assay Kit (Invitrogen). MCF-7 cells were seeded in a 96-well plate (TPP) with a density of $2 \times 10^4$ cells per well. After 24 h incubation at 37 °C, the media was replaced by a DPBS containing 0.24, 1.2 or 6 μM BP-$OC_{16}$ TP2 and the cells were incubated for 30 min at 37 °C. The cells incubated in DPBS without BP-$OC_{16}$ TP2 served as a control group. Afterwards, 50 μl of DPBS from each well was transferred to two 96-well plates and reaction mixture from the kit was applied to one of the plates. Absorbance at 490 and 630 nm wavelengths was measured with plate-reading spectrophotometer (BioTek) to determine the amount of extracellular LDH present in the plate. The other plate was used as a control to obtain absorbance values of BP-$OC_{16}$ TP2 at the same wavelengths, and subtract from the results of the first plate. Resulting absorbance values were recalculated as percentage values of cytotoxicity (according to manufacturer's protocol) and converted to viability of cells.

### 2.6 Data analysis

Fluorescence decays of studied BODIPYs were fitted using Edinburgh-F900 software package – F900.

Fluorescence lifetime ($\tau$) is expressed in eqn (1):

$$\tau = \frac{1}{k_r + k_{nr}} \quad (1)$$

where $k_r$ and $k_{nr}$ are radiative and non-radiative rate constants, respectively.

Fluorescence QY ($\phi$) is a relationship of $k_r$ and $k_{nr}$ (eqn (2)):

$$\phi = \frac{k_r}{k_r + k_{nr}} \quad (2)$$

Combining eqn (1) and (2) let us calculate $k_r$ and $k_{nr}$ values of fluorophores in toluene (displayed in Table 1):

$$k_r = \frac{\phi}{\tau} \quad (3)$$

$$k_{nr} = \frac{(1-\phi)}{\tau} \quad (4)$$

For biexponential fluorescence decays, intensity-weighted lifetimes $\tau_w$ (eqn (5)) were calculated:

$$\tau_w = \frac{\sum_i a_i \tau_i^2}{\sum_i a_i \tau_i} \quad (5)$$

where $a_i$ are the amplitudes and $\tau_i$ are the lifetimes of individual components. The goodness-of-fit parameter ($\chi^2$) was 1.5 or less for single decays (Table S1, ESI†). Polarities of pure solvents were evaluated using Lipperts equation (eqn (6)) which describes orientation polarisability ($\Delta f$) of the solvent:

$$\Delta f = \frac{\varepsilon - 1}{2\varepsilon + 1} - \frac{n^2 - 1}{2n^2 + 1} \quad (6)$$

where $\varepsilon$ is the relative permittivity and $n$ is the refractive index of a pure solvent.

Colocalisation analysis was performed using Fiji[31] with the Bioimaging and Optics Platform's (BIOP) version of JACoP (Just Another Colocalization Plugin).[32] We manually selected 20 cells from five different images as regions of interest (ROI). Prior to colocalisation analysis, we processed the images by subtracting background fluorescence and applying the Renyi-Entropy thresholding algorithm. To quantify colocalisation in each cell, we used Pearson's correlation coefficient (PCC) and thresholded Manders' colocalisation coefficients ($tM_1$ for the green channel and $tM_2$ for the red channel).[33] The results were expressed as means ± standard deviation.

Analysis of FLIM images was performed using SymPhoTime 64 software. A monoexponential reconvolution fitting model was used to determine the average fluorescence lifetime in each pixel of the FLIM image. The instrument response function (IRF) applied for fitting was calculated by the SymPhoTime 64 software. Further data processing and analysis was done using OriginPro 8.5.

## 3 Results and discussion

### 3.1 Absorbance and fluorescence spectra

At first, we investigated absorbance and fluorescence spectra of our newly developed BODIPY fluorophores. The absorbance spectra of all dyes in toluene had a higher energy band at 300–500 nm and the main absorption band in the region of 620–640 nm (Fig. 2(A)). Tetrasubstituted (TP4) showed a longer absorption wavelength ($\Delta\lambda$ = 10 nm) compared to the disubstituted (TP2) probes, which can be attributed to the two additional groups at the α,α′-positions leading to a further extension of the conjugation.

Similarly, the fluorescence spectra of tetrasubstituted dyes were red-shifted (682 nm) as compared with disubstituted ones (671 nm, Fig. 2(B)). The length of the alkoxy chain at the *meso*-phenyl ring had no impact on the position of absorbance and fluorescence bands. Overall, the new probes show a significant shift of the spectra as compared to the unmodified BODIPY-$C_{10}$, which is a green emitter ($\lambda_{max}$ = 515 nm).[20] The Stokes shift

Table 1 Experimental values of absorption ($\lambda_A$), fluorescence emission maxima ($\lambda_F$), Stokes shifts ($\tilde{\nu}_{SS}$), fluorescence quantum yields (QY), radiative ($k_r$), and non-radiative ($k_{nr}$) decay rates, molar extinction coefficients ($\varepsilon_c$) and the relative sensitivities to temperature ($S$) of BP-$OC_{10}$ TP2, BP-$OC_{16}$ TP2, BP-$OC_{10}$ TP4 and BP-$OC_{16}$ TP4 in toluene

| Derivative | $\lambda_A$, nm | $\lambda_F$, nm | $\tilde{\nu}_{SS}$, $cm^{-1}$ | QY, % | $k_r$, $10^8 \times s^{-1}$ | $k_{nr}$, $10^8 \times s^{-1}$ | $\varepsilon_c$, $M^{-1}\,cm^{-1}$ | $S$, %/°C |
|---|---|---|---|---|---|---|---|---|
| BP-$OC_{10}$ TP2 | 626 | 671 | 1071 | 12 | 0.7 | 5.2 | $4.44 \times 10^4$ | 0.4 |
| BP-$OC_{16}$ TP2 | 626 | 671 | 1071 | 13 | 0.8 | 5.2 | $4.38 \times 10^4$ | 0.4 |
| BP-$OC_{10}$ TP4 | 636 | 682 | 1061 | 23 | 0.8 | 2.7 | $2.56 \times 10^4$ | 0.2 |
| BP-$OC_{16}$ TP4 | 635 | 682 | 1085 | 23 | 0.8 | 2.7 | $3.75 \times 10^4$ | 0.2 |


This journal is © The Royal Society of Chemistry 2023

Published on 06 April 2023. Downloaded on 5/3/2023 1:03:14 PM.

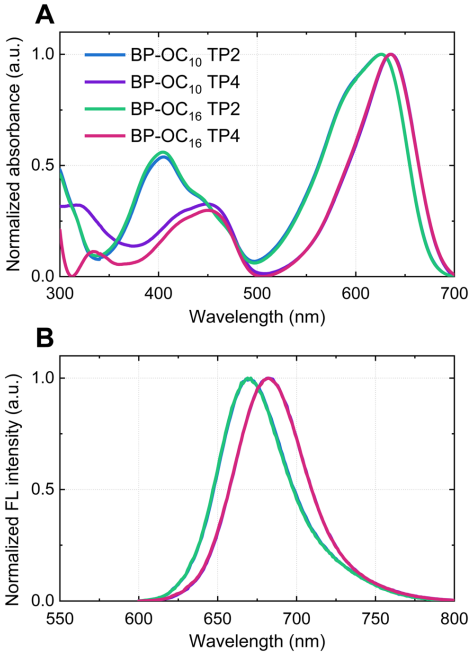


Fig. 2 Absorbance (A) and fluorescence emission (B) spectra of BP-$OC_{10}$ TP2 (blue), BP-$OC_{10}$ TP4 (purple), BP-$OC_{16}$ TP2 (green) and BP-$OC_{16}$ TP4 (magenta) obtained in toluene. Fluorescence emission spectra overlay of both TP2-substituted and TP4-substituted dyes.

was 1071 $cm^{-1}$ for TP2 dyes, meanwhile for BP-$OC_{10}$ TP4 and BP-$OC_{16}$ TP4 it was 1061 $cm^{-1}$ and 1085 $cm^{-1}$, respectively.

It is important to note that all dyes showed slight solvatochromism that was observed in normalised absorbance and fluorescence spectra measured in solvents of differing polarity (from apolar to the most polar: cyclohexane, toluene, chloroform, tetrahydrofuran, dimethyl sulfoxide, and methanol) (Fig. S1 and S2, ESI†). The largest difference of fluorescence maxima was observed between cyclohexane and dimethyl sulfoxide. Resulting red-shifts were 32, 33, 21 and 23 nm, respectively for BP-$OC_{10}$ TP2, BP-$OC_{16}$ TP2, BP-$OC_{10}$ TP4 and BP-$OC_{16}$ TP4, meaning that disubstituted probes are more solvatochromic (Fig. S2, ESI†). Meanwhile, absorbance spectra were affected less by polarity, the largest difference between absorbance maxima being only 11–12 nm (Fig. S1, ESI†).

Additionally, fluorescence spectra registered in non-viscous toluene ($\eta$ = 0.6 cP (dynamic viscosity), $n$ = 1.497, $\varepsilon$ = 2.385, $\Delta f$ = 0.0137) and viscous castor oil ($\eta$ = 920 cP, $n$ = 1.475, $\varepsilon$ = 4.478, $\Delta f$ = 0.1296) were compared. The influence of the increased viscosity was found to be minimal, leading only to a slight blue shift of the spectra, but not altering their form (Fig. S3, ESI†). Similarly, the augmentation of temperature blue-shifted the spectra, but had no impact on their shape (Fig. S4, ESI†).

Furthermore, QY measurements were conducted in toluene for all derivatives. Comparison of QY values between disubstituted and tetrasubstituted dyes indicates that attaching extra 2-thienyl groups to the BODIPY $\alpha,\alpha'$-positions increases QY value by about 10%. The length of the alkoxy chain at the *meso*-phenyl ring has no impact on QY values. QY values and other spectroscopic parameters of newly synthesised BODIPY derivatives are given below (Table 1).

### 3.2 Sensitivity of the fluorescence decay to polarity, viscosity and temperature

To test the photophysical properties of novel thiophene-modified BODIPY derivatives we measured their sensitivity to environmental polarity and evaluated the influence of viscosity and temperature. As a polarity parameter in this study, we use orientation polarisability ($\Delta f$, eqn (6)), which illustrates the effects of solvent polarity on the fluorophore clearer than a dielectric constant. Polarity sensitivity measurements performed in different solvents proved that all probes had monoexponential decays that were polarity-dependent and showed higher fluorescence lifetime in low polarity solvents (Fig. 3(A), (B) and Fig. S5A, B, ESI†). Monoexponential fitting curves of new derivatives are displayed in Fig. S6, ESI.† The dependence of fluorescence lifetime on solvent polarity is presented in Fig. S7, ESI.† Both disubstituted derivatives showed fluorescence lifetimes in 0.45–2.55 ns range, while tetrasubstituted dyes had a larger interval of fluorescence lifetimes, falling in the range of 0.67–4.09 ns (Table S1, ESI†). This means that additional electron-donating 2-thienyl groups increase the dynamic range of polarity sensitivity. Such effect achieved by the introduction of electron-withdrawing groups was demonstrated previously.[24] We also note that results presented in Table 1 demonstrate that $k_{nr}$ is significantly faster than $k_r$. Since all of the molecules in this study exhibit only slight solvatochromism (Fig. S2, ESI†), none of the thiophene-substituted derivatives should display drastic changes in $k_r$, according to the Strickler–Berg relation.[34] As $k_{nr}$ is 3 to 6 times faster than $k_r$, fluorescence lifetime is mostly determined by the former. Therefore, the polarity sensitivity of the probes is caused by changes of $k_{nr}$ in environments of different polarity.

It is known that BODIPY probes may show sensitivity to multiple parameters of the environment such as polarity, viscosity and temperature.[35,36] This would complicate the application of the probes as their reading could be affected by multiple other factors besides polarity. Therefore, viscosity dependence measurements were conducted (Fig. 3(C), (D) and Fig. S5C, D, ESI†). Apolar toluene and castor oil mixtures were used because of the high hydrophobicity of the dyes. Experiments reveal that all probes show negligible dependence on viscosity, which means that their relaxation pathways are not impacted by this environmental parameter. Although fluorescence decays of the TP2 dyes seem to show a slight dependence on viscosity (Fig. 3(C) and Fig. S5C, ESI†), this is an artefact caused by the autofluorescence of castor oil. After subtracting the fluorescence from pure castor oil, which was

Published on 06 April 2023. Downloaded on 5/3/2023 1:03:14 PM.

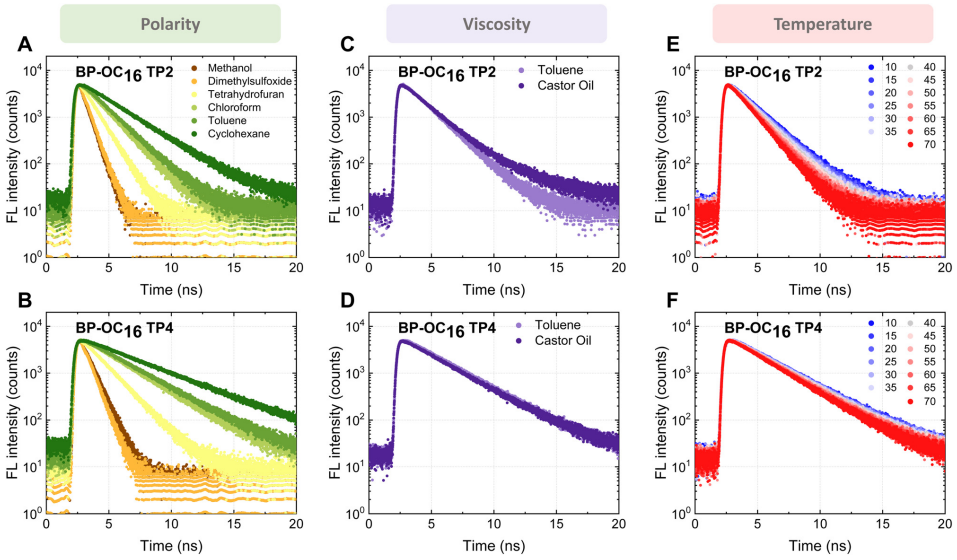


Fig. 3 The fluorescence decays of BP-$OC_{16}$ TP2 (top graphs) and BP-$OC_{16}$ TP4 (bottom graphs), and their sensitivity to polarity, viscosity, and temperature. Polarity dependence in solvents of differing polarity (A) and (B). Solvent polarity is quantified using their orientational polarisability. Viscosity dependence in toluene and castor oil (C) and (D). Temperature dependence measured in toluene, range 10–70 °C (E) and (F).

measured separately under identical experimental conditions, the corrected decay in castor oil fully overlaps with the one in toluene, which proves that the TP2 dyes are viscosity independent (Fig. S8, ESI†).

Lastly, temperature-dependent fluorescence decays recorded in toluene revealed slight sensitivity to temperature of all dyes (Fig. 3(E), (F) and Fig. S5E, F, ESI†). In the range of 10–70 °C TP2 dyes show shorter lifetimes than TP4 fluorophores. Moreover, the sensitivity of the probes to temperature was quantitatively evaluated by using the relative sensitivity parameter $S$ (eqn (7)).[37] The $S$ is an expression showing the percentage change of lifetime per one degree change:

$$S = -\frac{\left|\frac{\delta\tau}{\delta T}\right|}{\tau} \times 100\% \qquad (7)$$

where $\tau$ is the fluorescence lifetime, $\delta T$ is the change of the temperature in degrees Celsius (°C). The calculated values of relative sensitivity to temperature and polarity of all thiophene-modified probes (Table 1).

The sensitivity to temperature was two times larger for TP2 dyes (0.4%) as compared with the TP4 (0.2%) ones. Temperature-sensitive α- and β-substituted BODIPY fluorophores with aromatic groups were reported in the past.[36,38] Therefore, a slight degree of temperature sensitivity in the case of our compounds is not surprising.

### 3.3 Fluorescence decays in liquid-disordered and liquid-ordered vesicles

Having successfully characterised photophysical properties of the novel thiophene-modified BODIPY probes, we sought to test them in model lipid membranes to elucidate their capability to distinguish different lipid phases. Thus, the probes were inserted into LUVs, which can be prepared to represent either $L_d$ phase using DOPC or $L_o$ phase using a mixture of DPPC, cholesterol and DOPC by a ratio of 5 : 5 : 1.

Importantly, all probes decay monoexponentially in $L_d$ phase, but become biexponential as lipid order increases, as in $L_o$ phase (Fig. 4 and Fig. S9, ESI†). This is a well-known phenomenon of BODIPY probes, explained by the fact that these fluorophores have only one preferred orientation in $L_d$-phase bilayers, but are heterogeneously distributed in $L_o$-phase membranes, leading to biexponential decays.[39] Additionally, we calculated the difference of average fluorescence lifetimes between the $L_d$ and $L_o$ phases using eqn (5). Both TP4 dyes show a negligible difference between average fluorescence lifetime in $L_d$ and $L_o$ phases, which is respectively equal to 0.06 ns and 0.12 ns for probes with $-OC_{10}$ and $-OC_{16}$ chains (Table 1). In contrast, disubstituted dyes show an appreciable difference between average lifetimes in $L_d$ and $L_o$ phases. BP-$OC_{10}$ TP2 had a difference of 0.30 ns and for BP-$OC_{16}$ TP2 it was 0.42 ns, meaning that these probes were capable of differentiating between lipid phases using their fluorescence lifetime (Table 2). Moreover, we concluded that fluorophores bearing the longer

 This journal is © The Royal Society of Chemistry 2023

Published on 06 April 2023. Downloaded on 5/3/2023 1:03:14 PM.

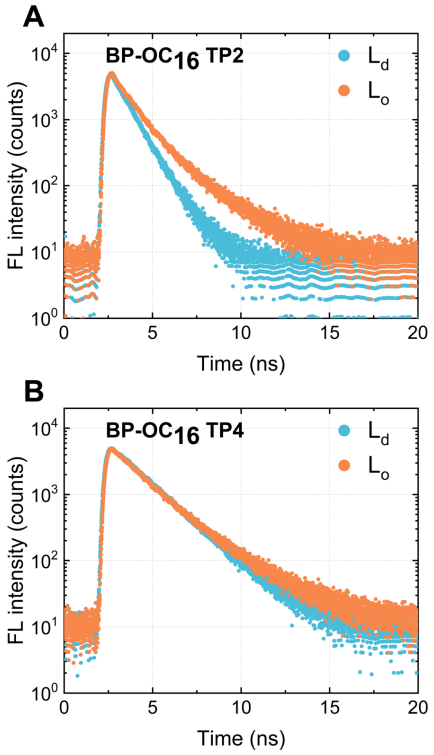


Fig. 4 Fluorescence lifetime decays of BP-$OC_{16}$ TP2 and TP4, measured in LUVs composed of DOPC ($L_d$ phase), DPPC : cholesterol : DOPC (5 : 5 : 1; $L_o$ phase).

Table 2 Mean fluorescence lifetimes of molecular probes in different lipid phases ($L_d$ and $L_o$) and difference between these lifetimes ($\Delta\tau_{L_o} - \tau_{L_d}$). Lifetimes were obtained by mono/biexponential fitting of decays measured in LUVs

| Derivative | $\tau_{L_d}$, ns | $\tau_{L_o}$, ns | $\Delta\tau_{L_o} - \tau_{L_d}$, ns |
|---|---|---|---|
| BP-$OC_{10}$ TP2 | 0.86 | 1.16 | 0.30 |
| BP-$OC_{16}$ TP2 | 0.84 | 1.26 | 0.42 |
| BP-$OC_{10}$ TP4 | 1.77 | 1.83 | 0.06 |
| BP-$OC_{16}$ TP4 | 1.71 | 1.83 | 0.12 |

alkoxy chains are more efficient because for both TP2 and TP4 probes the difference of lifetimes enlarge with the increased length of the aliphatic chain. This might suggest that the length of alkoxy chain increases the anchoring ability of the BODIPY probes and ensure their sufficient insertion into the lipid bilayer.

### 3.4 Cellular imaging

The aforementioned results indicate that from all the novel derivatives, BP-$OC_{16}$ TP2 is the most suitable molecular rotor for differentiating lipid phases using fluorescence lifetime. For this reason, we decided to test BP-$OC_{16}$ TP2 in live MCF-7 human breast cancer cells and see how the inner environment of the cells is affected by different chemotherapy drugs.

Firstly, we performed LDH assay to evaluate cytotoxicity of BP-$OC_{16}$ TP2 towards MCF-7 cell line. Results indicate that the dye has negligible cytotoxicity to the live cells (Fig. S10, ESI†). Afterwards, we utilised laser-scanning confocal microscopy to determine intracellular distribution of BP-$OC_{16}$ TP2. As shown in Fig. 5(A), after 30 min incubation BP-$OC_{16}$ TP2 acquires punctate-like distribution in vesicular structures. Further experiments demonstrated that BP-$OC_{16}$ TP2 colocalises with a commercial probe for LDs – BODIPY 493/503

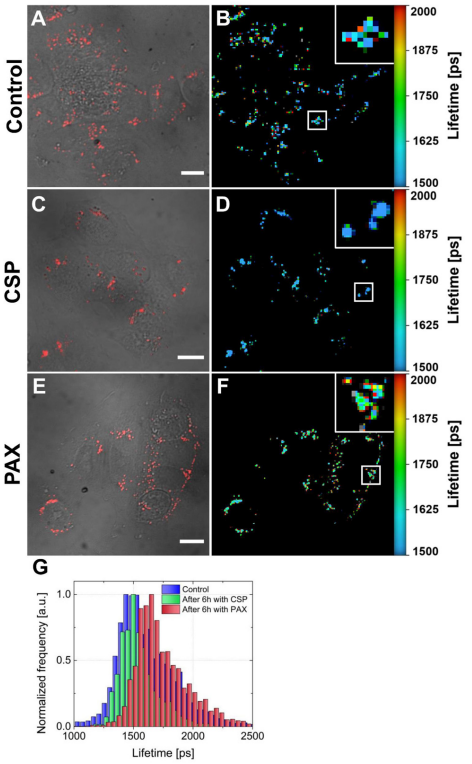


Fig. 5 Application of BP-$OC_{16}$ TP2 in live MCF-7 cells to monitor LD polarity after 6 h treatment with 93 μM cisplatin (CSP) or 7.2 nM paclitaxel (PAX). A, C, E – confocal fluorescence images merged with brightfield images. Scale bars – 15 μm. B, D, F – FLIM images with LDs selected as region of interest. G – lifetime histograms of the shown FLIM images. The mean lifetimes are 1487 ps (B – untreated cells), 1483 ps (D – cells treated with CSP) and 1608 ps (F – cells treated with PAX). The fluorescence was excited at 410 ± 5 nm and detected over the range of 621–755 nm. $\chi_r^2$ images obtained from the analysis of the aforementioned FLIM images are displayed in Fig. S13, ESI.†

Published on 06 April 2023. Downloaded on 5/3/2023 1:03:14 PM.

(mean PCC = 0.80 ± 0.09, mean $tM_1$ = 0.85 ± 0.07 and $tM_2$ = 0.87 ± 0.15, where $tM_1$ estimates the fraction of BODIPY 493/503 that colocalises with BP-$OC_{16}$ TP2, and *vice versa* for $tM_2$, $n$ = 20 cells). (Fig. S11, ESI†). The fluorescence spectrum of BP-$OC_{16}$ TP2 in LDs of MCF-7 cells closely resembled the spectrum observed in toluene (Fig. S12, ESI†), which means that the behaviour of the fluorophore in LDs is not drastically different to the one in solvents during characterisation. In addition, recorded FLIM image of live MCF-7 cells (Fig. 5(B)) revealed that BP-$OC_{16}$ TP2 exhibits monoexponential fluorescence decay with the mean lifetime of 1487 ps (Fig. S13, ESI†). Therefore, we conclude that BP-$OC_{16}$ TP2 does not form aggregates in the intracellular environment and can be utilised for conveniently measuring polarity of LDs in live cells.

To further test BP-$OC_{16}$ TP2 molecular rotor, we chose to investigate how different chemotherapeutics (CSP and PAX) affect the polarity of LDs in human breast cancer cells. CSP and PAX exhibit distinct molecular mechanisms of action: CSP mainly targets DNA, and PAX stabilizes microtubules.[40,41] MCF-7 cells were treated with 93 μM CSP or relatively low concentration of PAX (7.2 nM) for 6 h and then stained with BP-$OC_{16}$ TP2. Treatment with CSP yielded mean fluorescence lifetime value of 1483 ps (Fig. 5(D)) – almost identical to the fluorescence lifetime observed in untreated cells (1487 ps) (Fig. 5(B)), which is slightly lower than the lifetime of the probe in toluene (Table S1, ESI†). This concurs well with previous findings of Wang *et al.*, which demonstrated that polarity of LDs in human fibrosarcoma cells is almost unaltered after treatment with CSP.[12] In contrast, chemotherapy with PAX resulted in elevated fluorescence lifetime (1608 ps) (Fig. 5(F)). In addition, we conducted experiments with substantially higher concentration of PAX (Fig. S14, ESI†). Treatment of MCF-7 cancer cells with 5 μM PAX for 6 h resulted in a significant decrease of fluorescence lifetime (1310 ps), thus indicating that the polarity of LDs increases. The fact that chemotherapy with PAX changes polarity of LDs signifies that the effect of this anticancer drug is not limited to microtubules, even at relatively low PAX concentrations. Indeed, prior findings highlight that PAX directly affects endoplasmic reticulum and mitochondria of cells, thus triggering generation of intracellular reactive oxygen species (ROS).[42,43] Furthermore, it was demonstrated that after 1 h incubation with PAX, the drug causes a significant increase in extracellular superoxide and hydrogen peroxide concentrations, both of which mediate cytotoxic bystander effect in neighbouring cancer cells.[44] Finally, the results of the previous studies suggest that oxidative stress and ferroptosis increase LD polarity.[11,12] We hypothesise that the changes in LD polarity observed in our study after treatment with different concentrations of PAX may also be due to oxidative stress.

## 4 Conclusions

The majority of known fluorescent polarity probes are solvatochromic, which is not convenient for polarity sensing using FLIM as inconsistent spectral position and multiexponential nature of fluorescence decays complicates measurements and analysis. In this work, we prepared new polarity-sensitive, red-emitting BODIPY fluorophores that are suitable to be used as fluorescence lifetime probes for investigating intracellular environment. The BODIPY fluorophores contained 2-thienyl moieties at the β,β′-positions or at both α,α′- and β,β′-positions. In order to ensure their successful insertion into the lipid layer the probes were also modified with $-OC_{10}H_{21}$ and $-OC_{16}H_{33}$ alkoxy chains at the *meso*-phenyl ring. Besides red emission and polarity sensitivity, the best fluorophore of the group (BP-$OC_{16}$ TP2) demonstrated a capability to differentiate between $L_o$ and $L_d$ lipid phases in model lipid membranes. Moreover, it was shown to internalise inside LDs when used for cellular imaging while showing monoexponential fluorescence decay. Finally, by utilising BP-$OC_{16}$ TP2 with FLIM, we have successfully demonstrated a concentration dependent PAX effect on the polarity of LDs, whereas CSP did not alter polarity of LDs. The capability of BP-$OC_{16}$ TP2 to monitor the polarity of LDs will assist us to more effectively understand cellular response mechanisms to different chemotherapeutic agents. Overall, we report novel thiophene-modified red-emitting BODIPY polarity probe BP-$OC_{16}$ TP2 that has a great potential for intracellular polarity sensing using FLIM technique.

## Author contributions

R. Ž. (Rokas Žvirblis), synthesis, characterisation of new compounds, spectroscopic characterisation, data analysis, and writing – original draft preparation; K. M., spectroscopic characterisation, data analysis, and writing – original draft preparation; J. D.-V., synthesis and characterisation of new compounds; Dž. J., investigation, data analysis, visualisation of experimental data of live cells, and writing – original draft preparation; R. Ž. (Rugilė Žilėnaitė), spectroscopic characterisation and data analysis; V. K., supervision of experiments with live cells and writing – review and editing; S. T., supervision of organic synthesis and writing – review and editing; A. V., conceptualisation, writing – review and editing, supervision, and funding acquisition.

## Conflicts of interest

There are no conflicts to declare.

## Acknowledgements

Rokas Žvirblis would like to thank European Social Fund for funding his research project under the grant agreement with Lithuanian Academy of Sciences (no. 09.3.3-LMT-K-712-22-0167).

## Notes and references

1 A. L. Cruz, E. d A. Barreto, N. P. Fazolini, J. P. Viola and P. T. Bozza, Lipid droplets: platforms with multiple functions in cancer hallmarks, *Cell Death Dis.*, 2020, **11**, 105.

 This journal is © The Royal Society of Chemistry 2023

Published on 06 April 2023. Downloaded on 5/3/2023 1:03:14 PM.

2 N. Krahmer, R. V. Farese and T. C. Walther, Balancing the fat: lipid droplets and human disease, *EMBO Mol. Med.*, 2013, **5**, 973–983.
3 A. R. Thiam, R. V. Farese Jr and T. C. Walther, The biophysics and cell biology of lipid droplets, *Nat. Rev. Mol. Cell Biol.*, 2013, **14**, 775–786.
4 P. T. Bozza, I. Bakker-Abreu, R. A. Navarro-Xavier and C. Bandeira-Melo, Lipid body function in eicosanoid synthesis: An update, *Prostaglandins, Leukotrienes Essent. Fatty Acids*, 2011, **85**, 205–213.
5 F. Röhrig and A. Schulze, The multifaceted roles of fatty acid synthesis in cancer, *Nat. Rev. Cancer*, 2016, **16**, 732–749.
6 P. T. Bozza and J. P. Viola, Lipid droplets in inflammation and cancer, *Prostaglandins, Leukotrienes Essent. Fatty Acids*, 2010, **82**, 243–250.
7 P. Antunes, A. Cruz, J. Barbosa, V. D. Bonifácio and S. N. Pinto, Lipid Droplets in Cancer: From Composition and Role to Imaging and Therapeutics, *Molecules*, 2022, **27**, 1–13.
8 J. A. Olzmann and P. Carvalho, Dynamics and functions of lipid droplets, *Nat. Rev. Mol. Cell Biol.*, 2019, **20**, 137–155.
9 R. V. Farese and T. C. Walther, Lipid Droplets Finally Get a Little R-E-S-P-E-C-T, *Cell*, 2009, **139**, 855–860.
10 R. Rakotonirina-Ricquebourg, V. Costa and V. Teixeira, Hello from the other side: Membrane contact of lipid droplets with other organelles and subsequent functional implications, *Prog. Lipid Res.*, 2022, **85**, 101141.
11 A. H. Ashoka, P. Ashokkumar, Y. P. Kovtun and A. S. Klymchenko, Solvatochromic Near-Infrared Probe for Polarity Mapping of Biomembranes and Lipid Droplets in Cells under Stress, *J. Phys. Chem. Lett.*, 2019, **10**, 2414–2421.
12 K. N. Wang, L. Y. Liu, D. Mao, S. Xu, C. P. Tan, Q. Cao, Z. W. Mao and B. Liu, A Polarity-Sensitive Ratiometric Fluorescence Probe for Monitoring Changes in Lipid Droplets and Nucleus during Ferroptosis, *Angew. Chem., Int. Ed.*, 2021, **60**, 15095–15100.
13 A. S. Klymchenko and R. Kreder, Fluorescent Probes for Lipid Rafts: From Model Membranes to Living Cells, *Chem. Biol.*, 2014, **21**, 97–113.
14 G. M'Baye, Y. Mély, G. Duportail and A. S. Klymchenko, Liquid Ordered and Gel Phases of Lipid Bilayers: Fluorescent Probes Reveal Close Fluidity but Different Hydration, *Biophys. J.*, 2008, **95**, 1217.
15 J. R. Lakowicz, *Principles of fluorescence spectroscopy*, Springer, US, Boston, MA, 3rd edn, 2006, pp. 1–954.
16 C. Reichardt, *Solvent Effects in Organic Chemistry*, Wiley-VCH, Weinheim, 1984, pp. 1–629.
17 A. S. Klymchenko, Solvatochromic and Fluorogenic Dyes as Environment-Sensitive Probes: Design and Biological Applications, *Acc. Chem. Res.*, 2017, **50**, 366–375.
18 J. A. Levitt, P.-H. Chung and K. Suhling, Spectrally resolved fluorescence lifetime imaging of Nile red for measurements of intracellular polarity, *J. Biomed. Opt.*, 2015, **20**, 096002.
19 N. Boens, B. Verbelen and W. Dehaen, Postfunctionalization of the BODIPY Core: Synthesis and Spectroscopy, *Eur. J. Org. Chem.*, 2015, 6577–6595.
20 M. K. Kuimova, G. Yahioglu, J. A. Levitt and K. Suhling, Molecular rotor measures viscosity of live cells via fluorescence lifetime imaging, *J. Am. Chem. Soc.*, 2008, **130**, 6672–6673.
21 W. Miao, C. Yu, E. Hao and L. Jiao, Functionalized BODIPYs as Fluorescent Molecular Rotors for Viscosity Detection, *Front. Chem.*, 2019, **7**, 1–6.
22 C. Ma, W. Sun, L. Xu, Y. Qian, J. Dai, G. Zhong, Y. Hou, J. Liu and B. Shen, A minireview of viscosity-sensitive fluorescent probes: Design and biological applications, *J. Mater. Chem. B*, 2020, **8**, 9642–9651.
23 H. Xiao, P. Li and B. Tang, Small Molecular Fluorescent Probes for Imaging of Viscosity in Living Biosystems, *Chem. – Eur. J.*, 2021, **27**, 6880–6898.
24 K. Maleckait, D. Narkevičius, R. Žil nait, J. Dodonova-Vaitkūnien, S. Toliautas, S. Tumkevičius and A. Vyšniauskas, Give or take: Effects of electron-accepting/-withdrawing groups in red-fluorescent BODIPY molecular rotors, *Molecules*, 2022, **27**, 23.
25 S. Xuan, N. Zhao, X. Ke, Z. Zhou, F. R. Fronczek, K. M. Kadish, K. M. Smith and M. G. H. Vicente, Synthesis and Spectroscopic Investigation of a Series of Push-Pull Boron Dipyrromethenes (BODIPYs), *J. Org. Chem.*, 2017, **82**, 2545–2557.
26 Y. Chen, J. Zhao, H. Guo and L. Xie, Geometry relaxation-induced large Stokes shift in red-emitting borondipyrromethenes (BODIPY) and applications in fluorescent thiol probes, *J. Org. Chem.*, 2012, **77**, 2192–2206.
27 M. Olšinová, P. Jurkiewicz, M. Pozník, R. Šachl, T. Prausová, M. Hof, V. Kozmík, F. Teplý, J. Svoboda and M. Cebecauer, Di- and tri-oxalkyl derivatives of a boron dipyrromethene (BODIPY) rotor dye in lipid bilayers, *Phys. Chem. Chem. Phys.*, 2014, **16**, 10688–10697.
28 R. Sens and K. H. Drexhage, Fluorescence quantum yield of oxazine and carbazine laser dyes, *J. Lumin.*, 1981, **24–25**, 709–712.
29 R. Czarnomysy, K. Bielawski, A. Muszynska, A. Bielawska and A. Gornowicz, Biological evaluation of dimethylpyridine-platinum complexes with potent antiproliferative activity, *J. Enzyme Inhib. Med. Chem.*, 2016, **31**, 150–165.
30 S. Nakayama, Y. Torikoshi, T. Takahashi, T. Yoshida, T. Sudo, T. Matsushima, Y. Kawasaki, A. Katayama, K. Gohda, G. N. Hortobagyi, S. Noguchi, T. Sakai, H. Ishihara and N. T. Ueno, Prediction of paclitaxel sensitivity by CDK1 and CDK2 activity in human breast cancer cells, *Breast Cancer Res.*, 2009, **11**, 1–10.
31 J. Schindelin, I. Arganda-Carreras, E. Frise, V. Kaynig, M. Longair, T. Pietzsch, S. Preibisch, C. Rueden, S. Saalfeld, B. Schmid, J.-Y. Tinevez, D. J. White, V. Hartenstein, K. Eliceiri, P. Tomancak and A. Cardona, Fiji: an open-source platform for biological-image analysis, *Nat. Methods*, 2012, **9**, 676–682.
32 S. Bolte and F. P. Cordelières, A guided tour into subcellular colocalization analysis in light microscopy, *J. Microsc.*, 2006, **224**, 213–232.
33 E. M. M. Manders, F. J. Verbeek and J. A. Aten, Measurement of co-localization of objects in dual-colour confocal images, *J. Microsc.*, 1993, **169**, 375–382.

34 S. J. Strickler and R. A. Berg, Relationship between Absorption Intensity and Fluorescence Lifetime of Molecules, *J. Chem. Phys.*, 1962, **37**, 814–822.
35 A. Vyšniauskas, I. López-Duarte, N. Duchemin, T. T. Vu, Y. Wu, E. M. Budynina, Y. A. Volkova, E. Peña Cabrera, D. E. Ramírez-Ornelas and M. K. Kuimova, Exploring viscosity, polarity and temperature sensitivity of BODIPY-based molecular rotors, *Phys. Chem. Chem. Phys.*, 2017, **19**, 25252–25259.
36 A. Vyšniauskas, B. Cornell, P. S. Sherin, K. Maleckait, M. Kubánková, M. A. Izquierdo, T. T. Vu, Y. A. Volkova, E. M. Budynina, C. Molteni and M. K. Kuimova, Cyclopropyl Substituents Transform the Viscosity-Sensitive BODIPY Molecular Rotor into a Temperature Sensor, *ACS Sens.*, 2021, **6**, 2158–2167.
37 J. Zhou, B. del Rosal, D. Jaque, S. Uchiyama and D. Jin, Advances and challenges for fluorescence nanothermometry, *Nat. Methods*, 2020, **17**, 967–980.
38 T. T. Vu, R. Méallet-Renault, G. Clavier, B. A. Trofimov and M. K. Kuimova, Tuning BODIPY molecular rotors into the red: sensitivity to viscosity *vs.* temperature, *J. Mater. Chem. C*, 2016, **4**, 2828–2833.
39 M. R. Dent, I. López-Duarte, C. J. Dickson, N. D. Geoghegan, J. M. Cooper, I. R. Gould, R. Krams, J. A. Bull, N. J. Brooks and M. K. Kuimova, Imaging phase separation in model lipid membranes through the use of BODIPY based molecular rotors, *Phys. Chem. Chem. Phys.*, 2015, **17**, 18393–18402.
40 B. A. Weaver, How Taxol/paclitaxel kills cancer cells, *Mol. Biol. Cell*, 2014, **25**, 2677–2681.
41 S. Dasari and P. Bernard, Tchounwou, Cisplatin in cancer therapy: Molecular mechanisms of action, *Eur. J. Pharmacol.*, 2014, **740**, 364–378.
42 H. Jiang, X. W. Zhang, Q. L. Liao, W. T. Wu, Y. L. Liu and W. H. Huang, Electrochemical Monitoring of Paclitaxel-Induced ROS Release from Mitochondria inside Single Cells, *Small*, 2019, **15**, 1–5.
43 P. C. Liao, S. K. Tan, C. H. Lieu and H. K. Jung, Involvement of endoplasmic reticulum in paclitaxel-induced apoptosis, *J. Cell. Biochem.*, 2008, **104**, 1509–1523.
44 J. Alexandre, Y. Hu, W. Lu, H. Pelicano and P. Huang, Novel action of paclitaxel against cancer cells: Bystander effect mediated by reactive oxygen species, *Cancer Res.*, 2007, **67**, 3512–3517.

Published on 06 April 2023. Downloaded on 5/3/2023 1:03:14 PM.


This journal is © The Royal Society of Chemistry 2023

# BIBLIOGRAPHY


[1] M. K. Kuimova, Mapping viscosity in cells using molecular rotors, Physical Chemistry Chemical Physics **14**(37), 12671–12686 (2012), https://doi.org/10.1039/c2cp41674c.

[2] K. N. Clayton, G. D. Berglund, J. C. Linnes, T. L. Kinzer-Ursem, S. T. Wereley, DNA Microviscosity Characterization with Particle Diffusometry for Downstream DNA Detection Applications, Analytical Chemistry **89**(24), 13334–13341 (2017), https://doi.org/10.1021/acs.analchem.7b03513.

[3] M. Kubánková, I. López-Duarte, D. Kiryushko, M. K. Kuimova, Molecular rotors report on changes in live cell plasma membrane microviscosity upon interaction with beta-amyloid aggregates, Soft Matter **14**(46), 9466–9474 (2018), https://doi.org/10.1039/c8sm01633j.

[4] N. C. Bal, S. K. Maurya, D. H. Sopariwala, S. K. Sahoo, S. C. Gupta, S. A. Shaikh, M. Pant, L. A. Rowland, S. A. Goonasekera, J. D. Molkentin, M. Periasamy, Erratum: Sarcolipin is a newly identified regulator of muscle-based thermogenesis in mammals (Nature Medicine (2012) 18 (1575-1579)), Nature Medicine **18**(12), 1857 (2012), https://doi.org/10.1038/nm1212-1857b.

[5] Y. H. Tseng, A. M. Cypess, C. R. Kahn, Cellular bioenergetics as a target for obesity therapy, Nature Reviews Drug Discovery **9**(6), 465–481 (2010), https://doi.org/10.1038/nrd3138.

[6] D. Francis, P. W. Barlow, Temperature and the cell cycle., Symposia of the Society for Experimental Biology **42**, 181–201 (1988).

[7] N. Jiang, J. Fan, F. Xu, X. Peng, H. Mu, J. Wang, X. Xiong, Ratiometric fluorescence imaging of cellular polarity: Decrease in mitochondrial polarity in cancer cells, Angewandte Chemie - International Edition **54**(8), 2510–2514 (2015), https://doi.org/10.1002/anie.201410645.

[8] Y. D. Zhuang, P. Y. Chiang, C. W. Wang, K. T. Tan, Environment-sensitive fluorescent turn-on probes targeting hydrophobic ligand-binding domains for selective protein detection, Angewandte Chemie - International Edition **52**(31), 8124–8128 (2013), https://doi.org/10.1002/anie.201302884.

[9] M. W. Berns, T. Krasieva, C. H. Sun, A. Dvornikov, P. M. Rentzepis, A polarity dependent fluorescence "switch" in live cells, Journal of Photochemistry and Photobiology B: Biology **75**(1-2), 51–56 (2004), https://doi.org/10.1016/j.jphotobiol.2004.05.002.

[10] G. S. Zubenko, U. Kopp, T. Seto, L. L. Firestone, Platelet membrane fluidity individuals at risk for Alzheimer's disease: A comparison of results from fluorescence spectroscopy and electron spin

resonance spectroscopy, Psychopharmacology **145**(2), 175–180 (1999), https://doi.org/10.1007/s002130051046.

[11] X. Yang, D. Zhang, Y. Ye, Y. Zhao, Recent advances in multifunctional fluorescent probes for viscosity and analytes, Coordination Chemistry Reviews **453**(214336), 214336 (2022), https://doi.org/10.1016/j.ccr.2021.214336.

[12] T. T. Jia, Y. Li, H. Niu, Recent Progress in Fluorescent Probes for Diabetes Visualization and Drug Therapy, Chemosensors **10**(7) (2022), https://doi.org/10.3390/chemosensors10070280.

[13] A. M. Stark, S. Way, The use of thermovision in the detection of early breast cancer, Cancer **33**(6), 1664–1670 (1974), https://doi.org/10.1002/1097-0142(197406)33:6<1664::AID-CNCR2820330629>3.0.CO;2-7.

[14] J. Yin, W. Quan, X. Kong, C. Liu, B. Lu, W. Lin, Utilizing a solvatochromic optical agent to monitor the polarity changes in dynamic liver injury progression, ACS Applied Bio Materials **4**(4), 3630–3638 (2021), https://doi.org/10.1021/acsabm.1c00130.

[15] C. Lai, Y. Zhao, X. Zou, Y. Liang, W. Lin, Quantification of lipid droplets polarity for evaluating non-alcoholic fatty liver disease via fluorescence lifetime imaging, Sensors and Actuators B: Chemical **369**(132267), 132267 (2022), https://doi.org/10.1016/j.snb.2022.132267.

[16] W. Miao, C. Yu, E. Hao, L. Jiao, Functionalized BODIPYs as Fluorescent Molecular Rotors for Viscosity Detection, Frontiers in Chemistry **7**(November), 1–6 (2019), https://doi.org/10.3389/fchem.2019.00825.

[17] M. Homma, Y. Takei, A. Murata, T. Inoue, S. Takeoka, A ratiometric fluorescent molecular probe for visualization of mitochondrial temperature in living cells, Chemical Communications **51**(28), 6194–6197 (2015), https://doi.org/10.1039/c4cc10349a.

[18] H. Sunahara, Y. Urano, H. Kojima, T. Nagano, Design and synthesis of a library of BODIPY-based environmental polarity sensors utilizing photoinduced electron-transfer-controlled fluorescence ON/OFF switching, Journal of the American Chemical Society **129**(17), 5597–5604 (2007), https://doi.org/10.1021/ja068551y.

[19] J. A. Levitt, P. H. Chung, M. K. Kuimova, G. Yahioglu, Y. Wang, J. Qu, K. Suhling, Fluorescence anisotropy of molecular rotors, ChemPhysChem **12**(3), 662–672 (2011), https://doi.org/10.1002/cphc.201000782.

[20] K. Horikoshi, Cell Structure, https://training.seer.cancer.gov/anatomy/cells_tissues_membranes/cells/structure.html, [Accessed 19-Apr-2023] (2021).

[21] Britannica.com, Cell, https://www.britannica.com/science/cell-biology/Coupled-chemical-reactions, [Accessed 19-Apr-2023].

[22] X. Li, Z. Li, M. Zhao, Y. Nie, P. Liu, Y. Zhu, X. Zhang, Skeletal muscle lipid droplets and the athlete's paradox, Cells **8**(3), 249 (2019), https://doi.org/10.3390/cells8030249.

[23] I. M. Resta, F. Lucantoni, N. Apostolova, F. Galindo, Fluorescent styrylpyrylium probes for the imaging of mitochondria in live cells, Organic and Biomolecular Chemistry **19**(41), 9043–9057 (2021), https://doi.org/10.1039/d1ob01543e.

[24] R. V. Farese, T. C. Walther, Lipid Droplets Finally Get a Little R-E-S-P-E-C-T, Cell **139**(5), 855–860 (2009), https://doi.org/10.1016/j.cell.2009.11.005.

[25] Y. Fu, N. S. Finney, Small-molecule fluorescent probes and their design, RSC Advances **8**(51), 29051–29061 (2018), https://doi.org/10.1039/c8ra02297f.

[26] N. Hee Kim, D. Kim, Blue-Emitting BODIPY Dyes, in J. Bañuelos-Prieto, R. S. Llano (eds.), *BODIPY Dyes - A Privilege Molecular Scaffold with Tunable Properties* (IntechOpen, Rijeka, 2019), chapter 3.

[27] Y. W. Jun, H. R. Kim, Y. J. Reo, M. Dai, K. H. Ahn, Addressing the autofluorescence issue in deep tissue imaging by two-photon microscopy: The significance of far-red emitting dyes, Chemical Science **8**(11), 7696–7704 (2017), https://doi.org/10.1039/c7sc03362a.

[28] R. Weissleder, A clearer vision for in vivo imaging: Progress continues in the development of smaller, more penetrable probes for biological imaging, Nature Biotechnology **19**(4), 316–317 (2001), https://doi.org/10.1038/86684.

[29] S. Wang, B. Li, F. Zhang, Molecular Fluorophores for Deep-Tissue Bioimaging, ACS Central Science **6**(8), 1302–1316 (2020), https://doi.org/10.1021/acscentsci.0c00544.

[30] J. M. Nölle, C. Jüngst, A. Zumbusch, D. Wöll, Monitoring of viscosity changes during free radical polymerization using fluorescence lifetime measurements, Polymer Chemistry **5**(8), 2700–2703 (2014), https://doi.org/10.1039/c3py01684f.

[31] N. A. Hosny, C. Fitzgerald, A. Vyšniauskas, A. Athanasiadis, T. Berkemeier, N. Uygur, U. Pöschl, M. Shiraiwa, M. Kalberer, F. D. Pope, M. K. Kuimova, Direct imaging of changes in aerosol particle viscosity upon hydration and chemical aging, Chemical Science **7**(2), 1357–1367 (2016), https://doi.org/10.1039/c5sc02959g.

[32] S. C. Lee, J. Heo, J. W. Ryu, C. L. Lee, S. Kim, J. S. Tae, B. O. Rhee, S. W. Kim, O. P. Kwon, Pyrrolic molecular rotors acting as viscosity sensors with high fluorescence contrast, Chemical Communications **52**(94), 13695–13698 (2016), https://doi.org/10.1039/c6cc06521j.

[33] D. Li, X. Tian, A. Wang, L. Guan, J. Zheng, F. Li, S. Li, H. Zhou, J. Wu, Y. Tian, Nucleic acid-selective light-up fluorescent biosensors for ratiometric two-photon imaging of the viscosity of live cells and tissues, Chemical Science **7**(3), 2257–2263 (2016), https://doi.org/10.1039/c5sc03956h.

[34] M. Gao, Y. Hong, B. Chen, Y. Wang, W. Zhou, W. W. Wong, J. Zhou, T. A. Smith, Z. Zhao, AIE conjugated polyelectrolytes based on tetraphenylethene for efficient fluorescence imaging and lifetime imaging of living cells, Polymer Chemistry **8**(26), 3862–3866 (2017), https://doi.org/10.1039/c7py00564d.

[35] P. K. Ghosh, A. Vasanji, G. Murugesan, S. J. Eppell, L. M. Graham, P. L. Fox, Membrane microviscosity regulates endothelial cell motility, Nature Cell Biology **4**(11), 894–900 (2002), https://doi.org/10.1038/ncb873.

[36] M. E. Nipper, S. Majd, M. Mayer, J. C. Lee, E. A. Theodorakis, M. A. Haidekker, Characterization of changes in the viscosity of lipid membranes with the molecular rotor FCVJ, Biochimica et Biophysica Acta - Biomembranes **1778**(4), 1148–1153 (2008), https://doi.org/10.1016/j.bbamem.2008.01.005.

[37] L. Michels, V. Gorelova, Y. Harnvanichvech, J. W. Borst, B. Albada, D. Weijers, J. Sprakel, Complete microviscosity maps of living plant cells and tissues with a toolbox of targeting mechanoprobes, Proceedings of the National Academy of Sciences of the United States of America **117**(30), 18110–18118 (2020), https://doi.org/10.1073/pnas.1921374117.

[38] M. Páez-Pérez, I. López-Duarte, A. Vyšniauskas, N. J. Brooks, M. K. Kuimova, Imaging non-classical mechanical responses of lipid membranes using molecular rotors, Chemical Science **12**(7), 2604–2613 (2021), https://doi.org/10.1039/d0sc05874b.

[39] S. V. Dzyuba, BODIPY Dyes as Probes and Sensors to Study Amyloid-$\beta$-Related Processes, Biosensors **10**(12), 192 (2020), https://doi.org/10.3390/BIOS10120192.

[40] O. Nadiv, M. Shinitzky, H. Manu, D. Hecht, C. T. Roberts, D. LeRoith, Y. Zick, Elevated protein tyrosine phosphatase activity and increased membrane viscosity are associated with impaired activation of the insulin receptor kinase in old rats, Biochemical Journal **298**(2), 443–450 (1994), https://doi.org/10.1042/bj2980443.

[41] J. Yang, Y. Guo, M. Pistolozzi, J. Yan, Research progress of multi-functional fluorescent probes for Alzheimer's disease monitoring, Dyes and Pigments **193**(109466), 109466 (2021), https://doi.org/10.1016/j.dyepig.2021.109466.

[42] G. G. Yang, X. J. Hu, W. Liu, X. Xu, Real-time monitoring viscosity changes in lipid droplets in response to ER stress via a viscosity-sensitive ruthenium (II) fluorescent probe, Sensors and Actuators B: Chemical **370**(132403), 132403 (2022), https://doi.org/10.1016/j.snb.2022.132403.

[43] B. Dong, W. Song, Y. Lu, Y. Sun, W. Lin, Revealing the Viscosity Changes in Lipid Droplets during Ferroptosis by the Real-Time and in Situ Near-Infrared Imaging, ACS Sensors **6**(1), 22–26 (2021), https://doi.org/10.1021/acssensors.0c02015.

[44] S. Arai, S. C. Lee, D. Zhai, M. Suzuki, Y. T. Chang, A molecular fluorescent probe for targeted visualization of temperature at the endoplasmic reticulum, Scientific Reports **4**(Iii), 2–7 (2014), https://doi.org/10.1038/srep06701.

[45] M. M. Ogle, A. D. Smith McWilliams, M. J. Ware, S. A. Curley, S. J. Corr, A. A. Martí, Sensing Temperature in Vitro and in Cells Using a BODIPY Molecular Probe, Journal of Physical Chemistry B **123**(34), 7282–7289 (2019), https://doi.org/10.1021/acs.jpcb.9b04384.

[46] B. Valeur, *Molecular Fluorescence. Principles and Applications.* (Wiley-VCH Verlag GmbH, Weinheim, FRG, 2001).

[47] J. R. Lakowicz, *Principles of fluorescence spectroscopy* (Springer US, Boston, MA, 2006), third edition.

[48] S. Spange, N. Weiß, C. H. Schmidt, K. Schreiter, Reappraisal of Empirical Solvent Polarity Scales for Organic Solvents, Chemistry–Methods **1**(1), 42–60 (2021), https://doi.org/10.1002/cmtd.202000039.

[49] E. Shuang, Q. X. Mao, J. H. Wang, X. W. Chen, Carbon dots with tunable dual emissions: From the mechanism to the specific imaging of endoplasmic reticulum polarity, Nanoscale **12**(12), 6852–6860 (2020), https://doi.org/10.1039/c9nr10982j.

[50] J. Jiang, X. Tian, C. Xu, S. Wang, Y. Feng, M. Chen, H. Yu, M. Zhu, X. Meng, A two-photon fluorescent probe for real-time monitoring of autophagy by ultrasensitive detection of the change in lysosomal polarity, Chemical Communications **53**(26), 3645–3648 (2017), https://doi.org/10.1039/c7cc00752c.

[51] Y. Tang, S. Song, J. Peng, Q. Zhang, W. Lin, An ultrasensitive lipid droplet-targeted NIR emission fluorescent probe for polarity detection and its application in liver disease diagnosis, Journal of Materials Chemistry B **10**(36), 6974–6982 (2022), https://doi.org/10.1039/d2tb01145j.

[52] A. H. Ashoka, P. Ashokkumar, Y. P. Kovtun, A. S. Klymchenko, Solvatochromic Near-Infrared Probe for Polarity Mapping of Biomembranes and Lipid Droplets in Cells under Stress, Journal of Physical Chemistry Letters **10**(10), 2414–2421 (2019), https://doi.org/10.1021/acs.jpclett.9b00668.

[53] J. A. Olzmann, P. Carvalho, Dynamics and functions of lipid droplets, Nature Reviews Molecular Cell Biology **20**(3), 137–155 (2019), https://doi.org/10.1038/s41580-018-0085-z.

[54] K. N. Wang, L. Y. Liu, D. Mao, S. Xu, C. P. Tan, Q. Cao, Z. W. Mao, B. Liu, A Polarity-Sensitive Ratiometric Fluorescence Probe for Monitoring Changes in Lipid Droplets and Nucleus during Ferroptosis, Angewandte Chemie - International Edition **60**(27), 15095–15100 (2021), https://doi.org/10.1002/anie.202104163.

[55] I. Khan, A. Elhissi, M. Shah, M. A. Alhnan, W. Ahmed, *Liposome-based carrier systems and devices used for pulmonary drug delivery* (Woodhead Publishing Limited, 2013).

[56] R. P. Baker, S. Urban, *An Inducible Reconstitution System for the Real-Time Kinetic Analysis of Protease Activity and Inhibition Inside the Membrane*, volume 584 (Elsevier Inc., 2017), 1 edition.

[57] A. W. Leung, C. Amador, L. C. Wang, U. V. Mody, M. B. Bally, What drives innovation: The Canadian touch on liposomal therapeutics, Pharmaceutics **11**(3), 124 (2019), https://doi.org/10.3390/pharmaceutics11030124.

[58] X. L. Hao, B. Cao, D. Dai, F. G. Wu, Z. W. Yu, Cholesterol Protects the Liquid-Ordered Phase of Raft Model Membranes from the Destructive Effect of Ionic Liquids, Journal of Physical Chemistry Letters **13**(32), 7386–7391 (2022), https://doi.org/10.1021/acs.jpclett.2c01873.

[59] A. S. Klymchenko, R. Kreder, Fluorescent probes for lipid rafts: From model membranes to living cells, Chemistry and Biology **21**(1), 97–113 (2014), https://doi.org/10.1016/j.chembiol.2013.11.009.

[60] I. Schachter, R. O. Paananen, B. Fábián, P. Jurkiewicz, M. Javanainen, The Two Faces of the Liquid Ordered Phase, Journal of Physical Chemistry Letters **13**(5), 1307–1313 (2022), https://doi.org/10.1021/acs.jpclett.1c03712.

[61] M. L. Schmidt, J. H. Davis, Liquid Disordered-Liquid Ordered Phase Coexistence in Lipid/Cholesterol Mixtures: A Deuterium 2D NMR Exchange Study, Langmuir **33**(8), 1881–1890 (2017), https://doi.org/10.1021/acs.langmuir.6b02834.

[62] G. M'Baye, Y. Mély, G. Duportail, A. S. Klymchenko, Liquid ordered and gel phases of lipid bilayers: Fluorescent probes reveal close fluidity but different hydration, Biophysical Journal **95**(3), 1217–1225 (2008), https://doi.org/10.1529/biophysj.107.127480.

[63] Leica-microsystems.com, An Introduction to Fluorescence, https://www.leica-microsystems.com/science-lab/life-science/an-introduction-to-fluorescence/, [Accessed 19-Apr-2023].

[64] Libretexts.org, Fluorescence and Phosphorescence, https://chem.libretexts.org/Bookshelves/Physical_and_Theoretical_Chemistry_Textbook_Maps/Supplemental_Modules_(Physical_and_Theoretical_Chemistry)/Spectroscopy/Electronic_Spectroscopy/Fluorescence_and_Phosphorescence, [Accessed 19-Apr-2023].

[65] Tcspc.com, Origins of Multiexponential decays, https://www.tcspc.com/doku.php/some_origins_of_multiexponetial_decays_for_single_dyes, [Accessed 03-May-2023].

[66] M. Y. Berezin, S. Achilefu, Fluorescence lifetime measurements and biological imaging, Chemical Reviews **110**(5), 2641–2684 (2010), https://doi.org/10.1021/cr900343z.

[67] A. M. Brouwer, Standards for photoluminescence quantum yield measurements in solution (IUPAC technical report), Pure and Applied Chemistry **83**(12), 2213–2228 (2011), https://doi.org/10.1351/PAC-REP-10-09-31.

[68] M. Levitus, Tutorial: Measurement of fluorescence spectra and determination of relative fluorescence quantum yields of transparent samples, Methods and Applications in Fluorescence **8**(3), 033001 (2020), https://doi.org/10.1088/2050-6120/ab7e10.

[69] S. J. Strickler, R. A. Berg, Relationship between absorption intensity and fluorescence lifetime of molecules, The Journal of Chemical Physics **37**(4), 814–822 (1962), https://doi.org/10.1063/1.1733166.

[70] W. Becker, The bh TCSPC Handbook, Scanning (800), 1–566 (2010).

[71] TCSPC - What is Time-Correlated Single Photon Counting? — edinst.com, https://www.edinst.com/blog/what-is-tcspc/, [Accessed 08-May-2023].

[72] B. Crockett, J. van Howe, N. Montaut, R. Morandotti, J. Azaña, High-Resolution Time-Correlated Single-Photon Counting Using Electro-Optic Sampling, Laser Photonics Reviews **16**(10), 2100635 (2022), https://doi.org/10.1002/lpor.202100635.

[73] T. K. Meyvis, S. C. De Smedt, P. Van Oostveldt, J. Demeester, Fluorescence recovery after photobleaching: a versatile tool for mobility and interaction measurements in pharmaceutical research., Pharmaceutical research **16**(8), 1153–62 (1999), https://doi.org/10.1023/a:1011924909138.

[74] A. S. Verkman, Diffusion in cells measured by fluorescence recovery after photobleaching, Methods in Enzymology **360**(1996), 635–648 (2003), https://doi.org/10.1016/S0076-6879(03)60132-1.

[75] W. Baschong, L. Landmann, *Fluorescence microscopy* (Academic Press, San Diego, CA, 2005).

[76] D. Axelrod, D. E. Koppel, J. Schlessinger, E. Elson, W. W. Webb, Mobility measurement by analysis of fluorescence photobleaching recovery kinetics, Biophysical Journal **16**(9), 1055–1069 (1976), https://doi.org/10.1016/S0006-3495(76)85755-4.

[77] C. A. Day, L. J. Kraft, M. Kang, A. K. Kenworthy, Analysis of protein and lipid dynamics using confocal fluorescence recovery after photobleaching (FRAP), Current Protocols in Cytometry **Chapter 2**(SUPPL.62), Unit2.19 (2012), https://doi.org/10.1002/0471142956.cy0219s62.

[78] Z. W. Zhao, J. C. M. Gebhardt, D. M. Suter, X. S. Xie, Reply to "convergence of chromatin binding estimates in live cells", Nature Methods **10**(8), 692 (2013), https://doi.org/10.1038/nmeth.2574.

[79] H. C. Ishikawa-Ankerhold, R. Ankerhold, G. P. C. Drummen, Advanced Fluorescence Microscopy Techniques—FRAP, FLIP, FLAP, FRET and FLIM, Molecules **17**(4), 4047–4132 (2012), https://doi.org/10.3390/molecules17044047.

[80] G. A. Dunn, I. M. Dobbie, J. Monypenny, M. R. Holt, D. Zicha, Fluorescence localization after photobleaching (FLAP): A new method for studying protein dynamics in living cells, Journal of Microscopy **205**(1), 109–112 (2002), https://doi.org/10.1046/j.0022-2720.2001.001007.x.

[81] P. Schwille, Fluorescence correlation spectroscopy and its potential for intracellular applications, Cell Biochemistry and Biophysics **34**(3), 383–408 (2001), https://doi.org/10.1385/CBB:34:3:383.

[82] L. Yu, Y. Lei, Y. Ma, M. Liu, J. Zheng, D. Dan, P. Gao, A Comprehensive Review of Fluorescence Correlation Spectroscopy, Frontiers in Physics **9** (2021), https://doi.org/10.3389/fphy.2021.644450.

[83] A. Shahzad, G. Kohler, Fluorescence correlation spectroscopy (FCS): A promising tool for biological research, Applied Spectroscopy Reviews **46**(2), 166–173 (2011), https://doi.org/10.1080/05704928.2010.537005.

[84] R. Macháň, T. Wohland, Recent applications of fluorescence correlation spectroscopy in live systems, FEBS Letters **588**(19), 3571–3584 (2014), https://doi.org/10.1016/j.febslet.2014.03.056.

[85] Z. Wang, Y. Zheng, D. Zhao, Z. Zhao, L. Liu, A. Pliss, F. Zhu, J. Liu, J. Qu, P. Luan, Applications of fluorescence lifetime imaging in clinical medicine, Journal of Innovative Optical Health Sciences **11**(1), 1830001 (2018), https://doi.org/10.1142/S179354581830001X.

[86] J. M. Hum, A. P. Siegel, F. M. Pavalko, R. N. Day, Monitoring biosensor activity in living cells with fluorescence lifetime imaging microscopy, International Journal of Molecular Sciences **13**(11), 14385–14400 (2012), https://doi.org/10.3390/ijms131114385.

[87] W. Becker, Fluorescence lifetime imaging - techniques and applications, Journal of Microscopy **247**(2), 119–136 (2012), https://doi.org/10.1111/j.1365-2818.2012.03618.x.

[88] A. Pliss, X. Peng, L. Liu, A. Kuzmin, Y. Wang, J. Qu, Y. Li, P. N. Prasad, Single cell assay for molecular diagnostics and medicine:

Monitoring intracellular concentrations of macromolecules by two-photon fluorescence lifetime imaging, Theranostics **5**(9), 919–930 (2015), https://doi.org/10.7150/thno.11863.

[89] M. Kubánková, P. A. Summers, I. López-Duarte, D. Kiryushko, M. K. Kuimova, Microscopic Viscosity of Neuronal Plasma Membranes Measured Using Fluorescent Molecular Rotors: Effects of Oxidative Stress and Neuroprotection, ACS Applied Materials and Interfaces **11**(40), 36307–36315 (2019), https://doi.org/10.1021/acsami.9b10426.

[90] S. C. Lee, J. Heo, H. C. Woo, J. A. Lee, Y. H. Seo, C. L. Lee, S. Kim, O. P. Kwon, Fluorescent Molecular Rotors for Viscosity Sensors, Chemistry - A European Journal **24**(52), 13706–13718 (2018), https://doi.org/10.1002/chem.201801389.

[91] J. E. Chambers, M. Kubánková, R. G. Huber, I. López-Duarte, E. Avezov, P. J. Bond, S. J. Marciniak, M. K. Kuimova, An Optical Technique for Mapping Microviscosity Dynamics in Cellular Organelles, ACS Nano **12**(5), 4398–4407 (2018), https://doi.org/10.1021/acsnano.8b00177.

[92] A. Vyšniauskas, M. K. Kuimova, A twisted tale: Measuring viscosity and temperature of microenvironments using molecular rotors, International Reviews in Physical Chemistry **37**(2), 259–285 (2018), https://doi.org/10.1080/0144235X.2018.1510461.

[93] M. M. Ogle, A. D. Smith McWilliams, B. Jiang, A. A. Martí, Latest Trends in Temperature Sensing by Molecular Probes, ChemPhotoChem **4**(4), 255–270 (2020), https://doi.org/10.1002/cptc.201900255.

[94] H. Xiao, P. Li, B. Tang, Recent progresses in fluorescent probes for detection of polarity, Coordination Chemistry Reviews **427**, 213582 (2021), https://doi.org/10.1016/j.ccr.2020.213582.

[95] F. H. van der Linden, E. K. Mahlandt, J. J. Arts, J. Beumer, J. Puschhof, S. M. de Man, A. O. Chertkova, B. Ponsioen, H. Clevers, J. D. van Buul, M. Postma, T. W. Gadella, J. Goedhart, A turquoise fluorescence lifetime-based biosensor for quantitative imaging of intracellular calcium, Nature Communications **12**(1), 7159 (2021), https://doi.org/10.1038/s41467-021-27249-w.

[96] C. E. Rowland, C. W. Brown, I. L. Medintz, J. B. Delehanty, Intracellular FRET-based probes: a review, Methods and Applications in Fluorescence **3**(4), 042006 (2015), https://doi.org/10.1088/2050-6120/3/4/042006.

[97] S. Zadran, S. Standley, K. Wong, E. Otiniano, A. Amighi, M. Baudry, Fluorescence resonance energy transfer (FRET)-based biosensors: Visualizing cellular dynamics and bioenergetics, Applied Microbiology and Biotechnology **96**(4), 895–902 (2012), https://doi.org/10.1007/s00253-012-4449-6.

[98] L. Wu, C. Huang, B. P. Emery, A. C. Sedgwick, S. D. Bull, X. P. He, H. Tian, J. Yoon, J. L. Sessler, T. D. James, Förster

resonance energy transfer (FRET)-based small-molecule sensors and imaging agents, Chemical Society Reviews **49**(15), 5110–5139 (2020), https://doi.org/10.1039/c9cs00318e.

[99] A. Polita, S. Toliautas, R. Žvirblis, A. Vyšniauskas, The effect of solvent polarity and macromolecular crowding on the viscosity sensitivity of a molecular rotor BODIPY-C10, Physical Chemistry Chemical Physics **22**(16), 8296–8303 (2020), https://doi.org/10.1039/c9cp06865a.

[100] A. Vyšniauskas, I. López-Duarte, N. Duchemin, T. T. Vu, Y. Wu, E. M. Budynina, Y. A. Volkova, E. Peña Cabrera, D. E. Ramírez-Ornelas, M. K. Kuimova, Exploring viscosity, polarity and temperature sensitivity of BODIPY-based molecular rotors, Physical Chemistry Chemical Physics **19**(37), 25252–25259 (2017), https://doi.org/10.1039/c7cp03571c.

[101] H. Zhu, J. Fan, H. Mu, T. Zhu, Z. Zhang, J. Du, X. Peng, D-PET-controlled "off-on" Polarity-sensitive Probes for Reporting Local Hydrophilicity within Lysosomes, Scientific Reports **6**(October), 1–10 (2016), https://doi.org/10.1038/srep35627.

[102] T. T. Vu, R. Méallet-Renault, G. Clavier, B. A. Trofimov, M. K. Kuimova, Tuning BODIPY molecular rotors into the red: Sensitivity to viscosity: Vs. temperature, Journal of Materials Chemistry C **4**(14), 2828–2833 (2016), https://doi.org/10.1039/c5tc02954f.

[103] A. Athanasiadis, C. Fitzgerald, N. M. Davidson, C. Giorio, S. W. Botchway, A. D. Ward, M. Kalberer, F. D. Pope, M. K. Kuimova, Dynamic viscosity mapping of the oxidation of squalene aerosol particles, Physical Chemistry Chemical Physics **18**(44), 30385–30393 (2016), https://doi.org/10.1039/c6cp05674a.

[104] M. K. Kuimova, G. Yahioglu, J. A. Levitt, K. Suhling, Molecular rotor measures viscosity of live cells via fluorescence lifetime imaging, Journal of the American Chemical Society **130**(21), 6672–6673 (2008), https://doi.org/10.1021/ja800570d.

[105] L. Wang, Y. Xiao, W. Tian, L. Deng, Activatable rotor for quantifying lysosomal viscosity in living cells, Journal of the American Chemical Society **135**(8), 2903–2906 (2013), https://doi.org/10.1021/ja311688g.

[106] I. López-Duarte, T. Truc Vu, M. A. Izquierdo, J. A. Bull, M. K. Kuimova, A molecular rotor for measuring viscosity in plasma membranes of live cells, Chemical Communications **50**(40), 5282–5284 (2014), https://doi.org/10.1039/c3cc47530a.

[107] D. Su, C. L. Teoh, N. Gao, Q. H. Xu, Y. T. Chang, A simple bodipy-based viscosity probe for imaging of cellular viscosity in live cells, Sensors (Switzerland) **16**(9), 1397 (2016), https://doi.org/10.3390/s16091397.

[108] J. T. Mika, A. J. Thompson, M. R. Dent, N. J. Brooks, J. Michiels, J. Hofkens, M. K. Kuimova, Measuring the Viscosity of the Escherichia coli Plasma Membrane Using Molecular Rotors, Biophysical Journal **111**(7), 1528–1540 (2016), https://doi.org/10.1016/j.bpj.2016.08.020.

[109] P. S. Sherin, I. López-Duarte, M. R. Dent, M. Kubánková, A. Vyšniauskas, J. A. Bull, E. S. Reshetnikova, A. S. Klymchenko, Y. P. Tsentalovich, M. K. Kuimova, Visualising the membrane viscosity of porcine eye lens cells using molecular rotors, Chemical Science **8**(5), 3523–3528 (2017), https://doi.org/10.1039/c6sc05369f.

[110] I. E. Steinmark, A. L. James, P. H. Chung, P. E. Morton, M. Parsons, C. A. Dreiss, C. D. Lorenz, G. Yahioglu, K. Suhling, Targeted fluorescence lifetime probes reveal responsive organelle viscosity and membrane fluidity, PLoS ONE **14**(2), e0211165 (2019), https://doi.org/10.1371/journal.pone.0211165.

[111] X. Chen, Y. C. Liu, J. J. Cui, F. Y. Wu, Q. Xiao, A galactosidase-activatable fluorescent probe for detection of bacteria based on bodipy, Molecules **26**(19), 6072 (2021), https://doi.org/10.3390/molecules26196072.

[112] S. G. Awuah, Y. You, Boron dipyrromethene (BODIPY)-based photosensitizers for photodynamic therapy, RSC Advances **2**(30), 11169–11183 (2012), https://doi.org/10.1039/c2ra21404k.

[113] A. M. Durantini, D. A. Heredia, J. E. Durantini, E. N. Durantini, BODIPYs to the rescue: Potential applications in photodynamic inactivation, European Journal of Medicinal Chemistry **144**, 651–661 (2018), https://doi.org/10.1016/j.ejmech.2017.12.068.

[114] P. Ning, P. Dong, Q. Geng, L. Bai, Y. Ding, X. Tian, R. Shao, L. Li, X. Meng, A two-photon fluorescent probe for viscosity imaging in vivo, Journal of Materials Chemistry B **5**(15), 2743–2749 (2017), https://doi.org/10.1039/C7TB00136C.

[115] S. Toliautas, J. Dodonova, A. Žvirblis, I. Čiplys, A. Polita, A. Devižis, S. Tumkevičius, J. Šulskus, A. Vyšniauskas, Enhancing the Viscosity-Sensitive Range of a BODIPY Molecular Rotor by Two Orders of Magnitude, Chemistry - A European Journal **25**(44), 10342–10349 (2019), https://doi.org/10.1002/chem.201901315.

[116] Q. Ou, Q. Peng, Z. Shuai, Toward Quantitative Prediction of Fluorescence Quantum Efficiency by Combining Direct Vibrational Conversion and Surface Crossing: BODIPYs as an Example, Journal of Physical Chemistry Letters **11**(18), 7790–7797 (2020), https://doi.org/10.1021/acs.jpclett.0c02054.

[117] A. Prlj, L. Vannay, C. Corminboeuf, Fluorescence Quenching in BODIPY Dyes: The Role of Intramolecular Interactions and Charge Transfer, Helvetica Chimica Acta **100**(6), 1–9 (2017), https://doi.org/10.1002/hlca.201700093.

[118] Z. Lin, A. W. Kohn, T. Van Voorhis, Toward Prediction of Nonradiative Decay Pathways in Organic Compounds II: Two Internal Conversion Channels in BODIPYs, Journal of Physical Chemistry C **124**(7), 3925–3938 (2020), https://doi.org/10.1021/acs.jpcc.9b08292.

[119] T. Suhina, S. Amirjalayer, S. Woutersen, D. Bonn, A. M. Brouwer, Ultrafast dynamics and solvent-dependent deactivation kinetics of BODIPY molecular rotors, Physical Chemistry Chemical Physics **19**(30), 19998–20007 (2017), https://doi.org/10.1039/c7cp02037f.

[120] X. Liu, W. Chi, Q. Qiao, S. V. Kokate, E. P. Cabrera, Z. Xu, X. Liu, Y. T. Chang, Molecular Mechanism of Viscosity Sensitivity in BODIPY Rotors and Application to Motion-Based Fluorescent Sensors, ACS Sensors **5**(3), 731–739 (2020), https://doi.org/10.1021/acssensors.9b01951.

[121] F. Li, S. I. Yang, Y. Ciringh, J. Seth, C. H. Martin, D. L. Singh, D. Kim, R. R. Birge, D. F. Bocian, D. Holten, J. S. Lindsey, Design, synthesis, and photodynamics of light-harvesting arrays comprised of a porphyrin and one, two, or eight boron-dipyrrin accessory pigments, Journal of the American Chemical Society **120**(39), 10001–10017 (1998), https://doi.org/10.1021/ja9812047.

[122] B. Le Guennic, D. Jacquemin, Taking Up the Cyanine Challenge with Quantum Tools, Accounts of Chemical Research **48**(3), 530–537 (2015), https://doi.org/10.1021/ar500447q.

[123] R. Berraud-Pache, F. Neese, G. Bistoni, R. Izsák, Unveiling the Photophysical Properties of Boron-dipyrromethene Dyes Using a New Accurate Excited State Coupled Cluster Method, Journal of Chemical Theory and Computation **16**(1), 564–575 (2020), https://doi.org/10.1021/acs.jctc.9b00559.

[124] M. R. Momeni, A. Brown, Why do TD-DFT excitation energies of BODIPY/aza-BODIPY families largely deviate from experiment? Answers from electron correlated and multireference methods, Journal of Chemical Theory and Computation **11**(6), 2619–2632 (2015), https://doi.org/10.1021/ct500775r.

[125] J. Zhou, B. del Rosal, D. Jaque, S. Uchiyama, D. Jin, Advances and challenges for fluorescence nanothermometry, Nature Methods **17**(10), 967–980 (2020), https://doi.org/10.1038/s41592-020-0957-y.

[126] T. Förster, G. Hoffmann, Effect of viscosity on the fluorescence quantum yield of some dye systems, Zeitschrift fur physikalische chemie **75**(1-2), 63–76 (1971), https://doi.org/10.1524/zpch.1971.75.1$_2$.063.

[127] T. Karstens, K. Kobs, Rhodamine B and rhodamine 101 as reference substances for fluorescence quantum yield measurements [5], Journal of Physical Chemistry **84**(14), 1871–1872 (1980), https://doi.org/10.1021/j100451a030.

[128] K. P. Wall, R. Dillon, M. K. Knowles, Fluorescence quantum yield measurements of fluorescent proteins: A laboratory experiment for a biochemistry or molecular biophysics laboratory course, Biochemistry and Molecular Biology Education **43**(1), 52–59 (2015), https://doi.org/10.1002/bmb.20837.

[129] J. H. Brannon, D. Magde, Absolute quantum yield determination by thermal blooming. Fluorescein, Journal of Physical Chemistry **82**(6), 705–709 (1978), https://doi.org/10.1021/j100495a018.

[130] R. Sens, K. H. Drexhage, Fluorescence quantum yield of oxazine and carbazine laser dyes, Journal of Luminescence **24-25**(PART 2), 709–712 (1981), https://doi.org/10.1016/0022-2313(81)90075-2.

[131] Cold Spring Harbor Laboratory Press, PBS (pH 7.4) (2018).

[132] P. Blanchard, E. Brüning, *Density functional theory of atoms and molecules*, volume 69 (Oxford University Press, Oxford, 2015).

[133] R. E. Stratmann, G. E. Scuseria, M. J. Frisch, An efficient implementation of time-dependent density-functional theory for the calculation of excitation energies of large molecules, Journal of Chemical Physics **109**(19), 8218–8224 (1998), https://doi.org/10.1063/1.477483.

[134] W. Qin, T. Rohand, W. Dehaen, J. N. Clifford, K. Driesen, D. Beljonne, B. Van Averbeke, M. D. Van Auweraer, N. Boens, Boron dipyrromethene analogs with phenyl, styryl, and ethynylphenyl substituents: Synthesis, photophysics, electrochemistry, and quantum-chemical calculations, Journal of Physical Chemistry A **111**(35), 8588–8597 (2007), https://doi.org/10.1021/jp073547+.

[135] A. de Meijere, Bonding Properties of Cyclopropane and Their Chemical Consequences, Angewandte Chemie International Edition in English **18**(11), 809–826 (1979), https://doi.org/10.1002/anie.197908093.

[136] M. Baird, *The chemistry of the cyclopropyl group, Parts 1 and 2*, volume 12 (John Wiley & Sons, 1988).

[137] L. Gai, J. Mack, H. Lu, H. Yamada, D. Kuzuhara, G. Lai, Z. Li, Z. Shen, New 2,6-distyryl-substituted BODIPY isomers: synthesis, photophysical properties, and theoretical calculations, Chemistry **20**(4), 1091–1102 (2014).

[138] Y. Chen, J. Zhao, H. Guo, L. Xie, Geometry relaxation-induced large stokes shift in red-emitting borondipyrromethenes (BODIPY) and applications in fluorescent thiol probes, Journal of Organic Chemistry **77**(5), 2192–2206 (2012), https://doi.org/10.1021/jo202215x.

[139] H. Xiao, P. Li, B. Tang, Small Molecular Fluorescent Probes for Imaging of Viscosity in Living Biosystems, Chemistry - A European Journal **27**(23), 6880–6898 (2021), https://doi.org/10.1002/chem.202004888.

[140] M. Köllner, J. Wolfrum, How many photons are necessary for fluorescence-lifetime measurements?, Chemical Physics Letters **200**(1-2), 199–204 (1992), https://doi.org/10.1016/0009-2614(92)87068-Z.

[141] C. D. Brites, P. P. Lima, N. J. Silva, A. Millán, V. S. Amaral, F. Palacio, L. D. Carlos, Thermometry at the nanoscale, Nanoscale **4**(16), 4799–4829 (2012), https://doi.org/10.1039/c2nr30663h.

[142] K. Okabe, N. Inada, C. Gota, Y. Harada, T. Funatsu, S. Uchiyama, Intracellular temperature mapping with a fluorescent polymeric thermometer and fluorescence lifetime imaging microscopy, Nature Communications **3**(1), 705 (2012), https://doi.org/10.1038/ncomms1714.

[143] H. Itoh, S. Arai, T. Sudhaharan, S. C. Lee, Y. T. Chang, S. Ishiwata, M. Suzuki, E. B. Lane, Direct organelle thermometry with fluorescence lifetime imaging microscopy in single myotubes, Chemical Communications **52**(24), 4458–4461 (2016), https://doi.org/10.1039/c5cc09943a.

[144] V. J. Pansare, S. Hejazi, W. J. Faenza, R. K. Prud'Homme, Review of long-wavelength optical and NIR imaging materials: Contrast agents, fluorophores, and multifunctional nano carriers, Chemistry of Materials **24**(5), 812–827 (2012), https://doi.org/10.1021/cm2028367.

[145] Y. Ni, J. Wu, Far-red and near infrared BODIPY dyes: Synthesis and applications for fluorescent pH probes and bio-imaging, Organic and Biomolecular Chemistry **12**(23), 3774–3791 (2014), https://doi.org/10.1039/c3ob42554a.

[146] C. S. Kue, S. Y. Ng, S. H. Voon, A. Kamkaew, L. Y. Chung, L. V. Kiew, H. B. Lee, Recent strategies to improve boron dipyrromethene (BODIPY) for photodynamic cancer therapy: An updated review, Photochemical and Photobiological Sciences **17**(11), 1691–1708 (2018), https://doi.org/10.1039/c8pp00113h.

[147] E. Lager, J. Liu, A. Aguilar-Aguilar, B. Z. Tang, E. Peña-Cabrera, Novel meso-Polyarylamine-BODIPY hybrids: Synthesis and study of their optical properties, Journal of Organic Chemistry **74**(5), 2053–2058 (2009), https://doi.org/10.1021/jo802519b.

[148] J. Cui, H. Nie, S. Zang, S. Su, M. Gao, J. Jing, X. Zhang, A conformational transition based fluorescent probe for mapping lysosomal viscosity fluctuations by fluorescence lifetime imaging, Sensors and Actuators, B: Chemical **331**(January), 129432 (2021), https://doi.org/10.1016/j.snb.2020.129432.

[149] L. E. Shimolina, M. A. Izquierdo, I. López-Duarte, J. A. Bull, M. V. Shirmanova, L. G. Klapshina, E. V. Zagaynova, M. K. Kuimova, Imaging tumor microscopic viscosity in vivo using molecular rotors, Scientific Reports **7**(November 2016), 1–11 (2017), https://doi.org/10.1038/srep41097.

[150] I. V. Sazanovich, C. Kirmaier, E. Hindin, L. Yu, D. F. Bocian, J. S. Lindsey, D. Holten, Structural Control of the Excited-State Dynamics of Bis(dipyrrinato)zinc Complexes: Self-Assembling Chromophores for Light-Harvesting Architectures, Journal of the American Chemical Society **126**(9), 2664–2665 (2004), https://doi.org/10.1021/ja038763k.

[151] C. Reichardt, *Solvent Effects in Organic Chemistry* (Wiley-VCH, Weinheim, 2003).

[152] A. Y. Jee, E. Bae, M. Lee, Internal motion of an electronically excited molecule in viscoelastic media, Journal of Chemical Physics **133**(1), 14507 (2010), https://doi.org/10.1063/1.3454724.

[153] F. J. Santos, C. A. Nieto De Castro, J. H. Dymond, N. K. Dalaouti, M. J. Assael, A. Nagashima, Standard reference data for the viscosity of toluene, Journal of Physical and Chemical Reference Data **35**(1), 1–8 (2006), https://doi.org/10.1063/1.1928233.

[154] P. S. Steif, M. C. Palastro, Y. Rabin, Analysis of the effect of partial vitrification on stress development in cryopreserved blood vessels, Medical Engineering and Physics **29**(6), 661–670 (2007), https://doi.org/10.1016/j.medengphy.2006.07.010.

[155] S. Xuan, N. Zhao, X. Ke, Z. Zhou, F. R. Fronczek, K. M. Kadish, K. M. Smith, M. G. H. Vicente, Synthesis and Spectroscopic Investigation of a Series of Push-Pull Boron Dipyrromethenes (BODIPYs), Journal of Organic Chemistry **82**(5), 2545–2557 (2017), https://doi.org/10.1021/acs.joc.6b02941.

[156] R. Žvirblis, K. Maleckaitė, J. Dodonova-Vaitkūnienė, D. Jurgutis, R. Žilėnaitė, V. Karabanovas, S. Tumkevičius, A. Vyšniauskas, A red-emitting thiophene-modified BODIPY probe for fluorescence lifetime-based polarity imaging of lipid droplets in living cells, Journal of Materials Chemistry B **11**(17), 3919–3928 (2023), https://doi.org/10.1039/d3tb00305a.

[157] A. Vyšniauskas, B. Cornell, P. S. Sherin, K. Maleckaitė, M. Kubánková, M. A. Izquierdo, T. T. Vu, Y. A. Volkova, E. M. Budynina, C. Molteni, M. K. Kuimova, Cyclopropyl Substituents Transform the Viscosity-Sensitive BODIPY Molecular Rotor into a Temperature Sensor, ACS Sensors **6**(6), 2158–2167 (2021), https://doi.org/10.1021/acssensors.0c02275.

[158] M. R. Dent, I. López-Duarte, C. J. Dickson, N. D. Geoghegan, J. M. Cooper, I. R. Gould, R. Krams, J. A. Bull, N. J. Brooks, M. K. Kuimova, Imaging phase separation in model lipid membranes through the use of BODIPY based molecular rotors, Physical Chemistry Chemical Physics **17**(28), 18393–18402 (2015), https://doi.org/10.1039/c5cp01937k.

[159] B. A. Weaver, How Taxol/paclitaxel kills cancer cells, Molecular Biology of the Cell **25**(18), 2677–2681 (2014), https://doi.org/10.1091/mbc.E14-04-0916.

[160] S. Dasari, P. Bernard Tchounwou, Cisplatin in cancer therapy: Molecular mechanisms of action, European Journal of Pharmacology **740**, 364–378 (2014), https://doi.org/10.1016/j.ejphar.2014.07.025.

# NOTES

# NOTES

# NOTES

# NOTES

Vilnius University Press
Saulėtekio al. 9, LT-10222 Vilnius
e-mail: info@leidykla.vu.lt,
www.leidykla.vu.lt
Print run copies 20